INFORMATION TO USERS

This manuscript has been reproduced from the microfilm master. UMI films the text directly from the original or copy submitted. Thus, some thesis and dissertation copies are in typewriter face, while others may be from any type of computer printer.

The quality of this reproduction is dependent upon the quality of the copy submitted. Broken or indistinct print, colored or poor quality illustrations and photographs, print bleedthrough, substandard margins, and improper alignment can adversely affect reproduction.

In the unlikely event that the author did not send UMI a complete manuscript and there are missing pages, these will be noted. Also, if unauthorized copyright material had to be removed, a note will indicate the deletion.

Oversize materials (e.g., maps, drawings, charts) are reproduced by sectioning the original, beginning at the upper left-hand corner and continuing from left to right in equal sections with small overlaps. Each original is also photographed in one exposure and is included in reduced form at the back of the book.

Photographs included in the original manuscript have been reproduced xerographically in this copy. Higher quality 6" x 9" black and white photographic prints are available for any photographs or illustrations appearing in this copy for an additional charge. Contact UMI directly to order.

UMI®

Bell & Howell Information and Learning
300 North Zeeb Road, Ann Arbor, MI 48106-1346 USA
800-521-0600

Accurate and Efficient Analysis of Wireless Digital Communication Systems in Multiuser and Multipath Fading Environments

by

Annamalai, Annamalai Jr.

M. A. Sc., University of Victoria, 1997
B. Eng. (Hons.), Universiti Sains Malaysia, 1993

A Dissertation Submitted in Partial Fulfillment of the Requirements
for the Degree of

DOCTOR OF PHILOSOPHY

in the Department of Electrical and Computer Engineering

We accept this dissertation as conforming to the required standard

---

Dr. V. K. Bhargava, Supervisor, Dept. of Electrical and Computer Engineering

---

Dr. W. S. Lu, Member, Dept. of Electrical and Computer Engineering

---

Dr. K. F. Li, Member, Dept. of Electrical and Computer Engineering

---

Dr. D. Olesky, Outside Member, Dept. of Computer Science

Dr. H. Kobayashi, External Examiner, Princeton University

Supervisor: Prof. Vijay K. Bhargava

ABSTRACT

Testimonies of "wireless catching up with wireline" have begun. However, the nonstationary and hostile nature of the wireless channel impose the greatest threat to reliable data transmission over wireless links. The performance of a digital modulation scheme is degraded by many transmission impairments including fading, delay spread, co-channel interference and noise. Two powerful techniques for improving the quality of service over the wireless network are investigated: diversity reception and adaptive error control schemes. Owing to the growing interest in wireless communications, the importance of exact theoretical analysis of such systems cannot be understated. In light of these considerations, this dissertation focuses on accurate and efficient analysis of wireless digital communication systems in multiuser and multipath fading environments.

The evaluation of error probabilities in digital communication systems is often amenable to calculating a generic error probability of the form $Pr\{X \leq 0\}$, where X is a random variable whose probability distribution is known. We advocate a simple numerical approach based on the Fourier or Laplace inversion formulas and Gauss-Chebychev quadratures (GCQ) for computing this error probability. Using this result, and by formulating the outage probability of cellular mobile radio networks in the framework of statistical decision theory, we can unify the outage performance analysis for cellular mobile radio systems in generalized fading channels without imposing any restrictions on the desired signal and interferers statistics.

Next, we develop two unified analytical frameworks for evaluating the bit or symbol error probability (SER) of a broad class of coherent, differentially coherent and noncoherent digital communication systems with diversity reception in generalized fading channels. The exact SER is mostly expressed in terms of a single finite-range integral, and in some cases in the form of double finite-range integrals. Virtually "exact" closed-form expressions (in terms of a rapidly converging series) are also derived. This offers a convenient method to perform a comprehensive study of all common diversity combining techniques (maximal-ratio combining (MRC), equal-gain combining (EGC), selection combining (SDC) and switched combining (SWC)) with different modulation formats in a myriad of fading scenarios. In particular, our unified approach based on characteristic function (CHF) method allows us to unify the above problem in a single common framework. Nevertheless, the moment generating function (MGF) method often yields a

more concise solution than the CHF approach in the analysis of MRC, SDC and SWC diversity systems.

Subsequently, we examine the performance of a maximum amplitude selection diversity (MA/SD) rake receiver configuration in indoor wireless channels. The proposed low-complexity receiver structure is practically appealing because of its simplicity as well as its ability to operate effectively even at high signalling rates. We have also devised a robust packet combining mechanism to enhance the throughput and delay performance of spread-spectrum radio networks without incurring a substantial penalty in receiver complexity. A simple indirect method to estimate the channel state condition for successful implementation of a self-reconfigurable automatic repeat-request (ARQ) system, such as mixed-mode ARQ protocol or adaptive packet length strategy in a slowly varying mobile radio environment is also studied.

Examiners:

Dr. V. K. Bhargava, Supervisor, Dept. of Electrical and Computer Engineering

Dr. W. S. Lu, Member, Dept. of Electrical and Computer Engineering

Dr. K. F. Li, Member, Dept. of Electrical and Computer Engineering

Dr. D. Olesky, Outside Member, Dept. of Computer Science

Dr. H. Kobayashi, External Examiner, Princeton University

Table of Contents

List of Figures

List of Tables

Acknowledgments

First and foremost, I would like to express my deepest appreciation to my thesis supervisor and mentor, Prof. Vijay K. Bhargava. I greatly valued the freedom and flexibility with which he entrusted me, the generous financial support (both in terms of research assistantship and support for attendance at numerous technical meetings) he has provided and for offering the finest lab on campus from which I could perform my research in a timely manner.

I am very grateful to Professors Dale Olesky, Kin F. Li and Wu-Sheng Lu for serving on my supervisory committee, and Professor Hisashi Kobayashi for agreeing to be the external examiner in my Ph. D. oral examination. Their time and effort are highly appreciated. Special thanks to Professors H. Kobayashi and V. K. Bhargava for their many helpful suggestions which have improved the presentation of this thesis.

My sincere thanks are also extended to all my colleagues at the Digital Communications Research Laboratory for the friendship and assistance in various ways. In particular, I wish to express my gratitude towards Drs. Chinthananda Tellambura and Mao Zeng for having helped inspire this topic of research and for having provided numerous useful suggestions and constructive criticisms at several points throughout the last two years. I also thank Prof. Wu-Sheng Lu for his guidance in the optimization related task that I have undertaken. I am deeply indebted to Ms. Jing Su for her assistance in writing computer programs and generating several figures found in this thesis. It is not possible to mention all the people that have in some way influenced this work, and I apologize to those individuals whose names are omitted.

Last but not the least, I thank my family for their love and devoted support throughout my life. In particular, my parents have always been there for me and supported me in every way possible.

To
My beloved Parents

Chapter 1

Introduction

Marconi's innovative perception of the electromagnetic waves and the air interface in 1897 has been the first milestone on the important road to the shared use of the radio spectrum. But only after almost a century later, the mobile wireless communication started to take-off. Despite a series of disappointing false starts, the communication world in the late 1980s was rapidly becoming more mobile for a much broader segment of communication users than ever before. Historically, communication has been restricted primarily to voice traffic between two fixed locations rather than between two people. With the advent of wireless technology, a transition from point-to-point communication towards person-to-person communication (i.e., independent of location) has begun. Testimony to this is the rapidly increasing penetration of cordless and cellular phones, not just in North America but all across the world. In anticipation of the growing consumer demands, the next generation of wireless systems endeavors to provide person-to-person communication of both circuit and packet multi-media data.

Wireless access is an attractive alternative to copper wire because radio links cost much less than the wired networks for a vast range of applications. In addition, wireless links offer increased flexibility in a network design (specifically for less equitably or sparsely distributed services and for early deployments of new services) and possibly user mobility. Consequently, the developing countries can leap-frog into wireless technology to minimize the infrastructure and maintenance costs. The wireless local loop system is a natural solution since it provides the infrastructure in a fraction of time at a fraction

of cost. In developed nations, the most promising application of wireless access is mobile telephony - and its evolution towards the Personal Communication Networks (PCN). Satellite component of the PCN enables global connectivity. Therefore it is no surprise mobile cellular communications represents the fastest growing segment of wireless technology, particularly since the idea of "wireless Internet" is conceived.

Radio signals generally propagate according to three mechanisms: reflection, diffraction, and scattering. As a result of these three mechanisms, macrocellular radio propagation can be characterized by three nearly independent phenomenon: path loss variation with distance, slow log-normal shadowing, and fast multipath fading. In particular, the user mobility causes the radio link quality to be highly irregular. The nonstationary and hostile (noisy) nature of the wireless channel imposes the greatest threat to reliable data transmission over wireless links. Noise arises from sources such as thermal noise in the receiver, natural and man-made interference. Such a poor channel quality has been recognized as the largest obstacle facing the wireless communication systems designers. Frequency reuse in FDMA/TDMA cellular systems also introduces cochannel interference, one of the major factors that limits the capacity of cellular systems. Cochannel interference arises when the same carrier frequency is used in different neighbouring cells. This dissertation discusses and analyze some important issues in this subject, by focusing into the key techniques that can be used to facilitate transmission of voice, video and data in offering untethered personal communication services. These techniques include diversity reception and adaptive error control schemes (i.e., self-reconfigurable automatic repeat-request (ARQ) systems).

1.1 Significance of Research

In this dissertation, we address three major issues pertaining to analysis of wireless digital communication systems in generalized fading channel. The first part of the dissertation deals with accurate outage performance analysis for cellular mobile radio systems in an arbitrary fading environment. In the research literature, much effort has been expended to find closed-form expressions for outage in mobile radio systems. To get explicit formu-

las, it is often necessary to make restrictive assumptions (e.g., Nakagami fading severity parameter be a positive integer or identical statistical distributions for all the interferers) or even approximations (replacing a Rician random variable by a Nakagami random variable). Although the assumption that all the received signals (both desired and undesired) have the same statistical characteristics is quite reasonable for medium and large cell systems, its validity for pico- and microcellular systems is questionable. This is because an undesired signal from a distant cochannel cell may well be modelled by Rayleigh statistics but Rayleigh fading assumption may not be a good assumption for the desired signal since a line-of-sight path is likely to exist in a microcell. Therefore, it is evident that different statistics are needed to characterize the desired user signal and the interfering signals in a micro or picocellular radio systems. If the probability density function (PDF) of the total interference I is known, then the outage can readily be obtained. The PDF, $f_I(\xi)$, can be expressed as an L-fold convolution integral where L denotes the number of interfering signals. While there is no analytical solution to this integral in general, several early papers have taken this approach. Further Stuber [1] has pointed out that a more detailed analysis for the case of Rician faded desired signal with multiple Rician/Rayleigh interferers is required because the present analytical approaches do not lend themselves to analyze this case. He quotes, "... Unfortunately, this does not result in a simple multiplication of Laplace transform as before, and, hence, alternative methods for finding the exact PDF must be employed. This is an open research problem."[1, pp. 139]. In this dissertation we develop a general approach for computing the outage probability without imposing any restrictions on the desired signal or interfering signals statistics. First we advocate a simple numerical approach based on the Fourier or Laplace inversion formulas and Gauss-Chebychev quadratures (GCQ) for computing a generic error probability of the form $Pr\{X \leq 0\}$. Using this result, and by formulating the outage probability of cellular mobile radio networks in the framework of statistical decision theory, we can unify the outage performance analysis for cellular mobile radio systems in generalized fading channels. Further, our analysis has been generalized to include a more refined outage criterion (dual-threshold model) taking into account of the receiver noise. The outage analysis in turn can help the system designers to determine the cell cluster size and the minimum transmit power requirements.

The second part of the dissertation is devoted to unified analysis of diversity systems in generalized fading channels. Two analytical frameworks are outlined for evaluating the bit or symbol error probability (SER) of a broad class of coherent, differentially coherent and noncoherent digital communication systems in all common fading distributions. The first unifying theory is based on the moment generating function (MGF) method in conjunction with the use of alternate exponential representations for the one-dimension and two-dimension complementary error functions. The second approach is based on the characteristic function (CHF) method and relies on knowledge of three Fourier Transforms. The unified approach allows previously obtained results to be simplified both analytically and computationally and new results to be obtained for special cases that heretofore resisted solution in a simple form. The exact SER is mostly expressed in terms of a single finite-range integral, and in some cases in the form of double finite-range integrals. Virtually "exact" closed-form expressions (in terms of a rapidly converging series) are also derived. This offers a convenient method to perform a comprehensive study of all common diversity combining techniques (maximal-ratio combining (MRC), equal-gain combining (EGC), selection combining (SDC) and switched combining (SWC)) with different modulation formats. In particular, our approach based on the CHF method allows us to unify the above problem under a single common framework. Nevertheless, the MGF method often yields a more concise solution than the CHF approach in the analysis of MRC, SDC and SWC diversity systems. The generality and computational efficiency of our new results render themselves as powerful means for both theoretical analysis and practical applications.

We would like to point out that error performance analysis of EGC appears to be much more difficult than for MRC or SDC. The principle difficulty is finding a closed-form expression for the PDF of a sum of random fading amplitudes. Indeed, even for Rayleigh fading, the PDF is known only for the dual diversity case. According to Jakes, [2, pp. 321], "The problem of finding the distribution... is an old one, going back even to Lord Rayleigh, but has never been solved in terms of tabulated functions for $L \geq 3$." In the dissertation, we develop an alternative, direct technique to evaluate the exact perfor-

mance of EGC diversity systems. Our approach relies on the use of the Parseval theorem to transform the error integral into the frequency domain. Since the Fourier transform of the PDF is the CHF, which is available in this case, our solution is general and exact. To the best of our knowledge, no exact analytical expression for EGC diversity receivers have been reported previously for $L > 3$ even for the Rayleigh fading channel.

In this dissertation, we have also studied the performance of a low-complexity rake receiver structure, which is based on selecting the finger with the largest composite received signal, in indoor wireless channels. The proposed receiver structure is practically appealing because of its simplicity as well as its ability to operate effectively even at high signalling rates. We have also devised a robust packet combining mechanism to enhance the throughput and delay performance of spread-spectrum radio networks without incurring a substantial penalty in receiver complexity. Such a scheme is suitable for wireless data networks that demand stringent bit-error rate requirements but relatively insensitive to delay.

The third part of this dissertation focuses on accurate analysis and parameter optimization of several simple algorithms that are used estimate the channel state condition via an indirect method, for successful implementation of adaptive ARQ systems. The motivation for implementing an adaptive ARQ system arises from the fact that the wireless channel is time-varying and unlike forward error correction (FEC) schemes, the throughput of a fixed ARQ protocol falls rapidly with increasing channel error rates. Therefore, it is possible to improve the throughput performance by properly adapting the system parameters to the slowly varying channel conditions. In this dissertation we have examined two self-reconfigurable ARQ systems which use different block sizes (packet length) and multicopy transmission schemes as adaptation mechanisms. First, an accurate model for analyzing the transmission protocol with memory is developed. Subsequently, an efficient and systematic approach to acquire the suboptimal design variables is outlined.

Since the problems addressed in this dissertation is quite broad, the literature review pertinent to each topic will be discussed with greater detail in their chapters separately.

1.2 Thesis Outline

This thesis consists of nine chapters. In Chapter 2, we outline a unified approach to evaluating the outage probability in generalized fading channels without imposing any restrictions on the desired signal and the interfering signals statistics. The outage analysis in turn can help the system designers and planners to determine the cochannel reuse distance (i.e., cluster size) and the minimum transmit power requirements.

In Chapter 3, we outline two unified approaches for calculating the error performance of diversity systems in generalized fading channels. The approaches adopted here allows previously obtained results to be simplified both analytically and computationally and new results to be obtained for special cases that heretofore resisted solution in a simple form. Exact analytical expressions for the bit or symbol error probability (in the form of either a single or double finite-range integral(s)) and virtually "exact" closed-form solutions based on GCQ formula are derived for the maximal-ratio combining (MRC), equal-gain combining (EGC), selection combining (SDC) and switched combining (SWC) diversity systems with different modulation formats. The generality and computational efficiency of the new results presented in this chapter render themselves as powerful means for both theoretical analysis and practical applications.

Subsequently in Chapter 4, we present a comprehensive study of the M-ary quadrature amplitude modulation (MQAM) scheme with MRC and EGC diversity receivers over Nakagami-m fading channel. Specifically, we provide several methods for computing the average SER of MQAM in the hope of stimulating further applications. Both independent and correlated fading cases for MRC are considered. In fact, until recently, there was no exact analytical expression for evaluating the SER of square MQAM in generalized fading channel available in the research literature.

In Chapters 5, we rigorously examined the performance of a dual branch switch-and-stay (SWC) diversity system for different modulation formats via the MGF method. Subsequently in Chapter 6, we derive several closed-form and infinite series expressions for the MGF of SNR at the output of a dual-branch SDC combiner in bivariate (corre-

lated) Nakagami-m and Rayleigh fading channels.

In Chapter 7, we develop a theoretical framework to analyze the performance of maximum-amplitude selection diversity (MA/SD) systems in a Nakagami fading channel with arbitrary parameters. In addition, we derive a simple expression for bounding the remainder term of a Gauss-Chebychev quadrature (GCQ) formula using a complex-variable method. This new bound is highly desirable since it does not require the evaluation of higher order derivatives, which can be difficult, time consuming and tedious.

The steady-state performance of both slotted and unslotted random access packet-switched DS/CDMA networks in conjunction with packet combining is investigated in Chapter 8. This technique is highly advantageous for systems which can tolerate a certain delay and operate over highly time-varying channels. To facilitate the analysis, we have derived simple and computationally efficient lower and upper bounds for the average number of retransmissions and throughput of this new system with Poisson traffic assumption. The effects of the packet header failure rate and the feedback channel error probability on the system performance are examined.

In Chapter 9, we outline an efficient method to concurrently optimize a multiplicity of design variables for a mixed-mode ARQ protocol, both in noiseless and noisy feedback channels. In our multicopy transmission strategy, we either adapt the number of identical message blocks sent in each transmission or the number of copies of a block retransmitted to handle a negatively acknowledged codeword dynamically to the estimated channel condition.

Whereas in Chapter 10, we investigate the performance of an adaptive packet length strategy in mobile radio environment. In particular, we investigate four simple algorithms (indirect method to estimate the channel state condition) to implement such an adaptive system for slowly time-varying channels.

Finally in Chapter 11, conclusions and suggestions for future work are provided.

Chapter 2

A Unified Approach for Outage Analysis in Cellular Mobile Radio Systems

In cellular radio systems, the spectrum utilization efficiency may be improved by reducing the cluster size but at the expense of increased cochannel interference (CCI). The probability of outage is a useful statistical measure of performance in the presence of CCI [3]. The outage performance of digital radio systems has been studied extensively (see [4]-[11] among many others). The statistical fluctuations of the signal amplitude are often modelled by a Rayleigh, Rician or Nakagami distribution, or compound distributions like the lognormal-Nakagami, Suzuki and lognormal-Rice. These distributions can model most fading environments.

Consider evaluating the probability of outage (hereafter, simply referred to as outage) in an interference-limited mobile fading environment. The instantaneous signal powers are modelled as random variables (RVs) p_k, $k = 0, 1, 2, \ldots, L$, with mean $\bar{p}_k$. The subscript $k = 0$ denotes the desired user signal, and $k = 1, \ldots, L$ are for the interfering signals. The outage is given by,

$$P_{out} = Pr\{qI > p_0\} \tag{2.1}$$

where $I = p_1 + \ldots + p_L$ and q is the power protection ratio, which is fixed by the type of modulation and transmission technique employed and the quality of service desired. Typically, $9 < q < 20$ (dB). For instance, $q = 9.5dB$ for the digital pan-European GSM

system using GMSK modulation.

In the literature, various complicated formulas have been derived for the outage. In fact, computing the basic outage simply requires the cumulative distribution function (CDF) at zero of a linear sum of random powers. Since the MGF of the sum can be determined very easily, the outage follows at once from the Laplace or Fourier inversion formulas. Virtually-exact closed form solutions to the integrals can be attained using a GCQ sum.

However, in the past numerous ad-hoc attempts have been made to obtain closed-form expressions for the outage under different fading scenarios. To get explicit formulas, it is often necessary to make restrictive assumptions (e.g., Nakagami fading severity parameter be a positive integer [4] or identical statistical distributions for all the interferers [9]) or approximations (replacing a Rician RV by a Nakagami RV). Although the assumption that all the received signals (both desired and undesired) have the same statistical characteristics is quite reasonable for medium and large cell systems, its validity for pico- and microcellular systems is questionable. This is because an undesired signal from a distant cochannel cell may well be modelled by Rayleigh statistics but Rayleigh fading assumption may not be a good assumption for the desired signal since a line-of-sight path is likely to exist in a microcell. Therefore, it is evident that different statistics are needed to characterize the desired user signal and the interfering signals in a micro or picocellular radio systems. If the probability density function (PDF) of the total interference I is known, then the outage can readily be obtained. The PDF, $f_I(\xi)$, can be expressed as an L-fold convolution integral. While there is no analytical solution to this integral in general, several early papers have taken this approach. Another approach is to use the Laplace transform (LT) of the PDF, i.e., the moment generating function (MGF). If the RVs are independent, the MGF of total interference I,

$$\phi_I(s) = \int_0^\infty \exp(-s\xi) f_I(\xi)\, d\xi \tag{2.2}$$

is the product of the individual MGFs. While, in principle, inverting this MGF gives the

PDF of I, closed-form expressions are difficult or impossible under general conditions. This inversion can be circumvented if the desired signal power is a sum of exponential RVs. From Eq. (2.1), it follows that

$$P_{out} = \int_0^{\infty} F_0(q\xi) f_I(\xi)\, d\xi \tag{2.3}$$

where $F_0(.)$ is the cumulative distribution function (CDF) of p_0. If the desired signal amplitude is Rayleigh fading, then p_0 is an exponential RV with a CDF of the form $1-\exp(-p_0/\bar{p}_0)$. Therefore, by combining Eq. (2.2) and Eq. (2.3) the outage can be expressed using $\phi_I(s)$. If the desired signal amplitude is Nakagami faded with an integer fading index m, then p_0 is a sum of m exponential RVs (i.e., a Gamma RV) with a CDF of the form $1-\sum x^k \exp(-x)$. If $f(x)$ and $\phi(s)$ form an LT pair, so do $(-x)^k f(x)$ and $\phi^{(k)}(s)$, the kth derivative. Hence, the outage can be calculated using the first $m-1$ derivatives of the MGF of I. By approximating a Rice RV by a Nakagami RV, the above method can be used for the Rice-faded desired signal. These are some of the techniques that have appeared in the literature.

The main contributions of this chapter include the following: (a) First, we unify the previous results by expressing the *exact* outage in an interference-limited environment as a finite-range integral for all the common fading distributions. The MGFs of the desired and interfering signal powers constitute the integrand. Using the standard mathematical and software packages such as Maple and Matlab, it is extremely simple to evaluate (numerically) the integral with high accuracy, whereas explicit closed-form solutions tend to require much programming effort. Our approach here is partly motivated by this consideration. Moreover, the integral can be approximated by extremely accurate sums (Gauss-Chebychev quadrature formulas) requiring knowledge of the MGF at only a small number of points; (b) Next, we assess the suitability of Nakagami-m approximation for a Rician RV; (c) Third, we derive two unified expressions for the outage performance of a generalized threshold model which takes into account the receiver noise floor. The corresponding analysis can be handled either by treating the noise as interference or

by introducing a minimum signal power constraint (i.e., dual-threshold model). An assessment of the compatibility and applicability of these two approaches is also provided; (d) Finally we investigate the effect of correlated interferers on the outage performance in a Nakagami-m fading channel.

The outline of this chapter is as follows. In Section 2.1, we present the MGF and PDF for the signal power in different fading channel models. Our new methodology for outage analysis is outlined in Section 2.2. Selected numerical results are provided in Section 2.3. Finally in Section 2.4, the main points are summarized and conclusions restated.

2.1 Statistical Representation of the Fading Channels

Given a random variable X, the MGF indicates the expected value of the exponential of X, i.e., $\phi(s) = \mathrm{E}[e^{-sx}]$. Since our unified approach for computing the outage performance requires the knowledge of only the MGF of the received signal power (i.e., in an interference-limited environment as well as when receiver noise is treated as interference) or both MGF and PDF of the received signal power (i.e., for the dual-threshold model), we next identify the MGFs and PDFs for several commonly used fading channel models.

2.1.1 Rician and Rayleigh Fading

The PDF for the Rician-faded signal power is given by [1, (2.44)],

$$f(x) = \frac{1+K}{\bar{p}} \exp\left(-K - \frac{(1+K)x}{\bar{p}}\right) I_0\left(2\sqrt{\frac{K(K+1)x}{\bar{p}}}\right), x \geq 0 \qquad (2.4)$$

where $I_0(.)$ is the modified Bessel function of the first kind and K denotes the Rice parameter, which is the ratio of the power in the line-of-sight and specular components to that in the diffuse component. The Laplace transform of Eq. (2.4) gives the MGF for a non-centralized chi-squared RV [12, pp. 44],

$$\phi(s) = \frac{1+K}{1+K+s\bar{p}} \exp\left(\frac{-Ks\bar{p}}{1+K+s\bar{p}}\right) \tag{2.5}$$

In a limiting case when the power in the line-of-sight path approaches zero, the channel reverts to the Rayleigh fading channel. Therefore the PDF and MGF for Rayleigh fading case can be obtained by setting $K = 0$ in Eqs. (2.4) and (2.5), respectively.

2.1.2 Nakagami-m and Nakagami-q (Hoyt) Fading

Utilizing the transformation of RVs, the squared-envelope of a Nakagami-m distributed RV has the Gamma density,

$$f(x) = \left(\frac{m}{\bar{p}}\right)^m \frac{x^{m-1}}{\Gamma(m)} \exp\left(\frac{-mx}{\bar{p}}\right) \tag{2.6}$$

where m denotes the fading figure. It is evident that Eq. (2.6) reduces to the Rayleigh fading case when $m = 1$. When m is an integer, it is an m-stage Erlang distribution. The MGF for the Nakagami-m fading channel can be obtained from [4, Eq. (44)],

$$\phi(s) = \left(\frac{m}{m+s\bar{p}}\right)^m, \quad m \geq 0.5. \tag{2.7}$$

The PDF of the signal power for the Nakagami-q [13] is given by,

$$f(x) = \frac{1}{\bar{p}\sqrt{1-b^2}} \exp\left(\frac{-x}{\left[1-b^2\right]\bar{p}}\right) I_0\left(\frac{bx}{\left[1-b^2\right]\bar{p}}\right) \tag{2.8}$$

where $b = \left[1-q^2\right]/\left[1+q^2\right]$ and q $(0 \leq q < \infty)$ is the fading parameter. In particular, the Nakagami-q distribution reverts to the Rayleigh and the one-sided normal distribution when $b = 0$ and $b = 1$, respectively. It can be easily shown that the MGF of the received power for the Nakagami-q fading is,

$$\begin{aligned} \phi(s) &= \frac{1}{\sqrt{1+2s\bar{p}+s^2\left[1-b^2\right]\bar{p}^2}} \qquad \text{for} \quad -1 \leq b \leq 1. \\ &= \frac{1}{\sqrt{\left[s\bar{p}(1+b)+1\right]\left[s\bar{p}(1-b)+1\right]}} \end{aligned} \tag{2.9}$$

2.1.3 Lognormal-Rice and Suzuki Fading

Expressing the received fading envelope as the product of independent Rice and lognormal distributions, and then applying Hermitian integration, we can show

$$\phi(s) = \frac{1}{\sqrt{\pi}} \sum_{i=1}^{H} \frac{w_i(1+K)}{1+K+s\mu\exp\left[\sqrt{2}\sigma x_i\right]} \exp\left(\frac{-Ks\mu\exp\left[\sqrt{2}\sigma x_i\right]}{1+K+s\mu\exp\left[\sqrt{2}\sigma x_i\right]} \right) + R_H \quad (2.10)$$

where σ is the logarithmic standard deviation of shadowing, and μ is the local mean power. The abscissas x_i (ith root of an Hth order Hermite polynomial) and weights w_i are tabulated in [14] for $H \leq 20$ and R_H is a remainder term.

The PDF for the lognormal-Rice is given by,

$$f(x) = \int_0^{\infty} \frac{1+K}{\Omega} \exp\left(-K - \frac{(1+K)x}{\Omega} \right) I_0\left(2\sqrt{\frac{K(K+1)x}{\Omega}} \right) \times \frac{1}{\sqrt{2\pi}\sigma\Omega} \exp\left(\frac{-\ln^2(\Omega/\mu)}{2\sigma^2} \right) d\Omega \quad (2.11)$$

Since Suzuki distribution [10] is a special case of the lognormal Rician distribution, its MGF and PDF is readily obtained by setting $K = 0$ in Eqs. (2.10) and (2.11).

2.1.4 Lognormal-Nakagami-m Fading

Similar to our derivation of Eq. (2.10), the MGF of the received power in a Nakagami-m fading channel with lognormal shadowing can be expressed as,

$$\phi(s) = \frac{1}{\sqrt{\pi}} \sum_{i=1}^{N} \frac{w_i}{\left[1 + s\mu\exp\left\{\sqrt{2}\sigma x_i\right\}/m \right]^m} + R_H. \quad (2.12)$$

The PDF of the composite Gamma and lognormal shadowing for the Nakagami-m channel is,

$$f(x) = \int_0^{\infty} \left(\frac{m}{\Omega} \right)^m \frac{x^{m-1}}{\Gamma(m)} \exp\left(\frac{-mx}{\Omega} \right) \times \frac{1}{\sqrt{2\pi}\sigma\Omega} \exp\left(\frac{-\ln^2(\Omega/\mu)}{2\sigma^2} \right) d\Omega. \quad (2.13)$$

2.2 Outage Performance Analysis

2.2.1 Interference Limited Environment

The radio link performance in pico- and microcellular radio systems is usually limited by interference rather than noise and, therefore, the probability of co-channel interference is of primary concern. Then the probability of outage is dictated by the event that the instantaneous carrier-to-interference ratio falls below a specified receiver threshold level q.

Let us define

$$\gamma = \frac{p_0}{q} - \sum_{k=1}^{L} p_k \tag{2.14}$$

and therefore the MGF of γ is given by

$$\phi_\gamma(s) = \phi_0(s/q) \prod_{k=1}^{L} \phi_k(-s) , \tag{2.15}$$

where $\phi_k(s)$ is the MGF of p_k. It follows that the outage is given by

$$P_{out} = Pr(\gamma < 0) . \tag{2.16}$$

In the following, we outline two general methods for evaluating the outage probability expression illustrated by Eq. (2.16): (a) Laplace inversion method, and (b) Gil-Pelaez inversion theorem.

2.2.1.1 Laplace Inversion Method

This probability in the form of Eq. (2.16) can be written as [15][16],

$$\begin{aligned} P_{out} &= \frac{1}{2\pi}\int_{-\infty}^{\infty} \frac{\phi_\gamma(c+j\omega)}{c+j\omega} d\omega \\ &= \frac{1}{\pi}\int_{0}^{\infty} \frac{\text{Real}\,[\,(c-j\omega)\,\phi_\gamma(c+j\omega)\,]}{c^2+\omega^2} d\omega \end{aligned} \tag{2.17}$$

where $j^2 = -1$, $0 < c < a_{min} = min\{a_i | \ 1 \le i \le L\}$ with a_i being the i-th pole of $\phi_\gamma(s)$ in the left half plane (i.e., $a_i > 0$). Note that Eq. (2.17) emanates from the relation that the LT of CDF is $\phi(s)/s$, and therefore Eq. (2.17) is simply a Laplace inversion integral. Next, by substituting $\omega = c\tan(\theta/2)$ in Eq. (2.17), we get

$$P_{out} = \frac{1}{2\pi}\int_0^{\pi} \tilde{\phi}_\gamma(\theta)\, d\theta \tag{2.18}$$

where $\tilde{\phi}_\gamma(.)$ is given by,

$$\tilde{\phi}_\gamma(\theta) = \text{Real}\left[(1 - j\tan(\theta/2))\, \phi_\gamma(c + jc\tan(\theta/2)) \right]. \tag{2.19}$$

This *new* form (i.e., Eq. (2.18)) is both easily evaluated and well suited to numerical integration since it only involves *finite integration limits* and knowledge of the MGF. The *generality* and *simplicity* of this result is to be compared with other restrictive and more complex forms given in the research literature.

Further, using variable substitution $\theta = \text{acos}(x)$, and then applying the GCQ formula [[14], pp. 889] to the resultant integral, we get

$$P_{out} = \frac{1}{2n}\sum_{i=1}^{n} \tilde{\phi}_\gamma\left[\frac{(2i-1)\,\pi}{2n}\right] + R_n \tag{2.20}$$

where the remainder term R_n vanishes (decays) very rapidly (i.e., Eq. (2.20) is therefore a rapidly converging series).

Although the value of coefficient c can be selected anywhere between 0 and a_{min}, it is better to choose it such that $|\phi_\gamma(c + j\omega)|$ decays very rapidly as $\omega \to \infty$. The highest rate of decay is ensured if $s = c$ is a saddle point; i.e., at $s = c$, $s^{-1}\phi_\gamma(s)$ achieves its minimum on the real axis. However, this optimal value of c requires a numerical search. In practice it is sufficient to use $c = a_{min}/2$. For the MGFs listed in the previous section, this value can be determined at once. As well, in the Appendix 2A we have derived a simple expression for the remainder term,

$$R_n = \frac{\pi^2}{6n^2}\tilde{\phi}_\gamma''(\zeta) \quad \text{for some } 0 < \zeta < \pi. \tag{2.21}$$

This *new* expression is very attractive for numerical evaluation since it only involves a second order derivative of the MGF instead of $2n$-th order derivative of the MGF using the formula furnished in [14] (i.e., Eq. (2A.6)).

2.2.1.2 Gil-Pelaez Inversion Theorem

Our second approach relies on the characteristic function (CHF) of the decision variable γ given in Eq. (2.14) (i.e., Fourier transform of the PDF of γ) and the application of an inversion theorem [17]. It is noted that the CHF is related to the MGF via relationship

$$\psi_\gamma(t) = \phi_\gamma(-jt), \tag{2.22}$$

and Gil-Pelaez's inversion theorem provides the relationship between the CDF and the CHF,

$$F_\gamma(x) = \frac{1}{2} - \frac{1}{\pi}\int_0^\infty \frac{\text{Imag}\left[\psi_\gamma(t)\exp(-jtx)\right]}{t}dt \tag{2.23}$$

where notation $\psi_\gamma(t)$ denotes the CHF of γ.

From Eqs. (2.16) and (2.23), the outage probability can be directly calculated as

$$P_{out} = F_\gamma(0) = \frac{1}{2} - \frac{1}{\pi}\int_0^\infty \frac{\text{Imag}\left[\psi_\gamma(t)\right]}{t}dt. \tag{2.24}$$

Replacing $\psi_\gamma(t) = \phi_\gamma(-jt)$ and then using variable substitution $t = \tan(\theta/2)$, Eq. (2.24) may be rewritten in the desired form,

$$P_{out} = \frac{1}{2} - \frac{1}{\pi}\int_0^\pi \frac{\text{Imag}\left[\phi_\gamma(-j\tan(\theta/2))\right]}{\sin\theta}d\theta \tag{2.25}$$

which is suitable for numerical integration. Alternatively, substituting $t = \frac{1-x}{1+x}$ in Eq.

(2.24) and then applying GCQ rule, we get a closed-form formula for the outage probability in the form of a series expression,

$$\begin{aligned} P_{out} &= \frac{1}{2} - \frac{2}{\pi}\int_{-1}^{1} \frac{\mathrm{Imag}\left[\phi_\gamma\left(-j\frac{1-x}{1+x}\right)\right]}{\sqrt{1-x^2}} \frac{dx}{\sqrt{1-x^2}} \\ &= \frac{1}{2} - \frac{2}{n}\sum_{i=1}^{n} \frac{\mathrm{Imag}\left[\phi_\gamma\left(-j\tan^2\left(\frac{(2i-1)\pi}{4n}\right)\right)\right]}{\sin\left(\frac{(2i-1)\pi}{2n}\right)} + R_n \end{aligned} \tag{2.26}$$

Notice that formulas like Eq. (2.25) when evaluated numerically have the form of 0.5 minus a sum (e.g., see Eq. (2.26)). When the tails of the distribution are sought, the sum is also close to 0.5. As a consequence, many steps of numerical integration of the oscillatory integrand are needed to determine the sum accurately enough so that significant figures are not lost by roundoff errors, particularly for very small outage values. Since the Laplace inversion integral method circumvents this issue, we can anticipate that the rate of convergence of series shown in Eq. (2.20) to be much faster than that of Eq. (2.26).

2.2.1.3 Exact Closed-Form Formulas

In this subsection, we present exact closed-form expressions for two special cases of desired signal envelope fading. As pointed out in [8], the inversion of the MGF of I to obtain the PDF $f_I(\xi)$ can be circumvented if the desired signal power is a sum of exponential RVs.

Case A: Rayleigh fading

If the desired signal amplitude is Rayleigh faded, then it follows from Eq. (2.3) that

$$\begin{aligned} P_{out} &= \int_0^\infty [1 - \exp(-qy/\bar{p}_0)] f_I(y)\, dy \\ &= 1 - \phi_I(q/\bar{p}_0) \end{aligned} \tag{2.27}$$

where $\phi_I(s) = \prod_{k=1}^{L} \phi_k(s)$.

Case B: Nakagami fading with integer m

Similarly if the desired signal amplitude follows a Nakagami distribution with integer m, then the outage probability may be obtained directly from the Laplace transform derivative property,

$$\begin{aligned} P_{out} &= \int_0^{\infty} \left[1 - \exp\left(\frac{-m_0 q y}{\bar{p}_0} \right) \sum_{i=0}^{m_0 - 1} \frac{1}{i!} \left(\frac{m_0 q y}{\bar{p}_0} \right)^i \right] f_I(y)\, dy \\ &= 1 - \sum_{i=0}^{m_0 - 1} \frac{(-1)^i}{i!} s^i \frac{d^i}{ds^i} [\phi_I(s)] \Big|_{s = m_0 q / \bar{p}_0} \end{aligned} \tag{2.28}$$

It is worth pointing out that in arriving to Eqs. (2.27) and (2.28) we do not impose any restrictions on the interferers signal statistics. Hence these formulas are useful to gain some insights as to how the interferer statistics affect the outage performance.

2.2.2 Interference and Noise Limited Environment

Thus far, we have assumed that satisfactory reception is achieved as long as the short-term SIR exceeds the power protection ratio, thereby neglecting the receiver background noise. But in practice, thermal noise and/or receiver threshold exist(s) which may be of concern particularly in large cells (macro-cell). In the literature, there are two approaches to deal with this scenario. In the first technique, noise is treated as co-channel interference (e.g., [3]). Alternatively, a minimum signal power requirement is imposed as an additional criterion for satisfactory reception (e.g., [4] and [8]).

2.2.2.1 Treating Noise as Interference

Using a more refined criterion, we can redefine the outage event as the likelihood that the desired signal strength drops below the total interference power I by a CCI power protection margin q, and the total noise power N by the noise power protection margin r, i.e.,

$$P_{out} = Pr\{p_0 < qI + \Lambda\} = Pr\left\{\frac{p_0}{q} - \sum_{k=1}^{L} p_k < \frac{\Lambda}{q}\right\} \tag{2.29}$$

where $\Lambda = rN$ is a constant. Notice that when $\Lambda = 0$, Eq. (2.29) reduces to Eq. (2.16). Following the development of Eq. (2.17), we can now express the new *exact* outage probability as

$$P_{out} = \frac{1}{\pi}\int_0^{\infty} \frac{\text{Real}\left[\,(c - j\omega)\;(\phi_\gamma(c + j\omega))\exp\{(c + j\omega)\Lambda/q\}\,\right]}{c^2 + \omega^2} d\omega \tag{2.30}$$

or in the form of a finite-range integral,

$$P_{out} = \frac{1}{2\pi}\int_0^{\pi} \text{Real}\left[\,(1 - j\tan(\theta/2))\;(\phi_\gamma(c + jc\tan(\theta/2)))\right.$$
$$\left.\times \exp\left(\,[1 + j\tan(\theta/2)]\,\Lambda c/q\right)\,\right] d\theta \tag{2.31}$$

where $\phi_\gamma(.)$ is defined by Eq. (2.15).

From Eqs. (2.23) and (2.29), we have yet another *exact* expression for the refined outage criterion,

$$P_{out} = \frac{1}{2} - \frac{1}{\pi}\int_0^{\infty} \frac{\text{Imag}\left[\phi_\gamma(-jt)\exp(-jt\Lambda/q)\right]}{t} dt. \tag{2.32}$$

Eq. (2.29) may also be rewritten as

$$\begin{aligned} P_{out} &= 1 - \int_0^{\infty} f_I(y) \int_{qy+\Lambda}^{\infty} f_{p_0}(p_0)\, dp_0 dy \\ &= \int_0^{\infty} f_I(y)\, F_0(qy + \Lambda)\, dy \end{aligned} \tag{2.33}$$

When $\Lambda = 0$, Eq. (2.33) reduces to the familiar expression for outage in an interference-limited scenario (i.e., Eq. (2.3)). If we assume the desired signal to be Nakagami-faded with integer m_0, then following the development of Eq. (2.28) we have a simple closed-form expression for the refined outage probability,

$$P_{out} = 1 - \exp\left(\frac{-m_0\Lambda}{\bar{p}_0}\right)\left\{\sum_{i=0}^{m_0-1}\frac{1}{i!}\sum_{l=0}^{i}{}^{i}C_l\left(\frac{m_0\Lambda}{\bar{p}_0}\right)^{i-l}(-s)^l\frac{d^l}{ds^l}[\phi_I(s)]\right\}\Bigg|_{s=\frac{m_0 q}{\bar{p}_0}} \tag{2.34}$$

where ${}^{x}C_{y} = \frac{x!}{y!\,(x-y)!}$ is the coefficient of binomial expansion. For the special case of Rayleigh-faded desired signal amplitude ($m_0 = 1$), Eq. (2.34) reduces to

$$P_{out} = 1 - \exp\left(-\Lambda/\bar{p}_0\right)\phi_I(q/\bar{p}_0)\,. \tag{2.35}$$

2.2.2.2 Minimum Signal Power Constraint

The presence of thermal noise and the receiver threshold imply that the desired signal power must simultaneously exceed the total interference power by a protection ratio and a minimum power level. In other words, the effect of noise was included implicitly by setting a minimum reception threshold for the desired signal. Therefore, the probability of satisfactory reception can be expressed as the intersection of two probability events,

$$\begin{aligned} Pr\{S\} &= Pr\left\{\left[q\sum_{k=1}^{L}p_k < p_0\right] \cap [p_0 > \Lambda]\right\} \\ &= \int_{\Lambda}^{\infty} Pr\left\{q\sum_{k=1}^{L}p_k < p_0 \,\middle|\, p_0\right\} f(p_0)\,dp_0 \end{aligned} \tag{2.36}$$

where $\Lambda = rN$ is the minimum power requirement due to receiver noise floor. Then the probability of outage is given by,

$$\begin{aligned} P_{out} &= 1 - \int_{\Lambda}^{\infty} f_{p_0}(p_0)\int_{0}^{p_0/q} f_I(y)\,dy\,dp_0 \\ &= 1 - \int_{0}^{\infty} f_{p_0}(p_0+\Lambda)\,F_I\left(\frac{p_0+\Lambda}{q}\right)dp_0 \end{aligned} \tag{2.37}$$

Note that specifying a minimum signal requirement will cause a floor on the outage prob-

ability with or without co-channel interference because the deep fades will result in signal power level below the specified minimum.

Different from Eq. (2.37) (which involves L-fold convolution integral), we will solve the outage problem in the framework of hypothesis-testing and determine the outage probability directly from the MGF of a decision variable as in Section 2.2.1. The conditional probability illustrated by Eq. (2.36) can be expressed using a Laplace integral:

$$\begin{aligned} Pr\left\{ q\sum_{k=1}^{L} p_k < p_0 \middle| p_0 \right\} &= 1 - Pr\left\{ -\sum_{k=1}^{L} p_k < \frac{-p_0}{q} \middle| p_0 \right\} \\ &= 1 - \frac{1}{2\pi j}\int_{c-j\infty}^{c+j\infty} \frac{1}{s} \exp\left(-sp_0/q\right) \phi_I(-s)\, ds \end{aligned} \tag{2.38}$$

Then, we have

$$Pr\{S\} = 1 - F_0(\Lambda) - \frac{1}{2\pi j}\int_{c-j\infty}^{c+j\infty} \frac{G_0(s)}{s} \phi_I(-s)\, ds \tag{2.39}$$

where $G_0(s) = \int_{\Lambda}^{\infty} \exp\left(-sp_0/q\right) f(p_0)\, dp_0$, which is convergent.

Finally the probability of outage with minimum power requirement is given by

$$\begin{aligned} P_{out} &= F_0(\Lambda) + \frac{1}{2\pi}\int_{-\infty}^{\infty} \frac{G_0(c+j\omega)}{c+j\omega} \phi_I(-c-j\omega)\, d\omega \\ &= F_0(\Lambda) + \frac{1}{2\pi}\int_{0}^{\pi} \Phi_\gamma(\theta)\, d\theta \\ &= F_0(\Lambda) + \frac{1}{2n}\sum_{i=1}^{n} \Phi_\gamma\left[\frac{(2i-1)\pi}{2n}\right] + R_n \end{aligned} \tag{2.40}$$

where

$$\Phi_\gamma(\theta) = \text{Real}\left[\left(1 - j\tan(\theta/2)\right) G_0\left(c + jc\tan(\theta/2)\right) \prod_{k=1}^{L} \phi_k\left(-c - jc\tan(\theta/2)\right) \right].$$

When $\Lambda = 0$, Eq. (2.40) reverts back to Eq. (2.20) as anticipated.

As well, for the special case of Rayleigh-faded desired signal amplitude, we have a closed-form expression for $G_0(.)$, i.e.,

$$G_0(s) = \frac{\exp\left[-\Lambda\left(s/q + 1/\bar{p}_0\right)\right]}{1 + s\bar{p}_0/q}. \tag{2.41}$$

Alternatively, the probability of satisfactory reception illustrated by Eq. (2.36) may be restated as

$$Pr\{S\} = \frac{1}{2} - \frac{F_0(\Lambda)}{2} - \frac{1}{\pi}\int_0^\infty \frac{1}{t}\mathrm{Imag}\left[\phi_I(-jqt)\int_\Lambda^\infty \exp(-jtp_0) f(p_0)\, dp_0\right] dt \tag{2.42}$$

by invoking Gil-Pelaez inversion theorem. Hence,

$$P_{out} = \frac{1}{2} + \frac{F_0(\Lambda)}{2} + \frac{1}{\pi}\int_0^\infty \frac{1}{t}\mathrm{Imag}\left[\phi_I(-jqt)\int_\Lambda^\infty \exp(-jtp_0) f(p_0)\, dp_0\right] dt. \tag{2.43}$$

2.2.3 Correlated Nakagami-faded Interferers

When the interferers are correlated, the analysis proceeds in a similar manner as the independent fading scenario. But we need to find the corresponding CHF or MGF of $\gamma_I = \sum_k p_k$. For the correlated Nakagami fading environment, the joint CHF of γ_I may be written in the form

$$\psi_I(t_1, t_2, \ldots, t_L) = E\left[\exp\left\{j\sum_{k=1}^{L} t_k p_k\right\}\right] = \left|I - 2j\sigma^2 T\Upsilon\right|^{-\lambda} \tag{2.44}$$

where I is the $L \times L$ identity matrix, T is a diagonal matrix whose elements are $(t_1, \ldots, t_L)$, Υ is a square symmetric matrix of dimension L and λ is a constant.

For special cases of constant and exponential correlation models (and with the assumption of identical fading severity index and signal strength for all the interferers), the corre-

sponding MGFs can be easily shown to be Eqs. (2.45) and (2.46), respectively:

$$\phi_I(s) = \left(\frac{m^L}{[\bar{p}s(1-\rho+L\rho)+m]\,[\bar{p}s(1-\rho)+m]^{L-1}} \right)^m \tag{2.45}$$

$$\phi_I(t) \approx \left(\frac{mL}{mL+s\bar{p}\tau} \right)^{mL^2/\tau} \tag{2.46}$$

where $\tau = L + \frac{2\rho}{1-\rho}\left(L - \frac{1-\rho^L}{1-\rho}\right)$, ρ is the correlation coefficient and L is the number of co-channel interferers. Using these MGFs, we can investigate the effect of correlated interferers on the outage performance.

2.3 Computational Results and Remarks

We now provide a limited set of numerical results to show the efficiency of the unified expressions derived in this chapter for computing the outage performance of mobile radio systems. Since the application of Eq. (2.18) for complicated mobile radio scenarios (e.g., unequal interferers and mixed fading distributions) is straightforward, our main focus here is to verify the accuracy of Eq. (2.20). In the following, the notation $\hat{P}_{out}$ is the sum in the right hand side of Eq. (2.20) excluding the remainder term, and the signal-to-interference ratio (SIR) is defined as the ratio between the desired user mean signal power to the sum of all interfering mean signal powers (i.e., $\bar{p}_0 / \sum_k \bar{p}_k$). Then the accuracy of the truncated series (GCQ estimate) is given by,

$$\% \text{ error} = \left| \frac{P_{out} - \hat{P}_{out}}{P_{out}} \right| \times 100 \tag{2.47}$$

where P_{out} (i.e., the exact outage probability) is computed using Matlab's *quad8* function with an absolute tolerance of 10^{-15}.

Table 2.1 Sensitivity of the selection of parameter c on the number of samples required to achieve the desired accuracy for $\hat{P}_{out}$ with $L = 4$, $b_0 = 0.5$, $[b_k] = [0.4, 0, 0.2, 0.7]$, $[\bar{p}_k] = [1.2, 0.6, 0.9, 0.5]$ and $SIR/q = 15dB$.

c	ε	$\hat{P}_{out}$	Number of samples required to achieve the desired accuracy (i.e., % error < ε)	P_{out}
$\frac{a_{min}}{4}$	1×10^{-2}	$3.55258076 \times 10^{-2}$	17	$3.55270279 \times 10^{-2}$
	1×10^{-3}	$3.55273550 \times 10^{-2}$	37	
	1×10^{-5}	$3.55270313 \times 10^{-2}$	74	
$\frac{a_{min}}{2}$	1×10^{-2}	$3.55297886 \times 10^{-2}$	12	$3.55270279 \times 10^{-2}$
	1×10^{-3}	$3.55273144 \times 10^{-2}$	18	
	1×10^{-5}	$3.55270313 \times 10^{-2}$	36	
$\frac{3a_{min}}{4}$	1×10^{-2}	$3.55299713 \times 10^{-2}$	5	$3.55270279 \times 10^{-2}$
	1×10^{-3}	$3.55273719 \times 10^{-2}$	11	
	1×10^{-5}	$3.55270306 \times 10^{-2}$	24	

Table 2.2 Sensitivity of the selection of parameter c on the number of samples required to achieve the desired accuracy for $\hat{P}_{out}$ with $L = 2$, $K_0 = 2.5$, $[K_k] = [1.3, 0.9]$, $[\bar{p}_k] = [1.1, 0.6]$ and $SIR/q = 20dB$.

c	ε	$\hat{P}_{out}$	Number of samples required to achieve the desired accuracy (i.e., % error < ε)	P_{out}
$\frac{a_{min}}{4}$	1×10^{-2}	$2.97613620 \times 10^{-3}$	7	$2.97592131 \times 10^{-3}$
	1×10^{-3}	$2.97594797 \times 10^{-3}$	9	
	1×10^{-5}	$2.97592143 \times 10^{-3}$	14	
$\frac{a_{min}}{2}$	1×10^{-2}	$2.97589037 \times 10^{-3}$	5	$2.97592131 \times 10^{-3}$
	1×10^{-3}	$2.97592085 \times 10^{-3}$	6	
	1×10^{-5}	$2.97592130 \times 10^{-3}$	7	
$\frac{3a_{min}}{4}$	1×10^{-2}	$2.97578343 \times 10^{-3}$	25	$2.97592131 \times 10^{-3}$
	1×10^{-3}	$2.97589584 \times 10^{-3}$	27	
	1×10^{-5}	$2.97592118 \times 10^{-3}$	33	

In Table 2.1 and Table 2.2, we examine the sensitivity of the number of samples required to achieve a specified tolerance (% error $< \varepsilon$) for different selection of parameter c on Nakagami-Hoyt and Rician fading channel, respectively. Here we show that the suboptimal choice of c does not preclude the usage of Eq. (2.20) because n does not grow too large so as to become unmanageable (even with a relatively large deviation from the optimum value). This is particularly interesting in that the rule of thumb eliminates the need for a precise numerical search yet works very well in most instances. Furthermore, since a percentage accuracy of $\varepsilon \approx 10^{-2}$ may be adequate in practice, only approximately ten samples of the MGF are required to evaluate the outage in these examples.

Subsequently, in Table 2.3 we assess the accuracy of Eq. (2.20) for a shadowed Rician (desired)/Rician (interferer) mixed fading channel model with six interferers at different values of shadowing spread for the desired user signal. Our numerical results reveal that the rate of convergence of the series in this mixed fading scenario is also quite good. Hence, an extremely high accuracy can be easily attained with only a reasonable number of MGF samples (i.e., less than 25 samples).

Table 2.3 Comparison between the exact outage probability obtained using Eq. (2.18) and the truncated series expression (Eq. (2.20)) for different σ_0 and various n values. We have assumed $[\bar{p}_k] = [0.2, 0.6, 1.3, 0.7, 0.4, 1]$, $SIR/q = 20dB$, $[K_k] = [0.2, 3.3, 5.8, 2.7, 0.9, 4.4]$, $K_0 = 7$ and $c = a_{min}/2$.

σ_0	P_{out}	n	$\hat{P}_{out}$
0.5 dB	$5.842568875 \times 10^{-4}$	15	$4.919110147 \times 10^{-4}$
		20	$5.842568852 \times 10^{-4}$
		25	$5.842568875 \times 10^{-4}$
2.0 dB	$4.596188514 \times 10^{-3}$	15	$4.111391849 \times 10^{-3}$
		20	$4.596188503 \times 10^{-3}$
		25	$4.596188514 \times 10^{-3}$
3.5 dB	$2.555192659 \times 10^{-2}$	15	$1.593690332 \times 10^{-2}$
		20	$2.555192636 \times 10^{-2}$
		25	$2.555192659 \times 10^{-2}$

The accuracy of our simple expression in a mixed Nakagami/Rician fading scenario is examined in Table 2.4. The received signal amplitude of the desired user and the first two interferers are Nakagami faded, while the signal amplitude of the other three interferers are Rician faded. In this case, we select c such that

$$c = \frac{a_{min}}{2} = \frac{1}{2} min \left\{ \frac{m_1}{\bar{p}_1}, \frac{m_2}{\bar{p}_2}, \frac{1+K_3}{\bar{p}_3}, \frac{1+K_4}{\bar{p}_4}, \frac{1+K_5}{\bar{p}_5} \right\}. \tag{2.48}$$

We observe that the error performance improves as the fading severity parameter of the desired user increases, as anticipated. It is shown that Eq. (2.20) is simple yet yields remarkably accurate results even with only 10 sampling points of the MGF over a wide range of fading severity index as well as in complicated fading channel conditions.

Table 2.4 Comparison between the exact outage probability obtained using Eq. (2.18) and the truncated series formula for different m_0 and various n values. We have assumed $L = 5$, $N = 2$, $m_1 = 0.5$, $m_2 = 0.7$, $K_3 = 3.1$, $K_4 = 1.8$, $K_5 = 0$, $[\bar{p}_k] = [0.4, 0.7, 1.2, 0.9, 0.8]$, $SIR/q = 25dB$ and $c = a_{min}/2$.

m_0	P_{out}	n	$\hat{P}_{out}$	% error
0.6	$2.5500310127 \times 10^{-2}$	5	$2.5311177703 \times 10^{-2}$	7.417×10^{-1}
		10	$2.5499774104 \times 10^{-2}$	2.102×10^{-3}
		20	$2.5500310247 \times 10^{-2}$	4.717×10^{-7}
2.5	$2.2184764209 \times 10^{-6}$	5	$2.2177210607 \times 10^{-6}$	3.405×10^{-2}
		10	$2.2184846402 \times 10^{-6}$	3.705×10^{-4}
		20	$2.2184764237 \times 10^{-6}$	1.228×10^{-7}
3.5	$2.3176637079 \times 10^{-8}$	5	$2.3176039710 \times 10^{-8}$	2.577×10^{-3}
		10	$2.3176668244 \times 10^{-8}$	1.345×10^{-4}
		20	$2.3176637087 \times 10^{-8}$	3.594×10^{-8}

In some of the previous studies (e.g., [5]), the authors have suggested approximating a Rice RV by a Nakagami-m RV with a positive integer m to examine the outage performance of cellular mobile radio networks subject to Rician fading with nonidentical CCI statistics. This was done to circumvent the difficulty in performing the L-fold convolution integral to get $f_I(\xi)$. Hence, in Fig. 2.1 through Fig. 2.3 we investigate whether this is a valid (realistic) approximation.

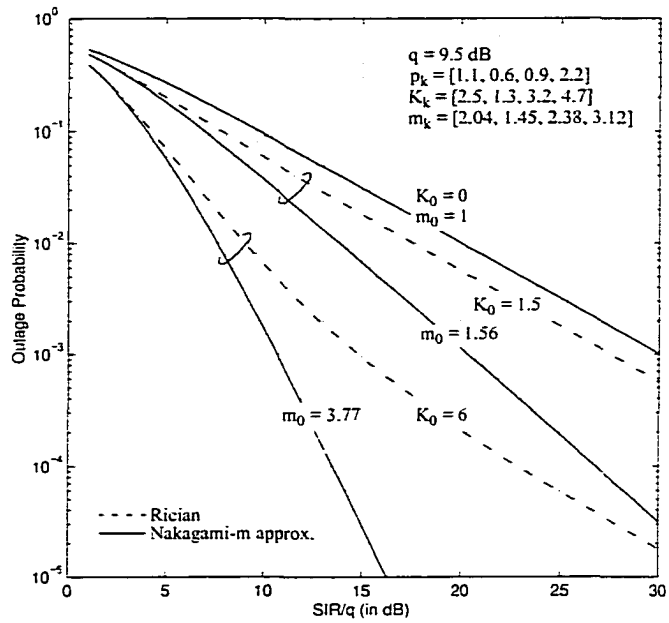

Fig. 2.1 Comparison of the outage probability between the Rician and its Nakagami-m approximation model.

In Fig. 2.1, we compare the outage performance of a cellular network where both the wanted signal and the four interfering signals are Rician-faded with its corresponding Nakagami-m approximation fading model. The fading severity index m (also known as fading figure) is obtained using the relationship $m = (K+1)^2/(2K+1)$. Notice that we did not round this value to the nearest positive integer, which would result in a further departure from the actual performance curve. The interference signal statistics (mean signal power and fading parameter) are given by $[\bar{p}_k] = [1.1, 0.6, 0.9, 2.2]$ and

$[K_k] = [2.5, 1.3, 3.2, 4.7]$. It is apparent from Fig. 2.1 that the Nakagami model for the desired signal yields misleadingly optimistic results. This observation may be attributed to the fact that the tails of the Rician and its Nakagami-m approximation distributions do not fit very closely. The difference in the behavior below the 1% point of the cumulative distribution function (CDF) of the power for these two distributions (see Fig. 2.2) may have led to a large difference in the required SIR/q to achieve a prescribed value of P_{out}. Comparison between these CDF curves also suggests that some basic results on Nakagami-m approximation model have been overlooked by some researchers previously.

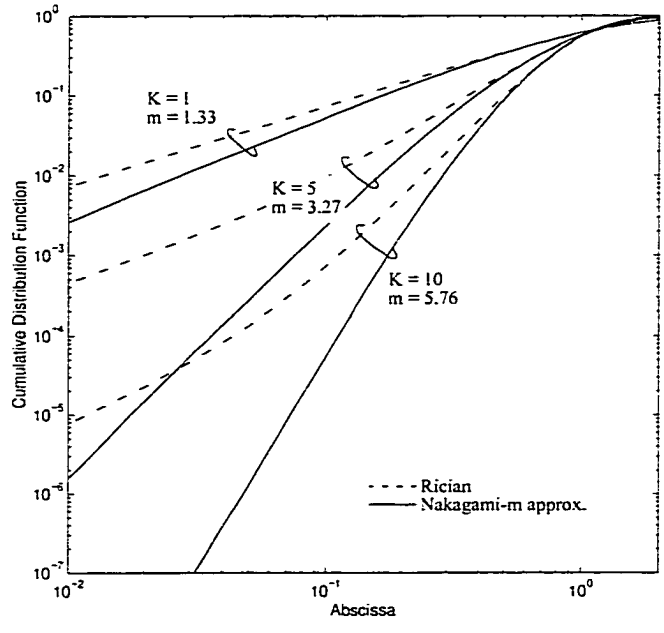

Fig. 2.2 Comparison between the CDFs of the normalized power for the Rician distribution and their corresponding Nakagami-m RVs.

It is noted that the real importance of the Nakagami-m fading model lies in the fact that it can often be used to fit experimental data and offers features of analytical convenience in comparison to the Rician distribution. However, the goodness-of-fit tests used by ionospheric physicists to match measured scintillation data to a Nakagami-m distribution do not give special weighting to the deep-fading tail of the distribution. As a result, we

sometimes have a better fit near the median of the distribution than in the tail region, although the tail behavior is of greater significance to communication systems performance analysis.

Diesta and Linnartz [6] also obtained a similar result by studying the behavior of the Laplace transform expressions for small arguments (i.e., corresponding to large SIR) by expanding into MacLaurin series. Further, they suggested that Nakagami PDF with $m > 1$ does not model deep fades, so it predicts much optimistic performance than Rician fading. Of course the Nakagami-m and Rician models are identical when $K_0 = 0$. From Fig. 2.1, we also find that the discrepancy between the actual and approximation model gets larger as K_0 decreases, for a given outage value. For instance, the difference in the required SIR/q to achieve $P_{out} = 10^{-3}$ is $7.2dB$ and $4.1dB$ when $K_0 = 1.5$ and $K_0 = 6$, respectively. But the Nakagami-m model predicts the exact performance that of Rician distribution when $K = 0$. We conclude that approximating a Rician RV of the desired signal by a Nakagami-m is only accurate for its extreme limiting cases -- Rayleigh fading ($K = 0$) and nonfading ($K = \infty$). The discrepancy becomes larger as SIR/q increases. The approximation is inaccurate even at moderate SIR/q values. This is particularly interesting because our unified expression handles the Rician-faded desired signal as well as the mixed-fading situation very well.

In Fig. 2.3, we confirm that one may accurately model the Rician-faded interfering signal by a Nakagami-m signal. Different from Fig. 2.1, we only model the unwanted Rician-faded signals using its equivalent Nakagami-m approximation and the desired signal is still modelled as Rician-faded (i.e., a mixed Rician/Nakagami fading case). Specifically, we show that the discrepancy observed in our Fig. 2.1 is attributed to the inaccurate modelling of the desired signal rather than the interfering signal statistics. The curves obtained by modelling the interferers as Nakagami-faded signals yields virtually identical results with that evaluated directly as Rician-faded interfering signals (we cannot distinguish their difference from Fig. 2.3 because the error due to the approximation is negligible). Fig. 2.3 also illustrates the effect of increasing the number of interferers on the outage performance. Note that the abscissa is the average single interferer power.

When $L = 1$ the interference statistics $\bar{p}_1 = 1.0$ and $K_1 = 2.2$, which also correspond to the first entry of vectors $\bar{p}_k$ and K_k, respectively. The penalty in the required SIR/q to achieve a prescribed outage gets larger with the CCI (i.e., higher number of interferers), as anticipated. As well, when the Rice factor of the wanted signal increases, a desired outage is achieved at smaller SIR/q because severity of the signal fading decreases.

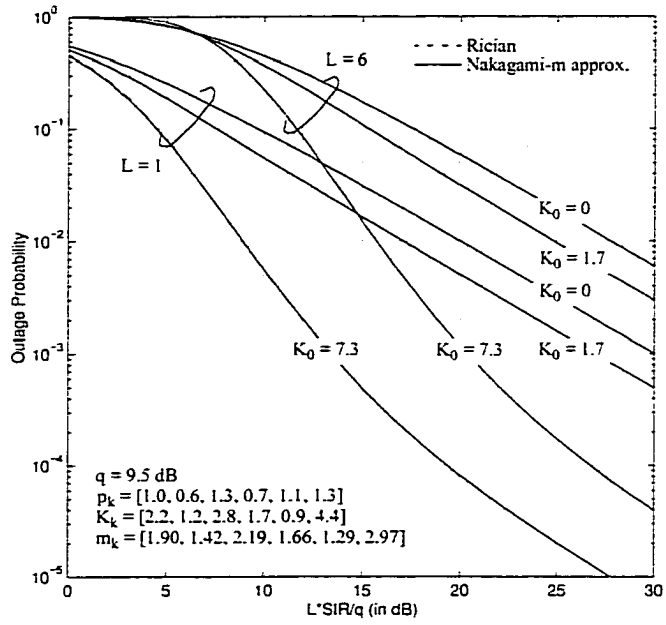

Fig. 2.3 Comparison of the outage between the Rician and its equivalent Nakagami-m approximation model of the interfering signals (the desired signal is modelled as Rician-faded for both cases) for different K_0 as well as number of interferers L.

In Fig. 2.4, we further substantiate the trends as well as the conclusions drawn from Fig. 2.3. In particular, we show that the outage performance is not too sensitive to the variations in the fading severity index of the interfering users. For simplicity, let us assume that all fading statistics of the interfering signals are identical. We see that the outage probability does not vary too much despite a considerable perturbation in the Rice

factor of the interfering signals if K_0 is small or if L is large. This observation in turn explains why there is negligible amount of error of the outage performance by modelling a Rician RV by a Nakagami-m RV for the interferer signals. However, note that the outage probability becomes more susceptible to the inaccuracies in modelling the interfering signals as K_0 increases when there are only a few number of interferers (i.e., single interferer case) since the spread between the curve gets larger.

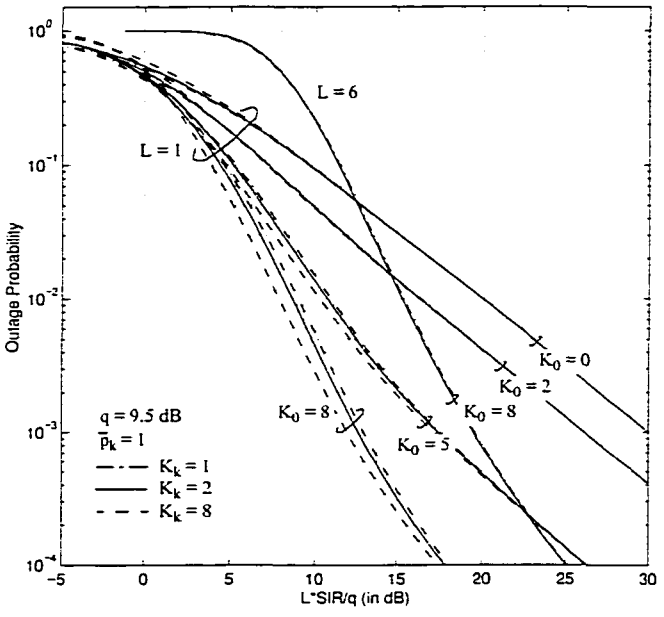

Fig. 2.4 Outage probability versus average signal power to a single interferer power ratio in a Rician (desired)/Rician (interferer) fading channel.

It can also be seen from Fig. 2.4 that as K_k ($k = 1, \ldots, L$) decreases, the outage probability gets larger for a given SIR/q in the moderate range (say 5 dB to 25 dB) if $K_0 > 0$. This can be explained by realizing that for a given SIR/q, K_0 and $\bar{p}_k$, $\bar{p}_0$ must be

increased if K_k decreases to keep $L \times SIR/q$ the same because

$$SIR = \frac{\bar{p}_0}{\sum_k \bar{p}_k} = \frac{(K_0 + 1)\bar{p}_{0\,(diffused)}}{\sum_k (K_k + 1)\bar{p}_{k\,(diffused)}} \tag{2.49}$$

where $\bar{p}_{i\,(diffused)}$ denotes the average power in the diffused path. If $K_0 \gg 0$, then the outage probability declines very rapidly even with a slight increase in $\bar{p}_0$ (i.e., 'waterfall curve') in the range of interest, which explains the above phenomena. At the other extreme (i.e., when the desired signal is Rayleigh-faded), the outage probability gets larger as K_k increases. If we change the abscissa to $\bar{p}_0$, then we will find that the outage will always be higher for a larger K_k, as anticipated.

In Fig. 2.5, we investigate the accuracy of modelling the shadowed Rician-faded desired signal PDF by its corresponding shadowed-Nakagami approximation. Here we assume that all the six interfering signals envelope follow the Nakagami distribution with the following statistics: m_k = [1.0, 0.5, 0.75, 0.6, 0.65, 0.9] (fading severity index) and $\bar{p}_k$ = [0.1, 0.6, 0.3, 0.7, 0.2, 0.5] (mean signal power). The Nakagami distribution with fading figure $m < 1$ models a fading channel condition that is more severe than the Rayleigh distribution (which cannot be represented using a Rician distribution). The Rice factor of the desired signal is assumed to be $K_0 = 6.1$. Hence, the fading severity parameter of the Nakagami approximation model is $m_0 = 3.819$. From Fig. 2.5, we see that the outage probabilities for the shadowed Nakagami-m channel and the shadowed Rician channel have good agreements for small SIR/q; otherwise the deviation can be substantial, in particular when the shadowing is not severe. The shadowing has the net effect of shifting the abscissa (i.e., SIR/q) when the departure begins to the right. Our results reveal that this approximation is plausible only in the limiting case (i.e., exact for the Suzuki fading environment) or if the desired signal experience heavy shadowing (i.e., large σ_0). Therefore the approximation performed in [11] is inadequate and cannot be justified for a general fading environment. However, the intuitive claim by the authors that the accuracy of approximating the shadowed Rician-faded desired signal by a shadowed-Nakagami improves when a strong specular path is available is correct.

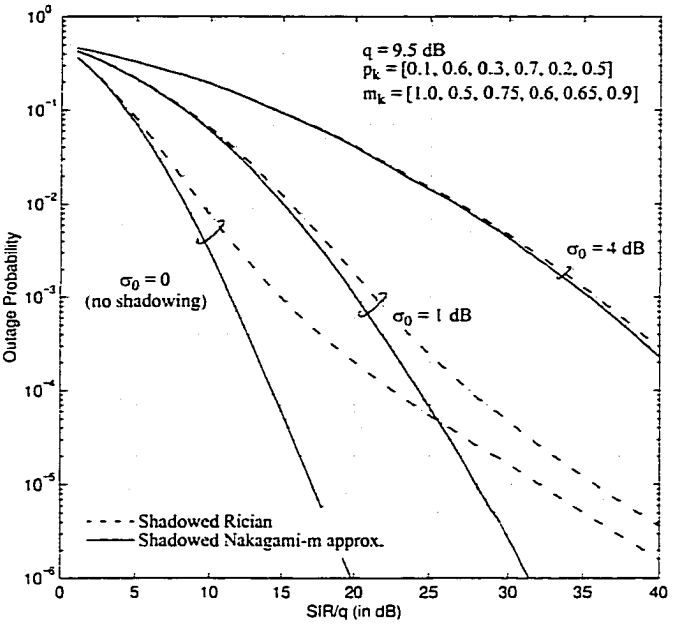

Fig. 2.5 Comparison of the outage between the shadowed Rician-faded desired signal case (K_0 = 6.1) and its equivalent shadowed Nakagami-m approximation model for different shadowing spreads σ_0 of the desired user signal.

Table 2.5 Comparison between the upper bound (Eq. (2.50)) for R_n and actual $R_n = P_{out} - \hat{P}_{out}$ (obtained using Eq. (2.18) and Eq. (2.20)) at different K_0.

Rice Factor K_0	Remainder term R_n			
	$n = 5$		$n = 10$	
	Upper bound	Exact	Upper bound	Exact
0	5.53×10^{-2}	3.877×10^{-7}	1.38×10^{-2}	3.278×10^{-13}
2.1	2.13×10^{-2}	1.487×10^{-7}	5.32×10^{-3}	1.254×10^{-13}
4.7	3.07×10^{-3}	2.119×10^{-8}	7.67×10^{-4}	1.763×10^{-14}
6.8	5.54×10^{-4}	3.758×10^{-9}	1.39×10^{-4}	3.075×10^{-15}

In Table 2.5, we provide an example to show the application of Eq. (2.21) to derive an upper bound on the remainder term. By taking the magnitude of R_n, we can rewrite Eq. (2.21) as,

$$R_n^{(max)} \leq \frac{\pi^2}{6n^2} \times max\left|\tilde{\phi}''(\zeta)\right| \quad \text{for } 0 < \zeta < \pi. \tag{2.50}$$

For the sake of illustration, consider the following interferers signal statistics: $K_k = [1.2, 0, 1.5]$ and $p_k = [0.7, 0.3, 0.5]$ for $k = 1, \ldots, L$, and $SIR/q = 20dB$. From Table 2.5, we observe that the remainder term diminishes very rapidly with the increasing number of MGF samples, as anticipated. R_n also decreases as K_0 increases, for a given moderate value of n. Comparison between the entries in the second and third column and/or fourth and fifth column of Table 2.5 reveal that the upper bound derived using Eq. (2.21) is quite loose. Consequently, if Eq. (2.50) is used to estimate the number of MGF samples required to achieve a specified accuracy, it will yield a rather pessimistic result. Nevertheless, this formula provides a useful information about the rate of convergence of the series given in Eq. (2.20), i.e., R_n diminishes by at least the reciprocal of n^2 with increasing n.

It is apparent from Table 2.6 that Laplace-inversion method is far more efficient than the Gil-Pelaez inversion formula (based on inverse Fourier method) especially at lower outage values. In other words, the rate of convergence of Eq. (2.20) is much faster than Eq. (2.26). An explanation for this observation is given in Section 2.2.1.2. Even if we reduce ε to 0.01%, the number of samples required is less than 10 for the Laplace inversion method. However, the corresponding n for Eq. (2.26) grows too large and becomes unmanageable for practical use. This observation in turn suggests that other numerical techniques (e.g., Gaussian quadrature) may be more appropriate to approximate Eq. (2.24) or (2.25) instead of using the Gauss-Chebychev formula. It is also important to highlight at this point that the number of samples required by the Laplace inversion method to achieve a prescribed accuracy is actually smaller than the value tabulated in Table 2.6 because we can further optimize the parameter c using the procedure outlined in Section 2.2.1.1.

Table 2.6 Comparison between the Laplace inversion method (Eq. (2.20)) and Gil-Pelaez Fourier inversion formula (Eq. (2.26)) for outage analysis in terms of the number of GCQ samples required to achieve an accuracy better than 1%. Interferers statistics: $SIR/q = 15dB$, $c = a_{min}/2$, $[\bar{p}_k] = [1.1, 0.9, 1.8, 1.2]$ and $[K_k] = [0.4, 1.3, 5.0, 2.7]$.

Rice factor K_0	Exact P_{out}	Number of GCQ samples required to achieve an accuracy of %error < 1%	
		Laplace Inversion Method	Gil-Pelaez Inversion Method
0	3.106373×10^{-2}	5	180
2.8	8.184924×10^{-3}	5	350
5.2	1.625258×10^{-3}	5	786
8.6	1.569834×10^{-4}	4	2527

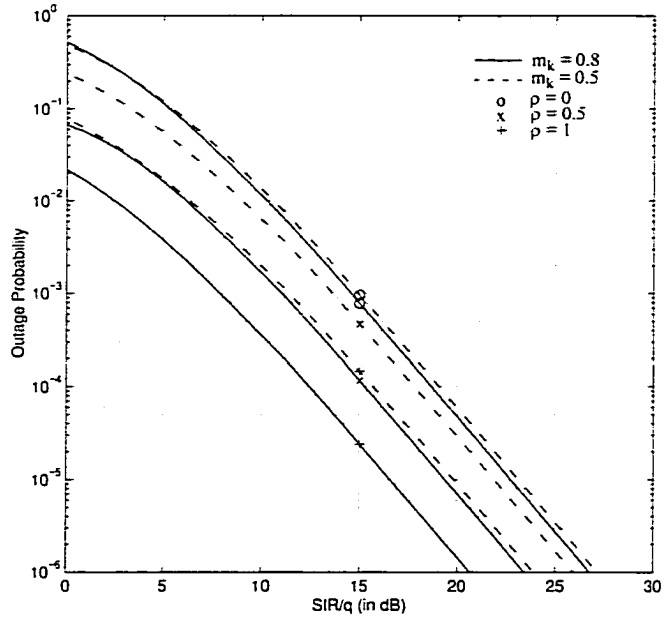

Fig. 2.6 Effect of correlated interferers (constant correlation model) on the outage performance with $m_0 = 2.5$.

In Fig. 2.6, we investigate the effect of correlated interferers on the outage performance. To generate this plot, we have assumed that there are four identical Nakagami-m co-channel interferers with fading severity index ($m = 0.5$ or $m = 0.8$) and signal strength $\bar{p} = 1.2$. The background noise is assumed to be negligible. From this figure, it is apparent that correlated interferers tends to be less harmful. One may also arrive to this conclusion by substituting Eq. (2.45) into Eq. (2.27) (i.e., the desired signal is assumed to be Rayleigh-faded) and then considering the two limiting cases of the correlation coefficient: $\rho = 0$ (uncorrelated case) and $\rho = 1$ (fully correlated case). Since $\frac{m}{L\bar{p}s + m} > \left(\frac{m}{m + \bar{p}s}\right)^L$ for practical values of m and $\bar{p}$, the outage probability will be smaller as ρ gets larger. Besides, the fading figure of the interferer signals plays an important role in the determination of the outage performance when the correlation is considered (because the spread between the curves for the two limiting cases of ρ becomes wider as m increases). Similar trends were also observed with the exponential correlation model (not shown in the figure).

From Fig. 2.7, we observe that the coarse approximation of the refined outage performance predicted by treating noise as CCI tends to yield slightly pessimistic result compared to the minimum power constraint approach. In fact, this upper bound gets tighter for both very small and very large SIR/q regions. However, the discrepancy between these two curves (at moderate SIR/q values) gets worse if the desired signal is not severely faded. When both the methods yield comparable performance and for small Λ, Eq. (2.30) or Eq. (2.32) will be preferred for rapid assessment of the system performance in a myriad of fading scenarios compared to Eq. (2.40) or Eq. (2.43)) since they require less programming effort. If the desired signal amplitude is Nakagami-faded (with integer m), then (2.34) is recommended. However, Eq. (2.40) should be used if accurate outage performance measure is desired (instead of an upper bound).

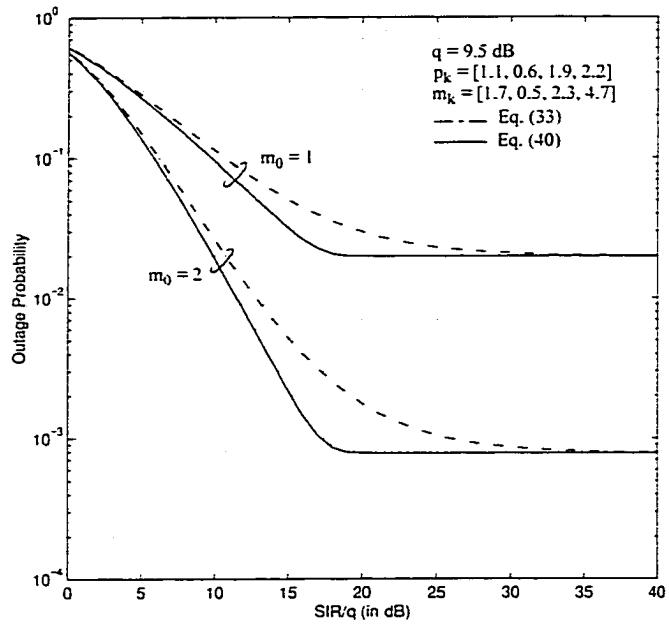

Fig. 2.7 Assessment of the compatibility and applicability of the two approaches that either treat noise as cochannel interference or consider a minimum detectable receiver signal threshold in the presence of receiver noise in a Nakagami-m fading channel.

2.4 Conclusions

In the research literature, much effort has been expended to find closed-form expressions for outage in mobile radio systems. This *ad hoc* development has led to various formulas. In contrast, we have developed several new unified outage expressions (in the form of a finite-range integral) for all common fading distributions. These exact outage expressions require the knowledge of only the MGF (for simple threshold model) or both MGF and PDF of the signal power (for the refined outage criterion). We also provide new closed-form expressions (based on GCQ approximation) that offers a convenient method to evaluate the outage. This general method allows for arbitrary fading parameters as well as dissimilar signal strengths, shadowing spreads and so on. It is a powerful tool for outage analysis -- not imposing any restrictions while being easy to program.

Moreover, we have shown that, in contrast to common belief, it is not very accurate to approximate the Rician or the shadowed Rician-faded wanted signal statistics by a Nakagami-m or the shadowed Nakagami-m distribution even at moderate SIR/q specifically if the desired signal is not shadowed heavily. Fortunately, the use of this approximation is unnecessary because our solution can handle Rice fading scenarios quite easily. The outage performance predicted by treating receiver noise as interference tends to be pessimistic compared to the case when a minimum signal power requirement is imposed. Their discrepancy gets larger if the desired signal experience less severe fading.

Appendix 2A

In this appendix, we will derive an alternative expression for the remainder term. In particular, we will show that the GCQ formula collapses to the mid-point trapezoidal rule for the class of integral considered in this chapter.

Consider the class of integral of the form,

$$A = \int_0^{\pi} f(x)\,dx. \tag{2A.1}$$

One may evaluate the above integral using a mid-point trapezoidal rule. The basic element of this rule is that as h tends to zero,

$$\int_a^{a+h} f(x)\,dx = hf(a+h/2) + \frac{h^3}{3}f''(a+h/2), \tag{2A.2}$$

which is obtained by expanding $f(x)$ at the vicinity of $x = a + h/2$ using Taylor series. The corresponding mid-point trapezoidal rule for an extended interval is

$$\int_0^b f(x)\,dx = h\sum_{k=0}^{n-1} f(kh + h/2) + R_n \tag{2A.3}$$

where $h = b/n$ and

$$R_n = \frac{b^3}{3n^2} f''(\zeta) \tag{2A.4}$$

for some $0 < \zeta < b$.

Alternatively, the integral illustrated in Eq. (2A.1) can be estimated directly by applying GCQ formula (after the variable substitution $x = \cos^{-1} t$), i.e.,

$$A = \frac{\pi}{n} \sum_{k=1}^{n} f\left[\frac{(2k-1)\pi}{2n}\right] + R_n \tag{2A.5}$$

where the remainder term is given by [[14], pp. 889],

$$R_n = \frac{\pi}{(2n)!\,2^{2n-1}} \frac{d^{2n}}{dt^{2n}} f\left[\cos^{-1} t\right]\Big|_{t=\psi} \quad \text{for } |\psi| < 1. \tag{2A.6}$$

If we substitute $\pi/n = h$ and replace $k-1$ by k in Eq. (2A.5), we have

$$A = h \sum_{k=0}^{n-1} f(kh + h/2) + R_n \tag{2A.7}$$

which is identical to Eq. (2A.3). Hence, it is evident that the GCQ formula collapses to mid-point trapezoidal rule for the class of integral in the form of Eq. (2A.1). Note also that we have two formulas for the remainder term but ψ and ζ are not the same. As we have noted earlier, it is easier to work with R_n in Eq. (2A.4) because it only requires the evaluation of the second order derivative of $f(x)$ and is *independent* of the sample size. Eq. (2.21) is obtained by applying Eq. (2A.4) to Eq. (2.18).

Chapter 3

Error Performance of Binary and M-ary Signalling Formats with Diversity Reception on Generalized Fading Channels

Diversity is a powerful communication receiver technique that provides wireless link improvements at a relatively low cost. The underlying premise is that if two or more statistically independent (or at least highly uncorrelated) replicas of a signal received over multiple diversity branches with comparable strengths, then it is improbable that all these signals will be in a fade at any given instant in time. Besides mitigating the deep fades experienced in wireless channels, diversity methods play a crucial role in minimizing the transmit power requirements, particularly in the reverse link, because the battery capacity of handheld subscriber units is usually limited. It also reduces the penalty in signal-to-noise ratio (SNR) due to co-channel interference.

To take advantage of the improvement in signal statistics due to diversity, several combining techniques have been proposed in the research literature, and they can be classified into two groups, namely switched combining and gain combining (see [2] and [21]). Four such techniques are considered here: maximal-ratio combining (MRC — the best known linear combining method), equal-gain combining (EGC), ideal selection diversity (SDC — perhaps the simplest combining method) and one type of switch-and-stay selection diversity (SWC).

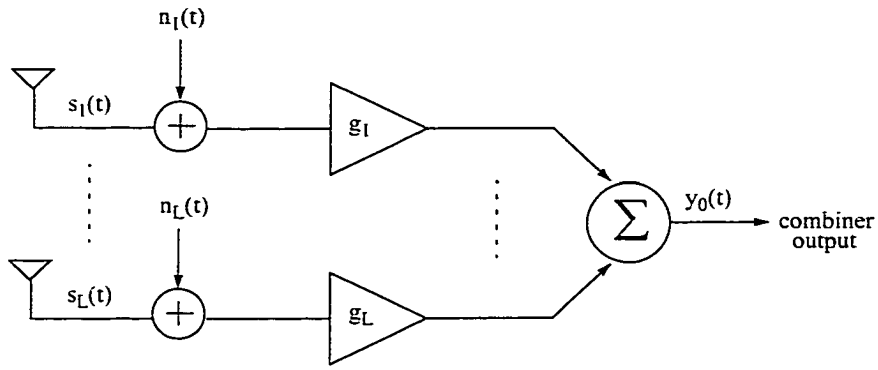

MRC: $g_k = \alpha_k \exp(-j\varepsilon_k) / \overline{n_k^2(t)}$

EGC: $g_k = \exp(-j\varepsilon_k)$

SDC: $g_k = \begin{cases} 1 \text{ if } k = l \\ 0 \text{ if } k \neq l \end{cases}$ where $\dfrac{\alpha_l^2}{\overline{n_l^2(t)}} = max\left\{\dfrac{\alpha_k^2}{\overline{n_k^2(t)}}\right\}$

SWC: $g_k = \begin{cases} 1 \text{ if } k = l \\ 0 \text{ if } k \neq l \end{cases}$ and $\dfrac{\alpha_l^2}{\overline{n_l^2(t)}} \geq \xi$

Fig. 3.1 Predetection diversity systems.

Let us consider an L-branch diversity combiner as shown in Fig. 3.1. Each of the L antennas is receiving locally coherent signal with statistically independent random amplitudes and random phases. Therefore, the received signal at the k-th antenna, $s_k(t)$, may be written as,

$$s_k(t) = \alpha_k e^{j\varepsilon_k} e^{j[2\pi f_c t + \theta(t)]} \tag{3.1}$$

where f_c is the carrier frequency, $\theta(t)$ is the information signal (desired phase modulation), ε_k is the random phase uniformly distributed between $[0, 2\pi)$, and α_k is the random fading amplitude process.

The additive zero-mean noise component is assumed to be independent of the signal and uncorrelated with the noise in any other branch. The composite signal plus noise in each branch is then multiplied by a voltage gain factor g_k and then summed in a linear combiner with replicas of the signal from all the other diversity branches. Thus, the

resultant predetection diversity signal output is

$$y_0(t) = \sum_{k=1}^{L} g_k [s_k(t) + n_k(t)] . \tag{3.2}$$

The values of the gain factors depend on the type of combining that is employed. For instance, the SDC measures the SNR at each branch (i.e. antenna) and selects the branch with the highest SNR value. Thus, if L branch diversity is employed and the mean noise power per branch is the same for all branches, the decision criteria reduces to $\max [\alpha_i]$, $i = 1, \ldots, L$, where α_i is the channel gain from the ith branch. However, the ideal SDC may not be practical for radio links that use continuous transmission (e.g., FDMA systems) because it requires continuous monitoring of all the diversity branches. This problem can be circumvented by adopting a suboptimal switched diversity scheme so that the rate of branch switching is reduced (which translates into a reduction of transient effects due to switching). In [34], Abu-Dayya and Beaulieu proposed a variation of the switch-and-stay diversity (SWC) strategy where the antenna switch is activated in the next switching instant as long as the measured local power in the current antenna is below the threshold level (i.e., envelope of the received signal need not necessarily cross the threshold in the negative direction). Therefore, the SWC scheme does not require comparison of present samples with past samples. In MRC, rather than selecting the single strongest signal, all the diversity branch are first co-phased, and then weighted in proportion to their SNR before summing. Different from MRC, the co-phased signals in an EGC combiner are simply added without having to weight the current SNR level of each signal. Therefore, MRC is known to be optimum in the sense that it yields the best statistical reduction of fading of any linear diversity combiner as well as provides the highest average output SNR.

While there are several excellent papers on the subject of fading channels and diversity reception, with many cases having been thoroughly analyzed, the approach adopted in this chapter results in "clean" derivations for the error probability expressions, and they are also numerically efficient. Two of the important techniques recurring throughout

this chapter are the use of moment generating functions (MGFs) or the characteristic functions (CHFs), and application of Gauss-Chebychev sampling to obtain rapidly converging series expressions for the average bit or symbol error rates (ASER).

The organization of this chapter is as follows. Section 3.1 briefly surveys some of the diversity techniques commonly used in cellular radio and satellite communication systems to mitigate the detrimental effects of signal fading. Subsequently in Section 3.2, the MGFs for several typical fading conditions are presented. Section 3.3 details the derivation of a generic conditional error probability (conditioned on the instantaneous SNR at the output of the predetection combiner) for a broad class of binary and M-ary (multilevel) modulation formats. The average error probability performance of various coherent, differentially coherent and noncoherent communication systems with predetection MRC, SDC and SWC are derived in Section 3.4 using the MGF method. In particular, we present new "closed-form" expressions (in the form of a truncated series expressions) for the ABER and/or ASER in a myriad of fading environments. The final expressions are sufficiently general to allow for arbitrary fading parameters as well as dissimilar mean signal strengths across the diversity branches. Moreover, this method is computationally stable and approximates the true value of average SER within any degree of accuracy. Yet another general approach for unified analysis of diversity systems on fading channels using the CHF method is discussed in Section 3.5. In particular, exact analytical expressions for the predetection EGC diversity receivers are derived. Finally, the main points are summarized in Section 3.6.

3.1 Diversity Techniques Commonly Used in Wireless Communications

3.1.1 Space Diversity

Historically, space diversity has been the most common form of diversity used in cellular radio networks, owing to its simple implementation and because it does not require additional frequency spectrum resources [23]. The uncorrelated diversity branches are attained from "sufficiently" spaced receiving antennas. The required antenna spacing

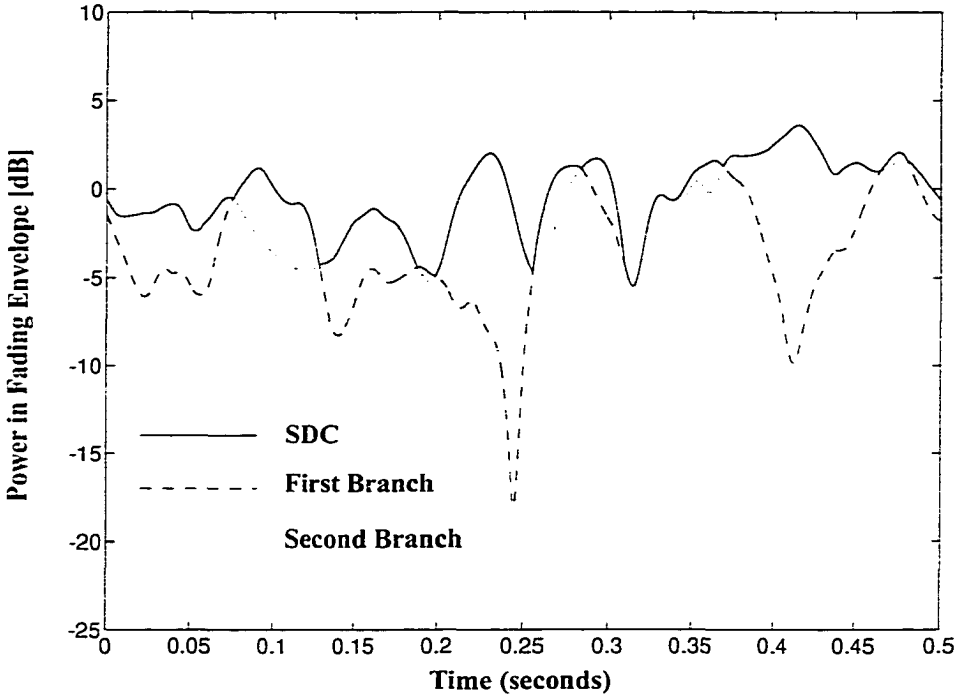

(a) Selection Diversity Combining

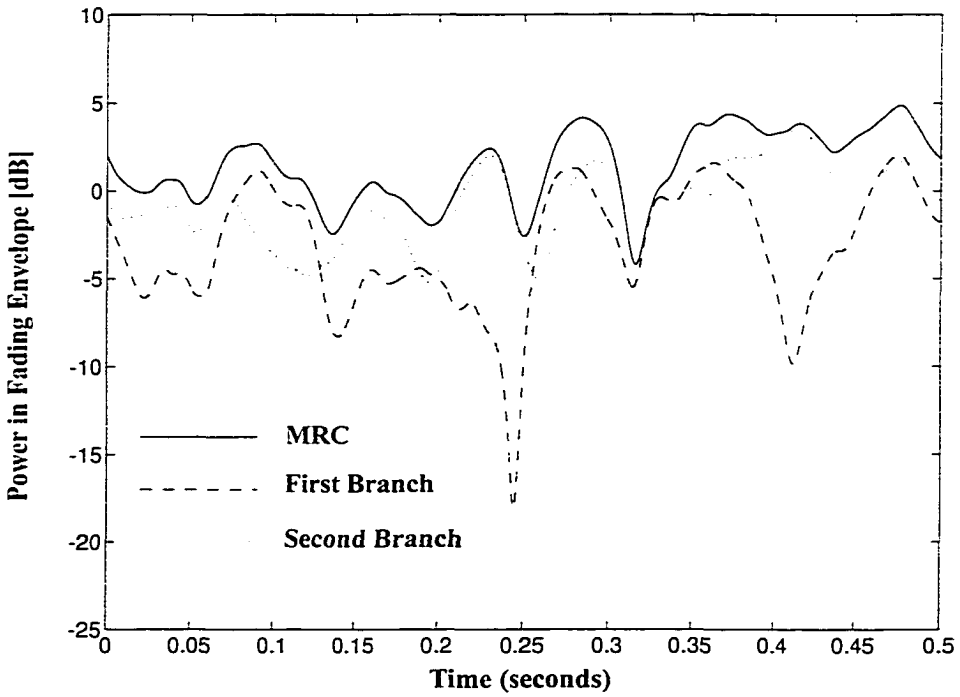

(b) Maximal Ratio Combining

Fig. 3.2 Effects of diversity on the received power in the Rician fading channel [24].

depends on the multipath angle spread. For the microscopic diversity, antenna separation of the order of 0.5λ–0.8λ is adequate because the multipath signals at the mobile usually arrive from all the directions in the azimuth. On the other hand, a larger coherence distance (typically 10λ–20λ) is required for the macroscopic diversity at the base station due to the small multipath angle spread. Empirical measurements also show that larger antenna heights require wider antenna separation [20].

Figure 3.2 illustrates the effects of two branch micro-diversity on the power S in the fading envelope for both SDC and MRC. This was obtained through simulation [24] with the following parameters: 900 MHz carrier frequency, a mobile speed of 15 kilometers per hour and a Rician factor $K = 2$. As micro-diversity has no effect on shadowing, shadowing was not simulated. This figure clearly illustrates the performance improvements obtained from diversity, especially with MRC. Note that for SDC, the combined signal strength will never exceed the strength of the best branch. However, for MRC, the combined signal strength will always exceed that of the best branch. Furthermore, since the channel gain of any branch may occasionally exceed unity in the multipath fading environment, with sufficient diversity branches (either MRC or SDC), the average signal strength in the multipath channel may actually exceed that of the non-fading channel.

3.1.2 Polarization Diversity

The implementation of space diversity at the base station is considerably less practical than at the mobile terminal because the narrow angle of incident fields requires large antenna separation. The comparatively high cost of using space diversity at the base station prompts the consideration of using orthogonal polarization to exploit polarization diversity. While the order of diversity is limited to two, it does allow antenna elements to be collocated. This is an important advantage in the personal communication service (PCS) base stations where low profile antennas (i.e., compact antenna assembly) are needed. More importantly, since the handset can be held at random orientations (due to hand-tilting) during a call, the use of cross-polarized antennas at the base station is highly desirable because at least one of the two antennas will be well matched to the signal launch polarization.

3.1.3 Frequency Diversity

Frequency diversity exploits the fact that if several replicas of a signal are transmitted on different carrier frequencies which are separated by at least the coherence bandwidth (which is related to the reciprocal of the multipath delay spread) of the channel, then it is unlikely that all the signals will experience simultaneous deep fades. However, this technique has the disadvantage that it not only requires additional spectrum (which is proportional to the diversity order), but also requires a higher transmitter power and as many receivers as the number of channels used for frequency diversity. A common form of frequency diversity is multicarrier (or multitone) modulation.

3.1.4 Time Diversity

In time diversity, redundant information is transmitted after a specified time spacing that exceeds the coherence time. The coherence time depends on the Doppler spread of the signal, which in turn is a function of the carrier frequency and mobile terminal velocity. The time diversity is usually exploited via interleaving, forward-error correction coding and automatic repeat-request. One fundamental drawback with this approach is that it introduces unacceptable delay in obtaining time diversity when the mobile terminal is moving very slowly. As well, the increased transmission power requirement makes it less efficient than the space diversity.

3.1.5 Angle (Directional) Diversity

Angle diversity is usually obtained by employing directional antennas in situations where the angle spread is very high because it attempts to reduce the Doppler spread. This form of diversity reception has been extensively utilized in indoor wireless local area networks.

3.1.6 Multipath Diversity

Path diversity is achieved by resolving and combining the multipath components of a transmitted signal if the signal bandwidth is much larger than the coherence bandwidth, such as in spread-spectrum systems. Resolvability is ensured if the multipath arrivals are

separated by at least one chip duration. Since the diversity branches are created after signal reception, multipath diversity is also referred as implicit diversity. The rake receiver and the adaptive equalizer are two typical examples that exploit path diversity. The most distinct feature of this technique is that no extra antenna, power, or spectrum are necessary to achieve the path diversity. However, the attainable diversity gain is dependent of the delay profile.

3.2 Fading Channel Models

To evaluate and simulate a channel based on the statistical models chosen, the probability density function (PDF), the cumulative distribution function (CDF) and the moment generating function (MGF) for each channel model are required. These functions are briefly described below.

Given a random variable $x(k)$ and any fixed value of x, the CDF of x is defined as

$$F(x) = \text{Prob}[x(k) \leq x] \tag{3.3}$$

Differentiating $F(x)$ with respect to x, the PDF $p(x)$ is obtained,

$$p(x) = \frac{d}{dx}F(x) . \tag{3.4}$$

The PDF indicates the relative frequency of occurrence of any fixed value of x. Finally, the MGF is defined as,

$$\phi(z) = \text{E}[e^{-zx}] = \int_{-\infty}^{\infty} e^{-zx}p(x)\,dx \tag{3.5}$$

where $\text{E}[x]$ is the expected value (also called mean or average value) of $x(k)$. (Note, the MGF is closely related to another statistical function, the characteristic function and is easily translated by the variable substitution $z = -jv$). By definition, Eq. (3.5) is the Laplace transform of the PDF $p(x)$. Thus, using the Laplace transform of a derivative property, the MGF may alternatively be written in terms of the CDF:

$$\phi(z) = \int_0^\infty e^{-zx} F'(x)\,dx = z\int_0^\infty e^{-zx} F(x)\,dx - F(0), x \geq 0 \tag{3.6}$$

where $F'(x)$ is the first derivative of $F(x)$. At this point, we would like to point out that the property illustrated in Eq. (3.5) can be directly used in the evaluation of MRC diversity systems while the latter (i.e., Eq. (3.6)) is useful in the analysis of selection diversity systems.

The random variable of interest here is the power in the fading envelope of the received signal. Since our new approach for computing the error performance requires only the knowledge of the MGF of SNR at the output of diversity combiner, in the following we will summarize the MGF of SNR (without diversity) for some of the commonly used fading channel models. Details may be found in [24].

3.2.1 Rician Channel

The MGF for the non-centralized chi-squared distribution (i.e., square of a Rician distributed fading amplitude) is well known, and is given by [12],

$$\phi_k(z) = \frac{1+K_k}{1+K_k+z\Omega_k}\exp\left(\frac{-zK_k\Omega_k}{1+K_k+z\Omega_k}\right) \tag{3.7}$$

where $\Omega_k = \mathrm{E}[\gamma_k]$, and K_k is the Rice factor of the kth diversity branch, defined as the ratio of the power in the line-of-sight (LOS) path to the power in the multipaths.

In a limiting case when the power in LOS path approaches zero, then $K \to 0$ and the channel reverts to the Rayleigh fading channel. Then the corresponding MGF of the exponential distribution is,

$$\phi_k(z) = \frac{1}{1+z\Omega_k}. \tag{3.8}$$

3.2.2 Nakagami Channel

The Nakagami distribution (m-distribution) is a versatile statistical distribution because it can accurately model a variety of fading environments. It has greater flexibility in matching some empirical data than the Rayleigh, lognormal or Rice distributions

owing to its characterization of the received signal as the sum of vectors with random moduli and random phases. As well, this statistical model includes the Rayleigh and the one-sided Gaussian distributions as special cases for the fading figure $m = 1$ and $m = 0.5$, respectively. Moreover, the m-distribution can closely approximate the Rician distribution via relationship $m = (K+1)^2/(2K+1)$ [25].

The MGF for this fading channel is given by

$$\phi_k(z) = \left(\frac{1}{1+z/\lambda_k}\right)^{m_k} \tag{3.9}$$

where $\lambda_k = m_k/\Omega_k$. It is evident that Eq. (3.9) reduces to Eq. (3.8) when $m = 1$ (i.e., Rayleigh fading).

3.2.3 Lognormal Rice Channel

The Rician distribution assumes a constant K. In reality, this may not be the case since as the mobile terminal moves through the cell, a variety of topographical surrounding are encountered. This is particularly evident in terrestrial environment where shadowing (physical obstruction of the signal path) is more severe. Hence, it is plausible to consider a combined distribution incorporating the effects of shadowing into the Rician distribution.

Expressing the received fading envelope as the product of independent Rice and lognormal distributions, the MGF can be shown to be,

$$\phi_k(z) = \frac{1}{\sqrt{\pi}}\int_{-\infty}^{\infty} \phi\left(z\mu_k \exp\left[\sqrt{2}\sigma_k x\right], K_k\right)\exp\left[-x^2\right]dx \tag{3.10}$$

where $x = \ln(\Omega_k/\mu_k) / \{\sqrt{2}\sigma_k\}$, σ is the logarithmic standard deviation of shadowing, and μ is the local mean power. Now applying Hermitian integration, a numerical approximation expression for Eq. (3.10) is obtained,

$$\phi_k(z) = \frac{1}{\sqrt{\pi}} \sum_{i=1}^{H} w_i \phi\left(z\mu_k \exp\left[\sqrt{2}\sigma_k x_i\right], K_k\right) + R_H \tag{3.11}$$

where x_i and w_i are tabulated in [14] for $H \leq 20$ and R_H is a remainder term.

3.2.4 Suzuki Channel

Suzuki fading characterizes the joint effects of Rayleigh fading and lognormal shadowing and models a shadowed multipath channel without a LOS path. Since Suzuki distribution is a special case of the lognormal Rician distribution, its MGF is readily obtained by setting $K = 0$ in Eq. (3.11), i.e.,

$$\phi_k(z) = \frac{1}{\sqrt{\pi}} \sum_{i=1}^{H} \frac{w_i}{1 + z\mu_k \exp\left[\sqrt{2}\sigma_k x_i\right]} + R_H. \tag{3.12}$$

3.2.5 Mixed Fading Channel

Owing to the time-varying nature of the wireless channels, a practical wireless channel may be more realistically modelled as a combination of different statistical distributions. The lognormal Rice or the lognormal Nakagami distribution may be further refined if additional information of the channel condition is available. For instance, Lutz et. al. [26] presented a two-state land mobile satellite channel model (see Fig. 3.3) based on channel measurements.

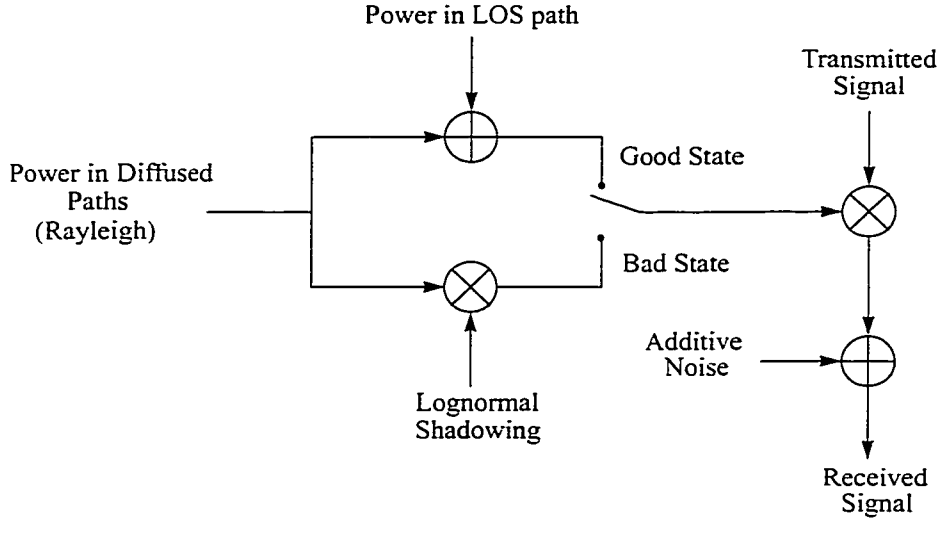

Fig. 3.3 Functional diagram of the satellite channel model.

In this model, the channel is in the good state for a fraction of the time $1-A$, and modelled as a Rician random process. For the remaining fraction of the time A, the channel is in the bad state modelled as a lognormally shadowed Rayleigh random process, or equivalently, a Suzuki random process. The net PDF of the received power is thus the weighted sum of the Rician and Suzuki PDFs, $p_{\text{Rice}}(\gamma)$ and $p_{\text{Suzuki}}(\gamma)$ respectively:

$$p(\gamma) = (1-A)\,p_{\text{Rice}}(\gamma) + A\,p_{\text{Suzuki}}(\gamma) \tag{3.13}$$

Similarly, using the definition of the MGF from Eq. (3.6), the net MGF is [10],

$$\phi(z) = \int_0^\infty e^{-zS} p(\gamma)\,d\gamma = (1-A)\,\phi_{\text{Rice}}(z) + A\,\phi_{\text{Suzuki}}(z) \tag{3.14}$$

where $\phi_{\text{Rice}}(z)$ and $\phi_{\text{Suzuki}}(z)$ are the MGFs for the Rician and Suzuki fading states given in (3.7) and (3.12), respectively.

3.3 Error Probability for Binary and M-ary Signalling Constellation in an AWGN Channel

Table 3.1 summarizes the instantaneous symbol error rate for a wide range of modulation schemes in an AWGN channel. One immediately recognizes that these expressions can be categorized into one of the four general forms: (a) function of only the $\text{erfc}(\sqrt{\gamma})$; (b) functions of both $\text{erfc}(\sqrt{\gamma})$ and $\text{erfc}^2(\sqrt{\gamma})$; (c) exponential form; and (d) finite-range integral with exponential integrand. Using the alternative exponential form for the complementary error functions, i.e., $\text{erfc}(\sqrt{\gamma}) = \frac{2}{\pi}\int_0^{\pi/2} \exp(-\gamma\csc^2\theta)\,d\theta$ and $\text{erfc}^2(\sqrt{\gamma}) = \frac{4}{\pi}\int_0^{\pi/4} \exp(-\gamma\csc^2\theta)\,d\theta$, we can show that the conditional error probability for a broad class of binary and two-dimension signalling constellations (for coherent, differentially coherent and noncoherent modulation formats) as a special case of the following generic form,

$$P_S(\varepsilon|\gamma) = \sum_u \int_0^{\eta_u} a_u(\theta) \exp(-\gamma b_u(\theta)) \, d\theta \tag{3.15}$$

where $a_u(\theta)$ and $b_u(\theta)$ are coefficients independent of the instantaneous SNR per symbol γ at the output of the predetection combiner, but may be dependent on θ.

Table 3.1 Instantaneous SER of several common modulation schemes.

Modulation Scheme	Conditional Error Probability $P_S(\varepsilon\|\gamma)$
Coherent binary signalling:	
(a) Coherent PSK	$0.5\text{erfc}(\sqrt{\gamma})$
(b) Coherent detection of differentially encoded PSK	$\text{erfc}(\sqrt{\gamma}) - \frac{1}{2}\text{erfc}^2(\sqrt{\gamma})$
(c) Coherent FSK	$0.5\text{erfc}(\sqrt{\gamma/2})$
Noncoherent binary signalling:	
(a) DPSK	$0.5\exp(-\gamma)$
(b) Noncoherent FSK	$0.5\exp(-\gamma/2)$
Quadrature signalling:	
(a) QPSK	$\text{erfc}(\sqrt{\gamma}) - 0.25\text{erfc}^2(\sqrt{\gamma})$
(b) MSK	$\text{erfc}(\sqrt{\gamma}) - 0.25\text{erfc}^2(\sqrt{\gamma})$
(c) $\pi/4$-DQPSK [37]	$\frac{1}{2\pi}\int_0^{\pi} \frac{\exp(-\gamma(2-\sqrt{2}\cos\theta))}{\sqrt{2}-\cos\theta} d\theta$
Multilevel signalling:	
(a) Square QAM	$2q\text{erfc}(\sqrt{p\gamma}) - q^2\text{erfc}^2(\sqrt{p\gamma})$ where $q = 1 - 1/\sqrt{M}$ and $p = 1.5\log_2 M/(M-1)$
(b) MPSK	$\frac{1}{\pi}\int_0^{\pi-\pi/M} \exp\left(\frac{-\gamma\sin^2(\pi/M)\log_2 M}{\sin^2\theta}\right) d\theta$
(c) MDPSK [38]	$\frac{\sin(\pi/M)}{\pi}\int_0^{\pi/2} \frac{\exp(-\gamma\log_2 M[1-\cos(\pi/M)\cos\theta])}{1-\cos(\pi/M)\cos\theta} d\theta$ or $\frac{1}{\pi}\int_0^{\pi-\pi/M} \exp\left(\frac{-\gamma\sin^2(\pi/M)\log_2 M}{1+\cos(\pi/M)\cos\theta}\right) d\theta$
(d) Two-dimension M-ary signal constellations [39]	$\frac{1}{2\pi}\sum_{k=1}^{S} Pr(S_k)\int_0^{\eta_k} \exp\left(\frac{-\gamma\alpha\sin^2(\Psi_k)}{\sin^2(\theta+\Psi_k)}\right) d\theta$ where S is the number of signal points, and $Pr(S_k)$ is the *a priori* probability that the kth signal point is transmitted.

Alternatively, we can express the conditional error probability in terms of the combiner output envelope $\vartheta = \sqrt{\gamma}$ as

$$P_S(\varepsilon|\ \vartheta) = \sum_u \int_0^{\eta_u} a_u(\theta) \exp\left[-\vartheta^2 b_u(\theta)\right] d\theta . \tag{3.16}$$

3.4 Unified Analysis of ASER using MGF Method

The ASER in the fading channels with an L-branch diversity may be derived by averaging the conditional error probability over the probability density function (PDF) of SNR at the output of the diversity combiner $p_\gamma(.)$ in a specified fading environment, i.e.,

$$P_S(\varepsilon) = \int_0^\infty P_S(\varepsilon|\ \gamma) p_\gamma(\gamma)\, d\gamma . \tag{3.17}$$

Substituting (3.15) into (3.17), interchanging the order of the integration, and then recognizing that the Laplace transform (LT) integral of the PDF of γ yields the MGF of the resultant SNR at the combiner output, we get

$$P_S(\varepsilon) = \sum_u \int_0^{\eta_u} a_u(\theta)\, \phi_\gamma(b_u(\theta))\, d\theta . \tag{3.18}$$

If the conditional error probability is in the exponential form, $P_S(\varepsilon|\gamma) = a\exp(-b\gamma)$, then (3.18) reduces to a closed-form expression. For instance, the average bit error rate performance for binary DPSK and noncoherent FSK with dual-branch SC is given by

$$P_S(\varepsilon) = a\phi_\gamma(b) \tag{3.19}$$

where $\{a = 1/2, b = 1\}$ for binary DPSK and $\{a = 1/2, b = 1/2\}$ for binary orthogonal FSK.

Now consider the instantaneous SER of the form $P_S(\varepsilon|\ \gamma) = a\ \mathrm{erfc}(\sqrt{b\gamma})$ (e.g., coherent binary PSK or FSK). In order to obtain an average error rate expression which is a function of the MGF of SNR at the combiner output, an alternate exponential form for

erfc (.) is required. Consider the definite integral and its solution given in [14, (7.4.11)],

$$\int_0^{\infty} \frac{\exp(\alpha^2 s^2)}{s^2 + z^2} dt = \frac{\pi}{2z} \exp(\alpha^2 z^2) \operatorname{erfc}(\alpha z), \quad \alpha > 0, z > 0 \tag{3.20}$$

Then the complimentary error function can be expressed in the desired form [10],

$$\operatorname{erfc}(\sqrt{b\gamma}) = \frac{2\sqrt{b}}{\pi} \int_0^{\infty} \frac{\exp\left[-\gamma\left[s^2 + b\right]\right]}{s^2 + b} ds, \quad b > 0, \gamma > 0 \tag{3.21}$$

Making the variable substitution $\tan\theta = s/\sqrt{b}$ and using the trigonometric property $1 + \tan^2\theta = \sec^2\theta$, we arrive to,

$$\operatorname{erfc}(\sqrt{b\gamma}) = \frac{2}{\pi} \int_0^{\pi/2} \exp(-b\gamma \sec^2\theta)\, d\theta \tag{3.22}$$

This form is both easily evaluated and well suited to numerical integration since the integrand is well behaved over the range of the integral. Substituting this alternative form (i.e., (3.22)) into (3.17), and then interchanging the order of integration and recognizing the integral with respect to γ is equal to the MGF of the fading channel evaluated at $b\sec^2\theta$, (3.17) reduces to,

$$\begin{aligned} P_S(\varepsilon) &= \frac{2a}{\pi} \int_0^{\infty} d\theta \int_0^{\pi/2} \exp(-b\gamma \sec^2\theta)\, p_{\gamma}(\gamma)\, d\gamma \\ &= \frac{2a}{\pi} \int_0^{\pi/2} \phi_{\gamma}(b\sec^2\theta)\, d\theta \end{aligned} \tag{3.23}$$

The ASER in (3.23) may also be re-written as

$$P_S(\varepsilon) = \frac{2a}{\pi} \int_0^{\pi/2} \phi_{\gamma}\left(b\csc^2\theta\right) d\theta \tag{3.24}$$

In general, a closed-form expression for (3.23) or (3.24) cannot be obtained. However, if the channel's MGF is of the form $\phi_{\gamma}(s) = (1 + sa)^{-L}$, one can directly solve (3.17) to obtain a closed form expression [10].

Using variable substitution $t = \cos(2\theta)$ in (3.24) and then applying Gauss-Chebychev quadrature (GCQ) formula [14, pp. 889], we obtain a rapidly converging series expres-

sion for the ASER:

$$\begin{aligned} P_S(\varepsilon) &= \frac{a}{\pi}\int_{-1}^{1} \phi_\gamma\left(b\csc^2\left(\frac{1}{2}\cos^{-1}t\right)\right)\frac{dt}{\sqrt{1-t^2}} \\ &= \frac{a}{n}\sum_{i=1}^{n} \phi_\gamma\left(b\csc^2\left(\frac{(2i-1)\pi}{4n}\right)\right) + R_n \end{aligned} \tag{3.25}$$

where n is a small positive integer, and the remainder term R_n can be bounded using procedure outlined in [30] or [31].

Similarly for $P_S(\varepsilon|\ \gamma) = a\mathrm{erfc}(\sqrt{b\gamma}) - c\mathrm{erfc}^2(\sqrt{b\gamma})$ (e.g., square QAM, quaternary PSK, coherent detection of differentially encoded PSK), the ASER is given by

$$\begin{aligned} P_S(\varepsilon) &= \frac{2a}{\pi}\int_0^{\pi/2} \phi_\gamma\left(b\csc^2\theta\right)d\theta - \frac{4c}{\pi}\int_0^{\pi/4} \phi_\gamma\left(b\csc^2\theta\right)d\theta \\ &= \frac{1}{n}\sum_{i=1}^{n} a\phi_\gamma\left(b\csc^2\left(\frac{(2i-1)\pi}{4n}\right)\right) + c\phi_\gamma\left(b\csc^2\left(\frac{(2i-1)\pi}{8n}\right)\right) + R_n \end{aligned} \tag{3.26}$$

because we can express $\mathrm{erfc}^2(.)$ as

$$\mathrm{erfc}^2(\sqrt{d\gamma}) = \frac{4}{\pi}\int_0^{\pi/4} \exp\left[-d\gamma\csc^2\theta\right]d\theta \tag{3.27}$$

by exploiting Simon's results in [28].

Next, we will highlight the use of GCQ formula for the ASER calculation in different propagation environments if $P_S(\varepsilon|\ \gamma) = \frac{a}{\pi}\int_0^{\eta} \exp\left[-b\gamma\csc^2\theta\right]d\theta$. For the sake of illustration, let us derive the rapidly converging series expressions for MPSK and MDPSK modulation formats with diversity reception over generalized fading channels. The evaluation of SER for M-phase signals with diversity combining and fading has been studied extensively in literature (see [32] and its references). Most authors place the emphasis on deriving explicit closed-form solutions for ASER and ABER. When it is difficult to obtain exact expressions, bounds are derived instead.

Proakis in [12] provides a comprehensive treatment of the problem for MRC under Rayleigh and Rician fading, and presents a general closed form expression for all signaling alphabet size M and the order of diversity L. However, the evaluation of the general expression requires $L-1$ th order derivatives for L channel reception. Alternative expressions have been derived in [32] for the Rayleigh fading channel. The derivation of these closed-form formulas tends to be a rather ad hoc affair, requiring some ingenuity in evaluating the necessary integrals. With the proliferation of standard mathematical software such as Maple and Matlab, it is extremely simple to evaluate (numerically) these integrals with high accuracy. Whereas explicit closed-form solutions tend to require much more programming effort. Our approach here is motivated by this consideration. Moreover, the integrals can be approximated by extremely accurate sums requiring knowledge of the MGF at only a small number of points.

Our derivation begins from the exact SER expression for MPSK in an AWGN channel provided in [33],

$$P_S(\varepsilon|\ \gamma) = \frac{1}{\pi}\int_0^{(M-1)\pi/M} \exp\left[-b\gamma \csc^2\theta\right] d\theta \tag{3.28}$$

where $b = (\log_2 M)\sin^2(\pi/M)$. Then the average symbol error probability in a slow and flat fading channel may be derived by averaging the error rate for the AWGN channel over the PDF of the SNR in a given fading channel, i.e.,

$$P_S(\varepsilon) = \frac{1}{\pi}\int_0^{(M-1)\pi/M} \phi_\gamma\left[b\csc^2\theta\right] d\theta\,. \tag{3.29}$$

Using variable substitution $t = \cos(M\theta/[M-1])$ in (3.29) and then applying GCQ approximation [14, pp. 889], we get a simple analytical expression for the ASER of MPSK in the form of a truncated series,

$$\begin{aligned} P_S(\varepsilon) &= \frac{M-1}{M\pi}\int_{-1}^{1} \phi_\gamma\left[b\csc^2\left[\frac{(M-1)}{M}\cos^{-1}t\right]\right]\frac{dt}{\sqrt{1-t^2}} \\ &= \frac{M-1}{nM}\sum_{i=1}^{n} \phi_\gamma\left[b\csc^2\left[\frac{(M-1)\,(2i-1)\,\pi}{2nM}\right]\right] + R_n \end{aligned} \tag{3.30}$$

where n is a small positive integer, and the remainder term is given by,

$$R_n = \frac{(M-1)^3\pi^2}{3M^3n^2}\left[\left(\frac{2b\cos\zeta}{\sin^3\zeta}\right)^2\phi_\gamma''\left(\frac{b}{\sin^2\zeta}\right)+\frac{2b\left(1+2\cos^2\zeta\right)}{\sin^4\zeta}\phi_\gamma'\left(\frac{b}{\sin^2\zeta}\right)\right] \tag{3.31}$$

for some $0<\zeta<(M-1)\pi/M$. Notations $\phi_\gamma'(s)$ and $\phi_\gamma''(s)$ in (3.31) are used to denote the first and second order derivatives of the MGF. When the derivatives are available, bounding on R_n is possible. The derivation of (3.31) relies on the fact that the GCQ rule collapses to the mid-point trapezoidal rule for the class of integral considered here.

The conditional SER of MDPSK is given by [33],

$$P_S(\varepsilon|\,\gamma) = \frac{\sin(\pi/M)}{\pi}\int_0^{\pi/2}\frac{\exp\left(-\gamma\log_2 M\left[1-\cos(\pi/M)\cos\theta\right]\right)}{1-\cos(\pi/M)\cos\theta}d\theta \tag{3.32}$$

Following our analysis for MPSK, the unconditional exact SER for MDPSK can be written in the form of a single integral with finite integration limits,

$$P_S(\varepsilon) = \frac{\sin(\pi/M)}{\pi}\int_0^{\pi/2}\frac{\phi_\gamma\left(\log_2 M\left[1-\cos(\pi/M)\cos\theta\right]\right)}{1-\cos(\pi/M)\cos\theta}d\theta\,. \tag{3.33}$$

Now applying the GCQ formulas on (3.33), we get a "closed-form" expression for SER of MDPSK in different fading environments,

$$P_S(\varepsilon) = \frac{\sin(\pi/M)}{2\pi n}\sum_{i=1}^{n}\frac{\phi_\gamma\left(\log_2 M\left[1-\cos(\pi/M)\cos\alpha\right]\right)}{1-\cos(\pi/M)\cos\alpha}+R_n \tag{3.34}$$

where $\alpha = (2i-1)\pi/4/n$ and the remainder term is given by,

$$R_n = \frac{\pi^2\sin(\pi/M)}{24n^2}\left[\phi_\gamma(p\delta)\left(\frac{2z^2\sin^2\zeta-\delta z\cos\zeta}{\delta^3}\right)+\phi_\gamma''(p\delta)\frac{(pz\sin\zeta)^2}{\delta}\right.$$
$$\left.+\,\phi_\gamma'(p\delta)\left(\frac{\delta pz\cos\zeta-2pz^2\sin^2\zeta}{\delta^2}\right)\right],\ \text{for}\ 0<\zeta<\pi/2 \tag{3.35}$$

where $p = \log_2 M$, $z = \cos(\pi/M)$ and $\delta = 1 - z\cos\zeta$.

Notice that the ASER formulas [see (3.18), (3.19), (3.23)-(3.26), (3.30) and (3.34)] are expressed in terms of only the MGF of the resultant SNR, $\phi_\gamma(.)$, which is dependent of the type of the diversity combining employed and the fading channel model. Therefore, in order to evaluate the error performance of any modulation formats listed in Table 3.1 in conjunction with a specific diversity combining scheme (MRC, SDC or SWC), we now need to determine only the $\phi_\gamma(.)$ for each type of the diversity combiners. Hence, in the following we will directly derive the MGF of the MRC, SDC and SWC combiner outputs over generalized fading channels.

3.4.1 Maximal-Ratio Diversity

It should be highlighted that the direct evaluation of (3.17) involves an L-fold convolution integral. Therefore, it is apparent that the MGF method is an attractive proposition for a rapid calculation of the ASER with MRC diversity receivers, especially when L is large. From the definition of the MGF, we can easily show that

$$\phi_\gamma^{(\mathrm{MRC})} = E\left[\exp\left(-s\sum_{k=1}^{L}\gamma_k\right)\right] = \prod_{k=1}^{L}\phi_k(s) \tag{3.36}$$

where $E[.]$ is the expected (average) value, L denotes the diversity order, and $\gamma_k = (E_S/N_0)\,\alpha_k^2$ where E_S/N_0 is the symbol energy-to-Gaussian noise spectral density ratio. In other words, the MGF of signal power at the MRC combiner output is simply the product of the MGF of the received signal power at each of the statistically independent diversity branches.

At this juncture, it is important to highlight that we do not impose any restrictions on the mean received signal strength and/or fading severity index for each of the L diversity branches. In fact, the fading statistics for different diversity branches may even be

modelled using different families of distributions. The MGFs of the signal power $\phi_k(.)$ for all common fading distributions are listed in Section 3.2. The approach presented here can be easily extended to analyze the performance of MRC in arbitrarily correlated Nakagami-m and Rayleigh fading channels. Details can be found in Chapter 4.

3.4.2 Selection Diversity

Once the MGF of the SNR at the output of selection combiner is determined, the ABER and/or ASER can be evaluated using the framework developed in Section 3.4. In fact, the final expression for the selection diversity will be identical to the MRC or SWC case, with the exception that the expression for the $\phi_\gamma(.)$ will now be different.

The CDF of SNR at the SDC combiner output is less than or equal to some value y is simply the product of the CDF of each of the individual diversity branches, i.e.,

$$F_\gamma^{(\mathrm{SDC})}(y) = \prod_{k=1}^{L} \mathrm{Prob}[\gamma_k \le y] = \prod_{k=1}^{L} F_{\gamma_k}(y) \tag{3.37}$$

Exploiting the relation between the MGF and CDF (through the use of the Laplace transform of a derivative property), the MGF of γ is given by

$$\phi_\gamma^{(\mathrm{SDC})}(s) = \int_0^\infty e^{-sy} \frac{d}{dy} F_\gamma^{(\mathrm{SDC})}(y)\, dy = s\int_0^\infty e^{-sy} F_\gamma^{(\mathrm{SDC})}(y)\, dy - F_\gamma^{(\mathrm{SDC})}(0) \tag{3.38}$$

For instance, the MGF of SNR with SDC in Rician and Nakagami-m fading are given by (3.39) and (3.40), respectively:

$$\phi_\gamma^{(\mathrm{SDC})}(s) = \sum_{i=1}^{N} \omega_i \prod_{k=1}^{L} \left\{ 1 - Q\left(\sqrt{2K_k}, \sqrt{\frac{2(1+K_k)\chi_i}{s\bar{\gamma}_k}} \right) \right\} + R_N \tag{3.39}$$

$$\phi_\gamma^{(\mathrm{SDC})}(s) = \sum_{i=1}^{N} \omega_i \prod_{k=1}^{L} \left\{ \frac{1}{\Gamma(m_k)} \Psi\left(m_k, \frac{m_k \chi_i}{s\bar{\gamma}_k} \right) \right\} + R_N \tag{3.40}$$

where $Q(\sqrt{2a}, \sqrt{2b}) = \int_b^\infty \exp(-t-a) I_0(2\sqrt{at})\, dt$ is the Marcum-Q function [21], χ_i and ω_i are the i-th abscissa and weight of the N-th order Laguerre polynomial [14], and $\Psi(a, x) = \int_0^x t^{a-1} \exp(-t)\, dt$ denotes the incomplete Gamma function [52].

3.4.3 Switched Diversity

The analysis of the switch-and-stay selection (SWC) diversity system is more involved compared to the ideal SDC scheme. In [65], the MGF for the SNR at the output of a dual-branch SWC combiner (statistically independent but with dissimilar fading statistics) is derived using a discrete-time model,

$$\begin{aligned}\phi_\gamma^{(\mathrm{SWC})}(s) &= A(\xi)\,[\lambda_1(\xi, s) + \phi_2(s) F_1(\xi)] \\ &\quad + [1-A(\xi)]\,[\phi_1(s) F_2(\xi) + \lambda_2(\xi, s)]\end{aligned} \tag{3.41}$$

where ξ is the fixed switching threshold and $A(\xi) = \dfrac{F_2(\xi)}{F_1(\xi) + F_2(\xi)}$. Notation $f_k(.)$, $F_k(.)$ and $\phi_k(.)$ correspond to the PDF, CDF and MGF of the received signal power in the k-th antenna. The marginal MGF $\lambda_k(\xi, s) = \int_\xi^\infty \exp(-su) f_k(u)\, du$ can be written in a closed-form for the Rician, Rayleigh and Nakagami-m channels:

$$\begin{aligned}\lambda_k(\xi, s) &= \frac{1+K_k}{s\Omega_k + K_k + 1} \exp\left(\frac{-sK_k\Omega_k}{s\Omega_k + K_k + 1}\right) \\ &\quad \times Q\left(\sqrt{\frac{2K_k(K_k+1)}{s\Omega_k + K_k + 1}}, \sqrt{\frac{2(s\Omega_k + K_k + 1)\xi}{\Omega_k}}\right) \quad \text{(Rician)}\end{aligned} \tag{3.42}$$

$$\lambda_k(\xi, s) = \frac{1}{s\Omega_k + 1} \exp\left[-\frac{\xi}{\Omega_k}(s\Omega_k + 1)\right] \quad \text{(Rayleigh)} \tag{3.43}$$

$$\lambda_k(\xi, s) = \frac{1}{\Gamma(m_k)} \left(\frac{m_k}{m_k + s\Omega_k}\right)^{m_k} \Gamma[m_k, \xi(s + m_k/\Omega_k)] \quad \text{(Nakagami-m)} \tag{3.44}$$

where $\Gamma(a,x) = \Gamma(a) - \Psi(a,x) = \int_x^{\infty} \exp(-t)\, t^{a-1} dt$.

When both the diversity branches are assumed to be independent and identically distributed, then (3.41) reduces to:

$$\phi_{\gamma}^{(SWC)}(s) = \phi_1(s) F_1(\xi) + \lambda_1(\xi, s) . \tag{3.45}$$

While the SWC strategy has the ability to reduce the transient effects compared to the ideal SDC scheme, its operation and the attainable diversity gain are largely dependent on the selection of the fixed threshold level. For instance, there will be constant switching between two antennas if a large value is assigned to the switching threshold because the probability of the received signal exceeding ξ will be small. In this case, the performance of SWC will be equivalent to the performance of a diversity branch selected in random, which resembles the behavior for no diversity case. On the other extreme (i.e., the value of ξ is set to be very small), the SWC combiner will be stuck in one of the diversity branches because the likelihood of received signal power staying above the specified threshold increases. Once again, the performance of the SWC will be close to the single diversity branch case. It is evident that the proper choice of ξ will minimize the average error probability.

In [66], an analytical expression to compute the optimal switching threshold ξ^* in a correlated fading channel with dissimilar signal strength across the two diversity branches is derived. For the special case of statistically independent and identically distributed diversity branches, the general expression collapses to

$$P_S(\varepsilon|\ \xi) = P_S^{(1)} = P_S^{(2)} \tag{3.46}$$

where $P_S^{(k)}$ corresponds to the ASER of the k-th diversity branch. Next we will identify three special cases of the conditional error probability $P_S(\varepsilon|\ \gamma)$ which lend themselves to closed-form formulas for the calculation of ξ^* in all common fading environments:

Case (a): If $P_S(\varepsilon|\ \gamma) = a\exp(-b\gamma)$, then $\xi^* = \dfrac{-\ln(\phi_1(b))}{b}$.

Case (b): If $P_S(\varepsilon|\ \gamma) = a\,\mathrm{erfc}(\sqrt{b\gamma})$, then $\xi^* = \dfrac{1}{b}\left(\mathrm{erfcinv}\left[P_S^{(1)}/a\right]\right)^2$.

Case (c): If $P_S(\varepsilon|\ \xi) = a\,\mathrm{erfc}(\sqrt{b\xi}) - c\,\mathrm{erfc}^2(\sqrt{b\xi})$, then by solving a quadratic equation formed using (3.46), we get $\xi^* = \dfrac{1}{b}\left\{\mathrm{erfcinv}\left[\dfrac{a-\sqrt{a^2-4cP_S^{(1)}}}{2c}\right]\right\}^2$.

A comprehensive study of dual-diversity SWC systems in generalized fading channels is treated in Chapter 5.

3.5 Unified Analysis of ASER using CHF Method

In Section 3.4, we tried to unify the performance analysis of the diversity receivers on fading channels by putting the conditional error probability in a desirable form (i.e., a finite range integral with exponential integrand) so that one can directly apply the Laplace transform to perform the averaging over the PDF of γ. Determining a desirable exponential form for an arbitrary $P_S(\varepsilon|\ \gamma)$ may not be a trivial task and in some cases it is impossible to partition the integral (3.17) into a product form. In fact, one cannot analyze the EGC receiver performance using the MGF approach. In light of the above considerations, we develope yet another general approach for calculating the error probability of all common diversity combining techniques over fading channels in a single common framework. Our novel derivation relies on the use of the Parseval's theorem to transform the product integral into the frequency domain, thereby circumventing the task to find and express the conditional error probability in a desirable form. But then we also need the Fourier transform (FT) of the conditional error probability, which surprisingly turns out to be very easily computed. As an application background, we will first derive exact analytical expressions for the EGC diversity receivers for both binary and M-ary modulation formats. Subsequently, we will show how this approach can be easily extended to other

diversity combining techniques.

3.5.1 Equal-Gain Diversity

In an equal gain combiner, the output of different diversity branches are first co-phased, equally weighted, and then summed to give the resultant output. The instantaneous SNR at the output of the EGC combiner is $\gamma = \vartheta^2$ where ϑ is defined as

$$\vartheta = \sqrt{\frac{E_b}{LN_0}} \sum_{l=1}^{L} \alpha_l \tag{3.47}$$

where α_l is the fading amplitude random variable (RV). Let $\bar{\gamma}_k = \Omega_k (E_S/N_0)$ denote the average SNR for the k-th branch, which is consistent with our definition for the MRC case.

The average bit or symbol error probability in fading channels can be obtained by averaging the conditional error probability over the PDF of the combined signal amplitude at the output of the EGC combiner, namely

$$P_S(\varepsilon) = \int_0^\infty P_S(\varepsilon|\vartheta) p_\vartheta(\vartheta)\, d\vartheta \tag{3.48}$$

where $p_\vartheta(.)$ denotes the PDF of RV ϑ.

In general, error performance analysis of EGC appears to be much more difficult than for MRC. The principal difficulty is finding a closed-form expression for the probability density function (PDF) of a sum of random fading amplitudes. Indeed, even for Rayleigh fading, the PDF is known only for the dual diversity case.

If the fading amplitudes are assumed to be independent, then the evaluation of ASER using the classical solution in the form of (3.48) will require L-fold convolution integrals. It is more insightful if we transform the PDF into frequency domain since the CHF of ϑ (i.e., sum of L fading amplitudes) is simply the product of the individual CHFs. However, it is difficult (or impossible) to invert the CHF $\psi_\vartheta^{(\mathrm{EGC})}(.)$ to get a

closed-form expression for the PDF of ϑ. Therefore, a Fourier series approach has previously been used [49, 50].

Using the inverse Fourier transform representation for the PDF, and then rearranging the order of integration, (3.48) can be restated as

$$\begin{aligned} P_S(\varepsilon) &= \int_0^{\infty} P_S(\varepsilon|\vartheta)\left[\frac{1}{2\pi}\int_{-\infty}^{\infty}\psi_{\vartheta}^{(\mathrm{EGC})}(\omega)\exp(-j\omega\vartheta)\,d\omega\right]d\vartheta \\ &= \frac{1}{2\pi}\int_{-\infty}^{\infty}\psi_{\vartheta}^{(\mathrm{EGC})}(\omega)\left[\int_0^{\infty}P_S(\varepsilon|\vartheta)\exp(-j\omega\vartheta)\,d\vartheta\right]d\omega \\ &= \frac{1}{2\pi}\int_{-\infty}^{\infty}\mathrm{FT}\left[P_S(\varepsilon|\vartheta)\right]\psi_{\vartheta}^{(\mathrm{EGC})*}(\omega)\,d\omega \end{aligned} \tag{3.49}$$

where notation $\psi_{\vartheta}^{(\mathrm{EGC})*}(.)$ denotes the complex conjugate of the CHF of ϑ. In fact, the final result of (3.49) follows directly from the application of Parseval's theorem [55, pp. 371] to transform the product integral in (3.48) into the frequency domain, thereby circumventing the need to find the PDF of ϑ. But we now need to compute the FT of $P_S(\varepsilon|\vartheta)$.

The FT of the generic conditional error probability (i.e., Eq. (3.16)) is given by

$$\begin{aligned} G_{\vartheta}(\omega) &= \frac{1}{2}\sum_u\int_0^{\eta_u}\frac{a_u(\theta)}{b_u(\theta)}\left\{\sqrt{\pi b_u(\theta)}\exp\left(\frac{-\omega^2}{4b_u(\theta)}\right)+j\omega\Phi\left(1,\frac{3}{2};\frac{-\omega^2}{4b_u(\theta)}\right)\right\}d\theta \\ &= \sum_u\int_0^{\eta_u}\frac{a_u(\theta)}{\sqrt{b_u(\theta)}}\left\{\frac{\sqrt{\pi}}{2}\exp\left(\frac{-\omega^2}{4b_u(\theta)}\right)+jF\left(\frac{\omega}{2\sqrt{b_u(\theta)}}\right)\right\}d\theta \end{aligned} \tag{3.50}$$

where $F(.)$ denotes the Dawson's integral,

$$F(x) = \exp\left[-x^2\right]\int_0^x\exp\left[t^2\right]dt = x\Phi\left(1,\frac{3}{2};-x^2\right) \tag{3.51}$$

and $\Phi(.,.;.)$ is the confluent hypergeometric series. The Dawson's integral can be computed more efficiently using a direct method (based on the sampling theorem) suggested by Rybicki [56] instead of evaluating sufficiently large number of terms in the series rep-

resentation of $\Phi\left(1, \frac{3}{2}; -x^2\right)$. For this reason, we have expressed $G_\vartheta(\omega)$ in terms of the Dawson's integral.

Substituting (3.50) into (3.49), and realizing that the imaginary part of this integral is zero (since the ASER is real), we get an exact analytical SER expression for binary and M-ary modulation formats with predetection EGC:

$$P_S(\varepsilon) = \frac{1}{\pi}\int_0^\infty \text{Real}\{G_\vartheta(\omega)\,\psi_\vartheta^{(\text{EGC})*}(\omega)\}\,d\omega = \frac{2}{\pi}\int_0^{\pi/2} \frac{\Lambda_\vartheta(\tan\theta)}{\sin(2\theta)}\,d\theta \tag{3.52}$$

where $\Lambda_\vartheta(\omega) = \text{Real}\{\omega G_\vartheta(\omega)\,\psi_\vartheta^{(\text{EGC})*}(\omega)\}$, and the CHF of ϑ in Nakagami, Rician and Rayleigh channels are given by (3.53), (3.54) and (3.55), respectively:

$$\psi_\vartheta^{(\text{EGC})}(\omega) = \prod_{k=1}^{L}\left\{\Phi\left(m_k, \frac{1}{2}; \frac{-\omega^2}{4L\lambda_k}\right) + j\omega\frac{\Gamma(m_k+1/2)}{\Gamma(m_k)\sqrt{L\lambda_k}}\Phi\left(m_k+\frac{1}{2}, \frac{3}{2}; \frac{-\omega^2}{4L\lambda_k}\right)\right\} \tag{3.53}$$

$$\psi_\vartheta^{(\text{EGC})}(\omega) = \prod_{k=1}^{L}\left\{\exp(-K_k)\sum_{i=0}^{\infty}\frac{K_k^i}{i!}\Phi\left(i+1, \frac{1}{2}; \frac{-\bar{\gamma}_k\omega^2}{4L(1+K_k)}\right)\right.$$

$$\left. + j\omega\sqrt{\frac{\bar{\gamma}_k}{L(1+K_k)}}\exp(-K_k)\sum_{i=0}^{\infty}\frac{\Gamma(i+3/2)\,K_k^i}{(i!)^2}\Phi\left(i+\frac{3}{2}, \frac{3}{2}; \frac{-\bar{\gamma}_k\omega^2}{4L(1+K_k)}\right)\right\} \tag{3.54}$$

$$\psi_\vartheta(\omega) = \prod_{k=1}^{L}\left\{\Phi\left(1, \frac{1}{2}; \frac{-\bar{\gamma}_k\omega^2}{4L}\right) + j\omega\sqrt{\frac{\pi\bar{\gamma}_k}{4L}}\exp\left(\frac{-\bar{\gamma}_k\omega^2}{4L}\right)\right\} \tag{3.55}$$

Notice that the evaluation of (3.52) for the most general case involves two-fold integrals. Next we will identify three special cases of the conditional error probability $P_S(\varepsilon|\,\vartheta)$ which allow the evaluation of the generic expression given in (3.52) to be further simplified into a single finite-range integral. This simplification is attributed to the availability of closed-form formulas for the FT of $P_S(\varepsilon|\,\vartheta)$:

Case (a): If $P_S(\varepsilon|\ \vartheta) = a\exp\left[-b\vartheta^2\right]$, then

$$G_\vartheta(\omega) = \frac{a}{\sqrt{b}}\left[\frac{\sqrt{\pi}}{2}\exp\left(\frac{-\omega^2}{4b}\right)+jF\left(\frac{\omega}{2\sqrt{b}}\right)\right] \tag{3.56}$$

Case (b): If $P_S(\varepsilon|\ \vartheta) = a\,\mathrm{erfc}\,(\sqrt{b}\,\vartheta)$, then

$$G_\vartheta(\omega) = \frac{a}{\omega}\left\{\frac{2}{\sqrt{\pi}}F\left(\frac{\omega}{2b}\right)+j\left[1-\exp\left(\frac{-\omega^2}{4b^2}\right)\right]\right\} \tag{3.57}$$

Case (c): If $P_S(\varepsilon|\ \vartheta) = a\,\mathrm{erfc}\,(\sqrt{b}\,\vartheta)-c\,\mathrm{erfc}^2(\sqrt{b}\vartheta)$, then

$$\begin{aligned} G_\vartheta(\omega) = {} & \frac{2a}{\omega\sqrt{\pi}}F\left(\frac{\omega}{2b}\right)-\frac{4c}{\omega\sqrt{\pi}}\left[F\left(\frac{\omega}{2b}\right)-F\left(\frac{\omega}{2b\sqrt{2}}\right)\exp\left(\frac{-\omega^2}{8b^2}\right)\right] \\ & +j\left\{\frac{a}{\omega}\left[1-\exp\left(\frac{-\omega^2}{4b^2}\right)\right]-\frac{c}{\omega}\left[1-\exp\left(\frac{-\omega^2}{4b^2}\right)-\frac{4}{\pi}F^2\left(\frac{\omega}{2b\sqrt{2}}\right)\right]\right\} \end{aligned} \tag{3.58}$$

Similar to the development in (3.25), we can replace the finite-range integral (3.52) with the series expression using GCQ approximation,

$$P_S(\varepsilon) = \frac{1}{n}\sum_{i=1}^{n}\frac{\Lambda_\vartheta\left[\tan\left(\frac{(2i-1)\,\pi}{4n}\right)\right]}{\sin\left[\frac{(2i-1)\,\pi}{2n}\right]}+R_n \tag{3.59}$$

3.5.2 Maximal-Ratio Diversity

Following the development in (3.49), it is straight-forward to show that (3.17) can be restated as

$$P_S(\varepsilon) = \frac{1}{2\pi}\int_{-\infty}^{\infty}\mathrm{FT}\left[P_S(\varepsilon|\gamma)\right]\psi_\gamma^{(\mathrm{MRC})*}(\omega)\,d\omega = \frac{2}{\pi}\int_0^{\pi/2}\frac{\Lambda_\gamma(\tan\theta)}{\sin(2\theta)}d\theta \tag{3.60}$$

where $\psi_\gamma^{(\mathrm{MRC})}(\omega) = \phi_\gamma^{(\mathrm{MRC})}(-j\omega)$ is the CHF of SNR at the MRC combiner output, $G_\gamma(\omega) = \mathrm{FT}\left[P_S(\varepsilon|\gamma)\right]$ and $\Lambda_\gamma(\omega) = \mathrm{Real}\left[\omega G_\gamma(\omega)\,\psi_\gamma^{(\mathrm{MRC})*}(\omega)\right]$.

It is clear that only the knowledge of $G_\gamma(.)$ is further required to investigate the error performance of different modulation formats. Since the FT of the generic error probability illustrated in (3.15) is given by

$$G_\gamma(\omega) = \sum_u \int_0^{\eta_u} \frac{a_u(\theta)}{b_u(\theta) - j\omega} d\theta \tag{3.61}$$

then (3.60) can be rewritten as

$$\begin{aligned} P_S(\varepsilon) &= \sum_u \int_0^{\eta_u} a_u(\theta) \left(\frac{1}{2\pi j} \int_{-\infty}^{\infty} \frac{1}{\omega - j b_u(\theta)} \phi_\gamma^{(\mathrm{MRC})}(-j\omega)\, d\omega \right) d\theta \\ &= \sum_u \int_0^{\eta_u} a_u(\theta) \left(\phi_\gamma^{(\mathrm{MRC})}(-j\omega) \Big|_{\omega = j b_u(\theta)} \right) d\theta \end{aligned} \tag{3.62}$$

The inner integral of (3.62) can be easily evaluated by directly applying the Cauchy integral formula. Then (3.62) reduces to

$$P_S(\varepsilon) = \sum_u \int_0^{\eta_u} a_u(\theta)\, \phi_\gamma^{(\mathrm{MRC})}(b_u(\theta))\, d\theta \tag{3.63}$$

which is identical to the result obtained in Section 3.4.1 using the MGF approach.
If the conditional error probability can be expressed in terms of the complementary error functions, then we may derive an alternative expression for computing the ASER by directly evaluating the FT of $P_S(\varepsilon|\gamma)$ and substituting the result in (3.60):

Case (a): If $P_S(\varepsilon|\gamma) = a\,\mathrm{erfc}(\sqrt{b\gamma})$, then

$$G_\gamma(\omega) = \frac{a}{j\omega}\left[\sqrt{\frac{b}{b - j\omega}} - 1\right] \tag{3.64}$$

Case (b): If $P_S(\varepsilon|\gamma) = a\,\mathrm{erfc}(\sqrt{b\gamma}) - c\,\mathrm{erfc}^2(\sqrt{b\gamma})$, then

$$G_\gamma(\omega) = \frac{a}{j\omega}\left[\sqrt{\frac{b}{b - j\omega}} - 1\right] + \frac{c}{j\omega}\left[1 - \frac{4}{\pi}\frac{\mathrm{atan}\left(\sqrt{1 - j\omega/b}\right)}{\sqrt{1 - j\omega/b}}\right] \tag{3.65}$$

However, the final expression for the ASER with MRC diversity obtained using the CHF approach can sometimes be slightly more complicated compared to the result attained via the MGF method. Nevertheless, the former is attractive because it allows us to unify the performance evaluation for all the common diversity combining techniques under a single common framework. It is also interesting to note the similarities between expressions (3.52) and (3.60).

3.5.3 Selection and Switched Diversity Systems

Similar to the analysis for the MRC case, the CHF of the SNR at the output of the SDC and the SWC combiners are related to their MGFs (derived in Sections 3.4.2 and 3.4.3) as $\psi_{\gamma}^{(SDC)}(\omega) = \phi_{\gamma}^{(SDC)}(-j\omega)$ and $\psi_{\gamma}^{(SWC)}(\omega) = \phi_{\gamma}^{(SWC)}(-j\omega)$, respectively. Once the CHF of SNR at the combiner output is determined, the ASER can be evaluated directly using the framework developed in Section 3.5.2. In fact, the final expression for the selection and/or switched diversity systems will be identical to the MRC case, with the exception that the expression for the $\psi_{\gamma}^{(MRC)}(.)$ is now replaced with $\psi_{\gamma}^{(SDC)}(.)$ or $\psi_{\gamma}^{(SWC)}(.)$, respectively.

3.6 Conclusions

Two unified approaches for evaluating the average error probability performance of diversity receivers in generalized fading channels are outlined. In the first approach, our derivation relies upon the properties of the MGF of the SNR at the combiner output, the use of an alternative exponential form for complementary error functions, and the application of a GCQ formula. In the second approach, we require the knowledge of Fourier transforms of the conditional error probability, the CHF of SNR, and the application of a GCQ formula. These unified approaches allow previously obtained results to be simpli-

fied both analytically and computationally and new results to be obtained for special cases that heretofore resisted solution in a simple form. Exact analytical expressions for the bit or symbol error probability (in the form of either a single or double finite-range integral(s)) and virtually "exact" closed-form solutions based on GCQ formula are derived for the MRC, EGC, SDC and SWC diversity systems with different modulation formats in a myriad of fading scenarios. This offers a convenient method to perform a comprehensive study of all common diversity combining techniques (MRC, EGC, SDC and SWC) with different modulation formats. The CHF method allows us to unify the above problem under a single common framework. Nevertheless, the MGF method sometimes yield a more concise solution than the CHF approach in the analysis of MRC, SDC and SWC diversity systems. The generality and computational efficiency of the new results presented in this chapter render themselves as powerful means for both theoretical analysis and practical applications.

Chapter 4

Exact Evaluation of Maximal-Ratio and Equal-Gain Diversity Receivers for M-ary QAM on Nakagami Fading Channels

In recent years, the M-ary QAM (MQAM) modulation scheme has received much attention for facilitating high-rate data transmission over wireless links due to its inherent spectral efficiency. For instance, using a 16-QAM modulation scheme coupled with pilot symbol assisted fading compensation technique and two antenna diversity reception, 64 kbps can be transmitted with almost same channel spacing as that of present analog systems [42]. While MQAM may be employed to increase the bandwidth efficiency, antenna diversity is usually needed to mitigate the effects of deep fades experienced on wireless links as well as to reduce the penalty in signal-to-noise ratio (SNR) due to co-channel interference. Besides, diversity methods can minimize the transmit power requirements, particularly in the reverse link, which is important because of the limited battery capacity of handheld subscriber units.

Among the various known linear diversity combining techniques, maximal-ratio diversity (MRC) is considered optimum because it yields the best statistical reduction of deep fades, as well as provides the highest average output SNR. Its main drawback, however, is that it requires sophisticated circuitry to accurately estimate the tap weights precisely. Equal gain diversity (EGC), on the other hand, can be implemented with much greater simplicity than the former, making it hardware feasible and cost viable. But this

is achieved at the expense of a slight degradation in performance.

While research into the performance of various modulation schemes in fading spans several decades, the symbol error rate (SER) performance of MQAM with MRC reception has been appearing only recently. The static SER of MQAM [[12], 5-2-79] involves terms of the form $Q(\sqrt{\gamma})$ and $Q^2(\sqrt{\gamma})$ where $Q(.)$ is the Gaussian probability integral. The averaging of the former over common fading distributions is well known, but the latter is less so. So the error performance of MQAM in some Rayleigh fading scenarios is given in [43]-[45]. In [46], we derive a simple expression (involving finite summations of the moment generating function (MGF)) for the SER of MQAM with MRC diversity over an arbitrary Nakagami fading channel by invoking a two-dimension GCQ formula. The use of an integral representation for $Q(\sqrt{\gamma})$ [[22], [10], [30], [28], [41], [40]] and $Q^2(\sqrt{\gamma})$ [28] have been suggested recently. More recently, Alouini and Goldsmith [41] exploited this idea to derive the SER of MQAM. Their related work also appeared in [40]. For the MRC case, the contribution of this paper differs from that of [40] and [41] in several ways: (a) virtually-exact closed-form expressions for MQAM with MRC diversity reception on arbitrary Nakagami fading are presented; (b) exact closed-form SER expressions for three special cases of Nakagami fading are derived; and (c) the SER performance of MQAM in correlated fading is derived.

In general, error performance analysis of EGC appears to be much more difficult than for MRC. The principal difficulty is finding a closed-form expression for the probability density function (PDF) of a sum of random fading amplitudes. Indeed, even for Rayleigh fading, the PDF is known only for the dual diversity case. There are no closed-form solutions for the PDF of a sum of Nakagami or Rician random variables (RVs). Altman and Sichak [47] have found an exact solution for the dual diversity system operating in a Rayleigh fading environment. For higher order of diversity, Jakes [2] has made use of a small argument approximation for the PDF suggested by Schwartz et. al. [21]. Recently Beaulieu [48] has devised an *approximate* infinite series technique to compute the PDF for the sum of independent Rayleigh RVs. Applying this technique, Abu-Dayya and

Beaulieu ([49] and [50]) analyze the performance of EGC for coherent and differential binary signalling schemes in Nakagami and Rician fading. In [40], the authors also derive an approximate solution for a binary case using Hermite integration. Here we develop an alternative direct technique to evaluate the exact performance of EGC diversity systems. Our approach relies on the use of the Parseval theorem to transform the error integral into the frequency domain. Since the Fourier transform of the PDF is the characteristic function (CHF), which is available in this case, our solution is general and *exact*. The resulting finite-range integral can be estimated very accurately with MGF samples using the GCQ formula. The generality and computational efficiency of our new expressions render themselves as a powerful tool for SER analysis under a myriad of fading scenarios.

This chapter has the following organization. The underlying steps in the derivation of average SER of MQAM using an L-fold MRC space diversity on a Nakagami fading channel is outlined in Section 4.1. Section 4.2 details the error performance of MQAM with predetection EGC. Subsequently in Section 4.3, selected numerical results are presented. Finally, the main points are summarized in Section 4.4.

4.1 Average SER of M-ary QAM with Maximal-Ratio Diversity Receiver

In the MQAM, a symbol is generated according to $\log_2 M$ bits of source data, and each symbol in a quadrant has different SER. Among the various known signal constellations, rectangular QAM signal is the most frequently used in practice because [12]: (a) its signal constellation is easily generated as two PAM signals impressed on phase-quadrature carriers; (b) the task of signal demodulated can be performed without much difficulty; and (c) the average transmitted power required to attain a given minimum distance with rectangular QAM is only slightly higher than that of the best MQAM signal constellation. When $\log_2 M$ is even (i.e., square QAM), the exact SER for MQAM in the AWGN channel is given by [12],

$$P_S^{(E)}(\varepsilon|\,\gamma_b) = 2q\mathrm{erfc}\left[\sqrt{p\gamma_b}\right] - q^2\mathrm{erfc}^2\left[\sqrt{p\gamma_b}\right] \tag{4.1}$$

where $q = 1-1/\sqrt{M}$, $p = 1.5\log_2 M/(M-1)$, and γ_b is the average received SNR per bit. On the other hand, when $\log_2 M$ is odd, there is no equivalent $\sqrt{M}$-ary PAM system. In this case, the symbol error probability is tightly upper bounded by,

$$P_S^{(O)}(\varepsilon|\,\gamma_b) \le 2\mathrm{erfc}\left[\sqrt{p\gamma_b}\right] - \mathrm{erfc}^2\left[\sqrt{p\gamma_b}\right] \tag{4.2}$$

if the detector bases its decisions on the optimum distance metric (maximum likelihood criterion).

It is noted that some previous related studies (e.g., [42]-[45] and [51]) have been restricted to AWGN and Rayleigh fading channels. While the Rayleigh fading model is plausible in macrocellular environments or in urban areas where a line-of-sight path seldom exists, the Rician fading model or the Nakagami channel with fading figure larger than unity is more appropriate for suburban areas, microcellular environments or satellite communication links. In fact, the Nakagami distribution (m-distribution [25]) is a versatile statistical distribution which can accurately model a variety of fading environments. It has greater flexibility in matching some empirical data than the Rayleigh, lognormal or Rice distributions owing to its characterization of the received signal as the sum of vectors with random moduli and random phases. It also includes the Rayleigh and the one-sided Gaussian distributions as special cases for fading figure $m = 1$ and $m = 0.5$, respectively. Moreover, the m-distribution can closely approximate the Rice distribution via relationship $m = (K+1)^2/(2K+1)$ [25], or by a linear map (coarse approximation) $m = 0.499853K + 0.762216$ for Rice factor $K \ge 2$.

4.1.1 Independent Fading

In this section we outlined several methods for computing the SER of MQAM with MRC diversity reception on a Nakagami fading environment. Each of these methods is unique, interesting and novel in its own right. Hence, we are presenting them in the hope

of stimulating further applications.

4.1.1.1 Computation of ASER using PDF of γ_b

As in [45], we assume matched filter detection and perfect channel estimation are available at the receiver. Then the average symbol error probabilities in a slow and flat Nakagami-fading channel may be derived by averaging the error rates for the AWGN channel over the PDF of the SNR in Nakagami fading,

$$P_S^{(E)}(\varepsilon) = \int_0^\infty P_S^{(E)}(\varepsilon|\,\gamma_b)\, p_{\gamma_b}(\gamma_b)\, d\gamma_b \equiv I_1 - I_2 \tag{4.3}$$

where

$$I_1 = \int_0^\infty 2q\,\mathrm{erfc}\left(\sqrt{p\gamma_b}\right) p_{\gamma_b}(\gamma_b)\, d\gamma_b \tag{4.4}$$

$$I_2 = \int_0^\infty q^2\,\mathrm{erfc}^2\left(\sqrt{\gamma_b p}\right) p_{\gamma_b}(\gamma_b)\, d\gamma_b \tag{4.5}$$

and $\gamma_b = \frac{E_b}{N_0}\sum_{l=1}^{L}\alpha_l^2 = \sum_{l=1}^{L}\gamma_l$ is the instantaneous SNR per bit with L-fold MRC diversity where α denotes the Nakagami distributed random variable. The PDF of γ_b is readily obtained by invoking basic Fourier inversion theorem,

$$p_{\gamma_b}(\gamma_b) = \frac{1}{2\pi}\int_{-\infty}^{\infty}\phi_{\gamma_b}(t)\exp(-jt\gamma_b)\, dt \tag{4.6}$$

where $\phi_{\gamma_b}(t)$ denotes the characteristic function (CHF) of γ_b [12],

$$\phi_{\gamma_b}(t) = \prod_{l=1}^{L}\int_0^\infty \exp(jt\gamma_l)\, p_\gamma(\gamma_l)\, d\gamma_l = \prod_{l=1}^{L}\left[\frac{\lambda_l}{\lambda_l - jt}\right]^{m_l} \tag{4.7}$$

with the assumption that the fading statistics across the L antennas are uncorrelated (achieved through sufficient antenna separation). The notation $p_\gamma(\gamma)$ in Eq. (4.7) corresponds to the PDF of the received SNR of a single diversity branch in Nakagami fading

environment, which has the chi-square PDF given in [[12], (14-3-14)]. Since $p_{\gamma_b}(\gamma_b)$ is real and the real part of the integrand is symmetric about $t = 0$, we get

$$p_{\gamma_b}(\gamma_b) = \frac{1}{\pi}\int_0^\infty \frac{\cos\left[\sum_{l=1}^{L} m_l \tan^{-1}(t/\lambda_l) - t\gamma_b\right]}{\prod_{l=1}^{L}\left[1 + (t/\lambda_l)^2\right]^{m_l/2}} dt \tag{4.8}$$

$$= \frac{1}{\pi}\int_0^\infty \frac{Re\{\exp[-jt\gamma_b + j\theta(t)]\}}{\zeta(t)}\, dt$$

where $\zeta(t) = \prod_{l=1}^{L}\left[1 + (t/\lambda_l)^2\right]^{m_l/2}$ and $\theta(t) = \sum_{l=1}^{L} m_l \tan^{-1}(t/\lambda_l)$. The parameter m_l in Eq. (4.8) denotes the fading figure of the lth diversity branch (i.e., antenna) and $\lambda_l = m_l/\bar{\gamma}_l$ where $\bar{\gamma}_l = \frac{E_b}{N_0}E\left[\alpha_l^2\right] = \frac{E_b}{N_0}\Omega_l$ corresponds to the average received SNR of the lth antenna.

Now consider the Fourier transform (FT),

$$G_1(\omega) = \int_0^\infty \exp(-j\omega t)\,\mathrm{erfc}(\sqrt{pt})\, dt = \frac{1}{j\omega}\left[1 - \frac{\sqrt{p}}{\sqrt{p + j\omega}}\right] \tag{4.9}$$

which is obtained using identity [[52], 6.283]. Substituting Eq. (4.8) into Eq. (4.4) and recognizing that the integration with respect to γ_b is the FT shown in Eq. (4.9), I_1 can be manipulated into the form,

$$I_1 = \frac{2q}{\pi}\int_0^\infty \frac{1}{\zeta(t)}\left\{\sin[\theta(t)]\left[1 - \frac{\sqrt{p}\cos\left[0.5\tan^{-1}(t/p)\right]}{\left[t^2 + p^2\right]^{0.25}}\right]\right.$$

$$\left. + \cos[\theta(t)]\frac{\sqrt{p}\sin\left[0.5\tan^{-1}(t/p)\right]}{\left[t^2 + p^2\right]^{0.25}}\right\}\frac{dt}{t} \tag{4.10}$$

by expressing $\sqrt{p + jt}$ in the polar form, $\sqrt{p + jt} = \left(p^2 + t^2\right)^{1/4}\exp\left[j0.5\tan^{-1}(t/p)\right]$.

In order to evaluate the integral illustrated by Eq. (4.5), let us first consider the following definite integral and its solution given in [[52], 8.258],

$$\int_0^{\infty} t\,\mathrm{erfc}^2(t)\exp\left(-\beta t^2\right)dt = \frac{1}{2\beta}\left[1-\frac{4}{\pi}\frac{\tan^{-1}\left(\sqrt{1+\beta}\right)}{\sqrt{1+\beta}}\right],\ Re\{\beta\} > -2. \tag{4.11}$$

After making the variable substitution $t = \sqrt{px}$ and replacing β with $j\omega/p$, we get a Fourier transform identity,

$$G_2(\omega) = \int_0^{\infty} \mathrm{erfc}^2\left(\sqrt{px}\right)\exp\left(-j\omega x\right)dx = \frac{1}{j\omega}\left[1-\frac{4}{\pi}\frac{\tan^{-1}\left(\sqrt{1+j\omega/p}\right)}{\sqrt{1+j\omega/p}}\right]. \tag{4.12}$$

By changing the order of integration in Eq. (4.5) and then applying the transformation formula Eq. (4.12), I_2 can be restated as,

$$I_2 = \frac{q^2}{\pi}\int_0^{\infty}\frac{1}{\zeta(t)}\left[\cos\left[\theta(t)\right]Re\left[G_2(t)\right]-\sin\left[\theta(t)\right]Im\left[G_2(t)\right]\right]dt \tag{4.13}$$

where

$$Re\left[G_2(t)\right] = \frac{2b\left[\tan^{-1}\left(\frac{a}{1-b}\right)-\tan^{-1}\left(\frac{-a}{1+b}\right)\right]-a\ln\left(\frac{a^2+(b+1)^2}{a^2+(b-1)^2}\right)}{\pi\sqrt{1+(t/p)^2}}, \tag{4.14}$$

$$Im\left[G_2(t)\right] = \frac{b\ln\left(\frac{a^2+(b+1)^2}{a^2+(b-1)^2}\right)-2a\left[\tan^{-1}\left(\frac{a}{1-b}\right)-\tan^{-1}\left(\frac{-a}{1+b}\right)\right]}{\pi\sqrt{1+(t/p)^2}}-1, \tag{4.15}$$

$$a = \left[1+(t/p)^2\right]^{0.25}\cos\left[0.5\tan^{-1}(t/p)\right], \tag{4.16}$$

and

$$b = \left[1+(t/p)^2\right]^{0.25}\sin\left[0.5\tan^{-1}(t/p)\right]. \tag{4.17}$$

Hence substituting Eqs. (4.10) and (4.13) into Eq. (4.3), we arrive to an exact analytical expression for SER of MQAM in Nakagami fading channel with arbitrary parameters.

This one-dimension integral can be computed numerically (e.g., trapezoidal integration rule). As before, the SER for rectangular QAM may be evaluated is upper bounded by,

$$P_S^{(O)}(\varepsilon) \leq P_S^{(E)}(\varepsilon)\Big|_{q=1} \tag{4.18}$$

In some previous work (e.g., [42], [43], [51]), the authors have used an approximate SER formula for MQAM in fading channel by ignoring the second integral in Eq. (4.3) since $\operatorname{erfc}^2\left[\sqrt{p\gamma_b}\right] \ll \operatorname{erfc}\left[\sqrt{p\gamma_b}\right]$ as $\gamma_b \to \infty$ (or for relatively large SNR per bit). However, the discrepancy between the exact SER and that of calculated via the coarse approximation described above can be quite large even for moderate values of $\bar{\gamma}_b$ [46].

4.1.1.2 Computation of ASER using PDF of γ_b and GCQ Formula

Our second approach for calculating accurate SER for MQAM in conjunction with MRC diversity is based on knowledge of two Fourier transform identities (Eq. (4.9) and Eq. (4.12)) and the application of GCQ formula [[14], (25.4.38)]. Combining Eqs. (4.10) and (4.13), we can write

$$P_S^{(E)}(\varepsilon) = I_1 - I_2 = \frac{q}{\pi}\int_0^{\infty} \frac{\psi(t)}{t\zeta(t)}dt \tag{4.19}$$

where

$$\psi(t) = Re\left\{e^{j\theta(t)-\pi/2}\left[2-q-\frac{2}{\sqrt{1+jt/p}}+\frac{4q}{\pi}\frac{\tan^{-1}\left(\sqrt{1+jt/p}\right)}{\sqrt{1+jt/p}}\right]\right\}.$$

Now making variable substitution $t^2+\frac{1}{2} = \frac{1}{1+x}$ in Eq. (4.19), we get

$$P_S^{(E)}(\varepsilon) = \frac{q}{\pi}\int_{-1}^{1} \frac{\xi(x)}{1-x^2}dx \tag{4.20}$$

where

$$\xi(x) = \psi\left(\sqrt{\frac{1-x}{2(1+x)}}\right)/\zeta\left(\sqrt{\frac{1-x}{2(1+x)}}\right).$$

Applying the GCQ formula of the first kind in Eq. (4.20), we have a closed-form expression for SER of MQAM with MRC diversity on Nakagami fading channel,

$$P_S^{(E)}(\varepsilon) = \frac{q}{n}\sum_{k=1}^{n} \xi\left[\frac{1}{\sqrt{2}}\tan\left(\frac{\pi(2k-1)}{4n}\right)\right] / \sin\left(\frac{\pi(2k-1)}{2n}\right) + R_n. \qquad (4.21)$$

Since the remainder term R_n vanishes quickly as n increases, Eq. (4.21) is a rapidly converging series.

4.1.1.3 Computation of ASER using MGF of γ_b and GCQ Formula

Different from the conventional method for computing SER (i.e., direct evaluation of Eq. (4.3)), our third approach relies upon the knowledge of the MGF of γ_b, the use of an alternative exponential forms for one-dimension and two-dimension complementary error functions as well as the application of GCQ rule [[30], [53], [31]]. The MGF technique has been applied successfully in [46] but I_2 was evaluated with the aid of a two-dimension GCQ formula, i.e.,

$$P_S^{(E)}(\varepsilon) = \frac{2q}{n}\sum_{i=1}^{n}\left\{\prod_{l=1}^{L}\left[1+\frac{\sec^2(\theta_i)}{\lambda_l/p}\right]^{-m_l} - \frac{q}{2n}\sum_{j=1}^{n}\prod_{l=1}^{L}\left[1+\frac{\sec^2(\theta_i)+\sec^2(\theta_j)}{\lambda_l/p}\right]^{-m_l}\right\} + R_n \qquad (4.22)$$

where n is a small positive integer, $\theta_j = (2j-1)\pi/4n$ and $\theta_i = (2i-1)\pi/4n$. In the following, we derive a much simpler closed-form SER formula for MQAM modulation scheme on Nakagami fading channels. The new expression reduces the number of MGF samples required to achieve a specified accuracy from n^2 (in case of Eq. (4.22)) to n. This is mainly attributed to the alternative exponential representation of the two-dimension complementary error function.

The MGF of γ_b is related to the CHF shown in Eq. (4.7) via relationship,

$$\phi(s) = \phi_{\gamma_b}(js) = \prod_{l=1}^{L}\left[\frac{\lambda_l}{s+\lambda_l}\right]^{m_l} \tag{4.23}$$

Next by exploiting the results from the definite integral [[52], (7.4.11)], the complementary error function can be represented via an alternative exponential form as,

$$\operatorname{erfc}(\sqrt{p\gamma}) = \frac{2\sqrt{p}}{\pi}\int_0^{\infty}\frac{1}{t^2+p}\exp\left[-\gamma\left[t^2+p\right]\right]dt, \quad p>0, \gamma>0. \tag{4.24}$$

From Appendix 4A, we have an alternative exponential form for the two-dimension complementary error function,

$$\operatorname{erfc}^2(\sqrt{\gamma p}) = \frac{4}{\pi}\int_0^{\pi/4}\exp\left[-\gamma\left[p\csc^2(\Theta)\right]\right]d\Theta. \tag{4.25}$$

It is noted that Eq. (4.25) may also be derived directly using the results from definite integrals [[52], (7.4.12)] and Eq. (4.24) with some algebraic manipulations. Substituting Eqs. (4.24) and (4.25) into Eq. (4.3), and recognizing

$$\int_0^{\infty}\exp(-\gamma_b s)\, p_{\gamma_b}(\gamma_b)\, d\gamma_b = \phi(s),$$

we get

$$P_S^{(E)}(\varepsilon) = \frac{4q\sqrt{p}}{\pi}\int_0^{\infty}\frac{\phi\left[t^2+p\right]}{t^2+p}dt - \frac{4q^2}{\pi}\int_0^{\pi/4}\phi\left[p\csc^2(\Theta)\right]d\Theta. \tag{4.26}$$

Eq. (4.26) can be manipulated into a desired form (so that one can apply GCQ formulas directly) using variable transformations $t^2+p = 2p/(x+1)$ and $y = \cos(4\Theta)$,

$$P_S^{(E)}(\varepsilon) = \frac{2q}{\pi}\int_{-1}^{1}\frac{\phi(2p/(x+1))}{\sqrt{1-x^2}}dx - \frac{q^2}{\pi}\int_{-1}^{1}\frac{\phi\left[p\csc^2\left[0.25\cos^{-1}(y)\right]\right]}{\sqrt{1-y^2}}dy. \tag{4.27}$$

Then using the GCQ approximation [22, (25.4.38)], leads Eq. (4.27) directly to a closed-form expression for the average SER of MQAM in a slow and flat Nakagami fading channel,

$$P_S^{(E)}(\varepsilon) = \frac{2q}{n}\sum_{i=1}^{n}\left\{\prod_{l=1}^{L}\left[1+\frac{p\sec^2(\theta_i)}{\lambda_l}\right]^{-m_l} - \frac{q}{2}\prod_{l=1}^{L}\left[1+\frac{p\csc^2(\theta_i/2)}{\lambda_l}\right]^{-m_l}\right\} + R_n \quad (4.28)$$

where $\theta_i = (2i-1)\pi/4n$. The remainder term R_n can be bounded using the results of Appendix A in [30] and/or [31]. However, this is not necessary in practice, since one simply computes Eq. (4.28) for several increasing values of n, and stops when the result converges to a prescribed accuracy. Since Eq. (4.28) can approximate the true SER within any degree of accuracy, it can be viewed as an *exact* closed-form solution. Note the implications of Eq. (4.28): we are simply sampling the MGF at n points. So as long as the MGF exists and computable, this method can work very effectively. In fact, its accuracy will be high if the high-order derivatives of the MGF vanishes rapidly. In Appendix 4A, we also present another method for computing I_2. The Gauss-Lobatto quadrature (GLQ) integration method also requires significantly fewer samples of MGF to evaluate the SER than the two-dimension GCQ technique (i.e., Eq. (4.22)) developed in [46].

Furthermore, using variable substitution $t = \sqrt{p}\tan(\Theta)$ in Eq. (4.26), we get a simple exact analytical expression for the SER of MQAM with MRC diversity receiver on generalized fading channels,

$$P_S^{(E)}(\varepsilon) = \frac{4q}{\pi}\int_0^{\pi/2}\phi\left[p\sec^2(\Theta)\right]d\Theta - \frac{q^2}{\pi}\int_0^{\pi/4}\phi\left[p\csc^2(\Theta)\right]d\Theta \quad (4.29)$$

which is identical to the results presented in [41]. This form is both easily evaluated and well suited to numerical integration since the integrand is well behaved over the finite-range of the integration limits.

4.1.1.4 Computation of ASER using Parseval's Theorem and GCQ Formula

Our fourth technique for evaluating the SER of MQAM with MRC diversity relies on knowledge of two Fourier Transforms (FTs), the application of the Parseval's theorem and GCQ formula. By applying Parseval's theorem in Eq. (4.3), we get

$$P_S^{(E)}(\varepsilon) = \frac{1}{2\pi}\int_{-\infty}^{\infty} \mathrm{FT}\left[P_S^{(E)}(\varepsilon|\gamma_b)\right]\phi_{\gamma_b}(\omega)\,d\omega$$
$$= \frac{1}{2\pi}\int_{-\infty}^{\infty}\left[2qG_1(\omega) - q^2 G_2(\omega)\right]\phi_{\gamma_b}(\omega)\,d\omega \tag{4.30}$$

where $\phi_{\gamma_b}(\omega)$, $G_1(\omega)$ and $G_2(\omega)$ are defined in Eqs. (4.7), (4.9) and (4.12), respectively. Notice that our method 4.1.1.1 and 4.1.1.4 are essentially the same. But the development of Eq. (4.30) is interesting because it lends itself into a unified-form of SER for MQAM with MRC diversity on arbitrary fading environments (not restricted to only Nakagami fading).

Now using variable substitution $\omega = \tan\theta$ in Eq. (4.30) and then applying GCQ formula, we get

$$P_S^{(E)}(\varepsilon) = \frac{1}{\pi}\int_0^{\pi/2} \vartheta(\tan\theta)\sec^2\theta\, d\theta$$
$$= \frac{q}{2n}\sum_{k=1}^{n} \vartheta\left[\tan\left(\frac{\pi(2k-1)}{4n}\right)\right]\sec^2\left[\frac{\pi(2k-1)}{4n}\right] + R_n \tag{4.31}$$

where $\vartheta(\omega) = Re\{[2G_1(\omega) - qG_2(\omega)]\phi_{\gamma_b}(\omega)\}$.

4.1.1.5 Exact Closed-Form Formulas for ASER of MQAM with MRC Diversity

Next, we will present exact closed-form SER formulas of MQAM with MRC diversity for three special cases of Nakagami fading: (a) identical $\lambda_l = m_l/\bar{\gamma}_l$ across the diversity branches and $\sum_l m_l$ is a positive integer; (b) fading severity index assumes an integer value and is common to all diversity branches, but λ_l for $l = 1, \ldots, L$ are dissimilar; and (c) distinct diversity branches and integer m_l's for $l = 1, \ldots, L$.

Case (a): Let us assume $\lambda_l = \lambda$ for $l = 1, \ldots, L$ and $\sum_l m_l = D$ is a positive integer. In this case, the random variable γ_b has a gamma PDF (obtained by inverting Eq. (4.23)),

$$p_{\gamma_b}(\gamma) = \frac{\lambda^D}{(D-1)!}\gamma^{D-1}\exp(-\lambda\gamma) . \tag{4.32}$$

Then, it can be readily shown that

$$\begin{aligned} I_1 &= 4q\int_0^\infty \frac{1}{2}\operatorname{erfc}(\sqrt{p\gamma})\, p_{\gamma_b}(\gamma)\, d\gamma \\ &= 4q\left[\frac{1}{2}\left(1-\sqrt{\frac{p}{\lambda+p}}\right)\right]^D \sum_{k=0}^{D-1}\binom{D-1+k}{k}\left[\frac{1}{2}\left(1+\sqrt{\frac{p}{\lambda+p}}\right)\right]^k \end{aligned} \tag{4.33}$$

using identity (14-4-15) in [12], and

$$\begin{aligned} I_2 &= \frac{q^2\lambda^D}{(D-1)!}\int_0^\infty \gamma^{D-1}\exp(-\lambda\gamma)\operatorname{erfc}^2(\sqrt{p\gamma})\, d\gamma \\ &= \frac{q^2\lambda^D(-1)^{D-1}}{(D-1)!}\left\{\frac{d^{(D-1)}}{ds}\left[\frac{1}{s}-\frac{4}{\pi}\frac{\tan^{-1}(\sqrt{1+s/p})}{s\sqrt{1+s/p}}\right]\Bigg|_{s=\lambda}\right\} \end{aligned} \tag{4.34}$$

by exploiting the Fourier transform identity in Eq. (4.12). For small values of D, the $(D-1)$ -th order differentiation in Eq. (4.34) can be computed by hand. For instance,

$$I_2 = q^2\left[1-4\Im+2\kappa\lambda-\frac{2\Im\lambda}{p+\lambda}\right] \text{ when } D = 2,$$

$$I_2 = q^2\left[1-4\Im+2\kappa\lambda-\frac{2\Im\lambda}{p+\lambda}+\frac{3\kappa\lambda^2}{2(p+\lambda)}+\frac{\kappa\lambda^2}{2p+\lambda}-\frac{3\Im\lambda^2}{2(p+\lambda)^2}\right] \text{ if } D = 3,$$

where $\Im = \dfrac{\operatorname{atan}(\sqrt{1+\lambda/p})}{\pi\sqrt{1+\lambda/p}}$ and $\kappa = \dfrac{p}{\pi(p+\lambda)(2p+\lambda)}$.

If D is large, then this differentiation may be performed with the aid of common mathematical software packages such as the Maple because the number of terms grows exponentially. Alternatively, by substituting $\operatorname{atan}(z)/z = {}_2F_1\left(\frac{1}{2}, 1; \frac{3}{2}; -z^2\right)$ [52, (9.121.27)] in Eq. (4.34), and then invoking Leibnitz' rule (i.e., n-th derivative of a product of two

functions) [52, (0.42)], and after simplifications, namely

$$\frac{d^{(n)}}{ds^{(n)}}(uv) = \sum_{k=0}^{n} \frac{n!}{(n-k)!k!} \frac{d^{(k)}}{ds^{(k)}}(v) \frac{d^{(n-k)}}{ds^{(n-k)}}(u), \tag{4.35}$$

and after simplifications, we get

$$I_2 = q^2\left[1 - \frac{4}{\pi}\sum_{k=0}^{D-1} \frac{1}{(2k+1)}\left(\frac{\lambda}{p}\right)^k {}_2F_1\left(\frac{1}{2}+k,\, 1+k; \frac{3}{2}+k; -1-\frac{\lambda}{p}\right)\right]. \tag{4.36}$$

In this case, the final SER expression can be computed recursively in terms of Gauss hypergeometric series. For the particular case of $m = 1$, Eq. (4.36) reduces to the results given in [45].

Case (b): Let us assume that the fading severity index is common to all diversity branches and assumes an integer value. However, the average received SNR per branch $\bar{\gamma}_l$ may be different. In this case, we can write the PDF of γ_b in the form,

$$p_{\gamma_b}(\gamma) = \sum_{l=1}^{L}\sum_{k=1}^{m} A_{lk} \frac{m^k \gamma^{k-1}}{(k-1)!\bar{\gamma}_l^k} \exp\left(\frac{-m\gamma}{\bar{\gamma}_l}\right) \tag{4.37}$$

where

$$A_{lk} = \frac{(-m)^{m-k}}{(m-k)!\,\bar{\gamma}_l^{m-k}} \frac{d^{m-k}}{dx^{m-k}}\left[\prod_{i=1, i\neq l}^{L}\left(1-\frac{\bar{\gamma}_i x}{m}\right)^{-m}\right]\Bigg|_{x=\frac{m}{\bar{\gamma}_l}} \tag{4.38}$$

Then it is straight-forward to show that the SER may be expressed as,

$$\begin{aligned} P_S^{(E)}(\varepsilon) = {} & 4q\sum_{l=1}^{L}\sum_{k=1}^{m} A_{lk}\left[\frac{1}{2}(1-\mu_l)\right]^k \sum_{i=0}^{k-1}\binom{k-1+i}{i}\left[\frac{1}{2}(1+\mu_l)\right]^i \\ & -q^2\sum_{l=1}^{L}\sum_{k=1}^{m} A_{lk}\frac{\lambda_l^k(-1)^{k-1}}{(k-1)!}\frac{d^{(k-1)}}{ds^{(k-1)}}\left[\frac{1}{s}-\frac{4}{\pi}\frac{\tan^{-1}(\sqrt{1+s/p})}{s\sqrt{1+s/p}}\right]\Bigg|_{s=\lambda_l} \end{aligned} \tag{4.39}$$

where $\mu_l = \sqrt{p\bar{\gamma}_l/(m+p\bar{\gamma}_l)}$. For the particular case of $m = 1$, Eq. (4.39) reduces to the SER formula for square MQAM on Rayleigh fading channel derived in [45].

Case (c): If the diversity branches are distinct and m_l's assume integer values, we obtain, upon performing the inverse Laplace transform of Eq. (4.23),

$$p_{\gamma_b}(\gamma) = \sum_{l=1}^{L} \sum_{k=1}^{m_l} \eta_l^{(m_l-k)} \frac{\gamma^{(k-1)} \lambda_l^k \exp(-\lambda_l \gamma)}{(k-1)!} \tag{4.40}$$

where

$$\eta_l^{(m_l-k)} = \frac{1}{(m_l-k)!\lambda_l^k} \left[\prod_{i=1}^{L} \lambda_i^{m_i}\right] \frac{d^{m_l-k}}{ds^{m_l-k}} \left[\prod_{i\neq l}^{L} (s+\lambda_l)^{-m_l}\right]\Bigg|_{s=-\lambda_l}. \tag{4.41}$$

Then, the corresponding exact SER may be evaluated as

$$P_S^{(E)}(\varepsilon) = 4q \sum_{l=1}^{L} \sum_{k=1}^{m_l} \eta_l^{(m_l-k)} \left[\frac{1}{2}\left(1-\sqrt{\frac{p}{\lambda_l+p}}\right)\right]^k \sum_{i=0}^{k-1} \binom{k-1+i}{i} \left[\frac{1}{2}\left(1+\sqrt{\frac{p}{\lambda_l+p}}\right)\right]^i$$
$$- q^2 \sum_{l=1}^{L} \sum_{k=1}^{m} \eta_l^{(m_l-k)} \frac{\lambda_l^k (-1)^{k-1}}{(k-1)!} \frac{d^{(k-1)}}{ds^{(k-1)}} \left[\frac{1}{s} - \frac{4}{\pi} \frac{\tan^{-1}(\sqrt{1+s/p})}{s\sqrt{1+s/p}}\right]\Bigg|_{s=\lambda_l} \tag{4.42}$$

To the best of the authors' knowledge, all the exact closed-form expressions for MQAM on Nakagami fading channel presented in this section are new.

4.1.2 Correlated Fading

When the diversity branches are correlated, the analysis proceeds in a similar manner as the independent fading scenario. But we need to find the corresponding CHF or MGF of the SNR at the output of the combiner. For the arbitrarily correlated Nakagami

fading environment, the joint CHF of the instantaneous SNR may be written in the form [54],

$$\phi_{\gamma}(t_1, \ldots, t_L) = \det(I - jTR\Lambda)^{-m} \tag{4.43}$$

where I is the $L \times L$ identity matrix, Λ is a positive definite matrix of dimension L (determined by the branch covariance matrix), T and R are two diagonal matrices defined as $T = \mathrm{diag}(t_1, \ldots, t_L)$ and $R = \mathrm{diag}(\bar{\gamma}_1/m, \ldots, \bar{\gamma}_L/m)$, respectively, and m is the fading parameter. Then the CHF of γ_b can be obtained from (4.43) by setting $t_1 = \ldots = t_L = t$, i.e.,

$$\phi_{\gamma_b}(t) = \det(I - jR\Lambda t)^{-m} = \prod_{k=1}^{L} (1 - j\lambda_k t)^{-m} \tag{4.44}$$

where λ_k are eigen values of matrix $R\Lambda$. Thus, we can readily evaluate the exact SER performance of MQAM with MRC diversity by substituting (4.44) into (4.30) or (4.31).

For special cases of constant and exponential correlation models (and with the assumption of identical fading severity index and signal strength across the diversity branches), the corresponding CHFs can be easily shown to be Eqs. (4.45) and (4.46), respectively:

$$\phi_{\gamma_b}(t) = \left(\frac{m^L}{[jt\bar{\gamma}(\rho - 1 - L\rho) + m]\,[jt\bar{\gamma}(\rho - 1) + m]^{L-1}} \right)^m \tag{4.45}$$

$$\phi_{\gamma_b}(t) \approx \left(\frac{mL}{mL - jt\bar{\gamma}\tau} \right)^{mL^2/\tau} \tag{4.46}$$

where $\tau = L + \frac{2\rho}{1-\rho}\left(L - \frac{1-\rho^L}{1-\rho}\right)$, ρ is the correlation coefficient and L denotes the order of diversity.

4.2 Average SER of M-ary QAM with Equal-Gain Diversity Receiver

The EGC is of considerable interest since it appears to offer comparable performance to the optimal MRC with much greater simplicity. The small argument approximation method [21] becomes inaccurate when L increases. A more refined analysis was presented recently by Beaulieu and Abu-Dayya by approximating the PDF of the sum of Nakagami RVs using an infinite series technique. In the following, we derive an exact analytical expression for EGC for MQAM on Nakagami fading channel in terms of a finite-range integral. Our new approach circumvents the problem of computing the PDF of the sum of RVs (corresponding to the amplitude of the received signal) which is normally encountered in the analysis of EGC diversity receivers. Furthermore, the integral can approximated very precisely using the GCQ formula requiring the evaluation of a function at only a small number of points. This simple expression also handles arbitrary fading parameters as well as dissimilar mean signal strengths across the diversity branches.

In an equal gain combiner, the output of different diversity branches are first cophased, equally weighted, and then summed to give the resultant output. The instantaneous SNR at the output of the EGC combiner is $\gamma_b = x^2$ where x is defined as

$$x = \sqrt{\frac{E_b}{LN_0}} \sum_{l=1}^{L} \alpha_l \tag{4.47}$$

where α_l is a Nakagami RV with the statistical parameters m_l and Ω_l as defined in Section 4.1. Let $\bar{\gamma}_k = \Omega_k (E_b/N_0)$ denote the average SNR for the k-th branch, which is consistent with our definition for the MRC case. The characteristic function (CHF) of x (the sum of L Nakagami RVs) in this case is simply the product of the individual CHFs, i.e.,

$$\phi_x(\omega) = \prod_{k=1}^{L} \int_0^{\infty} \frac{2}{\Gamma(m_k)} \left(\frac{m_k}{\bar{\gamma}_k}\right)^{m_k} \alpha^{2m_k-1} \exp\left(\frac{-m_k\alpha^2}{\bar{\gamma}_k} + j\frac{\omega\alpha}{\sqrt{L}}\right) d\alpha . \tag{4.48}$$

Recognizing the definite integral in Eq. (4.48) can be expressed in terms of parabolic cylinder function using identity [[52], (3.462)], we get

$$\phi_x(\omega) = \prod_{k=1}^{L} \frac{\Gamma(m_k + 1/2)}{2^{-m_k}\sqrt{\pi}} \exp\left(\frac{-\omega^2}{8\lambda_k L}\right) D_{-2m_k}\left(\frac{-j\omega}{\sqrt{2L\lambda_k}}\right) \tag{4.49}$$

where $\lambda_k = m_k/\bar{\gamma}_k$ and $D_{-v}(z)$ is the parabolic cylinder function of order v.

Using identity [[52], (9.240)],

$$D_{-2m_k}(z) = 2^{-m_k}\exp\left(\frac{-z^2}{4}\right) \times \left[\frac{\sqrt{\pi}}{\Gamma(m_k + 1/2)}\Phi\left(m_k, \frac{1}{2}; \frac{z^2}{2}\right) - \frac{\sqrt{2\pi}z}{\Gamma(m_k)}\Phi\left(m_k + \frac{1}{2}, \frac{3}{2}; \frac{z^2}{2}\right)\right] \tag{4.50}$$

we can express Eq. (4.49) in terms of the of the more familiar confluent hypergeometric function of the first kind $\Phi(a, b;c)$,

$$\phi_x(\omega) = \prod_{k=1}^{L} \left\{\Phi\left(m_k, \frac{1}{2}; \frac{-\omega^2}{4L\lambda_k}\right) + \frac{j\Gamma(m_k + 1/2)\,\omega}{\Gamma(m_k)\sqrt{L\lambda_k}}\Phi\left(m_k + \frac{1}{2}, \frac{3}{2}; \frac{-\omega^2}{4L\lambda_k}\right)\right\}. \tag{4.51}$$

The confluent hypergeometric function may be computed efficiently using a convergent series for small arguments and via a divergent expansion for large arguments [refer to Appendix 4B].

From Eq. (4.1), the conditional error probability for square MQAM is

$$P_S^{(E)}(\varepsilon|x) = 2q\,\mathrm{erfc}(\sqrt{p}x) - q^2\,\mathrm{erfc}^2(\sqrt{p}x) \tag{4.52}$$

and we are interested in calculating its average over the Nakagami PDF,

$$P_S^{(E)}(\varepsilon) = \int_0^\infty P_S^{(E)}(\varepsilon|x)\,p_x(x)\,dx \tag{4.53}$$

where $p_x(x)$ is the PDF of the sum of L Nakagami random variables. It is difficult (or

impossible) to invert Eq. (4.51) to get a closed-form expression for the PDF of x. Therefore, a Fourier series approach has previously been used [49]. Since we already have the Fourier transform (FT) of the PDF, by transforming the product integral in Eq. (4.53) to the frequency domain using Parseval's theorem [[55], pp 371] the need to find the PDF is circumvented. But we then also need the FT of $P_S^{(E)}(\varepsilon|x)$, which surprisingly turns out to be very easily computed. For our subsequent development, the following two FTs are needed:

$$\begin{aligned}\Psi(\omega) &= \omega\int_0^{\infty} \operatorname{erfc}(x)\exp(j\omega x)\,dx \\ &= \frac{2}{\sqrt{\pi}}F\left(\frac{\omega}{2}\right)+j\left[1-\exp\left(\frac{-\omega^2}{4}\right)\right]\end{aligned} \tag{4.54}$$

$$\begin{aligned}\varphi(\omega) &= \omega\int_0^{\infty} \operatorname{erfc}^2(x)\exp(j\omega x)\,dx \\ &= j-j\left[\exp\left(\frac{-\omega^2}{4}\right)+\frac{4j}{\sqrt{\pi}}F\left(\frac{\omega}{2}\right)-\frac{4j}{\sqrt{\pi}}F\left(\frac{\omega}{2\sqrt{2}}\right)\exp\left(\frac{-\omega^2}{8}\right)+\frac{4}{\pi}F^2\left(\frac{\omega}{2\sqrt{2}}\right)\right]\end{aligned} \tag{4.55}$$

which were obtained using integration by parts, and notation $F(.)$ denotes the Dawson's integral,

$$F(x) = \exp\left(-x^2\right)\int_0^x \exp\left(t^2\right)dt. \tag{4.56}$$

There are at least two methods for computing $F(x)$. First, it has the series representation (in terms of the confluent hypergeometric function),

$$F(x) = x\Phi\left(1,\frac{3}{2};-x^2\right). \tag{4.57}$$

Therefore, $F(x)$ can be computed using the procedure outlined in Appendix 4B (i.e., by evaluating sufficient number of terms in the series of $\Phi(a, c;x)$), which can handle

any real a and c. It turns out that when $a = 1$ and $c = 3/2$, there is a much more efficient, direct method to compute $\Phi\left(1, \frac{3}{2}; -x^2\right)$. In this chapter, we use this second approach due to Rybicki [56]. That is why Eq. (4.54) (which can also be expressed in terms of the confluent series) and Eq. (4.55) are expressed in terms of this function. Now applying Parseval's theorem in Eq. (4.53), we obtain

$$\begin{aligned} P_S^{(E)}(\varepsilon) &= \frac{1}{2\pi}\int_{-\infty}^{\infty} \mathrm{FT}\left[P_S^{(E)}(\varepsilon|x)\right]\phi_x^*(\omega)\,d\omega \\ &= \frac{1}{2\pi}\int_{-\infty}^{\infty} \frac{1}{\omega}\left[2q\Psi(\omega) - q^2\varphi(\omega)\right]\phi_x^*(\sqrt{p}\omega)\,d\omega \end{aligned} \tag{4.58}$$

Since the imaginary part of this integral is zero, we may re-write Eq. (4.58) as,

$$P_S^{(E)}(\varepsilon) = \frac{q}{\pi}\int_0^{\infty} \frac{\beta(\omega)}{\omega} d\omega \tag{4.59}$$

where

$$\beta(\omega) = Re\left\{\left[2\Psi(\omega) - q\varphi(\omega)\right]\phi_x^*(\sqrt{p}\omega)\right\}. \tag{4.60}$$

Using variable substitution $\omega = \tan\theta$ in Eq. (4.59), we can express this integral in a more desirable form (i.e., suitable for numerical integration),

$$P_S^{(E)}(\varepsilon) = \frac{2q}{\pi}\int_0^{\pi/2} \frac{\beta(\tan\theta)}{\sin(2\theta)} d\theta. \tag{4.61}$$

Note that Eqs. (4.59) and (4.61) are *exact* analytical solutions for MQAM with EGC diversity. Yet making another variable substitution $\omega^2 + \frac{1}{2} = \frac{1}{1+x}$ in Eq. (4.59) and then applying GCQ formula, we obtain a rapidly converging series representation for the EGC performance on Nakagami fading channel,

$$P_S^{(E)}(\varepsilon) = \frac{q}{\pi}\int_{-1}^{1} \frac{\beta\left[\sqrt{\frac{1-x}{2(1+x)}}\right]}{1-x^2}dx$$
$$= \frac{q}{n}\sum_{k=1}^{n} \beta\left[\frac{1}{\sqrt{2}}\tan\left(\frac{\pi(2k-1)}{4n}\right)\right] / \sin\left(\frac{\pi(2k-1)}{2n}\right) + R_n \qquad (4.62)$$

It is also interesting to note that Eqs. (4.21) and (4.62) are in similar forms.

4.3 Numerical Results

In this section we present selected numerical results to show the efficacy of MRC and EGC diversity receivers on generalized fading channel with arbitrary fading parameter. When applying the GCQ sum, we have used $n = 64$ and $n = 512$ for the MRC and EGC results, respectively. Note that these numbers were conservatively chosen to be large. In fact, as few as 8 samples can be sufficient in some cases. Fig. 4.1 depicts the SER performance curves of 4-QAM, 16-QAM and 64-QAM with the assumption that all the MRC or EGC space diversity branches undergo identical Nakagami fading with $m = 1.8$. This fading severity index corresponds to a Rician channel with Rice factor $K = 2$. From this figure, it is apparent that diversity reception is an effective technique for combatting the detrimental effects of deep fades experienced in wireless channels.

It is also observed that the penalty in SNR to achieve a given SER of MQAM system with a larger signal constellation size declines more rapidly than that of a smaller signal set, as the diversity order increases. This is true for both MRC and EGC diversity systems. In other words, the diversity improvement is greater as the constellation size M increases. When $L = 1$, the performance curves evaluated using Eq. (4.21) and/or Eq. (4.28) coincide with that evaluated via Eq. (4.59), as anticipated (i.e., corresponds to the non-diversity case). As well, the penalty in SNR for the EGC diversity receiver to achieve the same level of performance with the optimum diversity receiver is quite minimal. For instance, the difference for 4-QAM at $P_S = 10^{-4}$ is only about 0.4 dB and 0.6

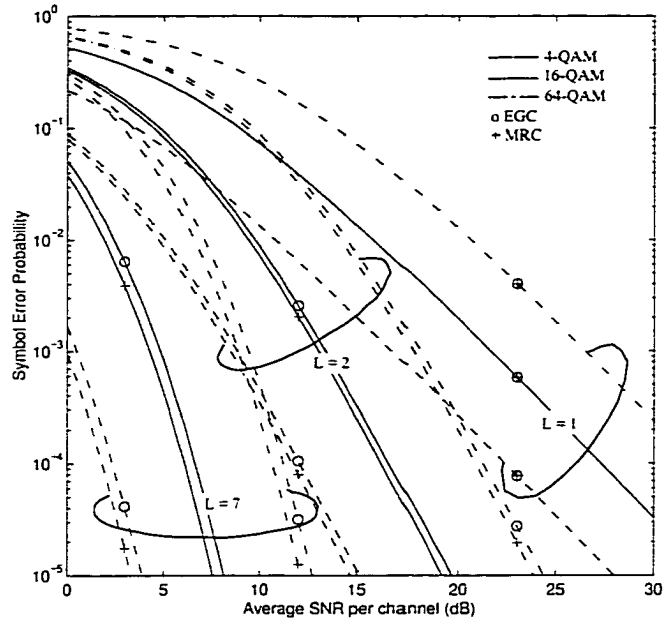

Fig. 4.1 Symbol error probability for MQAM with MRC and EGC diversity receivers on Nakagami fading with fading figure $m = 1.8$.

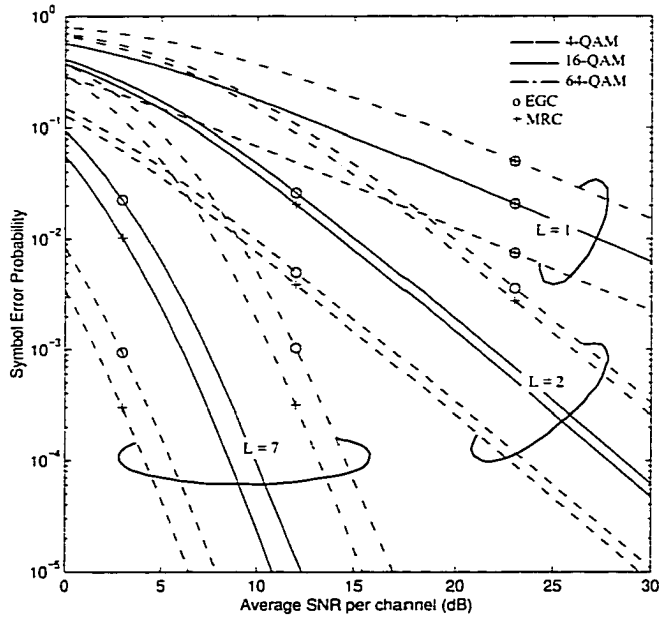

Fig. 4.2 Symbol error probability for MQAM with MRC and EGC diversity receivers on Nakagami fading with fading figure $m = 0.75$.

dB for $L = 2$ and $L = 7$, respectively.

Nakagami distribution can also model a multipath fading environment which is more severe than the Rayleigh fading. This is achieved when m is less than unity. More importantly, some empirical data suggests that some urban environment path fading statistics are more adequately described by a Nakagami distribution with fading figure $m = 0.75$ [59]. Hence in Fig. 4.2 we plot the SER curves for different QAM systems, with and without diversity reception, in this fading environment. Comparison between Fig. 4.1 and Fig. 4.2 reveals that the relative diversity advantage is more pronounced in a poorer channel condition. This is intuitively satisfying since the difference between the instantaneous received SNR on various diversity branches will be less as m increases. However, the SER performance is always better in a channel where a strong line-of-sight path exists for a specified average received SNR per branch $\bar{\gamma}_c$, and diversity order. We also observe that the discrepancy between the EGC and MRC diversity performance curves gets larger as the fading becomes more severe (i.e., smaller m).

Fig. 4.3 compares the exact SER with MRC (computed using Eq. (4.19) or (4.29)) with the approximate SER (which may be calculated via Eq. (4.10) or more efficiently by evaluating only the first term in Eq. (4.28)) for the system parameters considered in Fig. 4.1 and Fig. 4.2. Notice that the approximate SER for a dual-diversity 16-QAM is more than 10% higher than the true SER even at $\bar{\gamma}_c = 10$ dB when $m = 0.75$. The discrepancy between the approximate and the exact SER diminishes as the average received SNR per branch increases or for higher order of diversity. On the other hand, their difference becomes more apparent if the channel condition degrades (i.e., smaller m) or for a larger signal constellation size.

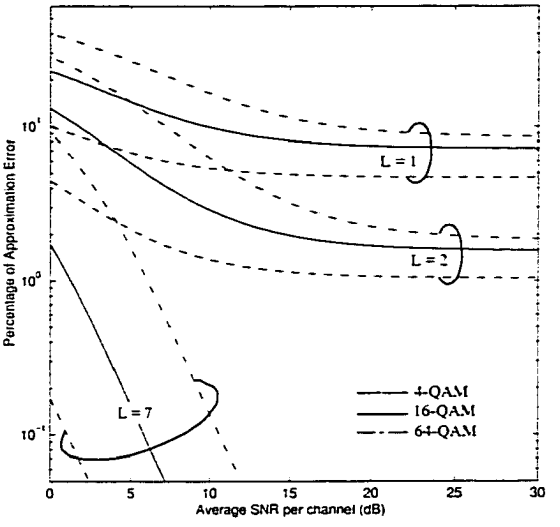

(a) m = 1.8

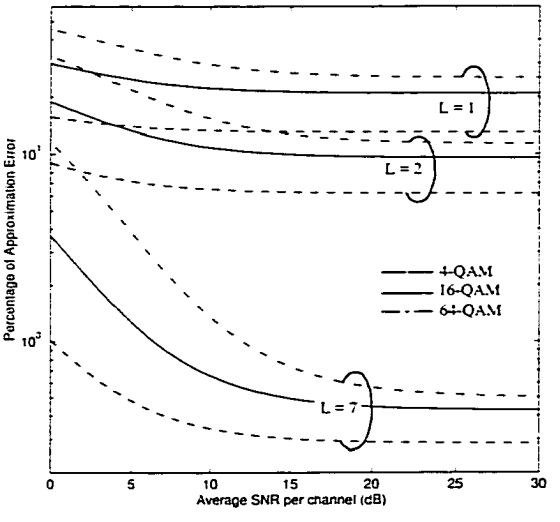

(b) m = 0.75

Fig. 4.3 Comparison between the exact and approximate SER of MQAM with MRC space diversity in different fading environments and for different diversity orders.

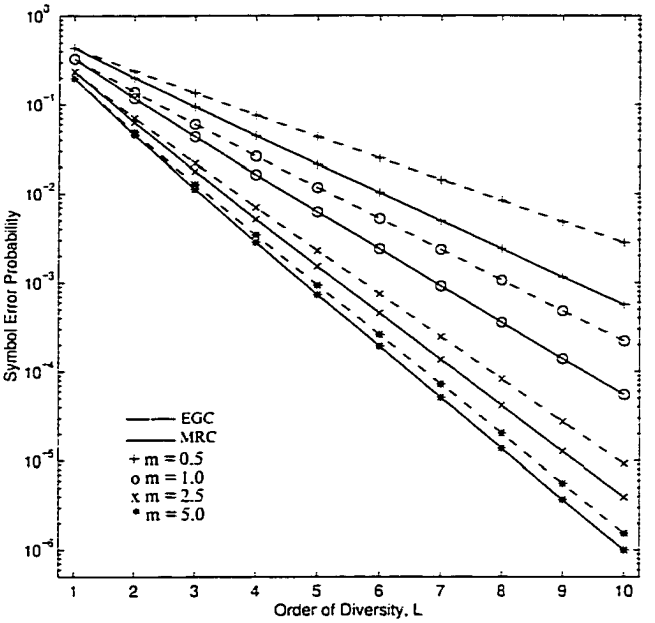

Fig. 4.4 Symbol error probability versus order of diversity for 64-QAM with MRC and EGC diversity receivers.

Next in Fig. 4.4, the SER performance of 64-QAM system plotted against the order of diversity for several fading severity indexes. All the diversity branches are assumed to have identical fading statistics and the received SNR per branch is assumed to be $\bar{\gamma}_c = 10dB$. It is obvious that the larger the number of diversity branches, the smaller the chance of the combined signal going into fade. However, the effective improvement in SNR for a fixed error performance does not improve in proportion to increasing L (see Fig. 4.1 and Fig. 4.2). The greatest improvement step occurs in going from a single-branch receiver to a two-branch receiver.

The results in Fig. 4.4 indicate that the discrepancy between the error performance of MRC and EGC diversity receivers becomes more apparent as the diversity order grows. This may be attributed to the fact that MRC yields better statistical reduction of deep fades as well as provides the higher average output SNR of the combined signal than EGC. Since the deviation between the EGC and MRC curves decline rapidly as m increases, we can conclude that the ability to mitigate the deep fades is the main factor

that has contributed the difference in the performance of the two receiver structures.

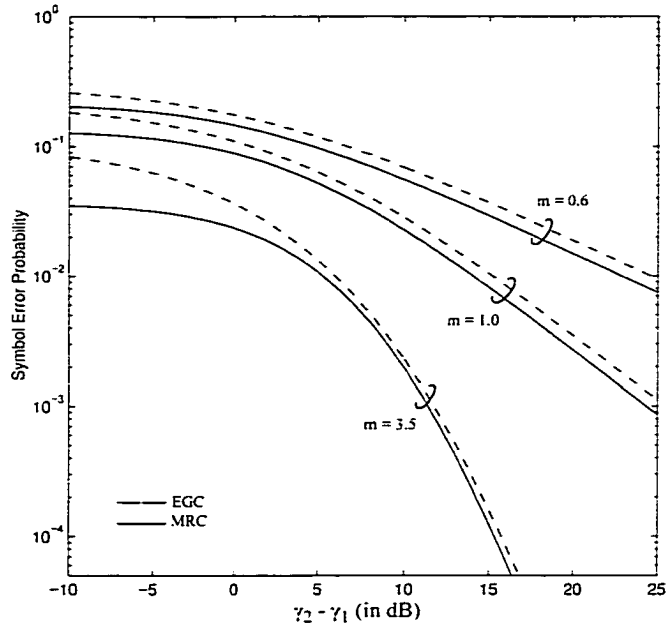

Fig. 4.5 Effect of unbalance mean signal strength ($\bar{\gamma}_1$ is fixed to 10 dB) on the SER performance of dual-diversity 16-QAM systems in different fading conditions.

In Fig. 4.5 and Fig. 4.6 we examine the sensitivity of the error probability for 16-QAM system with MRC or EGC diversity receivers in the presence of dissimilar mean signal strength and unequal fading parameters. It is clear that departure of the EGC performance curve from the MRC case is not very significant if the ratio $\bar{\gamma}_2/\bar{\gamma}_1$ is not excessively small and/or if the ratio m_2/m_1 is not too large.

From Fig. 4.5, it can be concluded that MRC makes much more effective use in diversity of relatively weak signals than can the EGC. Besides, equal noise levels in all branches is crucial to proper operation of EGC, since otherwise those branches with large noise levels would dominate the output SNR even if the branch itself were weak in signal level. This in turn suggests that a very weak signal should not be combined in the equal-gain diversity receiver configuration because it may cause a considerable degrada-

tion in the mean SNR (due to combination losses). Alternatively, one should equalize the noise levels across the diversity branches by introducing different gains in these branches, prior to the combiner.

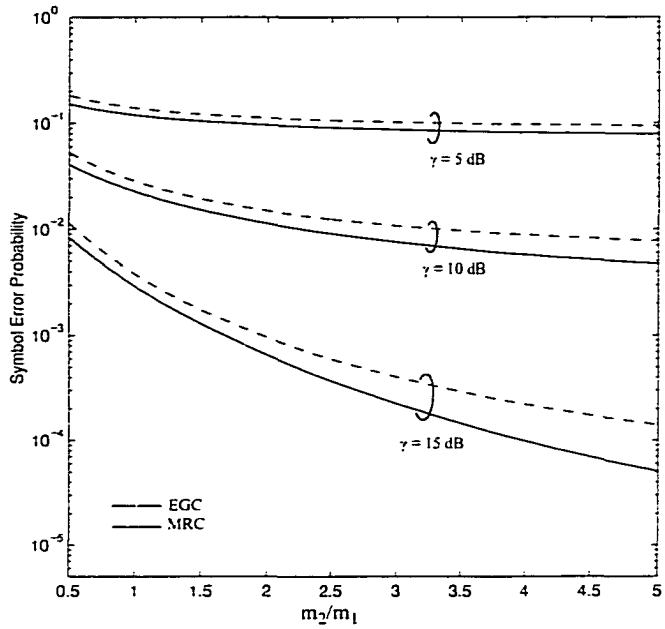

Fig. 4.6 Sensitivity of SER for 16-MQAM with dual-diversity MRC or EGC diversity receiver on Nakagami fading channels due to dissimilar fading severity index (m_1 is fixed to 1).

One way to explain the larger difference between the EGC and MRC performance curves as the ratio m_2/m_1 increases is by noting that fading severity index m has the diversity-like effect. Hence, the ability to mitigate the deep fades and average output SNR of the EGC combiner is inferior to the optimum MRC, specifically when the order of diversity increases (see Fig. 4.4).

4.4 Conclusions

Exact symbol error probability expressions have been derived for coherent MQAM systems employing MRC and EGC antenna diversity in a Nakagami fading environment with an arbitrary fading severity index and/or dissimilar signal strength. The SER formula is exact for square QAM. A tight bound for the rectangular signal constellations was also presented. In particular, the closed-form formula based on GCQ can be easily programmed and evaluated efficiently. Our results are sufficiently general to allow for arbitrary fading parameters as well as dissimilar mean signal strengths across the diversity branches. The generality and computational efficiency of the new results presented in this chapter rendering themselves as powerful means for both theoretical analysis and practical applications.

Appendix 4A

In this appendix we present an alternative technique for evaluating the term involving $\mathrm{erfc}^2(.)$ in Eq. (4.3) instead of the two-dimension GCQ method illustrated in [46], namely,

$$I_2 = \int_0^\infty q^2 \mathrm{erfc}^2\left[\sqrt{\gamma_b p}\right] p_{\gamma_b}(\gamma_b)\, d\gamma_b \tag{4A.1}$$

By definition,

$$\mathrm{erfc}^2(z) = \frac{4}{\pi}\int_z^\infty \int_z^\infty \exp\left[-\left[t^2+s^2\right]\right] dt ds \tag{4A.2}$$

where the region of integration is illustrated in Fig. 4.7.

Let $t = v\cos(\theta)$ and $s = v\sin(\theta)$ so that the double integral in (4A.2) reduces into a single integral, i.e.,

$$\mathrm{erfc}^2(z) = \frac{4}{\pi}\int_{\sqrt{2}z}^\infty v\exp\left(-v^2\right)\left[\cos^{-1}(z/v) - \sin^{-1}(z/v)\right] dv \tag{4A.3}$$

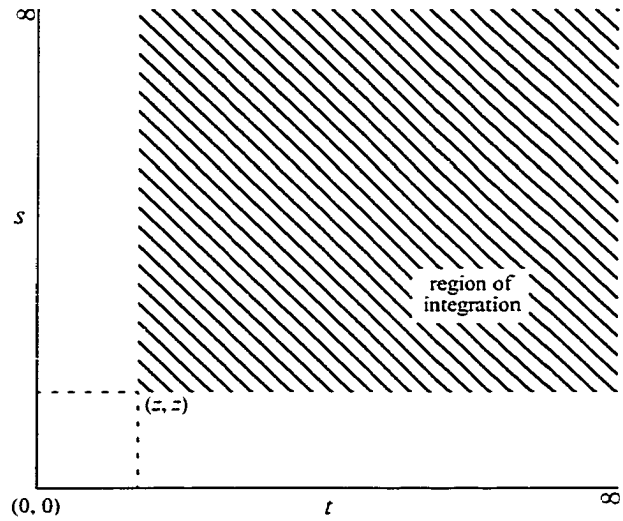

Fig. 4.7 Integration Region.

Now performing variable substitution $v = z\sqrt{1+x^2}$ in (4A.3), we arrive to,

$$\operatorname{erfc}^2(z) = \frac{4}{\pi}\int_1^\infty z^2 x \exp\left(-z^2\left[1+x^2\right]\right)\varnothing(x)\,dx \tag{4A.4}$$

where

$$\varnothing(x) = \cos^{-1}\left(\frac{1}{\sqrt{1+x^2}}\right) - \sin^{-1}\left(\frac{1}{\sqrt{1+x^2}}\right) \tag{4A.5}$$

Since $\frac{d}{dx}\left\{\exp\left(-z^2\left[1+x^2\right]\right)\right\} = -2z^2 x\exp\left(-z^2\left[1+x^2\right]\right)$, $\frac{d}{dx}\{\varnothing(x)\} = \frac{2}{1+x^2}$, $\varnothing(1) = 0$ and $\varnothing(x)\exp\left(-z^2\left[1+x^2\right]\right)\Big|_{x=1}^{x=\infty} = 0$, (4A.4) can be simplified as,

$$\operatorname{erfc}^2(z) = \frac{4}{\pi}\int_1^\infty \frac{\exp\left[-z^2\left[1+x^2\right]\right]}{1+x^2}dx \tag{4A.6}$$

by exploiting the identity $\int u\,dv = uv - \int v\,du$.

Then I_2 can be restated as,

$$I_2 = \frac{4q^2}{\pi}\int_1^{\infty} \frac{\phi\left[p\left[1+x^2\right]\right]}{1+x^2}dt = \frac{2q^2}{\pi}\int_0^1 \frac{\phi\left(2p/(1-z)\right)}{\sqrt{1-z^2}}dz \tag{4A.7}$$

where the second integral in (4A.7) is obtained via variable transformation $x^2 + 1 = 2/(1-z)$. Now applying GLQ formula [[14], (25.4.36)], we arrive to a simple expression for evaluating (4A.1):

$$I_2 = \frac{2q^2}{\pi}\sum_{i=1}^{n} w_i\left[\frac{\phi\left(2p/(1-z_i)\right)}{\sqrt{1+z_i}}\right] + R_n \tag{4A.8}$$

The abscissas and weights are given by $z_i = 1-\xi_i^2$ and $w_i = 2w_i^{(2n)}$ respectively, where ξ_i is the ith positive zero of Legendre function $P_{2n}(x)$, and $w_i^{(2n)}$ are the Gaussian weights of order $2n$. The remainder term R_n can be bounded using the procedure outlined in [30]. It is evident that this alternative method requires fewer samples of MGF (i.e., $2n \ll n^2$ samples for practical values of n) compared to the two-dimension GCQ formula. This is because the numerical approximation is performed over a single integral in GLQ, instead of the double integral in the latter approach.

Yet making another variable substitution $x = \cot(\Theta)$ in (4A.6), we get

$$\operatorname{erfc}^2(z) = \frac{4}{\pi}\int_0^{\pi/4} \exp\left(\frac{-z^2}{\sin^2(\Theta)}\right)d\Theta \tag{4A.9}$$

which is an alternative representation for the two-dimension complementary error function. It is noted that this new form is essentially the same as the results presented recently by Simon and Divsalar in [28].

Appendix 4B

In Appendix 4B, we present three series that are used in the calculations involving the confluent hypergeometric function of the first kind. The confluent series is defined as,

$$\Phi(a, c;x) = \sum_{r=0}^{\infty} \frac{(a)_r x^r}{(c)_r r!} \tag{4B.1}$$

where the polychamer symbol $(b)_r = b(b+1)\ldots(b+r-1)$. Note that if $-a$ is a positive integer, then the series is a finite polynomial of x, i.e.,

$$\Phi(a, c;x) = \sum_{r=0}^{-a} \frac{(a)_r x^r}{(c)_r r!}. \tag{4B.2}$$

In the mathematical sense, the series (4B.1) converges everywhere (i.e., the radius convergence is infinite). However, for large $|x|$ the series does not converge until $r \gg |x|$, by which time overflow problems may have occurred. Therefore (4B.1) is not computationally useful when $|x|$ is large. Note that when the series (4B.1) reduces to (4B.2), the convergence problem does not occur.

For EGC performance evaluation, both $\Phi\left(m, \frac{1}{2};-x^2\right)$ and $\Phi\left(m+\frac{1}{2}, \frac{3}{2};-x^2\right)$ are needed, where m can be real or integer. Beaulieu and Abu-Dayya provides a method to compute $\Phi\left(m+\frac{1}{2}, \frac{3}{2};-x^2\right)$ for positive integer m [[49], Appendix A], and their finite series simply follows from (4B.3) and (4B.2). They also provide a recursion to compute $\Phi\left(m, \frac{1}{2};-x^2\right)$ [[49], Appendix B], which again holds for positive integer m only. In contrast, the following procedure handles both real and integer m:

We now consider the calculation of $\Phi(a, c;-x)$ for $a, c > 0$ and x is a positive real number. For this case, it is better to apply Kummer's transformation formula,

$$\Phi(a, c;-x) = \exp(-x)\,\Phi(c-a, c;x). \tag{4B.3}$$

The advantage of this transformation is that if $m + 1/2$ or m is an integer, then the series required in Eq. (4.51) is a finite polynomial. Therefore, no convergence problems are encountered. For $x < 200$, we use

$$\Phi(a, c; -x) = \exp(-x) \sum_{r=0}^{\infty} \frac{(c-a)_r x^r}{(c)_r r!}, \tag{4B.4}$$

which can be computed via standard series evaluation techniques. For $x \geq 200$, we use the divergent expansion,

$$\Phi(a, c; -x) = \frac{x^{-a}\Gamma(c)}{\Gamma(c-a)} \sum_{r=0}^{\infty} \frac{(a)_r (a-c)_r}{x^r r!} + O\left(x^{a-c} \exp(-x)\right). \tag{4B.5}$$

It is sufficient to use the first term only. In this case, the reliability of the divergent series may be estimated as [[57], pp. 278],

$$\Phi(a, c; -x) = \frac{x^{-a}\Gamma(c)}{\Gamma(c-a)} \left[1 + O\left(|x|^{-1}\right)\right]. \tag{4B.6}$$

Appendix 4C

In this appendix, we outline a method that can be used to improve the computational efficiency of Eq. (4.19) if evaluated using a standard numerical integration technique such as the trapezoidal rule, as an alternative to GCQ formula (i.e., (4.21)). Assume that the integral in Eq. (4.19) is truncated at $t = u$ and we require the truncation error to be less than ε. It is easy to show that

$$|\psi(t)| \leq 4 + q + \frac{4q}{\pi} \tag{4C.1}$$

Thus, we have

$$K\int_{u}^{\infty}\frac{1}{t^{D+1}}dt \le \varepsilon \tag{4C.2}$$

where

$$K = \frac{q}{\pi}\left[4+q+\frac{4q}{\pi}\right]\prod_{l}\lambda_l^{m_l} \tag{4C.3}$$

and $D = \sum_{l} m_l$. From (4C.2), we obtain

$$u \ge \sqrt[D]{\frac{K}{D\varepsilon}}. \tag{4C.4}$$

Surprisingly the simple trapezoidal rule integration technique requires a lot more computational effort than the GCQ (for instance, in the order of 10^4 times at $\bar{\gamma}_b = 10dB$) even after truncating the integration limit to achieve a prescribed accuracy of $\varepsilon = 10^{-5}$.

Chapter 5

Unified Analysis of Switched Diversity Systems in Independent and Correlated Fading Channels

Among the various known diversity combining methods, selection diversity is the simplest and perhaps the most frequently used in practice. For instance, a form of selection diversity has been implemented in current digital cellular system (specified in the IS-54 common air interface) where the diversity branch is selected prior to the transmission of a TDMA burst. However, the ideal selective combining (SDC) that selects the branch with the highest signal-to-noise ratio (SNR) may not be practical for radio links that use continuous transmission because it requires continuous monitoring of all the diversity branches. This problem can be circumvented by adopting a suboptimal switched diversity scheme.

In Chapter 3, we have outlined two unified approaches to the performance evaluation of four common predetection diversity techniques on generalized fading channels. In particular, we have shown that the MGF or the CHF of SNR at the combiner output can be used to unify the performance evaluation of a broad class of modulation formats on fading channels. Therefore, in this chapter we directly derive the MGF of signal power at the output of a dual-branch SWC combiner. The first-order derivative of the MGF with respect to the switching threshold is also derived, which is exploited to determine the optimal switching threshold.

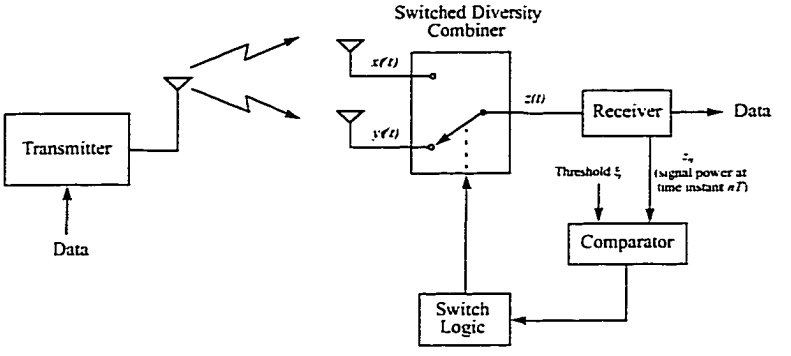

Fig. 5.1 Block diagram of a predetection switched diversity system.

Consider a two-branch switched diversity system depicted in Fig. 5.1. If the instantaneous envelope of the received signal falls below a predetermined threshold, the antenna switch is triggered, thus selecting the second branch. If the second branch is above the threshold, switching ceases. If the second branch is also in fade, we can immediately revert to the first branch, and if necessary, continue the rapid switching between the two antennas until one of them emerges above the threshold (i.e., switch-and-examine strategy), or we may switch to the second branch and remain there at least until the next switching instant regardless whether the instantaneous signal power in the second antenna is above or below the threshold (i.e., switch-and-stay strategy). Moreover, the switched diversity system has the advantage that only a single intermediate-frequency circuitry and a receiver "front-end" are used, thus avoiding the expense of extra diplexers and other high-frequency analog circuits.

Previous related studies on the switched diversity systems include the following: In [60], Rustako et. al. theoretically and experimentally examined a switched diversity system on independent Rayleigh channels using a continuous time signal model. In their switch-and-stay strategy, switching between the two antennas only occurs if there is a downward threshold crossing. Shortall [61] builds a prototype of a switched diversity system and experimentally examine the effect of the signal correlation on the receiver performance. Subsequently, Adachi et. al. [62] investigated the performance of a periodic switching diversity technique using digital FM with discriminator detection on Rayleigh

fading channels. Blanco and Zdunek [63] theoretically examined the performance of switched diversity system initially proposed in [60] for noncoherent frequency shift keying (NCFSK) in independent Rayleigh fading channels based on a discrete-time approach. Their analysis was extended in [64] for the Nakagami-m fading channels.

In [34], Abu-Dayya and Beaulieu proposed a different switch-and-stay strategy (which is referred to as SWC) and analyzed the performance of binary NCFSK on Nakagami-m fading channel based on a discrete-time model. Different from [63], the antenna switch in the SWC scheme is activated in the next switching instant as long as the measured local power in the current antenna is below the threshold level (i.e., the envelope of the received signal need not necessarily cross the threshold in the negative direction). Therefore, it does not require comparison of present samples with past samples. Moreover, the rate of branch switching is reduced with respect to the ideal selection diversity, which translates into a reduction of transient effects due to switching. Their analysis for both independent and correlated Nakagami-m signal fading has been extended to Rician fading in [35]. More recently, performance of BPSK signalling with SWC has been examined in [36] by exploiting an alternative exponential representation for the Gaussian probability integral. The authors' also derived a closed-form expression for evaluating the corresponding optimum threshold in Rayleigh and Nakagami-m fading channels when both the diversity branches are independent and identically distributed.

By contrast, in this chapter we derive a *generic* formula to study the performance of SWC for a wide range of binary and two-dimensional signal constellations in a myriad of fading environments. Different from [34]-[36], we directly determine the MGF of the resultant signal power statistic *without* imposing any restrictions. In fact, the signal statistics from different diversity branches may even be modelled using different families of distribution (i.e., mixed-fading). In particular, we examine the effect of power imbalance on the diversity receiver performance and the optimal switching threshold. This is an important consideration because in practice identical fading statistics across the diversity branches are rarely available. However, all the previous theoretical studies only considered the case of identical diversity branches for analytical simplicity. Once the MGF is

available, we can express the ASER in terms of a finite-range integral involving only the MGF. Since the derivative of the MGF with respect to the switching threshold can be obtained at once, the optimum switching threshold can be readily expressed in a closed-form in many instances.

The outline of this chapter is as follows. In Section 5.1, we derive the MGF of the local signal power at the output of the switched combiner, for both correlated and independent signal fading cases, taking into account of power imbalance, nonidentical fading severity index and/or the mixed-fading scenario. In Section 5.2, the optimization of the SWC strategy is considered. The optimum switching threshold for both independent and correlated signal fading can be attained either in a closed-form (for the identical fading statistic case) or by solving a nonlinear equation numerically (for the nonidentical fading statistics across the diversity branches). Selected numerical examples are presented in Section 5.3. Finally, the main points are summarized in Section 5.4.

5.1 Statistical Characterization of the SNR at the Output of the SWC Combiner

Table 3.1 summarizes the instantaneous symbol error rate for a wide range of modulation schemes in an AWGN channel. These conditional error probabilities (for binary and M-ary signal constellations) may be evaluated as

$$P_S(\varepsilon|\gamma) = \sum_k \int_0^{\eta_k} a_k(\theta) \exp(-\gamma b_k(\theta)) \, d\theta \tag{5.1}$$

Then the ASER in the fading channels with SWC can be derived by averaging the conditional error probability over the PDF of SNR at the output of the switched combiner in a specified fading environment. It is more insightful if we employ the MGF approach [10, 37] since the ASER can be expressed in terms of only the MGF of the resultant SNR. Further, closed-form formulas for the computing the optimum switching threshold can be determined in a straight-forward fashion for all common fading channels and for different modulation schemes if the diversity branches have identical fading statistics.

5.1.1 Correlated Fading and Nonidentical Diversity Branches

Similar to [34], [35], [63] and [64], our analysis is based on a discrete time model. The switching is performed at discrete instants of time $t = nT$, where n is an integer, and T is the interval between switching instants. The CDF of the resultant signal power at the output of the SWC combiner can be written as [34, Eq. (4)],

$$\begin{aligned} F_{z_n}(u) &= Pr\{z_n \le u\} \\ &= Pr\{z_n = x_n \text{ and } x_n \le u\} + Pr\{z_n = y_n \text{ and } y_n \le u\} \end{aligned} \tag{5.2}$$

where x_n and y_n denotes the local powers of the signals received by the two antennas at $t = nT$, and z_n is the local signal power at the output of the switched diversity receiver at $t = nT$.

If we assume the pair of samples from each diversity branch are independent[1] (i.e., x_{n-1} and x_n are independent; y_{n-1} and y_n are independent), then (5.2) can be restated as

$$\begin{aligned} F_{z_n}(u) = &\left[Pr\{\xi \le x_n \le u\} + Pr\{x_n < \xi \text{ and } y_n \le u\}\right] Pr\{z_{n-1} = x_{n-1}\} \\ &+ \left[Pr\{\xi \le y_n \le u\} + Pr\{y_n < \xi \text{ and } x_n \le u\}\right] Pr\{z_{n-1} = y_{n-1}\} \end{aligned} \tag{5.3}$$

where ξ denotes the switching threshold. In the following derivations, the time index n will be omitted for brevity. By differentiating (5.3) with respect to u, we obtain the PDF of the resultant signal power z_n:

$$\begin{aligned} f_z(u) = &\left[f_x(u)\, V(u-\xi) + \int_0^{\xi} f_{x,y}(X, u)\, dX\right] Pr\{z = x\} \\ &+ \left[f_y(u)\, V(u-\xi) + \int_0^{\xi} f_{x,y}(u, Y)\, dY\right] Pr\{z = y\}, \quad u \ge 0 \end{aligned} \tag{5.4}$$

---

1. This assumption is valid if T is large enough such that the fading process introduce small or no correlation in the time sequence of the samples in each branch. For small T, the justification of the final result (5.3) is explained in the Appendix of [34].

where $V(X) = 0$ for $X < 0$, and $V(X) = 1$ otherwise. Notations $f_x(.)$ and $F_x(.)$ correspond to the PDF and CDF of the signal power for antenna x, respectively; $f_{x,y}(.,.)$ is the joint PDF of x_n and y_n. Hence the MGF of z_n is given by

$$\begin{aligned}\phi_z(s) &= \left[\int_{\xi}^{\infty} \exp(-su) f_x(u)\, du + \int_0^{\xi} \phi_y(s, X)\, dX\right] Pr\{z = x\} \\ &\quad + \left[\int_{\xi}^{\infty} \exp(-su) f_y(u)\, du + \int_0^{\xi} \phi_x(s, Y)\, dY\right] Pr\{z = y\} \qquad (5.5)\end{aligned}$$

where $\phi_x(s, Y) = \int_0^{\infty} f_{x,y}(u, Y) \exp(-su)\, du$ & $\phi_y(s, X) = \int_0^{\infty} f_{x,y}(X, u) \exp(-su)\, du$ are the marginal MGFs.

Now let us calculate the antenna selection probabilities $Pr\{z = x\}$ and $Pr\{z = y\}$. If both diversity branches have identical fading statistics, then each of the two antennas will have an equal chance of being selected. However, when the sequences $\{x_n\}$ and $\{y_n\}$ are *not* identically distributed due to power imbalance, then the likelihood of staying in a "good" diversity branch will be higher because a branch with a higher mean received signal power will be favoured most of the time. The branch selection probabilities may be computed using a two-state Markov chain shown in Fig. 5.2.

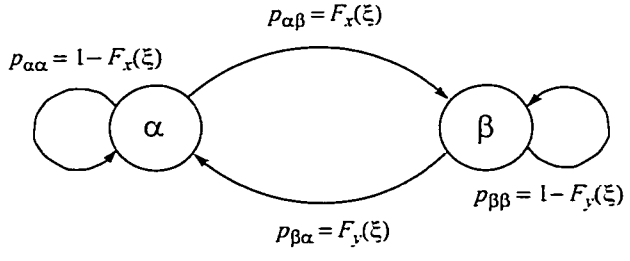

Fig. 5.2 A two-state Markov chain for calculating the antenna selection probabilities.

The states α and β correspond to the event that antenna x and antenna y is selected, respectively. The state transition probabilities, p_{ij}, is dictated by the probability that the power on a specified branch is either greater or smaller than the preset threshold. The

steady-state solution to this Markov chain yields the antenna selection probabilities:

$$Pr\{z = x\} = \frac{p_{\beta\alpha}}{p_{\alpha\beta} + p_{\beta\alpha}} = \frac{F_y(\xi)}{F_x(\xi) + F_y(\xi)} \equiv A(\xi) \tag{5.6}$$

$$Pr\{z = y\} = \frac{p_{\alpha\beta}}{p_{\alpha\beta} + p_{\beta\alpha}} = \frac{F_x(\xi)}{F_x(\xi) + F_y(\xi)} \equiv 1 - A(\xi) \tag{5.7}$$

Since $\int_{\xi}^{\infty} \exp(-su) f_x(u)\, du = \phi_x(s) - \int_0^{\xi} \exp(-su) f_x(u)\, du$ and substituting (5.6) and (5.7) into (5.5), we obtain a general expression for the MGF of the local signal power at the output of the switched combiner taking into account of the branch correlation as well as the dissimilar fading statistics, i.e.,

$$\begin{aligned}\phi_z(s) = {} & A(\xi)\left\{\phi_x(s) + \int_0^{\xi} [\phi_y(s, X) - \exp(-sX) f_x(X)]\, dX\right\} \\ & + [1 - A(\xi)]\left\{\phi_y(s) + \int_0^{\xi} [\phi_x(s, Y) - \exp(-sY) f_y(Y)]\, dY\right\}\end{aligned} \tag{5.8}$$

where $\phi_x(.)$ and $\phi_y(.)$ are the MGF of the signal power in antenna x and y, respectively (see Table 5.1 for a list of MGF of the signal power for several common fading channels). To the best of our knowledge, this result is new. From (5.1), the ABER or ASER with SWC is simply

$$P_S = \sum_k \int_0^{\eta_k} a_k(\theta)\, \phi_z(b_k(\theta))\, d\theta . \tag{5.9}$$

5.1.2 Independent Fading and Nonidentical Diversity Branches

If the antenna separation is greater than half-wavelength then it is reasonable to assume that the two diversity branches will be independent. However, their signal strength and fading severity index may be different in an actual mobile link since the radio waves take different propagation paths and may undergo different fading before arriving at the receiver.

Table 5.1 . PDF and MGF of signal power for several common fading models.

Channel Model	PDF and MGF of signal power X
Rayleigh	PDF: $f_x(X) = \frac{1}{\Omega}\exp\left(\frac{-X}{\Omega}\right)$ where $\Omega = E[X]$
	MGF: $\phi_x(s) = \frac{1}{1+s\Omega}$
Rician ($K \geq 0$)	PDF: $f_x(X) = \frac{1+K}{\Omega}\exp\left(-K-\frac{(1+K)X}{\Omega}\right) I_0\left(2\sqrt{\frac{K(K+1)X}{\Omega}}\right)$
	MGF: $\phi_x(s) = \frac{1+K}{1+K+s\Omega}\exp\left(\frac{-Ks\Omega}{1+K+s\Omega}\right)$
Nakagami-q ($-1 \leq b \leq 1$)	PDF: $f_x(X) = \frac{1}{\Omega\sqrt{1-b^2}}\exp\left(\frac{-X}{[1-b^2]\Omega}\right) I_0\left(\frac{bX}{[1-b^2]\Omega}\right)$
	MGF: $\phi_x(s) = \frac{1}{\sqrt{[s\Omega(1+b)+1][s\Omega(1-b)+1]}}$
Nakagami-m ($m \geq 0.5$)	PDF: $f_x(X) = \left(\frac{m}{\Omega}\right)^m \frac{X^{m-1}}{\Gamma(m)}\exp\left(\frac{-mX}{\Omega}\right)$
	MGF: $\phi_x(s) = \left(\frac{m}{m+s\Omega}\right)^m$
Correlated Nakagami-m with identical mean signal strength (i.e., $\Omega_x = \Omega_y$)	PDF: $f_{x,y}(X,Y) = \frac{(m/\Omega)^{m+1}}{\Gamma(m)\,[1-\rho]\,\rho^{(m-1)/2}}(XY)^{\frac{m-1}{2}} \times \exp\left(\frac{-m(X+Y)}{\Omega[1-\rho]}\right) I_{m-1}\left(\frac{2m\sqrt{\rho XY}}{\Omega[1-\rho]}\right)$
	MGF: $\phi_x(s,Y) = \left(\frac{m}{\Omega}\right)^m \frac{Y^{m-1}}{\Gamma(m)\,[1+s\Omega[1-\rho]/m]^m}\exp\left(\frac{-mY}{\Omega}\left[\frac{m+s\Omega}{m+s\Omega[1-\rho]}\right]\right)$ where ρ is the power correlation coefficient.
Correlated Nakagami-m with power imbalance	PDF: $f_{x,y}(X,Y) = \frac{\left[m/\sqrt{\Omega_x\Omega_y}\right]^{m+1}}{\Gamma(m)\,[1-\rho]\,\rho^{(m-1)/2}}(XY)^{\frac{m-1}{2}} \times\exp\left(\frac{-m(X+Y)}{\sqrt{\Omega_x\Omega_y}[1-\rho]}\right) I_{m-1}\left(\frac{2m\sqrt{\rho XY}}{\sqrt{\Omega_x\Omega_y}[1-\rho]}\right)$
	MGF: $\phi_x(s,Y) = \frac{Y^{m-1}}{\Gamma(m)}\left[\frac{m^2}{\Omega_y(m+s(1-\rho)\Omega_x)}\right]^m \exp\left(\frac{-mY}{\Omega_y}\left[\frac{m+s\Omega_x}{m+s\Omega_x(1-\rho)}\right]\right)$

For independent signal fading, the joint PDF is the product of the individual PDFs, and therefore (5.4) reduces to

$$f_z(u) = A(\xi)\{f_x(u)V(u-\xi) + F_x(\xi)f_y(u)\} + [1-A(\xi)]\{f_y(u)V(u-\xi) + F_y(\xi)f_x(u)\}. \quad (5.10)$$

The MGF of z_n is

$$\phi_z(s) = A(\xi)\{\int_{\xi}^{\infty} \exp(-su) f_x(u)\,du + \phi_y(s)F_x(\xi)\} + [1-A(\xi)]\{\phi_x(s)F_y(\xi) + \int_{\xi}^{\infty} \exp(-su) f_y(u)\,du\}. \quad (5.11)$$

One may also arrive to (5.11) directly from (5.8) by recognizing that the marginal MGFs $\phi_y(s, X) = f_x(X)\phi_y(s)$ and $\phi_x(s, Y) = f_y(Y)\phi_x(s)$ when the two diversity branches are statistically independent. Notice that (5.11) is still valid even if the received signal envelope in different antennas are modelled from different families of the fading distribution (i.e., mixed-fading model). As before, the ASER of the SWC with uncorrelated diversity branches is given by (5.9). However, $\phi_z(.)$ is evaluated using (5.11) instead of (5.8).

5.1.3 Correlated Fading and Identical Diversity Branches

If x_n and y_n are identically distributed, then $f_x(.) = f_y(.)$, $\phi_x(s, .) = \phi_y(s, .)$, $F_x(.) = F_y(.)$ and $Pr\{z = x\} = Pr\{z = y\} = 1/2$. Owing to the symmetry, (5.4) reduces to [35, Eq. (6)]. Similarly, the MGF of z_n illustrated in Eq. (5.8) may now be simplified as

$$\phi_z(s) = \phi_x(s) + \int_0^{\xi} [\phi_x(s, Y) - \exp(-sY) f_y(Y)]\,dY. \quad (5.12)$$

5.1.4 Independent Fading and Identical Diversity Branches

Following our treatment in Section 5.1.3, it is straight-forward to show that (5.4) reduces to [35, Eq. (7)] for the independent and identically distributed diversity branches. Hence the MGF of the resultant signal power is given by

$$\phi_z(s) = \phi_x(s) F_x(\xi) + \int_{\xi}^{\infty} \exp(-su) f_x(u)\, du. \tag{5.13}$$

5.2 Optimization of the SWC Strategy

If the switching threshold ξ is set to be very large, then there will be constant switching between the two antennas because the probability of the received signal exceeding ξ will be small. In this case, the performance of SWC will be equivalent to the performance of a diversity branch selected in random, which resembles the behaviour for no diversity case. On the other extreme (i.e., the value of ξ is set to be very small), the SWC combiner will be stuck in one of the diversity branches because the likelihood of received signal power staying above the specified threshold increases. Once again, the performance of the SWC will be close to the single diversity branch case.

It is evident that the performance of switched diversity strategy is dependent on the selection of the switching threshold, and proper choice of ξ will minimize the average error probability. Hence in the following, we will derive analytical expressions that will allow us to compute the optimum switching threshold (in the minimum error rate sense) either in a closed-form (for identical fading statistics) or numerically (for nonidentical fading statistics) for a broad class for a broad class of digital modulation formats in arbitrary fading environments.

5.2.1 Correlated Fading and Nonidentical Diversity Branches

Differentiating (5.8) with respect to ξ, we get

$$\begin{aligned}\frac{\partial}{\partial \xi}\phi_z(s) &= A(\xi)\,[\phi_y(s,\xi) - \exp(-s\xi) f_x(\xi)] + B(\xi)\,[\phi_x(s) - \phi_y(s)] \\ &\quad + [1 - A(\xi)]\,[\phi_x(s,\xi) - \exp(-s\xi) f_y(\xi)] \\ &\quad + B(\xi)\int_0^{\xi}\left[\phi_y(s,u) - \phi_x(s,u) + \{f_y(u) - f_x(u)\}\exp(-su)\right]du \qquad (5.14)\end{aligned}$$

where $A(\xi)$ is defined in (5.6) and

$$B(\xi) = \frac{\partial}{\partial \xi}A(\xi) = \frac{F_x(\xi) f_y(\xi) - F_y(\xi) f_x(\xi)}{[F_x(\xi) + F_y(\xi)]^2}. \qquad (5.15)$$

Now our task is to find the optimum ξ^* that minimizes the ASER. This value can be determined by solving $\frac{\partial P_S}{\partial \xi} = 0$ for ξ. By differentiating (5.9) under the integral sign, and exploiting the results of (5.14), we have

$$\begin{aligned}\frac{dP_S}{d\xi} &= \sum_k \int_0^{\eta_k} a_k(\theta)\,[A(\xi)\,\phi_y(b_k(\theta),\xi) + \{1 - A(\xi)\}\,\phi_x(b_k(\theta),\xi)]\,d\theta \\ &+ B(\xi)\sum_k \int_0^{\eta_k} a_k(\theta)\left[\int_0^{\xi}\left[\phi_y(s,u) - \phi_x(s,u) + \{f_y(u) - f_x(u)\}\exp(-su)\right]du\right]d\theta \\ &+ B(\xi)\left[P_S^{(x)} - P_S^{(y)}\right] - P_S(\varepsilon|\,\xi)\,[A(\xi) f_x(\xi) + \{1 - A(\xi)\} f_y(\xi)] \qquad (5.16)\end{aligned}$$

where notation $P_S^{(x)}$ and $P_S^{(y)}$ correspond to the ASER of the diversity branch x (i.e., obtained by replacing $\phi_z(s)$ in (5.9) with $\phi_x(s)$) and y, respectively. For this general case, no closed-form solution for ξ^* exists. Therefore, this value will be determined numerically.

5.2.2 Independent Fading and Nonidentical Diversity Branches

If the diversity branches are assumed to be statistically independent, then we may replace the marginal MGFs in (5.16) with $\phi_y(s,u) = f_x(u)\,\phi_y(s)$ and $\phi_x(s,u) = f_y(u)\,\phi_x(s)$. Then it can be easily shown that the optimal threshold is obtained by solving the following expression:

$$\begin{aligned} A(\xi) f_x(\xi) P_S^{(y)} + \{1 - A(\xi)\} f_y(\xi) P_S^{(x)} + B(\xi)\left[F_x(\xi) P_S^{(y)} - F_y(\xi) P_S^{(x)}\right] \\ + B(\xi) \sum_k \int_0^{\eta_k} a_k(\theta) \left[\int_\xi^\infty \left[\{f_y(u) - f_x(u)\} \exp(-su)\right] du\right] d\theta \\ - P_S(\varepsilon|\,\xi)\,[A(\xi) f_x(\xi) + \{1 - A(\xi)\} f_y(\xi)] = 0. \end{aligned} \tag{5.17}$$

5.2.3 Independent Fading and Identical Diversity Branches

If both the diversity branches are assumed to be independent and identically distributed, then the PDF, CDF and MGF of x_n and y_n are interchangeable. Moreover, $A(\xi) = 1/2$ and $B(\xi) = 0$. In this case, (5.17) reduces to

$$P_S(\varepsilon|\,\xi) = P_S^{(x)} = P_S^{(y)} \tag{5.18}$$

where $P_S^{(x)}$ or $P_S^{(y)}$ corresponds to the ASER without diversity reception. Next we will identify three special cases of the conditional error probability $P_S(\varepsilon|\,\gamma)$ which lend themselves to closed-form formulas for the calculation of ξ^* in all common fading environments.

A. Exponential Form: $P_S(\varepsilon|\,\gamma) = a\exp(-b\gamma)$

The instantaneous BER of some noncoherent binary modulation schemes (e.g., DPSK and NCFSK) can be expressed in the exponential form. Then $P_S = a\phi_z(b)$ for the switched diversity receiver, and their corresponding optimum switching threshold is (directly from (5.18)),

$$\xi^* = \frac{-1}{b} \ln\left(\frac{P_S^{(x)}}{a}\right) = \frac{-\ln(\phi_x(b))}{b}. \tag{5.19}$$

Substituting $b = 1/2$ and using appropriate expression for $\phi_x(.)$, we arrive to the previous expressions for the optimum threshold of NCFSK in Nakagami-m [34, Eq. (14)] and Rician [35, Eq. (12)] fading channels, respectively.

B. $P_S(\varepsilon|\ \gamma) = a\text{erfc}(\sqrt{b\gamma})$

The ASER of some coherent binary modulation schemes (e.g., CPSK and CFSK) with SWC is given by $P_S = \frac{2a}{\pi}\int_0^{\pi/2}\phi_z(b\csc^2\theta)\,d\theta$. Using (5.18), we get

$$\xi^* = \frac{1}{b}\Big(\text{erfcinv}\big[P_S^{(x)}/a\big]\Big)^2 = \frac{1}{b}\Big(\text{erfcinv}\Big[\frac{2}{\pi}\int_0^{\pi/2}\phi_x(b\csc^2\theta)\,d\theta\Big]\Big)^2. \tag{5.20}$$

where erfcinv (.) denotes the inverse of the complementary error function.

C. $P_S(\varepsilon|\ \xi) = a\text{erfc}(\sqrt{b\xi}) - c\text{erfc}^2(\sqrt{b\xi})$

The ASER for square QAM, QPSK and coherent detection of differentially encoded PSK with SWC is given by $P_S = \frac{2a}{\pi}\int_0^{\pi/2}\phi_z(b\csc^2\theta)\,d\theta - \frac{4c}{\pi}\int_0^{\pi/4}\phi_z(b\csc^2\theta)\,d\theta$. By solving the quadratic problem $c\text{erfc}^2(\sqrt{b\xi}) - a\text{erfc}(\sqrt{b\xi}) + P_S^{(x)} = 0$ for ξ (i.e., Eq. (5.18)), we obtain a closed-form expression for the optimal switching threshold,

$$\xi^* = \frac{1}{b}\left\{\text{erfcinv}\left[\frac{a-\sqrt{a^2-4cP_S^{(x)}}}{2c}\right]\right\}^2. \tag{5.21}$$

For instance, the optimal switching threshold for the QPSK or the 4-QAM modulation scheme is given by

$$\xi^* = \left(\text{erfcinv}\left(2\left[1-\sqrt{1-P_S^{(x)}}\right]\right)\right)^2 \tag{5.22}$$

where $P_S^{(x)} = \frac{2}{\pi}\int_0^{\pi/2}\phi_x(\csc^2\theta)\,d\theta - \frac{1}{\pi}\int_0^{\pi/4}\phi_x(\csc^2\theta)\,d\theta$.

5.2.4 Correlated Fading and Identical Diversity Branches

If the assumption of branch independence is slightly relaxed, then we may only get the optimal ξ in a closed-form for the exponential form of $P_S(\varepsilon|\ \gamma)$ in correlated Rayleigh and/or correlated Nakagami-m fading channels. Following our treatment for the independent signal fading, the optimal switching threshold for the differentially coherent or the noncoherent binary modulation format is obtained by solving $\frac{\partial}{\partial \xi}\phi_{\underline{z}}(b) = 0$ for ξ:

$$\phi_x(b, \xi) - f_x(\xi) \exp(-b\xi) = 0. \tag{5.23}$$

Substituting the marginal MGF for the correlated Nakagami-m fading channel with identical mean received signal strength (see Table 5.1) in (5.23), we get

$$\xi^* = m\left[\frac{m + b\Omega(1-\rho)}{b(1-\rho)(m+b\Omega)}\right]\ln\left(1 + \frac{b\Omega(1-\rho)}{m}\right). \tag{5.24}$$

which is a generalization of Eq. (24) in [34] for the differentially coherent binary signalling scheme and for arbitrary m values. By setting the power correlation coefficient $\rho = 0$, (5.24) reduces to (5.19). For other modulation formats listed in Table 3.1, ξ^* is given by the unique real positive root of (5.25), which will be determined numerically:

$$\sum_k \int_0^{\eta_k} a_k(\theta)\, \phi_x(b_k(\theta), \xi)\, d\theta - f_x(\xi) P_S(\varepsilon|\ \xi). \tag{5.25}$$

5.3 Numerical Results

In this section, we provide selected numerical examples to show the generality of the new results derived in this chapter. The performance of the SWC (with optimum switching threshold) for different M-ary signalling constellations in Rayleigh and Rician fading channels are shown in Fig. 5.3. For the Rician fading channel, the CDF of signal power (for a single branch) is given by

$$F_i(\xi) = 1 - Q\left(\sqrt{2K_i}, \sqrt{2(1+K_i)\xi/\Omega_i}\right) \tag{5.26}$$

and

$$\lambda_i(\xi, s) = \int_{\xi}^{\infty} \exp(-su) f_i(u)\, du = \frac{1+K_i}{s\Omega_i + K_i + 1} \exp\left(\frac{-sK_i\Omega_i}{s\Omega_i + K_i + 1} \right) \times Q\left(\sqrt{\frac{2K_i(K_i+1)}{s\Omega_i + K_i + 1}}, \sqrt{\frac{2(s\Omega_i + K_i + 1)\xi}{\Omega_i}} \right) \quad (5.27)$$

where $i \in \{x, y\}$, and $Q(\sqrt{2a}, \sqrt{2b}) = \int_b^{\infty} \exp(-t-a) I_0(2\sqrt{at})\, dt$ is the Marcum-Q function.

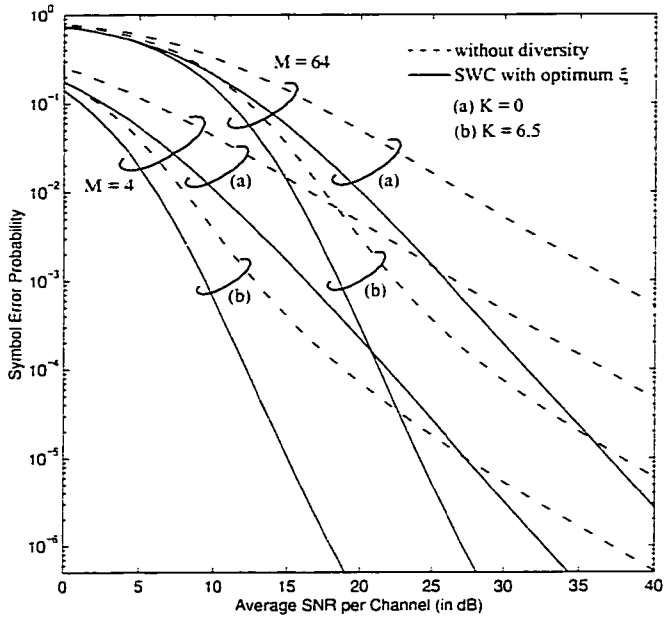

Fig. 5.3 Performance of MQAM with SWC in Rayleigh and Rician fading channels.

If the received signal envelopes from the two antennas are assumed to be independent and identically distributed, then $\Omega_i = \Omega$ and $K_i = K$. Substituting (5.26) and (5.27) into (5.13), we get a closed-form expression for $\phi_z(.)$, i.e.,

$$\phi_z(s) = \frac{1+K}{s\Omega + K + 1} \exp\left(\frac{-sK\Omega}{s\Omega + K + 1} \right) \times \left[1 - Q\left(\sqrt{2K}, \sqrt{\frac{2(1+K)\xi^*}{\Omega}} \right) + Q\left(\sqrt{\frac{2K(K+1)}{s\Omega + K + 1}}, \sqrt{\frac{2(s\Omega + K + 1)\xi^*}{\Omega}} \right) \right] \quad (5.28)$$

and the optimal threshold ξ^* is calculated using (5.21). For Rayleigh fading, (5.28) reduces to

$$\phi_z(s) = \frac{1}{s\Omega + 1}\left[1 - \exp(-\xi^*/\Omega) + \exp(-(s\Omega + 1)\xi^*/\Omega)\right] \tag{5.29}$$

since $Q(0, \beta) = \exp\left[-\beta^2/2\right]$.

From Fig. 5.3, it is apparent that the diversity reception is a simple yet powerful technique for mitigating the effect of deep fades experienced in wireless channels. For instance, the dual-branch SWC system can reduce the penalty in the required SNR to achieve an error rate of $P_S = 10^{-3}$ for the 64-QAM by approximately 11 dB in a Rayleigh fading channel with respect to the no diversity case. The diversity advantage is greater for a larger alphabet size and in a poorer channel condition (i.e., as $K \to 0$), as anticipated.

In Fig. 5.4, we examine the effect of power imbalance on the performance of BDPSK with SWC on a Rayleigh fading channel. Using (5.11) and (5.27), we can express the ABER as

$$\begin{aligned} P_S &= \frac{1}{2}\phi_z(1) \\ &= \frac{A(\xi^*)}{2}\left[\frac{F_x(\xi^*)}{\Omega_y + 1} + \lambda_x(\xi^*, 1)\right] + \frac{1 - A(\xi^*)}{2}\left[\frac{F_y(\xi^*)}{\Omega_x + 1} + \lambda_y(\xi^*, 1)\right] \end{aligned} \tag{5.30}$$

where

$$F_i(\xi) = 1 - \exp(-\xi/\Omega_i) \tag{5.31}$$

and

$$\lambda_i(\xi, 1) = \frac{1}{\Omega_i + 1}\exp\left(\frac{-\xi(\Omega_i + 1)}{\Omega_i}\right) \tag{5.32}$$

are obtained by setting $K = 0$ and $s = 1$ in (5.26) and (5.27). The optimum switching threshold is given by the real positive root of (5.33):

$$A(\xi)f_x(\xi)\left[\frac{1}{\Omega_y+1}\exp(-\xi)\right]+[1-A(\xi)]f_y(\xi)\left[\frac{1}{\Omega_x+1}\exp(-\xi)\right]$$
$$+B(\xi)\left[\frac{F_x(\xi)}{\Omega_y+1}-\frac{F_y(\xi)}{\Omega_x+1}+\lambda_x(\xi,1)-\lambda_y(\xi,1)\right]=0 \qquad (5.33)$$

where $A(\xi)$ and $B(\xi)$ are defined in (5.6) and (5.15), respectively.

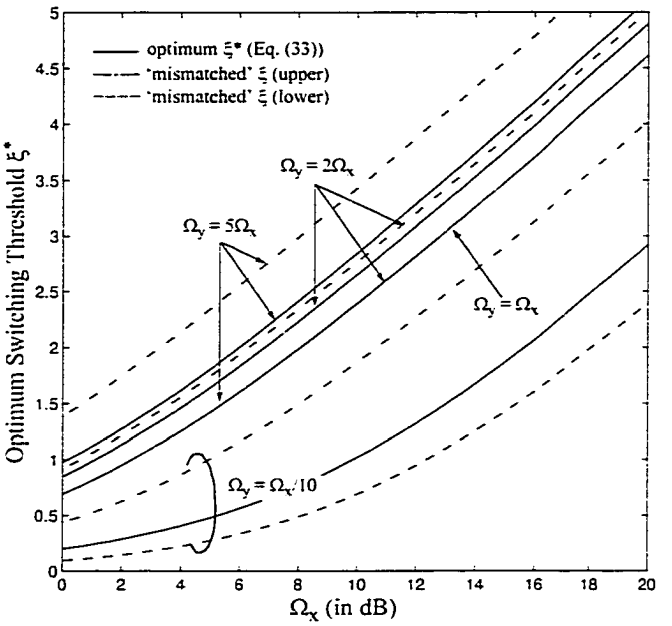

Fig. 5.4(a) Effects of power imbalance on the optimal switching threshold for BDPSK in a Rayleigh fading channel.

In Fig. 5.4(a), the optimum switching threshold is plotted as a function of Ω_x for the following four cases: (i) $\Omega_y = \Omega_x$; (ii) $\Omega_y = 2\Omega_x$; (iii) $\Omega_y = 5\Omega_x$; and (iv) $\Omega_x = 10\Omega_y$. We find that the optimum threshold (corresponding to the solid-line curves) decreases rapidly as the ratio Ω_y/Ω_x decreases. This trend can be explained by noting that when the power imbalance between the two diversity branches increases, then a lower threshold level is desirable so that the switched combiner will have an increased likelihood of choosing and staying in a "good" branch. Furthermore, a very large value for ξ only results in performance degradation due to bad switchings.

The optimal switching threshold for the independent and identically distributed (i.i.d.) case can be determined in closed-form for three different forms of conditional error probability, as derived in Section 5.2.3. For these cases, is also desirable if we can provide an estimate of ξ^* in a closed-form for the nonidentical fading statistics situation. Exploiting the trends from Fig. 5.4(a) and using (5.19), it is possible to bound the optimal threshold for the exponential form as

$$-\ln [\phi_{AL}(b)] / b \leq \xi^* \leq -\ln [\phi_{AU}(b)] / b \tag{5.34}$$

where $\phi_{AL}(.) = max \{\phi_x(.), \phi_y(.)\}$ (which corresponds to the MGF of the "weaker" branch), and the mean signal power used in $\phi_{AU}(.)$ is the average of signal power received from the two diversity branches, i.e., $\Omega_{AU} = (\Omega_x + \Omega_y)/2$. These bound are also plotted in Fig. 5.4(a). All the three curves coincide when $\Omega_y = \Omega_x$ and the optimal threshold is much closer to the upper limit if $0.25 < \Omega_y/\Omega_x < 4$, and the lower limit otherwise. It is also noted that the lower limit of the optimal threshold for case (ii) and (iii) is given by ξ^* of the i.i.d. case. We have also verified that the optimal threshold obtained using (5.19) and (5.33) are identical for case (i). Expressions similar to (5.34) can be easily derived for $P_S(\varepsilon|\gamma)$ in the form of a 1-D complementary error function or a combination of 1-D and 2-D complementary error functions.

In Fig. 5.4(b), we investigate the sensitivity of the ABER to the 'mismatch' in the switching threshold level. The solid and the dashed or the dash-dot curves correspond to the optimal threshold (calculated using (5.33)) and the threshold level predicted using (5.34), respectively. While there can be a noticeable difference in the switching threshold levels (e.g., see the curves corresponding to $\Omega_y = 2\Omega_x$ and $\Omega_y = 5\Omega_x$ in Fig. 5.4(a)), the ABER performance appears to be not too sensitive to this variation. In fact, we find that the lower bound given in (5.34) can be viewed as a good coarse approximation of ξ^*, and therefore attractive for rapid computation of the ASER or ABER. The discrepancy between the true and approximate ABER curves becomes appreciable only when the mean received signal power imbalance is very large.

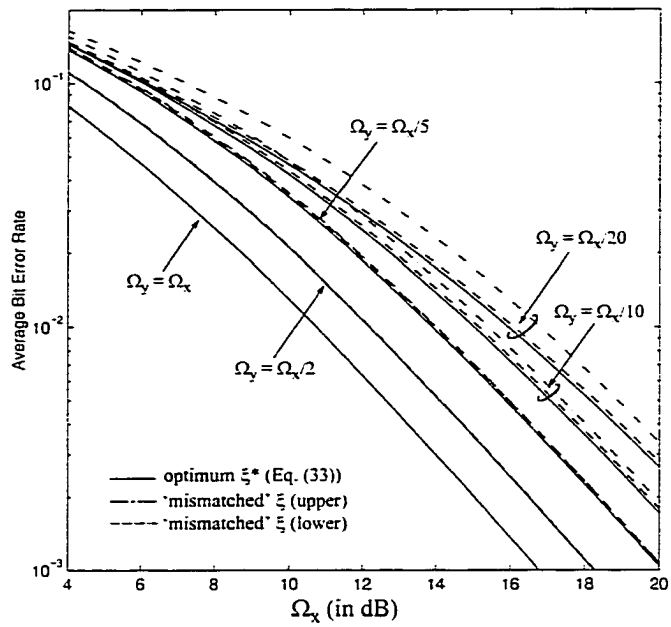

Fig. 5.4(b) Sensitivity of the average bit error rate performance of BDPSK to the mismatch in the optimal switching threshold on a Rayleigh fading channel.

Subsequently in Fig. 5.5, we study the effect of dissimilar fading severity index ($K_y \neq K_x$) on the performance of 8-PSK with SWC. The corresponding ASER of MPSK can be easily shown to be

$$P_S = \int_0^{\pi-\pi/M} \phi_z\left(\frac{\sin^2(\pi/M)\log_2 M}{\sin^2\theta}\right) d\theta \tag{5.35}$$

where $\phi_z(.)$ is obtained by substituting (5.26) and (5.27) into (5.11), and then setting $\Omega_i = \Omega$. From Fig. 5.5, we can conclude that the optimal switching threshold and the ASER are not severely affected by unequal fading index unless the perturbation is very large. Once again the optimum switching threshold point shifts to the left as the discrepancy between K_x and K_y gets larger. Now look at the $P_S^{(x)}$, $P_S^{(y)}$ and the SWC curves corresponding to case (c) with Ω = 10 dB. While the SWC will always perform better than any of the two identical diversity branches for the entire region of ξ (see the curves for case (a)), this may not be necessarily true if the branch statistics are not identical. If

ξ is chosen to be very large, the performance of SWC will be dictated by the average performance of the two diversity branches (due to the random switching). On the other extreme (i.e., ξ is set to a very small value), the SWC closely resembles the performance of the branch with better statistics. For the cases (b) and (c), we observe that the performance of SWC is actually slightly worse than $P_S^{(x)}$ as $\xi \to 0$. This is because there is always a finite probability that the "weaker" branch will be selected and the averaging of the error performance contribute to this phenomena. Comparison between the curves for case (b) and case (c) reveal that this gap actually diminishes as the difference between the fading severity indexes gets larger, as anticipated.

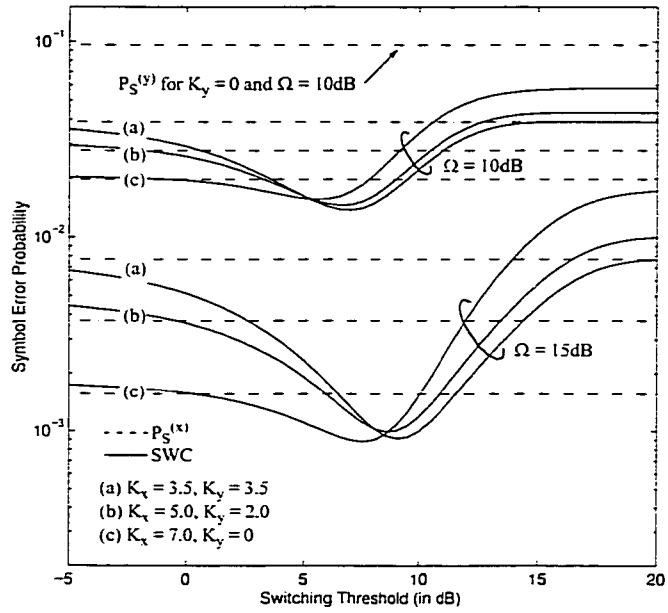

Fig. 5.5 Effects of nonidentical fading severity index on the optimal switching threshold level and the SER performance of 8-PSK signalling scheme.

In Fig. 5.6, we quantify the switched diversity receiver performance degradation due to branch correlation for the BDPSK modulation scheme. We have assumed both the diversity branches have equal mean received signal strength to isolate its effect on the ABER performance. For the correlated Nakagami-m channel, it is more convenient to rewrite (5.12) as (5.36) since both the integrals can be directly expressed in terms of the

incomplete Euler integrals:

$$\begin{aligned}\phi_z(s) &= \int_{\xi}^{\infty} \exp(-sY) f_y(Y)\, dY + \int_0^{\xi} \phi_x(s, Y)\, dY \\ &= \frac{1}{\Gamma(m)}\left(\frac{m}{m+s\Omega}\right)^m \left[\Gamma[m, \xi(s+m/\Omega)] + \gamma\left(m, \frac{\xi(s+m/\Omega)}{1+s\Omega(1-\rho)/m}\right)\right]\end{aligned} \tag{5.36}$$

where $\gamma(a, x) = \int_0^x \exp(-t)\, t^{a-1} dt,\ a > 0$ is the incomplete Gamma function, and its companion is defined as $\Gamma(a, x) = \Gamma(a) - \gamma(a, x) = \int_x^{\infty} \exp(-t)\, t^{a-1} dt$ (known as the complementary incomplete Gamma function). Now substituting (5.24) and (5.36) into (5.9), we get a simple closed-form expression for calculating the ABER of BDPSK with optimal switching threshold, namely $P_S = 0.5\phi_z(1)$. When the power correlation coefficient ρ increases, the switched diversity receiver performance degrades due to the increased likelihood of simultaneous deep signal fades at the branch inputs.

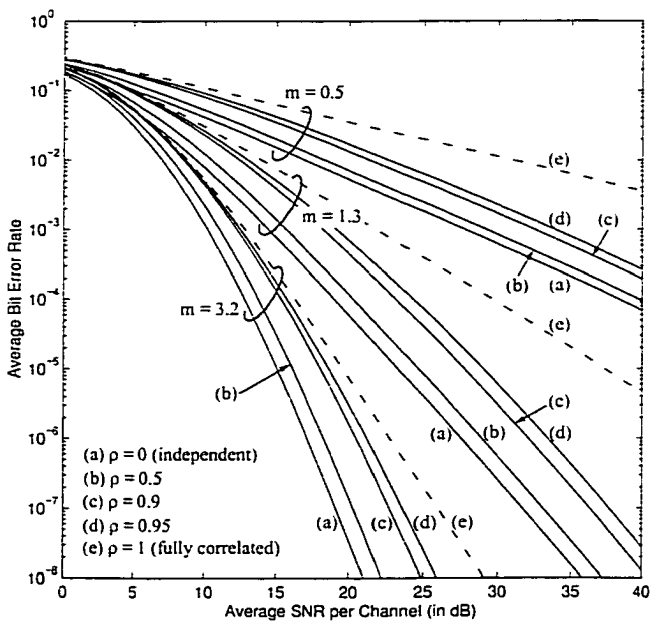

Fig. 5.6 Effect of branch correlations on the attainable switched diversity gain for BDPSK modulation format in Nakagami-m fading channels.

From Fig. 5.6, we can also conclude that the low branch correlation has negligible effect of the achievable diversity gain and the average SER performance does not seriously deteriorate unless $\rho \gg 0.5$. Even with a high value of correlation a significant diversity improvement can still be realized, particularly in channels that experience severe deep fades. For instance, the diversity gain in a Nakagami-m fading channel with fading index $m = 1.3$ is more than 9 dB and 6 dB at $P_S = 10^{-4}$ for $\rho = 0.5$ and $\rho = 0.9$, respectively. When the two branches are completely correlated, the ABER curve for SWC collapses to the no diversity case as expected.

Finally in Fig. 5.7, the ASER of $\pi/4$-DQPSK are plotted as a function of switching threshold for the correlated Rayleigh and Nakagami-m fading channels with nonidentical mean received signal strength. Using (5.8) and (5.9), and then following the development of (5.36), we can express the corresponding exact ASER in terms of a single integral with finite integration limits,

$$P_S = \frac{1}{2\pi}\int_0^{\pi} \frac{\phi_{\pm}(2-\sqrt{2}\cos\theta)}{\sqrt{2}-\cos\theta}\,d\theta = \frac{1}{2\pi}\int_0^{\pi} \phi_{\pm}\left(\frac{2}{2-\sqrt{2}\cos\theta}\right)d\theta \tag{5.37}$$

where $\phi_{\pm}(.)$ is now given by

$$\phi_{\pm}(s) = \frac{A(\xi)\,\Gamma[m, \xi(s+m/\Omega_x)] + [1-A(\xi)]\,\gamma\left[m, \dfrac{m\xi(m+s\Omega_x)}{\Omega_y(m+s\Omega_x(1-\rho))}\right]}{\Gamma(m)\,(1+s\Omega_x/m)^m}$$

$$+ \frac{[1-A(\xi)]\,\Gamma[m, \xi(s+m/\Omega_y)] + A(\xi)\,\gamma\left[m, \dfrac{m\xi(m+s\Omega_y)}{\Omega_x(m+s\Omega_y(1-\rho))}\right]}{\Gamma(m)\,(1+s\Omega_y/m)^m} \tag{5.38}$$

and $A(\xi)$ is evaluated using (5.6) with $F_i(\xi) = \gamma(m, m\xi/\Omega_i)/\Gamma(m)$ for $i \in \{x, y\}$. The second integral in (5.37) can be obtained from the first integral through geometric relations (see Eq. (10) in [38]). While ξ^* increases as the channel condition improves (i.e., the optimum threshold level in Figs. 5.7(a) and 5.7(b) shifts to the right of the x-axis as m increases), it declines as ρ gets larger. Fig. 5.7(a) also reveals that high branch correlation levels can seriously deteriorate the ASER performance in the presence

of power imbalance, specifically if the fading severity index is large. For instance, the SWC exhibits an inferior performance compared to the diversity branch y alone even at the optimum switching threshold when $\rho = 0.8$, $\Omega_x = 12dB$ and $\Omega_y = 15dB$.

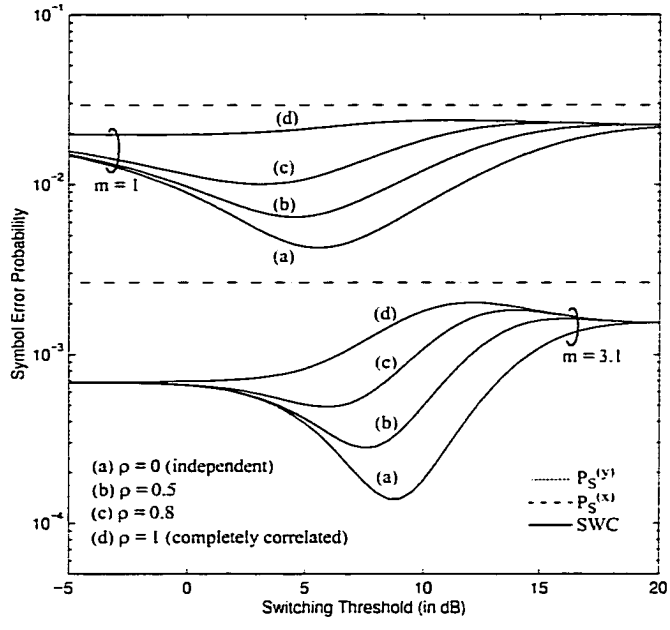

Fig. 5.7(a) Sensitivity of the ASER of π/4-DQPSK and the optimal switching threshold level to the branch correlations in the presence of dissimilar mean received signal strengths Ω_x = 12 dB and Ω_y = 15 dB.

It is also interesting to note that the optimal switching threshold remains almost unaffected despite a large deviation in the mean received signal strength across the diversity branches (see Fig. 5.7(b)). This in turn suggests that we can estimate ξ^* for the power imbalance case by computing the optimal threshold for the identical branches with $\Omega = min\{\Omega_x, \Omega_y\}$. This observation also validates the usefulness of the idea established in (5.34) for rapid calculation of the approximate ASER for several modulation formats (i.e., if a closed-form formula for computing ξ^* is available) when the restriction of identical fading statistics is relaxed.

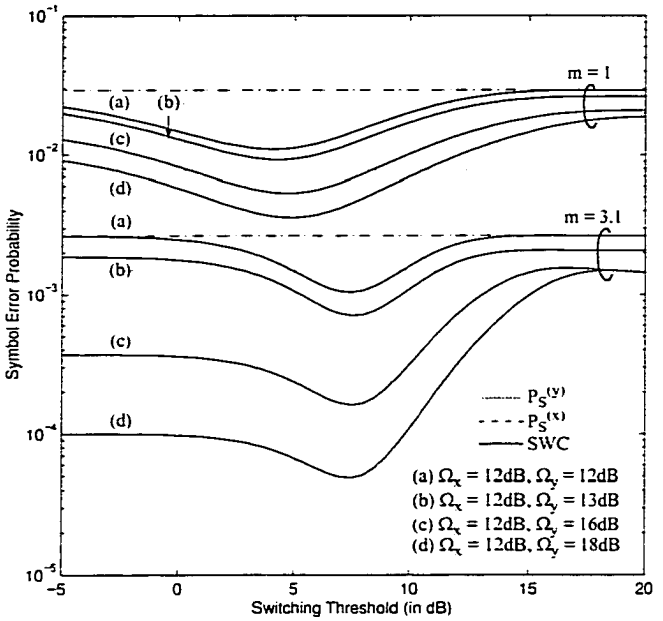

Fig. 5.7(b) Effects of unequal mean received signal strength on the ASER performance of π/4-DQPSK and the optimal switching threshold level when $\rho = 0.5$.

5.4 Conclusions

In this chapter, we outline a concise, unified approach for evaluating SWC receiver performance for a wide range of modulation formats and fading environments by directly deriving the MGF of SNR at the combiner output. The derivative of the MGF is used to determine the optimal (in the minimum error rate sense) switching threshold. Results of [34]-[36] are presented as special cases of our analysis. Closed-form expressions for the optimal switching threshold are derived for three generic forms of conditional SER probability by assuming identical fading statistics across the statistically independent diversity branches. When the effect of branch correlation is taken into account, a closed-form formula for the optimal switching threshold is only available for the exponential form of conditional error probability in Rayleigh and Nakagami-m fading channels with equal mean received signal strength.

Chapter 6

Analysis of Selection Diversity in Bivariate Nakagami Fading

The error performance of dual-diversity SCs over correlated Rayleigh and/or Nakagami-m fading channels has been analyzed by many authors (e.g., [21], [67]-[71]). The recent work of Simon and Alouini [71] has rekindled the interest in this topic. In [71], the authors differentiate an integral representation for the cumulative distribution to get the PDF. Their resulting expressions depend on the branch power ratios and the power correlation coefficient ρ [71, Eq. (3)]. They then use the PDF to average the conditional error probability for different modulation formats. Alternatively, if one derives the SC output MGF first, the performance of a broad class of modulation formats can be obtained at once. Previously, Okui [67] derived a Gauss hypergeometric series for the MGF of the SC output signal-to-noise ratio (SNR). However, his result [67, Eq. (7)] holds for the case of equal average SNRs only. Fedele *et. al.* [69] generalize the results in [67] by considering the effect of dissimilar mean received signal strengths.

Motivated by Simon and Alouini's work and the fact that SC output MGF is the key to the performance analysis, we attempted to derive closed-form solutions for the average symbol error probability of binary noncoherent and differentially coherent modulation formats using an approach similar to that of [71] -- which utilizes certain integral representations of $Q_m(a, b)$. These take different forms depending on $a > b$, $a = b$ or

$a < b$ [72, 73]. During our attempt, we have discovered a number of related results which are worthy of reporting. Our results provide some new insights and supplement [67, 69, 71]. Our major results and comments are as follows:

(a) Using the integral representation of $Q_m(a, b)$ [72], an *exact closed-form* expression for the MGF of SC output in correlated Nakagami-m fading for positive integer m can be derived. As shown in Appendixes 6B-6D, this however leads to fairly long expressions, which are somewhat complicated from a programming point of view.

(b) We became aware of a circular contour integral representation for the generalized Marcum-Q function [12]. Interestingly, unlike [72] or [73], it is valid whether $a > b$, $a = b$ or $a < b$. As well, it encapsulates the modified bessel series expansions for $Q_m(a, b)$, which are used in [72, 73]. Therefore, not surprisingly, we show that the representations due to both Simon [72] and Helstrom [73] follow from this contour representation. We also derive a new, single integral representation for $Q_m(a, b)$ that is valid for $a > b$, $a = b$ or $a < b$.

(c) We have used this contour representation to derive exact closed-form expression for the SC output MGF in correlated Nakagami-m fading for positive integer m. Unlike [71], the resulting formula applies regardless of the values of the branch power ratios and ρ. For instance, the independent fading case can be treated directly by setting $\rho = 0$. Therefore, it leads to a compact, unified analysis of a broad class of modulation formats for dual-diversity SC in Nakagami-m fading.

(d) We also derive an infinite series formula for the SC output MGF with non-integer m.

(e) We show that Okui's ${}_2F_1(.,.;.;.)$ formula can be reduced to a finite series for the case of integer m and for $m = 1/2$.

In Section 6.1, we first introduce the circular contour integral representation for the generalized Marcum-Q function, and subsequently show that the alternative integral representations for $Q_m(a, b)$ due to Helstrom, and then later by Simon can be easily obtained from this representation by proper variable substitution. Section 6.2 details the

derivation of the SC output MGF for both integer and non-integer fading severity indexes in bivariate Nakagami-m fading. In Section 6.3, we present several generic expressions for calculating the average bit or symbol error probability of a broad class of modulation formats for a dual-diversity SC. The average error rate is expressed either in a closed-form (e.g., for binary signalling with differentially coherent or noncoherent detection schemes) or in terms of a single integral with finite integration limits. Finally, the main points are summarized in Section 6.4.

6.1 Integral Representations for $Q_m(a, b)$

Proakis [12, pp. 885] provides the contour integral representation for the generalized Marcum-Q function,

$$Q_m(a, b) = \frac{1}{2\pi j} \oint_{\Gamma} \frac{e^{g(z)}}{z^m (1-z)} dz \tag{6.1}$$

where $g(z) = a^2 (1/z - 1)/2 + b^2 (z-1)/2$ and Γ is a circular contour of radius r that encloses origin. The singularities of the integrand are at $z = 0$ and $z = 1$. Therefore, by Cauchy's theorem we can choose any $0 < r < 1$. Now if we choose $r = 1$, then we need to remove the singularity at $z = 1$ on Γ by suitably deforming Γ (see Fig. 6.1b). This representation holds regardless of $a > b$, $a = b$ or $a < b$, and for any positive integer m. In the following, we will show that both Helstrom's [73] and Simon's [72] integral representations readily follow from (6.1) for integer values of m.

(i) Consider the case $a < b$ (see Fig. 6.1a) where the circular contour Γ encloses origin with a radius less than unity. Therefore, z in (6.1) can be written as $z = re^{j\theta}$ with $r < 1$ and $0 \le \theta < 2\pi$. Now select $r = a/b$, so we immediately get

$$Q_m(a, b) = \frac{e^{-a^2/2 - b^2/2}}{2\pi} \left(\frac{b}{a}\right)^m \int_0^{2\pi} \frac{e^{ab\cos\theta - j(m-1)\theta}}{\left[b/a - e^{j\theta}\right]} d\theta, \quad m \in Z \tag{6.2}$$

where Z is the set of positive integers. Taking the magnitude of the integrand, we obtain the new bound

$$Q_m(a,b) \le e^{-(a-b)^2/2}\left(\frac{b}{a}\right)^m \frac{a}{\sqrt{a^2+b^2}} \tag{6.3}$$

which holds for any integer $m \ge 1$, whereas the bound due to Simon [72, Eq. (12)] holds only for $m = 1$.

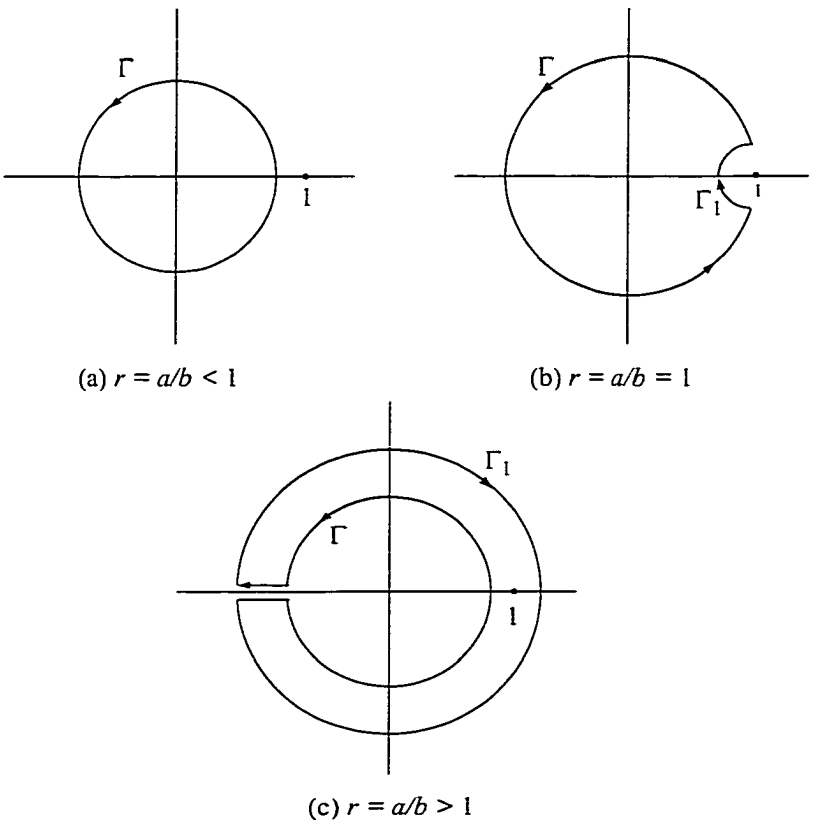

Fig. 6.1 Contours of a line integral for: (a) $r < 1$; (b) $r = 1$; and (c) $r > 1$.

(ii) Consider the case $a = b$ (see Fig. 6.1b). Now $g(z) = a^2(z + 1/z)/2 - a^2$ and Γ as shown in Fig. 6.1b. Hence,

$$Q_m(a,b) = \frac{e^{-a^2}}{2\pi}\int_{\varepsilon}^{2\pi-\varepsilon}\frac{e^{a^2\cos\theta - j(m-1)\theta}}{\left[1-e^{j\theta}\right]}d\theta + \frac{1}{2\pi j}\oint_{\Gamma_1}\frac{e^{g(z)}}{z^m(1-z)}dz \tag{6.4}$$

where Γ_1 is the half-circle contour centered on $z = 1$ with radius ε. On Γ_1, $z = 1-\varepsilon e^{j\alpha}$ and $-\pi/2 \le \alpha \le \pi/2$. Taking the real value of the first integral on the right hand side and letting $\varepsilon \to 0$, we obtain

$$Q_m(a,b) = \frac{1}{2}\int_0^{2\pi} e^{-a^2(1-\cos\theta)}\frac{\sin\left[(m-1/2)\,\theta\right]}{\sin(\theta/2)}\frac{d\theta}{2\pi} + \frac{1}{2}, \quad m \in Z \tag{6.5}$$

This result (i.e., Eq. (6.5)) is in fact identical to [73, pp. 528] derived by Helstrom.

(iii) If $a > b$, $r = a/b$ is greater than unity. So we need to consider the closed contour shown in Fig. 6.1c. The inner circle Γ has a radius less than unity, while the outer circle Γ_1 has a radius of a/b. Inside the closed contour, the only singularity of the integrand occurs at $z = 1$. Hence using Cauchy's theorem, we find

$$\frac{1}{2\pi j}\oint_{\Gamma}\frac{e^{g(z)}}{z^m(1-z)}dz + \frac{1}{2\pi j}\oint_{\Gamma_1}\frac{e^{g(z)}}{z^m(1-z)}dz = \lim_{z=1}\frac{e^{g(z)}}{z^m} \tag{6.6}$$

The first integral is $Q_m(a,b)$ and $z = (a/b)e^{j\theta}$ on Γ_1. Therefore, we get

$$Q_m(a,b) - 1 = \frac{e^{-a^2/2-b^2/2}}{2\pi}\left(\frac{b}{a}\right)^m\int_0^{2\pi}\frac{e^{ab\cos\theta - j(m-1)\theta}}{\left[b/a - e^{j\theta}\right]}d\theta, \quad m \in Z \tag{6.7}$$

Note that (6.2) and (6.7) are identical to Helstrom's results [73], except the integrands are in a complex format, and hence are slightly more compact. Since the integrals are real-valued, taking the real parts of the integrands in (6.2) and (6.7) gives the exact same integral representations of Helstrom.

Similarly, Simon's results [72, 40] are very closely related. For instance, consider the $a < b$ case. As in the derivation of (6.2), we can select $z = (a/b)je^{j\theta}$. Note that the magnitude of z is still less than unity, i.e., $|z| < 1$. Hence using this new substitution in (6.1), we find

$$Q_m(a,b) = \frac{e^{-a^2/2-b^2/2}}{2\pi}\left(\frac{b}{a}\right)^m \int_0^{2\pi} \frac{e^{-ab\sin\theta - j(m-1)\,[\theta+\pi/2]}}{\left[b/a - je^{j\theta}\right]} d\theta, \quad m \in Z \tag{6.8}$$

Again, this representation is very compact, yet it is identical to [72, Eq. (7)], [72, Eq. (10)] and [40, Eq. (14a)].

6.1.1 Yet Another Simple Integral Representation for $Q_m(a,b)$

While the contour in Fig. 6.1b is used for the $a = b$ case, it can also be used when $a \neq b$. Therefore, if we use $z = e^{j\theta}$ in (6.1) along with the contour in Fig. 6.1b, we may obtain a new integral representation for the generalized Marcum-Q function. Now $g(z) = \frac{1}{2}\left(a^2+b^2\right)[\cos\theta - 1] + \frac{j}{2}\left(b^2-a^2\right)\sin\theta$. Hence,

$$Q_m(a,b) = \frac{1}{2\pi}\int_{\varepsilon}^{2\pi-\varepsilon} \frac{e^{\frac{1}{2}\left[a^2+b^2\right](\cos\theta - 1 - j\sin\theta) - j(m-1)\theta}}{\left[1-e^{j\theta}\right]} d\theta + \frac{1}{2\pi j}\oint_{\Gamma_1} \frac{e^{g(z)}}{z^m(1-z)} dz \tag{6.9}$$

Taking the real value of the first integral on the right hand side and letting $\varepsilon \to 0$, we obtain

$$\begin{aligned} Q_m(a,b) &= \frac{1}{2} + \frac{1}{2}\int_0^{2\pi} \frac{e^{\frac{1}{2}(\cos\theta - 1)\left[a^2+b^2\right]}}{1-\cos\theta}\psi(\theta)\frac{d\theta}{2\pi} \\ &= \frac{1}{2} + \frac{1}{4\pi}\int_0^{2\pi} e^{-\sin^2(\theta/2)\left[a^2+b^2\right]} \frac{\sin\left[\dfrac{(2m-1)\theta + \left[a^2-b^2\right]\sin\theta}{2}\right]}{\sin(\theta/2)} d\theta \end{aligned} \tag{6.10}$$

where $\psi(\theta) = \cos\left[(m-1)\theta + \frac{1}{2}\left(a^2-b^2\right)\sin\theta\right] - \cos\left[m\theta + \frac{1}{2}\left(a^2-b^2\right)\sin\theta\right]$ and $m \in Z$. To the best of our knowledge, the above expression is *new*, and it holds for $a < b$, $a = b$ or $a > b$. Also notice that if $a = b$, (6.10) reduces to (6.5).

Since the integrand in (6.10) contains a factor $\left[a^2-b^2\right]$ inside the sin (.) term, it is not

suitable for the average error rate analysis of noncoherent digital communication systems over fading channels where $a = a'\sqrt{\gamma}$, $b = b'\sqrt{\gamma}$ and a' and b' are modulation format dependent constants. In this case, further averaging over the distribution of γ is necessary. However, it can be utilized to obtain very concise outage expressions.

6.2 Derivation of the MGF of SNR at the Output of a Dual-Branch SC Combiner

The joint probability density function (PDF) of the bivariate Nakagami-m fading is given by [74],

$$f(x,y) = \frac{4(xy)^m}{\Gamma(m)\Omega_1\Omega_2(1-\rho)\left(\sqrt{\Omega_1\Omega_2\rho}\right)^{m-1}} \times \exp\left(\frac{-1}{1-\rho}\left[\frac{x^2}{\Omega_1}+\frac{y^2}{\Omega_2}\right]\right) I_{m-1}\left(\frac{2\sqrt{\rho}xy}{\sqrt{\Omega_1\Omega_2}(1-\rho)}\right) \tag{6.11}$$

where $x \geq 0$, $y \geq 0$, $\rho = cov[x^2, y^2]/\sqrt{var[x^2]\,var[y^2]}$, $\rho \neq 0, 1$, $\Omega_1 = \{\overline{x^2}/m\}$, $\Omega_2 = \{\overline{y^2}/m\}$ and m is a positive number greater than $1/2$.

Then the CDF of signal envelope at the output of SC combiner is

$$F(r) = \int_0^r \int_0^r f(x,y)\,dxdy. \tag{6.12}$$

Now differentiating (6.12) with respect to r, we obtain the PDF of the signal envelope,

$$f(r) = \int_0^r f(x,r)\,dx + \int_0^r f(r,y)\,dy. \tag{6.13}$$

From the definition of the m-th order generalized Marcum-Q function [12],

$$Q_m(a,b) = 1 - \int_0^b x\left(\frac{x}{a}\right)^{m-1} \exp\left(\frac{-x^2-a^2}{2}\right) I_{m-1}(ax)\,dx \tag{6.14}$$

we can show that

$$\int_0^b x^m \exp\left(-cx^2\right) I_{m-1}(ax)\,dx = \frac{a^{m-1}}{(2c)^m}\exp\left(\frac{a^2}{4c}\right)\left[1-Q_m\left(a/\sqrt{2c}, b\sqrt{2c}\right)\right] \quad (6.15)$$

if $a>0$, $b>0$ and $c>0$.

Substituting (6.11) into (6.13) and using identity (6.15), we get

$$\begin{aligned} f(r) &= \psi_2(r)\left[1-Q_m\left(r\sqrt{\frac{2\rho}{(1-\rho)\Omega_2}}, r\sqrt{\frac{2}{(1-\rho)\Omega_1}}\right)\right] \\ &\quad + \psi_1(r)\left[1-Q_m\left(r\sqrt{\frac{2\rho}{(1-\rho)\Omega_1}}, r\sqrt{\frac{2}{(1-\rho)\Omega_2}}\right)\right] \end{aligned} \quad (6.16)$$

where $\psi_j(r) = \dfrac{2r^{2m-1}}{\Gamma(m)\Omega_j^m}\exp\left(\dfrac{-r^2}{\Omega_j}\right), j \in \{1,2\}$, is introduced for ease of notation.

Now, the desired MGF may be evaluated as

$$\phi(s) = \int_0^\infty \exp\left(-sr^2\right) f(r)\,dr. \quad (6.17)$$

6.2.1 Integer Fading Severity Index

Clearly, the solution to the definite integral (6.18) is required to solve our problem on hand:

$$\begin{aligned} I_m(p,a,b) &= \int_0^\infty x^{2m-1}\exp\left(-px^2\right)\left[1-Q_m(ax,bx)\right]dx \\ &= \frac{\Gamma(m)}{2p^m} - \int_0^\infty x^{2m-1}\exp\left(-px^2\right)Q_m(ax,bx)\,dx \end{aligned} \quad (6.18)$$

where Real $\{p\} > 0$. From (6.1), we have

$$Q_m(ax,bx) = \frac{1}{2\pi j}\oint_\Gamma \frac{\exp\left[x^2 g(z)\right]}{z^m(1-z)}dz \quad (6.19)$$

where $g(z) = a^2(1/z-1)/2 + b^2(z-1)/2$ and Γ is a circular contour of radius less than unity that encloses origin. This representation holds regardless of $a>b$, $a=b$ or $a<b$.

Now substituting (6.19) into (6.18) and performing the integration with respect to x first (changing the order of integration is valid because both the integrals are convergent), we find

$$I_m(p,a,b) = \frac{\Gamma(m)}{2}\left[\frac{1}{p^m} - \frac{1}{2\pi j}\oint_\Gamma \frac{dz}{(1-z)\,z^m\,[p-g(z)]^m}\right] \tag{6.20}$$

which can be rewritten as

$$I_m(p,a,b) = \frac{\Gamma(m)}{2}\left[\frac{1}{p^m} - \left(\frac{-2}{b^2}\right)^m \frac{1}{2\pi j}\oint_\Gamma \frac{dz}{(1-z)\left[z^2-\alpha_0 z+\alpha_1\right]^m}\right] \tag{6.21}$$

where $\alpha_0 = \left(2p+a^2+b^2\right)/b^2$ and $\alpha_1 = (a/b)^2$. The denominator of the integrand in (6.21) has two positive roots, namely

$$\begin{bmatrix} r_1 \\ r_2 \end{bmatrix} = \frac{1}{2}\left[\alpha_0 \mp \sqrt{\alpha_0^2 - 4\alpha_1}\right] = \frac{2p+a^2+b^2 \mp \sqrt{\left[2p+(a+b)^2\right]\left[2p+(a-b)^2\right]}}{2b^2}.$$

It can be easily shown that $0 < r_1 < 1$ and $r_2 > 1$. Therefore, applying the residue theorem, we get

$$I_m(p,a,b) = \frac{\Gamma(m)}{2}\left[\frac{1}{p^m} - \left(\frac{2}{b^2}\right)^m \frac{d^{(m-1)}}{dz}\left\{\frac{1}{(1-z)\,(r_2-z)^m}\right\}\Bigg|_{z=r_1}\right]. \tag{6.22}$$

Now invoking the Liebnitz' differentiation rule [52, (0.42)]

$$\frac{d^{(n)}}{dx}(uv) = \sum_{k=0}^{n} \frac{n!}{(n-k)!\,k!}\frac{d^{(k)}}{dx}(u)\frac{d^{(n-k)}}{dx}(v), \tag{6.23}$$

and after simplifications, we obtain a closed-form solution for $I_m(p,a,b)$:

$$I_m(p,a,b) = \frac{\Gamma(m)}{2}\left\{\frac{1}{p^m} - \frac{(2b)^{2m}}{[Y(Y-X)]^m}\sum_{k=0}^{m-1}\frac{\Gamma(m+k)}{k!\,\Gamma(m)}\left[\frac{1}{2}(1-X/Y)\right]^k\right\} \tag{6.24}$$

where $X = 2p+a^2-b^2$ and $Y = \sqrt{\left[2p+(a+b)^2\right]\left[2p+(a-b)^2\right]}$.

Obviously (6.24) holds only for integer m. Besides, we would like to point out that (6.24) is equivalent to [67, Eq. (6)] but simpler than the latter. Therefore, the MGF of SNR at the SC combiner output in bivariate Nakagami fading can be conveniently evaluated using expression (6.25):

$$\begin{aligned}\phi(s) &= \sum_{i=1, j\neq i}^{2} \frac{2}{\Gamma(m)\,\Omega_i^m} I_m\left(s+\frac{1}{\Omega_i}, \sqrt{\frac{2\rho}{(1-\rho)\,\Omega_i}}, \sqrt{\frac{2}{(1-\rho)\,\Omega_j}}\right) \\ &= \sum_{i=1, j\neq i}^{2} \left\{ \frac{1}{(1+s\Omega_i)^m} - \frac{(2A_{ij})^{2m}}{[\Omega_i B_{ij}(B_{ij}-1)]^m} \sum_{k=0}^{m-1} \frac{\Gamma(m+k)}{k!\,\Gamma(m)} \left[\frac{1}{2}\left(1-\frac{1}{B_{ij}}\right)\right]^k \right\}\end{aligned} \tag{6.25}$$

where

$$A_{ij} = \frac{\sqrt{\Omega_j(1-\rho)/2}}{\Omega_j/\Omega_i - 1 + s\Omega_j(1-\rho)} \text{ and } B_{ij} = \frac{\sqrt{[s\Omega_i\Omega_j(1-\rho) + \Omega_i + \Omega_j]^2 - 4\rho\Omega_i\Omega_j}}{s\Omega_i\Omega_j(1-\rho) + \Omega_j - \Omega_i}.$$

.In Appendix 6A, we also show that it is possible to derive yet another closed-form formula (finite series expression) for the MGF with the aid of the integral formula identity [67, Eq. (6)].

6.2.2 Non-Integer Fading Severity Index

If the fading severity index is not an integer value, then the methods discussed thus far are no longer applicable because we cannot simplify the contour integral through the use of residue theorem. In this case, the infinite series found by Tan and Beaulieu for computing the CDF of bivariate Rayleigh and Nakagami-m fading is a good alternative. The CDF of SNR at the SC combiner output is given by [74, Eq. (3)],

$$F(r) = \frac{(1-\rho)^m}{\Gamma(m)} \sum_{k=0}^{\infty} \frac{\rho^k}{k!\,\Gamma(m+k)} \gamma\left[m+k, \xi_1 r^2\right] \gamma\left[m+k, \xi_2 r^2\right] \tag{6.26}$$

where $\xi_i = \frac{1}{\Omega_i(1-\rho)}, i \in \{1, 2\}$ and $\gamma(\alpha, x) = \int_0^x \exp(-t)\, t^{\alpha-1} dt$, $[\mathrm{Re}\{\alpha\} > 0]$ is the incomplete Gamma function. Therefore, the PDF of the signal envelope can be readily expressed as

$$\begin{aligned} f(r) &= \frac{d}{dr}F(r) \\ &= \sum_{i=1, j\neq i}^{2} \frac{(1-\rho)^m}{\Gamma(m)} \sum_{k=0}^{\infty} \frac{2\xi_i^{m+k}\rho^k}{\Gamma(m+k)\,k!} r^{2m+2k-1} \exp\left[-\xi_i r^2\right] \gamma\left[m+k, \xi_j r^2\right] \end{aligned} \tag{6.27}$$

Substituting (6.27) into (6.17) and after simplifications (with the aid of [52, (6.455.2)]), we obtain the desired MGF as,

$$\begin{aligned} \phi(s) = \sum_{i=1, j\neq i}^{2} \frac{(1-\rho)^m}{\Gamma(m)} \sum_{k=0}^{\infty} \frac{\rho^k}{\Gamma(m+k)\,k!} \left[\frac{\xi_i\xi_j}{(s+\xi_i+\xi_j)^2}\right]^{m+k} \frac{\Gamma(2m+2k)}{m+k} \\ \times {}_2F_1\left[1, 2(m+k); m+k+1; \frac{\xi_i}{s+\xi_i+\xi_j}\right]. \end{aligned} \tag{6.28}$$

To the best of our knowledge, the expression (6.28) is new and holds for arbitrary $m \geq 0.5$ values. This MGF can be used to unify the performance evaluation of various modulation formats in Nakagami-m fading with arbitrary parameters. Although the above expression also holds for integer m, the finite polynomials derived in Section 6.2.1 is recommended to increase the computational efficiency.

6.3 ASER of Binary and M-ary Modulation Formats with Dual-Diversity SC

In this section, we present some applications of our new MGFs as a tool for unified analysis of a broad class of modulation formats employing dual branch SC in Nakagami fading with arbitrary parameters. Craig [76] outlined a simple method for computing the conditional error probability of an arbitrary two dimension signalling constellation.

Using an alternative exponential form for the $\mathrm{erfc}(\sqrt{\gamma})$ and $\mathrm{erfc}^2(\sqrt{\gamma})$, we can show that the conditional error probability for the binary and M-ary signalling constellations (coherent, differentially coherent and noncoherent modulation formats) as a special case of the following generic form [66],

$$P_S(\varepsilon|\gamma) = \sum_k \int_0^{\eta_k} a_k(\theta) \exp(-\gamma b_k(\theta)) d\theta \tag{6.29}$$

where $a_k(\theta)$ and $b_k(\theta)$ are coefficients independent of γ but may be dependent on θ. Then the ASER can be expressed in terms of only the MGF of the resultant SNR:

$$P_S = \sum_k \int_0^{\eta_k} a_k(\theta) \phi(b_k(\theta)) d\theta. \tag{6.30}$$

It is clear that the evaluation of generic ASER expression only involves a single integral with finite integration limits since we have a closed-form solution for the MGF. Unlike the development of [71, Eq. (59)], no further manipulations are necessary. Furthermore, the evaluation for the independent fading case can be directly obtained by substituting $\rho = 0$ in our expressions. More importantly, our expressions (e.g., (6.25), (6A.4), (6A.5), (6.28)) are not conditioned on the ratio between the arguments of the Marcum-Q function.

If the conditional error probability is in the exponential form, namely $P_S(\varepsilon|\gamma) = a\exp(-b\gamma)$, then we also have a closed-form expression for the ASER. For instance, the average bit error rate performance for binary DPSK and noncoherent FSK with dual-branch SC is given by

$$P_S = a\phi(b) \tag{6.31}$$

where $[a = 1/2, b = 1]$ for binary DPSK and $[a = 1/2, b = 1/2]$ for binary orthogonal FSK. As well, when $m = 1$ (Rayleigh fading), we get

$$\phi(s) = \sum_{i=1, j\neq i}^{2} \frac{(2A_{ij})^2}{[\Omega_i B_{ij}(1+B_{ij})]} \tag{6.32}$$

where A_{ij} and B_{ij} are as defined in (6.25). Eqs. (31) and (32) in [71] follow at once from (6.32). Also notice that (6.32) (unlike Eq. (32) in [71]) is independent of the ratio between the arguments of the generalized Marcum-Q function even when $\rho \neq 0$. Similarly for integer m and $\rho = 0$, Eq. (57) in [71] follows at once from (6.25).

If the conditional error probability is of the form $P_S(\varepsilon|\gamma) = a\text{erfc}(\sqrt{b\gamma})$ (e.g., coherent binary PSK or FSK), then the ASER can be expressed as

$$P_S = \frac{2a}{\pi}\int_0^{\pi/2} \phi\left[b\csc^2\theta\right] d\theta . \tag{6.33}$$

Similarly for $P_S(\varepsilon|\gamma) = a\text{erfc}(\sqrt{b\gamma}) - c\text{erfc}^2(\sqrt{b\gamma})$ (e.g., square QAM, quaternary PSK, coherent detection of differentially encoded PSK) the ASER is given by

$$P_S = \frac{2a}{\pi}\int_0^{\pi/2} \phi\left[b\csc^2\theta\right] d\theta - \frac{4c}{\pi}\int_0^{\pi/4} \phi\left[b\csc^2\theta\right] d\theta . \tag{6.34}$$

6.4 Conclusions

This chapter makes a number of contributions: (a) we derive closed-form expressions for the MGF for integer m; (b) we derive an infinite series expression for the MGF for non-integer m; (c) we point out that Okui's result can be represented as a finite polynomial expression for integer m and inverse $\sin(.)$ function for $m = 1/2$; (d) we show that the two previously reported alternative integral representation for $Q_m(a, b)$ can be directly obtained from the contour integral representation [12]; (e) we derive a new, single integral representation for $Q_m(a, b)$ (with finite integration limits) that is valid for $a > b$, $a = b$ or $a < b$; and (f) we also show that closed-form expressions for

the MGF of SC combiner output in a bivariate Nakagami-m fading can be obtained using integral representations for $Q_m(a, b)$ given in [72] and [73]. The details are provided in Appendixes 6B-6D for completeness and comparison purposes (also some of the derivations such as (6C.4) or (6C.6) seem not to be reported anywhere else). To enable the error analysis, we derive the required MGF for both cases of identical and dissimilar mean received signal strengths. The evaluation for the independent fading case can be directly obtained by setting the power correlation coefficient to zero in our expressions. The closed-form formulas can be directly used to determine the error performance of a broad class of modulation formats with dual-diversity SC over independent and correlated Nakagami-m and Rayleigh fading channels.

Appendix 6A

Using the integral formula identity [67, Eq. (6)],

$$\int_0^\infty x^{2m-1}\exp\left(-px^2\right)\left[1-Q_m(ax, bx)\right]dx = \frac{2^{2m-1}\Gamma(2m)\,b^{2m}}{\Gamma(m+1)\left[Y(X+Y)\right]^m} \times {}_2F_1\left[1-m, m; (1+m; (1-X/Y)/2)\right], \quad p>0, m\geq 0.5 \qquad (6A.1)$$

we can easily get an analytical expression for the MGF of SNR at the SC combiner output involving Gauss hypergeometric series ${}_2F_1(.,.;.;.)$, i.e.,

$$\phi(s) = \frac{2^{2m}\Gamma(2m)}{\Gamma(m)\Gamma(m+1)} \times \sum_{i=1, j\neq i}^{2} \frac{(A_{ij})^{2m}}{\left[\Omega_i B_{ij}(1+B_{ij})\right]^m}\, {}_2F_1\left(1-m, m; 1+m; \frac{1}{2}(1-1/B_{ij})\right) \qquad (6A.2)$$

where ${}_2F_1(a, b; c; z) = \sum_{n=0}^{\infty} \frac{(a)_n (b)_n z^n}{(c)_n n!}$ is convergent for $|z|<1$, A_{ij} and B_{ij} as defined in (6.25), and notation $(.)_n$ denotes the Pochhammer's symbol. Eq. (6A.2) generalizes the result in [67] for the case of dissimilar signal strengths. For the particular case of

$\Omega_1 = \Omega_2$, (6A.2) reduces to [67, Eq. (7)]. It is also noted that (6A.2) is valid for arbitrary $m \geq 1/2$.

For integer $m \geq 2$, the Gauss hypergeometric series has also a finite series representation:

$$ {}_2F_1\left[1-m, m; 1+m; \frac{1}{2}(1-1/B_{ij})\right] = \sum_{n=0}^{m-1} \frac{(1-m)_n (m)_n}{(1+m)_n \, n!} \left[\frac{1}{2}(1-1/B_{ij})\right]^n \quad (6A.3) $$

since $1-m$ is equal to a negative integer. In fact, (6A.3) is also valid for $m = 1$ since ${}_2F_1(0, b; c; z) = {}_2F_1(a, 0; c; z) = 1$ and therefore the right-hand side of the finite series reduces to unity. Hence, (6A.2) may be conveniently evaluated using

$$ \phi(s) = \frac{\Gamma(2m)}{\Gamma(m)\Gamma(m+1)} \times \sum_{i=1, j\neq i}^{2} \frac{(2A_{ij})^{2m}}{[\Omega_i B_{ij}(1+B_{ij})]^m} \sum_{n=0}^{m-1} \frac{(1-m)_n (m)_n}{(1+m)_n \, n!} \left[\frac{1}{2}\left(1-\frac{1}{B_{ij}}\right)\right]^n \quad (6A.4) $$

for positive integer m.

One may also express (6A.4) in terms of Jacobi polynomial using identity [52, (8.962.1)]:

$$ \phi(s) = \sum_{i=1, j\neq i}^{2} \frac{(2A_{ij})^{2m}}{[\Omega_i B_{ij}(1+B_{ij})]^m} P_{m-1}^{(m,-m)}(1/B_{ij}) \quad (6A.5) $$

If $m = 1/2$, then (6A.2) may be simplified as

$$ \phi(s) = \frac{4\sqrt{2}}{\pi} \sum_{i=1, j\neq i}^{2} \frac{A_{ij}}{\sqrt{\Omega_i\left[B_{ij}^2 - 1\right]}} \sin^{-1}\left(\sqrt{(1-1/B_{ij})/2}\right) \quad (6A.6) $$

with the aid of identity [52, (9.121.26)].

Although the preceding development constitute only minor extensions of [67], none of the recent papers on this subject highlighted the availability of closed-form solutions for the above cases. In fact, more complicated formulas were derived instead and they are not in

closed-form (e.g., simplicity of the results given by (6A.4) and/or (6A.5) should be compared to Eq. (55) given in [71]).

Appendix 6B

Recently, Simon and Alouini obtained an analytical expression for the MGF in terms of a single finite-range integral by utilizing an exponential representation for the generalized Marcum-Q function [73, 75] when integer $m > 1$. In what follows, we will show that it is also possible to obtain closed-form expressions for the desired MGF (for both the identical and nonidentical diversity branches situations) in Nakagami fading directly from the integral representation of $Q_m(ar, br)$. From [73], we know that the integral form for $Q_m(\alpha, \beta)$ varies according to $\alpha < \beta$, $\alpha = \beta$ or $\alpha > \beta$:

$$Q_m(\alpha, \beta) = \begin{cases} H_m(\alpha, \beta) & \text{if } \alpha < \beta \\ 1/2 + H_m(\alpha, \alpha) & \text{if } \alpha = \beta \\ 1 + H_m(\alpha, \beta) & \text{if } \alpha > \beta \end{cases} \tag{6B.1}$$

where the finite-range integral $H_m(\alpha, \beta)$ is defined by [73, C-26]

$$H_m(\alpha, \beta) = \alpha\left(\frac{\beta}{\alpha}\right)^m \exp\left[\frac{-(\beta-\alpha)^2}{2}\right] \times \frac{1}{2\pi}\int_0^{2\pi} \exp\left[-\alpha\beta(1-\cos\theta)\right] \frac{\beta\cos(m-1)\theta - \alpha\cos m\theta}{\alpha^2+\beta^2-2\alpha\beta\cos\theta}\, d\theta. \tag{6B.2}$$

6B.1 Identical Diversity Branches

When $\Omega_1 = \Omega_2 = \Omega$, (6.16) reduces to

$$f(r) = 2\psi(r)\left[1 - Q_m\left(r\sqrt{\frac{2\rho}{(1-\rho)\Omega}}, r\sqrt{\frac{2}{(1-\rho)\Omega}}\right)\right] \text{ for } 0 < \rho < 1. \tag{6B.3}$$

For this case, it is obvious that we can replace $Q_m(ar, br)$ with $H_m(ar, br)$ since $b > a$. Combining (6B.3), (6B.2), (6.17) and then invoking identity [52, (3.381.4)], we obtain

$$\phi(s) = \frac{2}{(s\Omega+1)^m} - \left(\frac{b}{\Omega a}\right)^m \frac{a}{\pi}\int_0^{2\pi} \frac{b\cos(m-1)\theta - a\cos m\theta}{\left[a^2+b^2-2ab\cos\theta\right](s_1 - ab\cos\theta)^m} d\theta \qquad (6B.4)$$

where $a = \sqrt{\frac{2\rho}{(1-\rho)\Omega}}$, $b = \sqrt{\frac{2}{(1-\rho)\Omega}}$ and $s_1 = s + \frac{a^2+b^2}{2} + \frac{1}{\Omega}$.

By introducing parameters $a_1 = \frac{a^2+b^2}{2ab} > 1$ and $a_2 = \frac{s_1}{ab} > 1$, (6B.4) may be restated in a more desirable form,

$$\phi(s) = \frac{2}{(s\Omega+1)^m} - \frac{\lambda}{2\pi}\int_0^{2\pi} \frac{b\cos(m-1)\theta - a\cos m\theta}{(a_1-\cos\theta)(a_2-\cos\theta)^m} d\theta \qquad (6B.5)$$

where $1/\lambda = \Omega^m a^{2m} b$. The denominator of the integrand in (6B.5) can be expressed in terms of partial fractions as,

$$\begin{aligned} \frac{1}{(a_1-\cos\theta)(a_2-\cos\theta)^m} &= \frac{\mu^m}{(a_1-\cos\theta)^m} - \sum_{k=1}^{m} \frac{\mu^{m+1-k}}{(a_2-\cos\theta)^k} \\ &= \sum_{k=0}^{m} \frac{\Psi_k}{(\delta_k-\cos\theta)^{\eta_k}} \end{aligned} \qquad (6B.6)$$

where $\delta_k = \begin{cases} a_1 \text{ if } k=0 \\ a_2 \text{ if } k\geq 1 \end{cases}$, $\Psi_k = \begin{cases} \mu^m & \text{if } k=0 \\ -\mu^{m+1-k} & \text{if } k\geq 1 \end{cases}$, $\eta_k = \begin{cases} 1 \text{ if } k=0 \\ k \text{ if } k\geq 1 \end{cases}$ and $\mu = 1/(a_2-a_1)$.

Finally, the desired closed-form solution is obtained by substituting (6B.6) into (6B.5) and using the results from Appendix 6C:

$$\begin{aligned} \phi(s) &= \frac{2}{(s\Omega+1)^m} - \lambda \sum_{k=0}^{m} \Psi_k \left[b I_{\eta_k}^{(m-1)}(\delta_k) - a I_{\eta_k}^{(m)}(\delta_k) \right] \\ &= \frac{2}{(s\Omega+1)^m} - \frac{2}{\Omega^m} I(s+1/\Omega, m, a, b) \end{aligned} \qquad (6B.7)$$

where $I_{\eta_k}^{(m)}(\delta_k)$ and $I(s+1/\Omega, m, a, b)$ are computed with the aid of (6C.4) or (6C.6) and (6D.5).

6B.2 Nonidentical Diversity Branches

Let us denote $\rho_0 = \Omega_2/\Omega_1$ and assume that $\Omega_1 > \Omega_2$ without any loss of generality. Now we can rewrite (6.16) as

$$f(r) = \psi_2(r)\left[1 - Q_m(\tilde{a}r, \tilde{b}r)\right] + \psi_1(r)\left[1 - Q_m(\hat{a}r, \hat{b}r)\right] \tag{6B.8}$$

where $\tilde{a} = \sqrt{\frac{2\rho}{(1-\rho)\Omega_2}}$, $\tilde{b} = \sqrt{\frac{2}{(1-\rho)\Omega_1}}$, $\hat{a} = \sqrt{\frac{2\rho}{(1-\rho)\Omega_1}}$ and $\hat{b} = \sqrt{\frac{2}{(1-\rho)\Omega_2}}$.

It is clear that $\hat{b} > \hat{a}$ always, and therefore $Q_m(\hat{a}r, \hat{b}r)$ may be replaced with $H_m(\hat{a}r, \hat{b}r)$. However, $\tilde{a} > \tilde{b}$ if $\rho > \rho_0$; $\tilde{a} = \tilde{b}$ if $\rho = \rho_0$; and $\tilde{a} < \tilde{b}$ if $\rho < \rho_0$.

Using (6B.1), we can express (6B.8) in a desired form, i.e.,

$$\begin{aligned} f(r) = {} & \psi_2(r)\left[u(\rho_0 - \rho) - \frac{\delta(\rho - \rho_0)}{2}\right] - \psi_2(r) H_m(\tilde{a}r, \tilde{b}r)\,\hat{\delta}(\rho - \rho_0) \\ & - \psi_2(r) H_m(\tilde{a}r, \tilde{a}r)\,\delta(\rho - \rho_0) + \psi_1(r)\left[1 - H_m(\hat{a}r, \hat{b}r)\right] \end{aligned} \tag{6B.9}$$

where $u(t) = \begin{cases} 1 & \text{if } t \geq 0 \\ 0 & \text{if } t < 0 \end{cases}$ denotes unit-step function, $\delta(t) = \begin{cases} 1 & \text{if } t = 0 \\ 0 & \text{if } t \neq 0 \end{cases}$ is the unit-impulse function and its complementary is given by $\hat{\delta}(t) = \begin{cases} 0 & \text{if } t = 0 \\ 1 & \text{if } t \neq 0 \end{cases}$.

A closed-form expression (finite series representation) for the corresponding MGF can be readily obtained using (6.17) and Appendix 6D:

$$\begin{aligned} \phi(s) = {} & \frac{1}{(s\Omega_2 + 1)^m}\left[u(\rho_0 - \rho) - \frac{\delta(\rho - \rho_0)}{2}\right] \\ & - \frac{1}{\Omega_2^m} I\left(s + 1/\Omega_2, m, \tilde{a}, \tilde{b}\right)\hat{\delta}(\rho - \rho_0) - \frac{1}{\Omega_2^m} I(s + 1/\Omega_2, m, \tilde{a}, \tilde{a})\,\delta(\rho - \rho_0) \\ & + \frac{1}{(s\Omega_1 + 1)^m} - \frac{1}{\Omega_1^m} I\left(s + 1/\Omega_1, m, \hat{a}, \hat{b}\right) \end{aligned} \tag{6B.10}$$

When $\Omega_1 = \Omega_2$, (6B.10) reduces to (6B.7) since $\rho < \rho_0$. While we have derived much simpler expressions for the MGF of SC combiner output (e.g., Eq. (6.25) and (6A.5)), the results presented in Appendix 6C and 6D may still serve as a useful reference since they provide new closed-form formulas for some integrals related to the Marcum-Q function.

Appendix 6C

Consider an integral of the form

$$I_n^{(m)}(a) = \frac{1}{2\pi}\int_0^{2\pi} \frac{\cos(m\theta)}{[a-\cos(\theta)]^n} d\theta \tag{6C.1}$$

where $m \geq 0$, $n \geq 1$, $a > 1$, m and n are integers. Now making variable substitution $z = \exp(j\theta)$, (6C.1) can be restated in terms of a circular contour integral with unit radius, i.e.,

$$I_n^{(m)}(a) = \frac{(-2)^n}{2\pi j} \oint_{|c|=1} \frac{z^{m+n-1}}{\left[z^2 - 2az + 1\right]^n} dz. \tag{6C.2}$$

Since the denominator of the integrand in (6C.2) has two positive roots, namely $r_1 = a - \sqrt{a^2-1} < 1$ and $r_2 = a + \sqrt{a^2-1} > 1$, the contour integral has an n-th order pole. Invoking the residue theorem, we get

$$I_n^{(m)}(a) = \frac{(-2)^n}{(n-1)!} \frac{d^{(n-1)}}{dz} \left\{ \frac{z^{m+n-1}}{(z-r_2)^n} \right\} \Bigg|_{z=r_1}. \tag{6C.3}$$

Now applying the Liebnitz' differentiation rule (see Eq. (6.23)) and after simplifications, we obtain a closed-form solution for $I_n^{(m)}(a)$:

$$I_n^{(m)}(a) = 2^n \left[a - \sqrt{a^2-1}\right]^{m-n} \times \sum_{k=0}^{n-1} \binom{m+n-1}{k} \binom{2n-k-2}{n-1} \left[\frac{a-\sqrt{a^2-1}}{2\sqrt{a^2-1}}\right]^{2n-k-1} \tag{6C.4}$$

For instance, $I_1^{(m)}(a) = \left[a-\sqrt{a^2-1}\right]^m / \sqrt{a^2-1}$, which is similar to [52, (3.613.1)].

Alternatively, using identity [52, (9.112)] we can show that the integral (6C.1) is associated with the Gauss hypergeometric series via relationship,

$$I_n^{(m)}(a) = \frac{2^n \Gamma(n+m)\,\zeta^{n+m}}{m!\,\Gamma(n)}\, {}_2F_1\left[n, n+m; 1+m; \zeta^2\right] \tag{6C.5}$$

where notation $\zeta = a-\sqrt{a^2-1}$. Now applying Kummer's transformation formula [52, (9.131.1)], we get

$$\begin{aligned} I_n^{(m)}(a) &= \frac{2^n \Gamma(n+m)\,\zeta^{n+m}}{m!\,\Gamma(n)\left(1-\zeta^2\right)^n}\, {}_2F_1\left[n, 1-n; 1+m; \frac{\zeta^2}{\zeta^2-1}\right] \\ &= \frac{2^n \Gamma(n+m)\,\zeta^{n+m}}{m!\,\Gamma(n)\left(1-\zeta^2\right)^n} \times \sum_{k=0}^{n-1} \frac{(1-n)_k (n)_k}{(1+m)_k\, k!}\left(\frac{\zeta^2}{\zeta^2-1}\right)^k \\ &= \frac{2^n \zeta^{n+m}}{\left(1-\zeta^2\right)^n} P_{n-1}^{(m,-m)}\left(\frac{1+\zeta^2}{1-\zeta^2}\right) \end{aligned} \tag{6C.6}$$

where $P_n^{(\alpha,\beta)}(x)$ denotes the Jacobi polynomial.

Appendix 6D

Let us define

$$I(c, m, a, b) \equiv \frac{2}{\Gamma(m)} \int_0^\infty r^{2m-1} \exp\left(-cr^2\right) H_m(ar, br)\, dr \tag{6D.1}$$

where m assumes a positive integer value.

Substituting (6B.2) into (6D.1) and rearranging the order of integration, we get

$$\begin{aligned} I(c, m, a, b) &= \frac{1}{2\pi} \int_0^{2\pi} \frac{b\cos(m-1)\theta - a\cos m\theta}{a^2+b^2-2ab\cos\theta} \times \frac{2a}{\Gamma(m)}\left(\frac{b}{a}\right)^m \\ &\quad \times \int_0^\infty r^{2m-1} \exp\left[-r^2\left(c + \frac{1}{2}(b-a)^2 + ab(1-\cos\theta)\right)\right] dr d\theta \,. \end{aligned} \tag{6D.2}$$

Since the integration with respect to the random variable r can be carried out using the identity

$$\int_0^\infty x^{2n-1}\exp\left(-qx^2\right)dx = \frac{\Gamma(n)}{2q^n} \quad \text{for } q>0, n>\frac{1}{2}, \tag{6D.3}$$

equation (6D.2) reduces to

$$I(c,m,a,b) = \frac{1}{2a^{2m}b}\times\frac{1}{2\pi}\int_0^{2\pi}\frac{b\cos(m-1)\theta - a\cos m\theta}{(\vartheta_1-\cos\theta)(\vartheta_2-\cos\theta)^m}d\theta \tag{6D.4}$$

where $\vartheta_1 = \dfrac{a^2+b^2}{2ab}$ and $\vartheta_2 = \dfrac{2c+a^2+b^2}{2ab}$.

By expressing the integrand of (6D.4) in terms of partial fractions [see Eq. (6B.6)], and then using the result of Appendix 6B, we can show that $I(c,m,a,b)$ also has a closed-form solution:

$$\begin{aligned} I(c,m,a,b) = \frac{1}{2a^{2m}b}\Bigg(&\left(\frac{ab}{c}\right)^m\left[bI_1^{(m-1)}(\vartheta_1) - aI_1^{(m)}(\vartheta_1)\right] \\ &-\sum_{k=1}^{m}\left(\frac{ab}{c}\right)^{m+1-k}\left[bI_k^{(m-1)}(\vartheta_2) - aI_k^{(m)}(\vartheta_2)\right]\Bigg). \end{aligned} \tag{6D.5}$$

For the special case of $m = 1$, (6D.5) reduces to

$$I(c,1,a,b) = \frac{1}{2c}\left[\frac{a^2-b^2+2c}{\sqrt{\left[(a+b)^2+2c\right]\left[(a-b)^2+2c\right]}} - 1\right]. \tag{6D.6}$$

Chapter 7

A Reduced Complexity Rake Receiver Structure for High Speed Indoor Wireless Communications

Direct-sequence spread-spectrum multiple access (DS/CDMA) has been proposed for future personal communication networks (PCN) due to its inherent advantages in terms of statistical multiplexing, fading immunity, soft-handover capability, interference suppression and overlay communication. In addition to multiuser interference, the deep fades experienced on wireless channels remain a serious problem to ensure a reliable communication, particularly for the narrowband systems.

Diversity reception has long been recognized as a powerful technique for mitigating the detrimental effects of channel fading. In Chapter 3, we have briefly reviewed various forms of diversity techniques commonly used in the cellular radio communications. A thorough treatment of the diversity schemes and the signal combining techniques may be found in [21] and [2]. Among these approaches, selecting the branch with largest received composite signal for demodulation is the simplest option but yields inferior performance compared to the optimal maximal-ratio combiner (if accurate channel fading estimate is available).

In wideband DS/CDMA systems, it is natural to exploit the autocorrelation properties of the pseudo-random spreading signature waveforms to resolve and combine the multipath components to obtain multipath diversity. Resolvability can be achieved if the

signal bandwidth is larger than the coherence bandwidth of the channel. In other words, a multipath can be resolved if the time difference between the first arriving signal and the consecutive multipaths is greater than a chip duration. Various diversity combining techniques may be employed to achieve a good compromise between the performance and implementation complexity. Kavehrad and McLane [78] analyzed the average bit-error rate (BER) performance for the conventional selection diversity[1] (SNR/SD) and the maximal-ratio diversity (MRC) over a frequency-selective Rayleigh fading channel by assuming a uniform multipath intensity profile (MIP). In [79], Eng and Milstein studied the performance of MRC in a Nakagami fading environment with a decaying multipath intensity profile. Subsequently in [80], the authors examined the performance of a preselection maximal-ratio combiner over Rayleigh fading channels. The analysis was extended in [81] for a Nakagami fading environment. In this chapter we will investigate the performance of a low-complexity rake receiver architecture[2] which simply selects the finger with the largest magnitude of the received composite signal (and therefore suitable for high-speed wireless links).

In a related work [82], Chyi et. al. investigated the performance of two receiver structures for M-ary orthogonal signalling over frequency non-selective Rayleigh fading channels. More recently, Neasmith and Beaulieu [83] have investigated the performance of four receiver structures for noncoherent FSK signalling and two receiver structures for DPSK signalling employing selection diversity over a frequency non-selective Rayleigh fading channel. They have shown that in an identical mean signal strength scenario, the

---

1. If the L th order diversity is employed and the mean noise power is assumed to be identical for all branches, then the decision criterion reduces to $\max[\alpha_i]$, $i = 1, \ldots, M$, where α_i is the channel gain from the i th branch. In this situation, it is evident that selecting the branch with the largest SNR is equivalent to selecting the branch with the largest signal power or amplitude.

2. In practice, measurements of SNR may be difficult or expensive especially for high signalling rates. To be most effective, the system should be able to make its selection in a period of time equal to or less than the interval of the shortest signal that will be transmitted. Consequently, the branch with the largest amplitude of the received composite signal is chosen.

practical S+N (or in our case MA/SD) rule (based on choosing the diversity branch with the largest amplitude of the received composite signal, i.e., signal plus noise) yields superior performance compared to that of SNR/SD scheme (which is based on choosing the diversity branch with the largest signal to noise ratio) owing to the stochastic nature of the noise. Subsequently in [84], performance of two different selection diversity rules have been examined in the presence of a specular component for asynchronous DS/CDMA systems with coherent BPSK demodulation. Our result validates the previously established and explained phenomena concerning selection diversity systems that appeared in [82] and [83], but for coherent signal detection. Moreover, numerical results in [84] reveal that the MA/SD scheme exhibits comparable performance with that of the maximal-ratio combiner in environments where a strong specular path is available (better channel conditions) and for small diversity orders. It should be emphasized, however, that these conclusions were drawn based on the assumptions that all the statistically independent diversity branches have identical fading parameters and equal mean signal strengths. As well, the analysis is restrictive in the sense that the fading figure was confined to the set of elements that are multiples of 0.5 and assumed to be identical on each diversity branch.

By contrast, in this chapter we move away from these restrictions and study the effectiveness of the new selection diversity rule in more realistic channel conditions. Due to the random nature of the propagation channel, it is more realistic to assume that the mean signal strengths and/or the fading parameter may be different (and may assume an arbitrary value) for the different diversity branches. This may well be the case in an actual mobile link, since the radio waves take different paths and may undergo different fading before arriving at the receiver. Subsequently, the performance of the proposed rake receiver configuration is compared with that of MRC by considering the effect of Gaussian error in the combiner weighting factors.

7.1 System Model

The delay spread encountered in indoor radio channels are very small and the maximum multipath delay spread is typically in the range of 200-300 ns. For instance, the chip duration (after Nyquist pulse shaping) of a DS/CDMA signal which uses the binary modulation format and employs a transmission bandwidth of 1.25 MHz will not give rise to path diversity in an indoor wireless channel, resulting in a frequency non-selective fading channel. However, the maximum multipath delay spread is usually less than the symbol duration T_b, and therefore intersymbol interference (ISI) can be assumed to be negligible. The application of micro-diversity techniques becomes even more crucial in indoor wireless channels (characterized by high-rate traffic but with low mobility users), because in such scenarios, coding with interleaving approach will not work effectively to combat multipath fading. This is because the interleaving time span need to cover independent fades, and therefore requires a very large memory. At the base-station, antenna diversity may be employed to achieve the desired performance. Whereas, multipath diversity is more feasible for portable units.

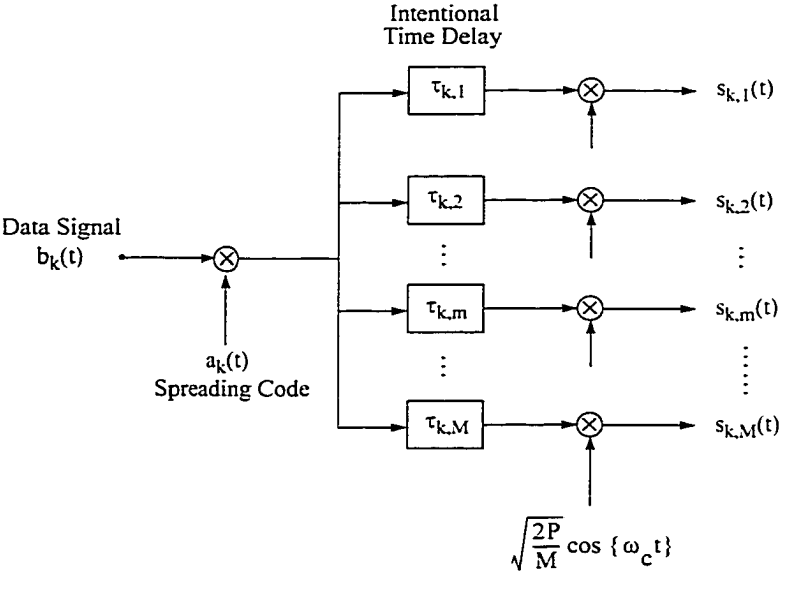

Fig. 7.1 Transmitter Diversity with Intentional Time-Offset

An effective way to overcome this problem is by implementing transmitter diversity [77], which artificially creates multipath of sufficient delays for the rake processor to work effectively [see Fig. 7.1]. The signals received from the neighboring antennas are distinguished by PN temporal processing. When path diversity is available, the transmitter diversity will increase the effective order of diversity. The impact of the emulated frequency-selective channel via transmitter diversity is two fold. First, due to the increased diversity order, the required signal-to-noise ratio for a prescribed error rate is lowered. Secondly, the variance of the multi-access interference is reduced, thereby increasing capacity. However, it should also be realized that while multipath allows us to gain diversity advantage by employing a rake receiver, it has the undesirable effect of accentuating the effect of multiple-access interference.

7.2 Error Probability Analysis

The sample (decision statistic) of the received composite signal at a sampling instant can be described in a compact form as in [84],

$$\zeta_j \equiv \alpha_j b_0 + n_j \tag{7.1}$$

where $\alpha_j = \sqrt{P/2}\, T_b \beta_j$ is the fading sample, n_j is the MAI (multipath and multi-user interference plus AWGN noise) sample with variance σ_j^2, and b_0 is the polarity of the data bit being detected. Also, α_j and n_j are assumed to be statistically mutually independent Nakagami and Gaussian random variables, respectively. Subscript j corresponds to the jth copy of a signal available at the rake receiver for detection, $j \in \{1, 2, \ldots, M\}$, where M corresponds to the order of diversity (i.e., number of resolvable multipaths). Since α_j is a Nakagami random variable, it has a probability density function (PDF) of the form,

$$f_\alpha(R) = \frac{2m^m R^{2m-1}}{\Gamma(m)\,\Omega^m} \exp\left(\frac{-mR^2}{\Omega}\right) u(R) \tag{7.2}$$

where $u(.)$ denotes the unit-step function and $\Gamma(.)$ corresponds to the Gamma func-

tion. The scalar m in Eq. (7.2) is defined as the ratio of moments, called the fading figure, $m = \Omega^2 / E\left[(R^2 - \Omega)^2\right] \geq 0.5$, where $E[.]$ denotes the statistical average (or mean) function, and $\Omega = E\left[R^2\right]$.

7.2.1 Maximum Amplitude Selection Diversity (MA/SD)

When the branch with the largest received composite signal amplitude is chosen [see Fig. 7.2], the average probability of bit error is given by,

$$P_b = 1 - \sum_{j=1}^{M} Pr\{\zeta_j > 0 \mid b_0 = +1, |\zeta_j| > |\zeta_i| \text{ for all } i \neq j\} \tag{7.3}$$

Using the transformation $z_j = \zeta_j / \sigma_j$, $j = 1, 2, \ldots, M$, Eq. (7.3) can be re-stated as,

$$P_b = 1 - \sum_{j=1}^{M} \int_0^{\infty} g_\zeta(z_j) \prod_{i=1, i\neq j}^{M} \left[\int_{-\frac{\sigma_j}{\sigma_i} z_j}^{\frac{\sigma_j}{\sigma_i} z_j} g_\zeta(z_i)\, dz_i \right] dz_j \tag{7.4}$$

where $g_\zeta(z_j)$ denotes the density function of the decision variable z_j when $b_0 = +1$.

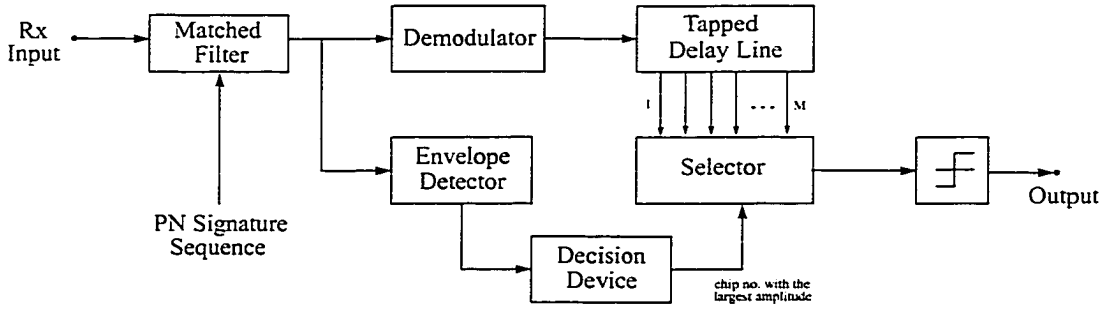

Fig. 7.2 Block diagram of the proposed MA/SD rake receiver.

Assuming that $b_0 = +1$ was transmitted, the random variable z_i is the sum of a Gaussian and a Nakagami distributed random variables. Therefore, the PDF of $g_\zeta(z_i)$ can be

obtained easily through convolution of their individual density functions [84],

$$g_{\zeta}(z_j) = \int_0^{\infty} \frac{1}{\sqrt{2\pi}} \exp\left(\frac{-(z_j - x)^2}{2}\right) \frac{2m^m x^{2m-1}}{\Gamma(m)\left[\Omega_j/\sigma_j^2\right]^m} \exp\left(\frac{-mx^2}{\Omega_j/\sigma_j^2}\right) dx. \tag{7.5}$$

After some mathematical manipulations, (7.5) can be re-stated as,

$$g_{\zeta}(z_j) = \frac{2m^m \Gamma(2m)}{\sqrt{2\pi}\Gamma(m)\,(2m+\bar{\gamma}_j)^m} \exp\left(\frac{-z_j^2(4m+\bar{\gamma}_j)}{4(2m+\bar{\gamma}_j)}\right) D_{-2m}\left(-z_j\sqrt{\frac{\bar{\gamma}_j}{2m+\bar{\gamma}_j}}\right) \tag{7.6}$$

where $\bar{\gamma}_j = \Omega_j/\sigma_j^2 = 2\bar{\gamma}_{bj}$ is the mean signal-to-noise plus interference ratio (SNIR) of the jth rake finger, $\bar{\gamma}_{bj}$ denotes the average SNR per bit, and $D_{-v}(z)$ is the function of the parabolic cylinder [52] of order v and argument z. It is noted that $D_{-2m}(z)$ can be computed efficiently using the recurrence relationship given by Eq. (7.7) if m is a multiple of 0.5 :

$$D_{p+1}(z) - zD_p(z) + pD_{p-1}(z) = 0 \tag{7.7}$$

with

$$D_{-1}(z) = \sqrt{\frac{\pi}{2}} \exp\left(\frac{z^2}{4}\right) \operatorname{erfc}\left(\frac{z}{\sqrt{2}}\right) \tag{7.8}$$

and

$$D_{-2}(z) = \exp\left(-\frac{z^2}{4}\right) - z\exp\left(\frac{z^2}{4}\right)\sqrt{\frac{\pi}{2}} \operatorname{erfc}\left(\frac{z}{\sqrt{2}}\right). \tag{7.9}$$

Using identities 19.3.7 and 19.12.2 in [85], $D_{-v}(z)$ can be written in the form of Whittaker function $W_{\mu,\kappa}(x)$:

$$D_{-v}(z) = 2^{\frac{1}{4}-\frac{v}{2}} z^{-\frac{1}{2}} W_{\frac{1}{4}-\frac{v}{2},\frac{1}{4}}\left(\frac{z^2}{2}\right), \tag{7.10}$$

and in terms of the confluent hypergeometric function of the second kind $U(a, c, z)$ via relationship $W_{\mu,\kappa}(x) = \exp\left(\frac{-x}{2}\right) x^{\frac{2\kappa+1}{2}} U\left(\frac{2\kappa+1}{2} - \mu, 2\kappa+1, x\right)$:

$$D_{-v}(z) = 2^{-\frac{1}{2}(v+1)} z \exp\left(\frac{-z^2}{4}\right) U\left(\frac{v+1}{2}, \frac{3}{2}, \frac{z^2}{2}\right) \tag{7.11}$$

Now applying $U(a, c, z) = z^{1-c} U(a+1-c, 2-c, z)$ (Kummer's transformation formula), Eq. (7.11) reduces to,

$$D_{-v}(z) = 2^{-\frac{v}{2}} \exp\left(\frac{-z^2}{4}\right) U\left(\frac{v}{2}, \frac{1}{2}, \frac{z^2}{2}\right) \tag{7.12}$$

Since $U(a, c, z) = \frac{\Gamma(1-c)}{\Gamma(1+a-c)} {}_1F_1(a; c; z) + \frac{\Gamma(c-1)}{\Gamma(a)} z^{1-c} {}_1F_1(1+a-c; 2-c; z)$ [86], and substituting Eq. (7.12) into Eq. (7.6), the PDF of $g_\zeta(z_i)$ can be re-stated in terms of the more familiar confluent hypergeometric function of the first kind,

$$g_\zeta(z_i) = \frac{2^{-m_i+1} m_i^{m_i} \Gamma(2m_i)}{\sqrt{2\pi}\,\Gamma(m_i)\,(2m_i+\bar{\gamma}_i)^{m_i}} \exp\left(\frac{-z_i^2}{2}\right) \left\{ \frac{\sqrt{\pi}}{\Gamma\left(m_i+\frac{1}{2}\right)} {}_1F_1\left(m_i; \frac{1}{2}; \frac{z_i^2}{2}\left[\frac{\bar{\gamma}_i}{2m_i+\bar{\gamma}_i}\right]\right) \right.$$
$$\left. + \frac{\sqrt{2\pi} z_i}{\Gamma(m_i)} \sqrt{\frac{\bar{\gamma}_i}{2m_i+\bar{\gamma}_i}} {}_1F_1\left(m_i+\frac{1}{2}; \frac{3}{2}; \frac{z_i^2}{2}\left[\frac{\bar{\gamma}_i}{2m_i+\bar{\gamma}_i}\right]\right) \right\} \tag{7.13}$$

Unlike Eq. (10) in [84] (which is restrictive because the fading parameter m is confined to the set of elements that are multiples of 0.5, i.e., $m \in \{0.5, 1.0, 1.5, 2, \ldots\}$), Eq. (7.13) enables us to compute the bit error rate performance with arbitrary fading severity parameters. In other words, m may now assume any real value that is greater than or equal to $1/2$. The average probability of bit error described by Eq. (7.4) can be evaluated numerically by using the adaptive Simpson's integration method. Also for the particular case of $m = 1$ (Rayleigh fading), Eq. (7.13) reduces to Eq. (A.4) in [84] by utilizing the following three known identities: $1 + \mathrm{erf}(x) = \mathrm{erfc}(-x)$, ${}_1F_1(a; a; x) = \exp(x)$ and ${}_1F_1\left(1; \frac{1}{2}; x^2\right) = 1 + \sqrt{\pi}\, x \exp\{x^2\} \mathrm{erf}(x)$.

7.2.2 Maximum SNR Selection Diversity (SNR/SD)

The conventional selection diversity model specifies that of M diversity branches, the one providing the largest SNR be selected for data recovery. If we assume that $b_0 = +1$ was transmitted, then the conditional error probability is given by,

$$Pr\{\zeta_j < 0 \mid b_0 = +1\} = \sum_{j=1}^{M} Pr\left\{\zeta_j < 0, \gamma_j = \frac{\alpha_j^2}{\sigma_j^2} > \frac{\alpha_i^2}{\sigma_i^2} = \gamma_i \text{ for all } i \neq j\right\} \tag{7.14}$$

In [78], statistics from the self-interference, multiple-access interference and the Gaussian noise are assumed to be same on each diversity branch. Consequently, the selection diversity process is simplified by considering the largest path gain as the best estimate of the transmitted signal,

$$\alpha_{max} = \max_{1 \le j \le M} \{\alpha_j\} . \tag{7.15}$$

Assuming that the data bits are equiprobable, and owing to the statistical symmetry property of the decision variable, the average bit error rate (for integer m) can be expressed as,

$$P_b = \sum_{j=1}^{M} \int_0^{\infty} Q\left(\sqrt{\gamma_j}\right) \frac{m_j^{m_j} \gamma_j^{m_j - 1}}{\Gamma(m_j)\, \bar{\gamma}_j^{m_j}} \exp\left(\frac{-m_j \gamma_j}{\bar{\gamma}_j}\right) \times \prod_{i=1, i \neq j}^{M} \left[1 - \exp\left(\frac{-m_i \gamma_j}{\bar{\gamma}_i}\right) \sum_{k=0}^{m_i - 1} \frac{1}{k!} \left(\frac{m_i \gamma_j}{\bar{\gamma}_i}\right)^k\right] d\gamma_j \tag{7.16}$$

where $\bar{\gamma}_j$ corresponds to the mean SNIR of the j th diversity branch (finger) and $Q(.)$ is the Gaussian probability integral,

$$Q(x) = \frac{1}{\sqrt{2\pi}} \int_x^{\infty} \exp\left(\frac{-u^2}{2}\right) du = \frac{1}{2} \operatorname{erfc}\left(\frac{x}{\sqrt{2}}\right) \tag{7.17}$$

When all the diversity branches have identical fading statistics, Eq. (7.16) can be expressed as,

$$P_b = \frac{M}{2\sqrt{\pi}\,(m-1)!}\sum_{w=0}^{M-1}\sum_{k=0}^{w(m-1)} C_w^{N-1}(-1)^w A_k^w \times \int_0^\infty \gamma^{m+k-1}\exp\left(-(w+1)\gamma\right)\Gamma\left(\frac{1}{2},\frac{\bar{\gamma}}{2m}\gamma\right)d\gamma \tag{7.18}$$

where ${}^aC_b = \frac{a!}{(a-b)!b!}$ is the binomial expansion coefficient, $A_0^w = 1$, $A_1^w = w$, $A_{w(m-1)}^w = [1/(m-1)!]^w$ and $A_k^w = \frac{1}{k}\sum_{i=1}^{V}\frac{i(w+1)-k}{i!}A_{k-1}^w$ is evaluated recursively for $2 \le k \le w(m-1)-1$ and $V = min(k, m-1)$. Since the definite integral in Eq. (7.18) has a known closed-form solution, the average BER formula reduces to,

$$P_b = \frac{M}{2\sqrt{\pi}\,(m-1)!}\sum_{w=0}^{M-1}\sum_{k=0}^{w(m-1)} \frac{C_w^{N-1}(-1)^w A_k^w \Gamma(m+k+0.5)}{\left(1+w+\frac{\bar{\gamma}}{2m}\right)^{m+k+0.5}(m+k)} \times \sqrt{\frac{\bar{\gamma}}{2m}}\,{}_2F_1\left(1, m+k+\frac{1}{2}, m+k+1, \frac{1}{1+\bar{\gamma}/(2m(w+1))}\right) \tag{7.19}$$

As discussed in Chapter 3, there is a much simpler way to compute the average BER of the SNR/SD diversity receivers. Moreover, the moment generating function (MGF) approach is sufficiently general to handle arbitrary fading parameter and unequal mean received signal powers. By exploiting the alternative exponential representation for the complementary error function, i.e., $\mathrm{erfc}(\sqrt{x}) = \frac{2}{\pi}\int_0^{\pi/2}\exp(-x\sec^2\theta)\,d\theta$, the average BER can be expressed in terms of a finite range integral,

$$P_b = \frac{1}{\pi}\int_0^{\pi/2}\phi_\gamma^{(SC)}(\sec^2\theta)\,d\theta \tag{7.20}$$

which requires only the knowledge of the MGF of SNR at the output of the selection combiner. Using the relation between the MGF and cumulative distribution function (CDF) from the Laplace transform of a derivative property, we can easily compute the MGF of the SNR at the output of the SNR/SD selection combiner as,

$$\phi_{\gamma}^{(SC)}(z) = \int_{-\infty}^{\infty} e^{-zx} F'(x)\,dx = z\int_{0}^{\infty} e^{-zx} F(x)\,dx - F(0) \tag{7.21}$$

where $F(x)$ is the CDF of x. Following the steps outlined in Chapter 3, it can be easily shown that the $\phi_{\gamma}^{(SC)}(.)$ in a Nakagami fading channel is given by,

$$\phi_{\gamma}^{(SC)}(z) = \sum_{i=1}^{N} \omega_i \prod_{k=1}^{L} \left[\Psi(m_k, m_k \chi_i / (z\bar{\gamma}_k)) / \Gamma(m_k)\right] + R_N \tag{7.22}$$

where $\Psi(a, x) = \int_0^x t^{a-1} \exp(-t)\,dt$ is the incomplete gamma function, χ_i and ω_i are the ith abscissa and weight of the N-th order Laguerre polynomial, and R_N corresponds to the remainder term.

7.2.3 Maximal-Ratio Combining (MRC)

Maximal-ratio combining is known to be optimum in the sense that it yields the best statistical reduction of fading in any linear diversity combiner. In this technique, the M diversity branches are first co-phased and then weighted in proportion to their signal level before summing. It is worth noting that the approximate bit error rate expression found in [79] is only accurate if the discrepancy between the mean signal strengths are small (exact for the equal mean signal strength case). On the other hand, the closed-form formula derived in [84] is exact even if the variances of the mean signal strengths are large, but limited to integer m. In [87], Efthymoglou et. al. presented a more general expression (i.e., for arbitrary fading parameters) by invoking the Gil-Pelaez inversion theorem, but the result is in the form of an integral:

$$P_b = \frac{1}{2\pi}\int_0^{\infty} \prod_{k=1}^{M} \left[1 + \left(\frac{t}{\lambda_k}\right)^2\right]^{-m_k/2} \left\{ \frac{\sin\left[0.5\tan^{-1}(t)\right]}{\left[t^2+1\right]^{0.25}} \cos\zeta + \left[1 - \frac{\cos\left[0.5\tan^{-1}(t)\right]}{\left[t^2+1\right]^{0.25}}\right] \sin\zeta \right\} \frac{dt}{t} \tag{7.23}$$

where $\zeta = \sum_{k=1}^{M} m_k \tan^{-1}(t/\lambda_k)$ and $\lambda_k = m_k/\bar{\gamma}_k$.

An alternative but considerably simpler analytical expression is obtained in [22] and [10] by using the MGF method,

$$P_b = \frac{1}{\pi}\int_0^{\pi/2} \prod_{k=1}^{M} \left[1 + \frac{\sec^2\phi}{\lambda_k}\right]^{-m_k} d\phi \tag{7.24}$$

More recently, we have estimated this expression very precisely involving only a finite sum of the MGF samples [27] (and therefore, our new expressions allows for a rapid evaluation of MRC diversity performance in different fading environments without imposing any constraint while being very easy to program):

$$P_b \approx \frac{1}{2n}\sum_{i=1}^{n} \prod_{k=1}^{M} \left[1 + \frac{\sec^2(\theta_i)}{\lambda_k}\right]^{-m_k} \tag{7.25}$$

where n is a small positive integer (typically, $n \leq 15$), and $\theta_i = (2i-1)\pi/4/n$. In Appendix 7A, we have derived a relatively tight bound for the remainder term.

7.3 Numerical Results

In this section, we first compare the performance of the proposed MA/SD selection rule with the traditional SNR/SD and the optimal MRC receiver structures in Rayleigh and Nakagami fading channels. Subsequently, we will investigate the effect of noninteger and/or nonidentical fading figures across all the fingers of a rake receiver, as well as the imbalance in the mean received signal strength levels on the receiver performance.

Fig. 7.3 compares the ABER performance of BPSK signals with three different combining techniques and varying diversity order over a Rayleigh fading channel. Obviously all the diversity combining methods yield the identical result for a single diversity branch. We have also verified that when the average signal power is zero (i.e., $\bar{\gamma}_b = 0$ or $\bar{\gamma}_b$ (in dB) $\rightarrow -\infty$), the probability of bit-error is 0.5 (not shown in this figure), which is anticipated for BPSK signals. It is also apparent from this figure that the largest diversity gain is obtained using 2-branch diversity and diminishing returns are obtained with

increasing order of *M*. This is typical for all diversity techniques. Another interesting point to note is that the MA/SD selection rule outperforms the traditional selection scheme. The explanation for this phenomena has been furnished in [83]. As an example, the differences in required SNR per bit predicted by the MA/SD selection model with respect to the conventional selection scheme for dual-diversity and four-fold diversity systems are 0.9 dB and 1.4 dB respectively, at an average BER of 10^{-3}. As we can see, the difference becomes more evident with a larger number of diversity branches. This may be attributed to the increased number of choices among statistically independent (Gaussian) noise samples.

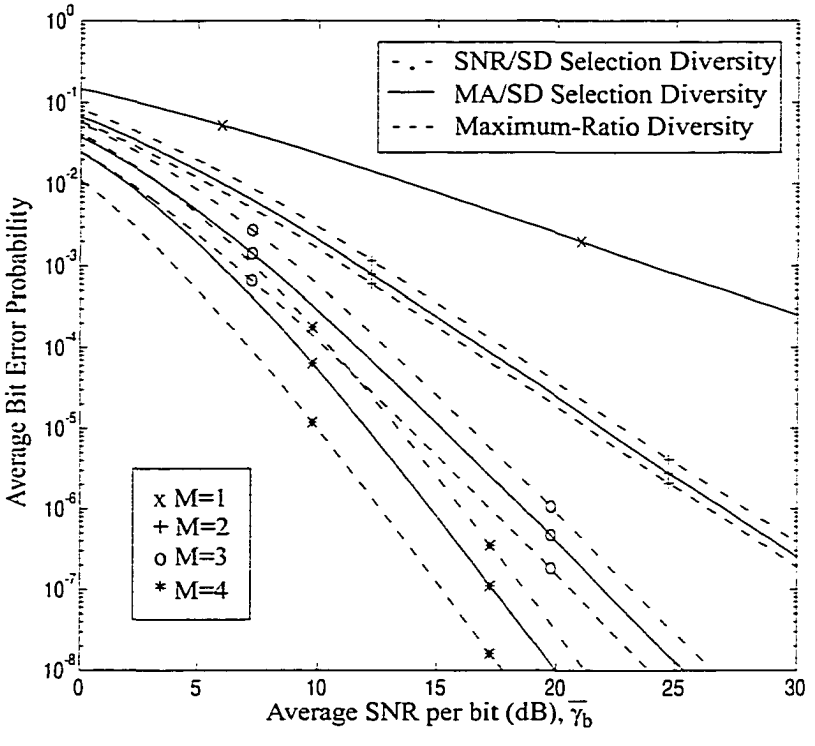

Fig. 7.3 Performance comparison of different diversity combining techniques and varying diversity order (M=1, 2, 3 and 4) for 2-PSK signals over a Rayleigh fading channel (m=1).

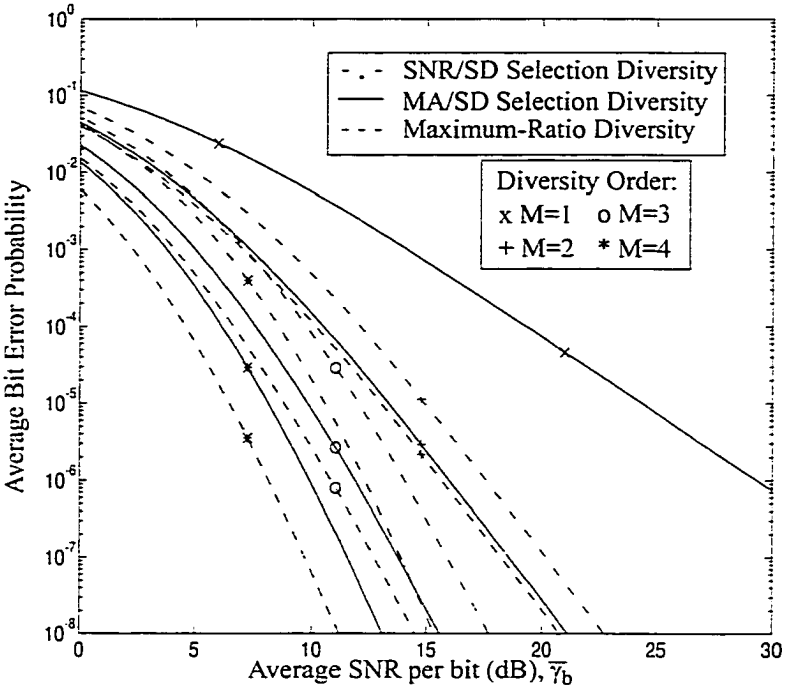

Fig. 7.4 Bit error rate performance for binary PSK signals over a Nakagami fading channel with fading figure m=2, as a function of mean received signal-to-noise ratio.

Fig. 7.4 depicts the bit error performance for binary PSK signals over a Nakagami fading channel with fading figure $m = 2$. Similar trends as in the Rayleigh fading case are observed here, except that the results are slightly better. Also notice that the results in these figures clearly illustrate the advantage of diversity as a means of overcoming the severe penalty in SNR/bit caused by fading. A few important conclusions can be drawn by comparing Fig. 7.3 and Fig. 7.4. First, the fade distribution affects the diversity gain. The relative advantage of diversity is greater for Rayleigh than Nakagami ($m > 1$) fading because as the fading figure m increases, there is less difference between the instantaneous receiver SNR on the various diversity branches. However, the performance is always better with Nakagami ($m > 1$) fading than Rayleigh fading for a given average received signal-to-noise ratio and diversity order. Next, the discrepancy between the SNR/SD and MA/SD selection systems becomes more pronounced in environments that

have strong specular paths (large m). Finally it is observed that the performance of the MA/SD scheme is much closer to the maximum-ratio diversity than the conventional selection scheme for small diversity orders. This observation becomes more noticeable in good channel conditions. However, the reverse is true when the number of diversity branches grows.

Fig. 7.5 illustrates the bit error rate performance of a rake receiver with two fingers as a function of the average received SNR per finger for eight different combinations of fading figures, but both diversity branches have identical mean signal strengths (corresponds to the uniform MIP). We found that the performance curves for these cases vary considerably. This suggests that the effect of noninteger and/or nonidentical fading parameters cannot be ignored in the analysis of a diversity receiver operating in a Nakagami fading environment. This is particularly interesting because the new expression derived in this paper allows us to predict the bit error rate performance of the MA/SD rake receiver accurately for arbitrary channel parameters, i.e., without imposing any restrictions on the fading parameters and/or the mean received signal strengths.

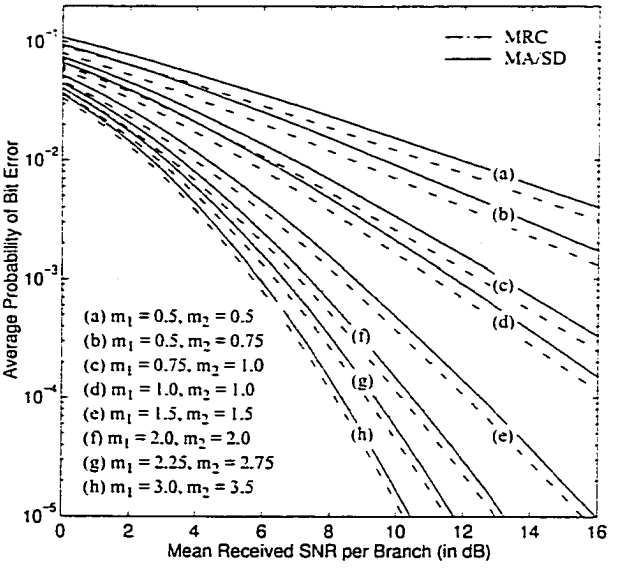

Fig. 7.5 Bit error rate performance of a dual-finger rake receiver in Nakagami fading environment with different fading parameters.

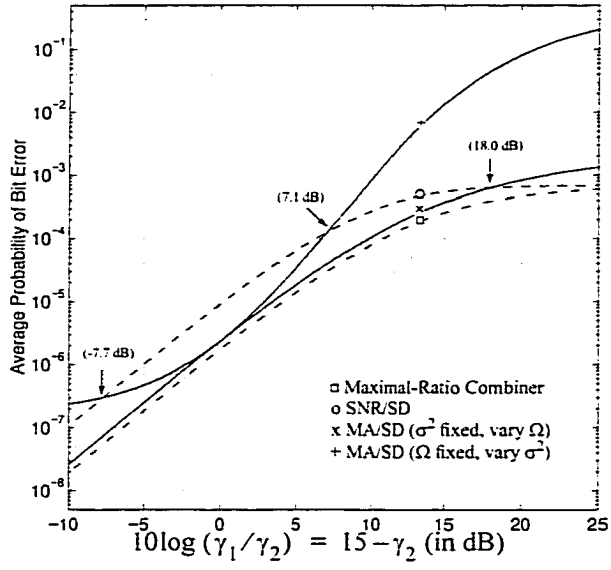

Fig. 7.6 Effects of unequal mean signal strengths on the BER performance of MA/SD, SNR/SD and MRC receiver structures with fading figure $m_1 = m_2 = 2$, $\bar{\gamma}_1$ is fixed at 15 dB, and $M = 2$.

The effect of unequal mean signal strength on the performance of a rake receiver with two fingers is illustrated graphically in Fig. 7.6. Here we assume that both these multipath diversity branches have identical fading parameters ($m_1 = m_2 = 2$) to isolate its effect on the system performance. As well, it is important to investigate the variations in the variance of MAI σ^2 and unbalances in the mean received signal power Ω separately, especially noting that the ratio σ_j/σ_i in Eq. (7.4) is different for these two cases. The unique trends cited in [84] are also apparent from this figure: (a) the diversity gain is maximized when the statistically independent diversity branches possess equal mean signal strength; (b) the MA/SD rule outperforms the traditional SNR/SD model if the discrepancy in the mean received SNR across the diversity branches is small (however, if the variation is extremely large, a very noisy branch can easily upset the system performance because it introduces ambiguity in the selection process); (c) it is observed that the MA/SD scheme is less susceptible to the variations in the mean received signal power levels compared to the fluctuations of the MAI power; (d) the SNR/SD selection diversity sys-

tem performs identically to the variations in σ^2 and Ω, which is anticipated.

Fortunately in practice, the assumption of equal MAI power in all the rake fingers is valid in most instances (because number of interfering users is the same for all the resolvable multipath signals). Consequently, the proposed MA/SD technique will always perform better than the traditional selection diversity model as long as the variations in the mean received signal power are not excessively large. But careful consideration should be placed in the case of time-diversity or macro-diversity reception because the above assumption may become void.

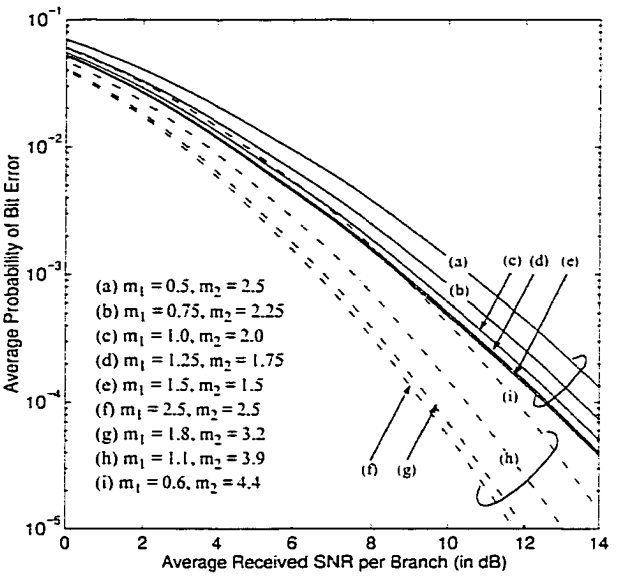

Fig. 7.7 Effect of nonidentical fading parameter on the performance of a rake receiver employing MA/SD.

Fig. 7.7 and Fig. 7.8 illustrate the effect of nonidentical fading parameters on the error performance of MA/SD and MRC rake receivers, respectively. A close look at the trends of these curves suggest that the effect of nonidentical fading figure along the multipath signals is somewhat similar to that exhibited by a rake receiver with unequal mean received signal power levels. From these figures we also observe that the best performance is realized when the received multipath signals undergo the same level of fading. Therefore the assumptions of identical fading figure and/or mean signal strengths tend to

yield rather optimistic results. A comparison between Fig. 7.7 and Fig. 7.8 reveals that the MA/SD system is more sensitive to nonidentical fading than that of MRC because the spread of the best-case and worst-case performance is much wider for the former.

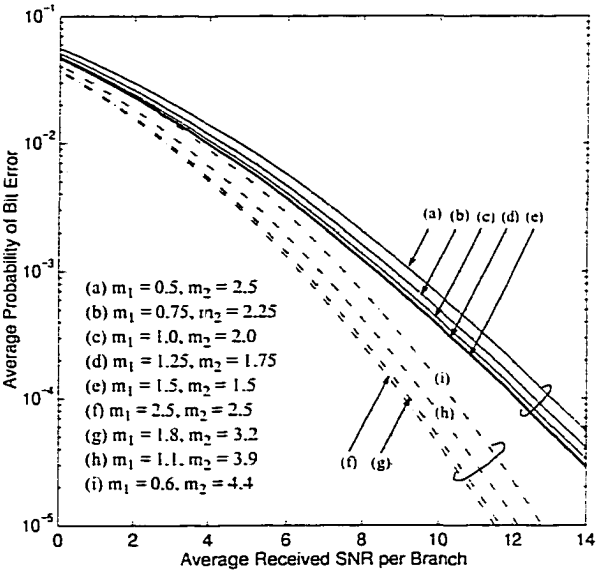

Fig. 7.8 Effect of nonidentical fading parameter on the performance of a rake receiver employing MRC.

7.4 Comparison between MA/SD and Imperfect MRC

In the maximal-ratio diversity system, the complex weighting factors on each branch of the combiner are adjusted to remain proportional to the complex conjugate of the fading signal phasor on each respective branch. Stein [21] has examined the effect of errors in MRC by computing the reduction in average output SNR for a fixed phasor error or a fixed amplitude error in the weighting factors. A more comprehensive study on this subject was performed by Gans [88] by considering the Gaussian errors in the combiner weighting factors. The Gaussian errors may be induced either due to inaccurate signal estimation or to decorrelation of the medium distortion on the pilot compared to that on the signal.

In case of the Rayleigh fading channel with uniform MIP, the probability density function of an MRC combiner with imperfect channel estimation is [88],

$$p(\gamma) = \frac{\left[1-\rho^2\right]^{M-1}\exp(-\gamma/\bar{\gamma})}{\bar{\gamma}} \sum_{k=0}^{M-1} \frac{1}{k!}\binom{M-1}{k}\left\{\frac{\rho^2\gamma}{\left[1-\rho^2\right]\bar{\gamma}}\right\}^k \tag{7.26}$$

where $\bar{\gamma}$ denotes the mean SNR per branch, and ρ is the correlation coefficient. Notice that when $\rho = 1$ (perfect correlation), perfect MRC combining is realized. On the other extreme, i.e., $\rho = 0$, there is no correlation between the pilot and the signal fading. As a result, the net performance is equivalent to the performance of a rake receiver without diversity (i.e., $M = 1$). Then it can be easily shown that the average bit error rate performance of a MRC rake receiver without perfect channel estimation is given by,

$$P_b = \left[1-\rho^2\right]^{M-1} \sum_{k=0}^{M-1}\binom{M-1}{k}\left[\frac{\rho^2}{1-\rho^2}\right]^k \left[\frac{1}{2}\left(1-\sqrt{\frac{\bar{\gamma}}{1+\bar{\gamma}}}\right)\right]^{k+1} \times \sum_{i=0}^{k}\binom{k+i}{i}\left[\frac{1}{2}\left(1+\sqrt{\frac{\bar{\gamma}}{1+\bar{\gamma}}}\right)\right]^i \tag{7.27}$$

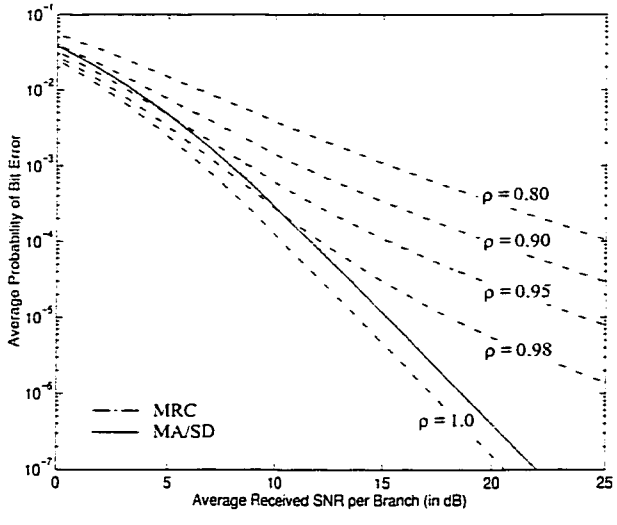

Fig. 7.9 Comparison between MA/SD rake receiver with imperfect MRC in a Rayleigh fading ($m = 1$) channel and uniform MIP. M is assumed to be 3 (three fingers).

It is apparent from Fig. 7.9 that inaccurate estimation of combiner weighting factors leads to serious degradation of the performance of the MRC rake receiver. In this situation, the proposed MA/SD receiver outperforms MRC because it is independent of such type of errors i.e., combination loss).

7.5 Conclusions

An analytical framework to evaluate the performance of a practical rake receiver structure in various propagation environments has been developed. The results obtained are sufficiently general to allow for arbitrary fading parameters as well as different mean signal strengths in the multipath signals. The selection rule based on choosing the finger with the largest composite received signal lends itself to a low-complexity receiver architecture, besides yielding improved performance over the traditional SNR/SD scheme in many realistic channel conditions. As well, inaccurate fading estimation leads to serious degradation in the performance of MRC receivers, and in this case, the proposed MA/SD becomes superior to MRC.

Appendix 7A

In this appendix, we will derive a simple expression for the remainder term, and therefore complement our previous work [27] by providing the error analysis for the resulting estimate of the truncated series.

Eq. (7.25) is a simple and efficient formula for computing the MRC diversity performance in Nakagami fading channel with arbitrary parameters. The expression simply involves summing up n samples of the MGF of the output SNR of the maximal-ratio combiner. However, there is remainder term R_n associated with Eq. (6) in [27], which vanishes as n gets large. So, the natural question is how large n should be or how to choose n for a specified error tolerance? The direct solution is to keep increasing n until the difference between the successive values of the expression is less than the specified error tolerance. However, this approach does not provide any indication about the conver-

gence rate of the expression. Alternatively, if a bound on magnitude of R_n as a function of n is available, a suitable value of n can be directly chosen so that the error magnitude is less than the accuracy threshold. This is the approach developed in this appendix. In other words, we provide a bound on the magnitude of R_n by an *a priori* error analysis. This bound also indicates the range of average SNR values for which our expression breaks down.

In [27], we have shown that the average BER for binary signals with MRC diversity reception over a frequency-nonselective Nakagami fading channel is in the form,

$$P_b = \int_{-1}^{1} \frac{f(x)}{\sqrt{1-x^2}} dx \tag{7A.1}$$

where

$$f(x) = \frac{1}{2\pi} \prod_{l=1}^{L} \left(\frac{x+1}{x+1+2a^2/\lambda_l} \right)^{m_l} \tag{7A.2}$$

where $\lambda_l = m_l/\Omega_l$ and the coefficient a in (7A.2) indicate the type of modulation [$a = 1$ for antipodal signaling (PSK) and $a = 1/\sqrt{2}$ for orthogonal signaling (FSK)]. Parameters L, Ω_l and m_l denote the diversity order, average SNR per branch and fading figure of the lth branch, respectively. Using Gauss-Chebychev (GCQ) approximation [[14], pp. 889] to evaluate (7A.1), we get [[27], Eq. (6)],

$$\hat{P}_b = \frac{1}{2n} \sum_{j=1}^{n} \prod_{l=1}^{L} \left[1 + \frac{a^2 \sec^2(\theta_j)}{\lambda_l} \right]^{-m_l} \tag{7A.3}$$

where $\theta_j = (2j-1)\pi/4/n$. The exact BER is given by $P_b = \hat{P}_b + R_n$. In [27], we asserted that the remainder term decreases to zero as n gets large, without offering any further proof. Taking the magnitude of the remainder term [14, pp. 889], we have an upper bound on R_n,

$$|R_n| \le \frac{\pi}{(2n)!\,2^{2n-1}} \left| f^{(2n)}(\zeta) \right| \quad \text{for } -1 < \zeta < 1 \tag{7A.4}$$

where notation $f^{(n)}(x)$ denotes the n th derivative of function $f(x)$, and ζ is unknown. However, evaluating higher order derivatives of $f(x)$ depicted in (7A.2) is difficult and tedious. Therefore, using a complex-variable technique, we bound $|f^{(2n)}(\zeta)|$ in terms of maximum $|f(z)|$ on some contour containing [-1, 1] in its interior within the region of analyticity of $f(z)$. The n-th derivative of an analytic function is given by the formula in [[89], pp. 65],

$$f^n(\zeta) = \frac{n!}{2\pi}\int_{C_\rho}\frac{f(z)}{(z-\zeta)^{n+1}}dz \tag{7A.5}$$

for any ζ inside the analytic region and C_ρ can be any arbitrary contour with $\rho > 1$. Here we choose circular contour $C_\rho = \rho\exp(i\theta)$ for $0 \le \theta \le 2\pi$, where $i^2 = -1$ (see Fig. 7.10).

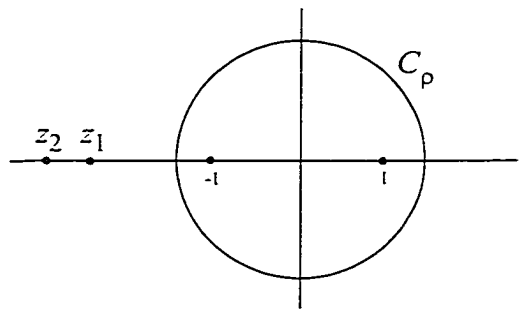

Fig. 7.10 Circular contour of integration.

Consider any ζ on the real axis between -1 and $+1$, and let

$$M(f; C_\rho) = \max_{z \in C_\rho} |f(z)|.$$

By taking absolute value of integral (7A.5) and using the maximum value of $|f(z)|$ and minimum value of $|z-\zeta|$ on C_ρ, we get

$$|f^n(\zeta)| \le \frac{n!}{2\pi}\frac{2\pi\rho M(f; C_\rho)}{|\rho-1|^{n+1}} = \frac{n!\rho M(f; C_\rho)}{|\rho-1|^{n+1}}. \tag{7A.6}$$

In order for (7A.6) to be a valid bound, $\rho > 1$ and $f(z)$ should be analytic in the interior of C_ρ (i.e., there are no poles of $f(z)$ in the interior). The analytic region of $f(z)$ fol-

lows readily. Since it has poles at $z_l = -\left[1 + 2a^2/\lambda_l\right]$, which should not lie inside C_ρ, let $\hat{\rho} = \min\left\{1 + \left[2a^2/\lambda_l\right] \;\middle|\; 1 \le l \le L\right\}$.

Then $f(z)$ is analytic inside C_ρ for $1 < \rho < \hat{\rho}$. On the circular contour, the maximum of $|f(z)|$ occurs at $\theta = 0$ or $\theta = \pi$. Hence combining (7A.4) and (7A.6) we have,

$$|R_n| \le \min_{1<\rho<\hat{\rho}} \left[\frac{2\pi\rho}{4^n(\rho-1)^{2n+1}} \max\left\{|f(\rho)|, |f(-\rho)|\right\}\right] \tag{7A.7}$$

Note that $|f(\rho)| > |f(-\rho)|$ only when ρ is near unity. Eq. (7A.7) shows that the remainder term vanishes rapidly for a larger sample size n and higher average received SNR per channel Ω. The constrained minimization of (7A.7) also can be solved easily using common mathematical software packages such as Maple and Matlab.

This new bound (i.e., Eq. (7A.7)) is highly desirable since it does not require the evaluation of higher order derivatives, which can be difficult, time consuming and tedious. More importantly, it allows us to choose an appropriate value for n that satisfies a prescribed error tolerance. Since (7A.7) is an upper bound, it is not necessary to perform this minimization with a very high accuracy. In fact, choosing $\rho = \hat{\rho}/2$ may be sufficient for large SNR values. Thus,

$$|R_n| \le \left\{\frac{\rho}{4^n(\rho-1)^{2n+1}} \prod_{l=1}^{L} \left|\frac{1-\rho}{\left[1+2a^2/\lambda_l\right]-\rho}\right|^{m_l}\right\}\Bigg|_{\rho=\frac{\hat{\rho}}{2}} \to \left(\frac{m}{\Omega}\right)^{2n} \tag{7A.8}$$

Note also that for large SNR values, $\hat{\rho} \approx 2a^2\Omega/m$ where Ω/m is the minimum Ω_l/m_l across the diversity branches. Thus, the term inside the product sign are nearly unity, and the remainder term decreases as $2n$-th power of the SNR. Note also for small SNR values (i.e., $\Omega \to 0$), $\hat{\rho} \to 1$. Then the above bound becomes very loose. Thus for extremely small SNR values $\Omega \ll 1$, our expression (7A.3) breaks down as indicated by the loose bound on R_n. It means that the expression is not valid for $\Omega \to -\infty$ (dB), so increasing n is not enough.

In the case of identical diversity branch statistics and $2n+1 > M$ where $M = \sum_l m_l$, the value of ρ that minimizes the term $(\rho-1)^{2n+1-M}\left[1+2a^2/\lambda-\rho\right]^M$ in (7A.7) is

$$\rho^* = \left[(2n+1-M)\left[1+2a^2/\lambda\right]+M\right]/(2n+1)$$

Therefore,

$$|R_n| \le \frac{\rho^*}{4^n(\rho^*-1)^{2n+1-M}\left[1+2a^2/\lambda-\rho^*\right]^M} \tag{7A.9}$$

Next, a few selected numerical examples for the error bound (7A.7) and its tightness are provided. The analysis of tightness of the error bound is quite tricky because the bound decreases very rapidly (see the tables) as n increases. Since the exact $R_n = P_b - \hat{P}_b$, we need to compute P_b with accuracy (say) 10^{-50}, much more exact than the floating point precision. In the most general case, P_b can only be expressed as an integral (not an explicit closed-form formula) and it is impossible to achieve such a level of accuracy. Therefore, in the following antipodal signaling (BPSK) examples, we have assumed that all the diversity branches have identical Ω and same fading figure although the general expression can handle both unequal mean signal strengths and dissimilar fading parameters. In this case, using [[12], (14-4-15)] with $\bar{\gamma}_c = \Omega/m$ and replacing L by mL, the exact BER expression is given by,

$$P_b = \left[\frac{1}{2}(1-\mu)\right]^{mL}\sum_{k=0}^{mL-1}\binom{mL-1+k}{k}\left[\frac{1}{2}(1+\mu)\right]^k \tag{7A.10}$$

where $\mu = \sqrt{\Omega/(m+\Omega)}$ and mL is an integer. Using Maple to compute Eq. (7A.3) and Eq. (7A.10) with the accuracy up to 80 decimals, we can investigate the tightness of upper bound for R_n. Table 7.1 reveals that Eq. (7A.7) is a valid upper bound for the remainder term even at SNR levels as low as 0 dB. The bound becomes tighter with the increase in Ω, as anticipated.

Table 7.1 Comparison between the upper bound for R_n (Eq. (7A.7)) and actual $R_n = P_b - \hat{P}_b$ (Eqs. (7A.3) and (7A.10)) at different SNR levels ($L = 2, m = 1$).

Mean received SNR per channel, Ω	Remainder term R_n			
	$n = 5$		$n = 10$	
	Upper bound	Exact	Upper bound	Exact
0 dB	2.3051×10^{-4}	9.0986×10^{-8}	9.4226×10^{-10}	4.4543×10^{-15}
2 dB	1.9796×10^{-6}	3.6995×10^{-9}	8.1820×10^{-14}	5.7406×10^{-18}
5 dB	1.7014×10^{-9}	1.5248×10^{-11}	7.1236×10^{-20}	7.5404×10^{-23}
15 dB	1.4492×10^{-19}	7.0916×10^{-21}	6.1659×10^{-40}	1.2234×10^{-41}

Table 7.2 Bound on R_n for different L ($\Omega = 5$dB, $m = 1$)

Diversity order, L	Number of samples, n		
	5	10	15
1	2.8937×10^{-10}	5.6225×10^{-21}	8.0925×10^{-32}
2	1.7014×10^{-9}	7.1236×10^{-20}	1.5751×10^{-30}
5	1.2818×10^{-8}	8.4363×10^{-18}	7.6542×10^{-28}
10	6.4100×10^{-11}	1.2535×10^{-16}	2.1064×10^{-25}
15	2.2983×10^{-15}	1.1257×10^{-17}	1.2247×10^{-24}

Table 7.2 shows the upper bound on R_n for different diversity orders. The remainder term diminishes very rapidly with the increasing number of MGF samples for a given order of diversity, as expected. Although the remainder term increases with the increasing diversity order initially, this value will be always smaller than R_n obtained with a much smaller n. From the column entry corresponding to $n = 5$, we notice that R_n will reduce eventually with L if the order of diversity becomes very large.

The effects of Ω and m on the remainder term are illustrated in Table 7.3 and Table 7.4, respectively. These numerical results validate the asymptotic trends that can be derived from (7A.8). Comparison between Table 7.2 and Table 7.4 reveals that L and m have similar effects on the bound of the remainder term.

Table 7.3 Bound on R_n for various Ω ($L = 3, m = 2$)

Mean received SNR per channel, Ω	Number of samples, n		
	10	15	20
1 dB	4.1055×10^{-3}	6.1349×10^{-6}	3.8758×10^{-9}
3 dB	3.3038×10^{-7}	5.0089×10^{-12}	3.1855×10^{-17}
5 dB	2.7974×10^{-11}	4.2981×10^{-18}	2.7498×10^{-25}
10 dB	2.2040×10^{-21}	3.4665×10^{-33}	2.2403×10^{-45}

Table 7.4 Bound on R_n for various m ($\Omega = 7$dB, $L = 2$)

Fading figure, m	Number of samples, n		
	5	10	15
0.5	2.5371×10^{-15}	4.8384×10^{-31}	6.8116×10^{-47}
1.0	1.5981×10^{-11}	6.7310×10^{-24}	1.4909×10^{-36}
1.5	3.0000×10^{-9}	1.6696×10^{-19}	3.3356×10^{-30}
3.0	8.1388×10^{-6}	9.1476×10^{-12}	8.1168×10^{-19}

From the numerical examples, we find that the BER expression (7A.3) developed in [27] is virtually exact for sufficiently large n (say, 20 samples) and SNR over 0 dB. The expression only breaks down when the SNR approaches $-\infty$ dB.

Chapter 8

A Robust Diversity Combining Scheme for Spread Spectrum Packet Radio Networks

Random access protocols such as ALOHA are attractive in wireless environments due to their simplicity, and because they do not require centralized coordination. However, the traditional narrowband ALOHA suffers from its low maximum throughput, inherent system instability, and rapid rising delay under intensive traffic loading. Although its performance can be improved by employing a carrier-sensing technique, it is rather difficult to achieve a reliable carrier sensing in a wireless environment due to hidden terminal problems. Besides, there exists a maximum data rate that can be transmitted via a narrowband ALOHA channel (limited by the intersymbol interference). In order to facilitate high data rate transmissions, the only choice until now has been the awkward use of multiple ALOHA channels in parallel (e.g., Inmarsat networks).

On the other hand, wideband code division multiaccess (CDMA) is an attractive signalling scheme for high-speed packet radio networks because it has good signal capture, along with spread spectrum advantages [90], such as immunity to external interference and jamming, robustness against intersymbol interference, antimultipath capability, and low probability of intercept. Consequently, employing spread spectrum signaling in a random access packet-switched radio network may provide a possible solution to attain the high throughputs and high data rates required for new applications of today — an important milestone towards achieving the promised ubiquitous personal communication services (PCS).

However, the advantages of packet CDMA are generally offset by channel bandwidth utilization levels due to the large processing gain required for reliable multiuser operation [91]. This motivates the application of forward error correction (FEC) coding which is known to provide significant capacity increases both in fixed assigned CDMA and slotted packet CDMA. Besides multiuser interference, the wireless medium can severely degrade the system performance. In order to cope with the detrimental effects of channel fading and multiuser interference, some form of diversity reception is needed. Fortunately, an automatic repeat-request (ARQ) strategy can be easily incorporated into packet-switched networks, thereby allowing these systems to operate at higher raw error rates.

In the conventional random-access packet-switched direct sequence CDMA (hereafter, simply referred to as DS/CDMA ALOHA) [91][92], erroneous packets will be discarded, and decoding of a newly received copy is attempted at the receiver without using any prior knowledge from previously received copies of the same packet (which were not decoded successfully). Simply discarding the noisy packets seem to be wasteful, particularly when one realizes that a portion of a packet may have been received correctly[1]. Chase [93] has suggested combining the noise corrupted packets at the codeword level to form a single more reliable packet, thus minimizing the average number of retransmissions required before a packet is received successfully. Whereas in [94], the authors analyzed the efficacy of packet combining with an average diversity combiner for continuous data transmission. In [95], packet combining technique has been applied to a slotted frequency hopped spread spectrum multiple access (FH/SSMA) system. It should be pointed out, however, that in [95] the authors have neglected the effects of channel fading and additive white Gaussian noise in their analysis, by assuming co-channel interference as the only source of error. Furthermore, only a lower bound on the throughput performance (worst-case analysis) of the proposed system was presented.

---

1. Since the severity of the errors in a packet is a monotonically increasing function of the number of simultaneous transmissions, a large portion of the packet may not be affected if the number of active users is not excessively high.

By contrast, in this chapter we examine the performance of slotted and unslotted random access asynchronous DS/CDMA radio networks with retransmission diversity combining, in a Rayleigh multipath fading environment. The analysis can be easily extended to other fading conditions by exploiting the results in Chapter 3. In our system, the combining operation occurs at the bit level, and the resulting decisions are produced by employing maximal-ratio diversity at the output of the rake receiver. Specifically, we outline a novel mechanism to ensure a reliable packet combining operation, and investigate the effects of the time-varying multiuser interference (due to bursty nature of the traffic) on the system performance by validating the tightness of the upper and lower bounds for the throughput and packet error probability. Computationally efficient formulas for evaluating the performance of these systems will be presented. Finally, the sensitivity of the system performance to the channel impairments, such as packet header failure and missed acknowledgment messages, will be studied.

An outline of this chapter is as follows: The assumptions required for analytical tractability, traffic flow model and the system operation are described in Section 8.1. Section 8.2 details the bound estimations for the packet error probability and the throughput performance for both slotted and unslotted DS/CDMA ALOHA networks with packet combining. Subsequently, in Section 8.3, an error performance analysis for a combined packet-diversity and rake receiver with finite tap-statistics is outlined. Numerical results are presented in Section 8.4. Finally in Section 8.5, the main points are summarized.

8.1 DS/CDMA Packet Radio Network

8.1.1 Analytical Model

When the spread-spectrum multiple access channel is operated in a random access packet mode, the analysis proceeds in a manner that is analogous to that for ALOHA channels, with the difference that $m > 1$ simultaneous transmissions do not necessarily produce a collision, but result in a soft degradation in error rate. The assumptions used in

this chapter are similar to those adopted in [91], [92], [95] and [96]. We shall describe them briefly, in order to be complete.

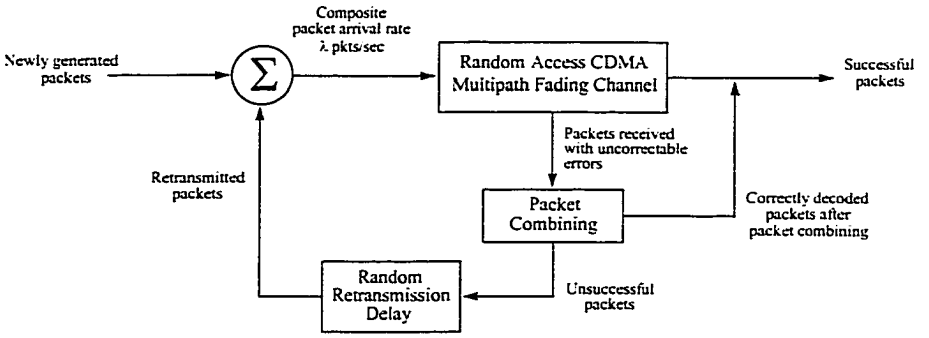

Fig. 8.1 Schematic of traffic flow in the proposed random access DS/CDMA system.

A schematic representation of traffic flow in a random access DS/CDMA system with packet combining is shown in Fig. 8.1. Each transceiver can be in either one of two operation modes: origination mode or backlog mode. In the origination mode, there is no backlogged packet to be retransmitted, and new packets are transmitted in any given slot with probability p_o. When a packet retransmission is requested, the user enters the backlogged mode, where the probability of retransmission of this packet in the next slot is geometrically distributed with probability p_r. If $p_o = p_r = p$, the composite packet arrival distribution becomes binomial with parameters p and K_{MAX} (number of subscribers). Further simplification occurs when $p_o = p_r = p \to 0$ and $K_{MAX} \to \infty$, because the binomial distribution approaches the Poisson traffic model with an arrival rate equal to the traffic intensity. The composite packet arrival distribution $f_\mu(m)$ is [91],

$$f_\mu(m) = \frac{(\lambda T)^m}{m!} e^{-\lambda T} \tag{8.1}$$

with a finite composite arrival rate λ, and packet reception interval T. Hence, $\mu = \lambda T$ is the offered traffic (average number of attempted transmissions per slot).

Modeling the time-varying nature of the multiple access interference is simplified if the bit error probabilities in adjacent bits of a packet are independent to each other. This condition is satisfied when the spreading signature sequences are truly random and if perfect chip level synchronization is achieved [97]. The second requirement is a constraint that is needed for analytical purposes and tends to impact the achievable performance adversely. However, the statistical independence assumption becomes quite realistic if the system is operating in a fast fading environment or in an ideally interleaved condition. Although the latter has delay or latency ramifications, these are less critical than those due to retransmissions. Furthermore, packet combining can reduce correlation and tends to make the occurrence of bit errors random. It is also reasonable to assume that errors in different packets occur independently, since the CDMA spreading codes are generally sufficiently random to allow for this.

8.1.2 Network Description

When the information bits from a particular user are ready for transmission, parity bits for error detection based on a high error detecting code C_0 are appended to them, yielding an information sequence of k_d bits. Subsequently, they are encoded for error correction by a different code C_1 (e.g., an (N_d, k_d, t_d) BCH code) to form a packet of N_d bits. For simplicity, let us assume that the same cyclic code will be used for both error correction and error detection. The FEC code is capable of correcting up to t_d random errors per packet. The encoded binary data are then phase modulated to yield a constant-envelope data-modulated carrier before the direct-sequence spreading operation (which is accomplished by multiplying with the user's signature waveform). Similar operations are performed by K other active users in the system.

The transmitted signal is perturbed by self-interference and channel attenuation due to multipath fading, multiuser interference, and additive white Gaussian noise. In order to capture the signal from user i, the received composite signal is assumed to go through a rake receiver with M taps (fingers), where $M \leq L$, and L corresponds to the maximum number of resolvable multipaths. First, the received signal is despread independently for

each multipath component by multiplying the spreading signature code of the ith user, delayed by an amount equal to the estimated multipath delay. The modulated signal is then down-converted to a baseband signal and passed through a bank of correlators prior to diversity combining. In the maximal-ratio combiner, the voltage signal from each of the M path diversity branches are first co-phased, and then weighted in proportion to their signal level before summing. The sampled decision statistic at the output of the rake demodulator (before a hard decision for the bit is made by the threshold detector) is stored in a register until the packet is successfully received or decoded. When a received packet is detected in error, the receiver first attempts to correct the error. If the received packet is not detected in error or does not contain an uncorrectable error pattern, a positive acknowledgment (ACK) message is sent to the transmitter, indicating that the packet has been successfully decoded and delivered to the user. Then, the content of the corresponding registers are flushed.

In case of a decoding failure, a negative acknowledgment (NAK) message is sent to request for a retransmission. The transmitter reschedules the same packet for transmission after a certain random delay. When the retransmitted packet is received, the receiver again attempts to correct errors (if any). If the decoding is successful, an ACK message will be sent to the transmitter, as before. However, if the decoding is not successful, then the packet combining mechanism will be initiated [see Fig. 8.1]. It is worth noting that an acknowledgment message (either NAK or ACK) will not be sent to the transmitter until the packet combining process is completed. The retransmissions continue until the receiver is able to reconstruct the transmitted packet. Theoretically, a message might be repeated forever while awaiting an ACK. Usually, a system implementation will contain a retransmission limit (i.e., truncated ARQ protocol) beyond which the message is returned undelivered. Such a strategy is also important for delay sensitive applications that impose an upper bound on the time delay, at the expense of packet reliability (quality of service).

Similar to [98], we assume that the feedback channel error can only make ACK and NAK messages indistinguishable and the transmitter will handle this erred ACK or NAK

message (erasure symbol) as a NAK. Such an assumption is reasonable since the undetectable error probability can be made very small by proper selection of error detecting codes. The following two additional protocols are required for a noisy feedback channel: (a) Each time the transmitter sends out a packet, the timer for the packet is initialized and started. If the response from the receiver is not obtained for the packet after a reasonable period of time, it is assumed that the response is a NAK; (b) If the receiver receives a packet that has already been accepted, an ACK is sent to the transmitter and the packet is discarded.

8.1.3 Packet Identification Mechanisms

If the pseudo-random (PN) spreading code is unique for each user, the signal will appear as random noise for unintended recipients. This protection level (also known as the processing gain, PG) is given by the ratio between the PN sequence chipping rate and the encoded source rate. It is evident that the spreading-despreading operation helps to reduce or possibly eliminate the probability of erroneous or incorrect combining of packets from different users in a receiver oriented protocol.

Consider now the packets received by a particular user. The receiver is expected to determine if a received packet is a new packet or a retransmission of a previously transmitted packet (in case of decoding failure) before it is routed to the combiner. In a practical operating environment, the receiver may not be able to determine the packet sequence number with certainty unless it is completely free of errors or contains a correctable error pattern. As a consequence, the receiver may incorrectly combine two or more different packets intended for the same user. In this case, there is obviously no reason for additional diversity! Hence, it is evident that the results presented in [94] and [95] are contingent upon perfect knowledge about the sequence numbers of the noisy packets (although no such mechanisms were proposed therein).

Decoding of the newly received packets first prior to the combining operation helps to reduce this error event[2]. But this step still does not guarantee a reliable packet combin-

ing operation. Alternatively, packet retransmissions can be sent on a different carrier frequency (in this case, additional RF bandwidth is required) or using different spreading sequences (each user will be assigned a pair of signature codes). However, these approaches are not justifiable in practice due to the inefficient use of the limited resources, and increased hardware complexity (the former scheme requires an additional modulator-demodulator circuitry, whereas the latter approach requires a second correlator at the receiver front-end with its own signature waveform generation circuitry). In light of these considerations, in this chapter we present two simple yet robust mechanisms that will enable the receiver to distinguish a new packet from a retransmitted copy intended for the same user or eliminate the need for such a requirement in a receiver oriented protocol, even in the presence of feedback channel errors.

8.1.3.1 Idle ARQ

The simplest resolution to this issue is to ensure each user operates in a stop-and-wait ARQ operation mode (i.e., the transmitter will not send a new packet until it receives a positive acknowledgment for the current packet). While this strategy is plausible for terrestrial communications where the propagation delay is negligible or small, such a system will yield a very low throughput if a typical long round trip delay scenario or high-speed modems are considered.

8.1.3.2 Extra Protection for the Packet Header

Since the packet header contains at least source identification and packet sequence number which are used in packet combining process, it is natural to protect this header information (k_h bits) by using a powerful FEC. In our scheme, the message itself is contained within a packet, with source address and packet sequence number preceding the

2. By performing this "checking" process and only triggering the combining operation if the newly received packet was not decoded successfully, we can assure that the performance of the packet combining system will not be any poorer than that of the traditional type-I hybrid ARQ scheme, even if all the packets were combined incorrectly.

message in a header [see Fig. 8.2 (b)]. The header is encoded separately from the message so that the header may be read before making a decision as to whether to read the following message section. When the packet header preceding a message is not decoded correctly, then the packet (i.e., message) will be discarded, and a retransmission will be requested. However, if the packet header is detected correctly but not the message, then the packet combining operation will be triggered. An ACK will be sent on return channel if both packet header and the message were received successfully. It is worth noting that the likelihood of the event that a packet header is missed but its corresponding message block is received correctly is negligible because the header is normally protected with a very low rate code and its block size is usually much smaller than the message block length, i.e., $N_h \ll N_d$. From now onwards, we shall assume that packet combining systems will adopt this scheme, unless stated otherwise.

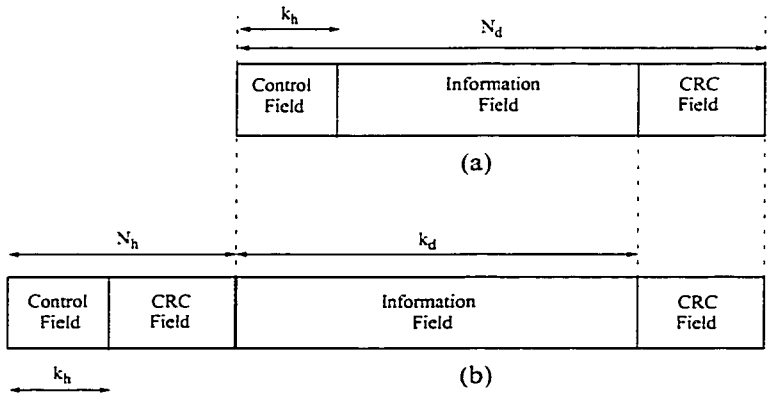

Fig. 8.2 Data frame format for: (a) conventional DS/CDMA ALOHA (i.e., without packet combining); and (b) packet combining systems.

Thus far, we have assumed a receiver oriented protocol and subsequently proposed two methods to ensure a reliable packet combining operation. But disadvantages of the receiver oriented protocol include transmitters that must select proper spreading codes and the possibility of overlapping messages from two transmitters intended for the same

receiver. Two other spreading protocols, i.e., the transmitter oriented protocol and the approach where a common spreading sequence is used for the entire network (i.e., spread ALOHA), yield the possibility of a receiver accidentally combining packets not intended for it unless the header is first correctly decoded and the packet destination is examined. In all these cases, our second approach of providing extra protection to the packet header (which contains the packet sequence number as well as the source and the destination addresses) will ensure a reliable packet combining operation.

8.2 Throughput Analysis

In this chapter several performance quality indices of a packet radio network are considered. The average packet error probability or the average bit error rate metric is related to a particular link performance, whereas throughput and average time delay are representative of network performance, in terms of channel bandwidth utilization efficiency and stability. As in [91], the steady-state throughput β is defined as the expected number of successful transmissions per time slot. Then, the throughput of a conventional slotted random access DS/CDMA is given by,

$$\beta = \sum_{m=1}^{K_{MAX}} m P_C(m) f_\mu(m) = \mu \sum_{K=0}^{K_{MAX}-1} P_C(K+1) f_\mu(K) \tag{8.2}$$

where $P_C(m)$ denotes the packet success probability conditioned on $m = K+1$ simultaneous transmissions during that packet transmission interval, μ is the offered load, and K_{MAX} corresponds to the maximum number of users that can be simultaneously handled by the system, because the number of receivers or available codewords is limited.

Exact evaluation of the throughput performance with packet combining is rather involved, specifically because the packet success probability is dependent not only on the most recently received packet, but also related to previously received copies of that packet. In particular, the time-varying co-channel interference produces a nonstationary packet error probability. This is true for both slotted and unslotted radio networks under

consideration. Moreover, in an unslotted system the interference level changes even during the reception of a packet because some transmissions are started while others are completed during that interval. Since the time-varying nature of multiuser interference imposes considerable analytical and computational difficulties, we resort to bounding techniques to investigate the system performance. Subsequently, the tightness of the upper and lower bounds for the frame-error rate and throughput are validated.

8.2.1 Bound Estimation for Packet Error Probability

Let $D^{(i)}(K_1, K_2, \ldots\ldots, K_i)$ be the event that after combining i copies of the same packet, decoded data block still contains an uncorrectable error pattern, conditioned on $K_j + 1$ simultaneous users during transmission of the j th copy, $j = 1, 2, \ldots, i$. The probability of this event is denoted as $P_i = p\{D^{(i)}(K_1, K_2, \ldots\ldots, K_i)\}$. Since a decoding failure of the combined packet after the i th reception will initiate the request of an $i+1$ th transmission of that packet, it is evident that the packet error rate with i number of transmissions, $P_B^{(i)}$, is equal to the repeat-request probability (RRP) of the $i+1$ th transmission:

$$P_B^{(i)} = p\{D^{(1)}(K_1), D^{(1)}(K_2), D^{(2)}(K_1, K_2), D^{(1)}(K_3), D^{(3)}(K_1, K_2, K_3), \ldots$$

$$\ldots, D^{(1)}(K_i), D^{(i)}(K_1, K_2, \ldots, K_i)\} \qquad (8.3)$$

For instance, $P_B^{(1)}$ corresponds to the RRP of the first retransmission (i.e., the probability that original packet contains an uncorrectable error pattern), while $P_B^{(2)}$ denotes the RRP of the second retransmission (i.e., both the original and first retransmitted packets was not decoded successfully, and the new packet formed from the two available packets at the receiver still contains an uncorrectable error pattern) and so on. Evaluation of expression (8.3) is rather difficult because the events $p\{D^{(1)}(K_1)\}$, $p\{D^{(2)}(K_1, K_2)\}$, ..., and $p\{D^{(i)}(K_1, K_2, \ldots, K_i)\}$ are not independent. However, it is possible to derive the upper and lower bounds. Realizing

$P_B^{(i)} = p\{D^{(1)}(K_1), D^{(1)}(K_2), D^{(2)}(K_1, K_2), \ldots, D^{(1)}(K_i) \mid D^{(i)}(K_1, \ldots, K_i)\} \times p\{D^{(i)}(K_1, K_2, \ldots, K_i)\}$, the upper bound is given by P_i. Whereas the lower bound can be obtained by assuming that $P_1, P_2, \ldots, P_i$ are all independent events. Using the upper and lower bounds for the RRP, the packet error probability is bounded by,

$$P_E(K_2) \times P_E(K_3) \times \ldots \times P_E(K_i) \prod_{j=1}^{i} P_j \leq P_B^{(i)} \leq P_i \tag{8.4}$$

where $P_E(K_x) = p\{D^{(1)}(K_x)\}$. Note that the block error rate of the conventional system (type-I hybrid ARQ) is given by $P_B^{(i)} = P_E(K_1) \times P_E(K_2) \times \ldots \times P_E(K_i)$, which is equivalent to the performance of a simple time-diversity strategy without packet combining (diversity combining).

8.2.2 Bound Estimation for Average Number of Transmissions

Now consider the following three situations: (a) the interference level is constant[3] and equal to z over the entire interval $[0, T]$; (b) the maximum number of interfering users among the i combined packets is equal to $z = K^*$, where $K^* = max(K_1, K_2, \ldots, K_i)$; and (c) the minimum number of interfering users between the i combined packets is $z = K_*$, where $K_* = min(K_1, K_2, \ldots, K_i)$. Consequently, the error probability for P_i is bounded by,

$$p\{D^{(i)} \mid K_*\} \leq p\{D^{(i)}(K_1, K_2, \ldots, K_i)\} \leq p\{D^{(i)} \mid K^*\} \tag{8.5}$$

where

3. This condition is satisfied in a slotted system because the users have to wait until the beginning of some time-slot to transmit or retransmit their packets. However, it becomes void in an unslotted case because the number of interfering transmissions changes during the reception of a packet. Consequently, one may have to resort to bounding techniques even to analyze the performance of a conventional unslotted system (without packet combining).

$$p\{D^{(i)} \mid K\} = p\{D^{(i)}(K, K, \ldots, K)\}$$
$$= 1 - \sum_{x=0}^{t_d} \binom{N_d}{x} \left[P_b^{(i)}(K+1)\right]^x \left[1 - P_b^{(i)}(K+1)\right]^{N_d - x} \tag{8.6}$$

and $P_b^{(i)}(.)$ is the average probability of bit-error of a rake-rake receiver configuration (combined packet and spread spectrum diversity), which can be calculated as in Section 8.3. In order to use the bounds depicted in (8.5), it is necessary to find the distribution of K^* and K_*. In what follows, mathematical expressions for the probability density functions of K^* and K_* are developed, and employed to obtain the upper and lower bounds on the average number of transmissions required to transmit a packet successfully, and the corresponding throughput performance for the DS/CDMA ALOHA systems with packet combining.

8.2.2.1 Slotted DS/CDMA ALOHA

In this section, we consider a time-slotted asynchronous direct-sequence CDMA packet radio network that operates in a random access mode. It is considerably easier to implement a slotted system than to synchronize the chip duration among all the terminals in the network. Since the users in this system are required to wait until the beginning of some time-slot to transmit or re-transmit their packets, there is no loss in generality in assuming a constant number of interfering transmissions throughout the entire packet.

Let $R_{av}(K_1, K_2, \ldots, K_\infty)$ denote the average number of transmissions necessary to transmit a given packet successfully, conditioned on K_i other users transmitting simultaneously during the ith transmission of this packet. Utilizing the upper and lower bounds of the RRP, $R_{av}(K_1, K_2, \ldots, K_\infty)$ can be bounded by,

$$1 + \sum_{i=1}^{\infty} P_E(K_2) \times \ldots \times P_E(K_i) \prod_{j=1}^{i} P_j \le R_{av}(K_1, K_2, \ldots, K_\infty) \le 1 + \sum_{i=1}^{\infty} P_i \tag{8.7}$$

For analytical tractability, we further assume that the packet arrivals in the different time slots are independent Poisson random variables. Then the unconditional average number of transmissions, R_{av}, is obtained by averaging (8.7) over (8.1) [99],

$$R_{av} = 1 + \sum_{i=1}^{\infty} \left\{ \sum_{K_1=0}^{\infty} f_{\mu}(K_1) \sum_{K_2=0}^{\infty} f_{\mu}(K_2) \cdots \sum_{K_i=0}^{\infty} f_{\mu}(K_i) \right\} \times P_B^{(i)} \tag{8.8}$$

After some algebraic manipulations [see Appendix 8A], (8.8) can be easily shown to be upper and lower bounded by (8.9) and (8.10), respectively, by considering the maximum and the minimum number of interfering users among the combined packets,

$$R_{av-AU} = 1 + \sum_{i=1}^{\infty} \sum_{K^*=0}^{\infty} \left\{ \left[\sum_{s=0}^{K^*} \frac{\mu^s}{s!} e^{-\mu} \right]^i - \left[\sum_{s=0}^{K^*-1} \frac{\mu^s}{s!} e^{-\mu} \right]^i \right\} \times p\{D^{(i)} | K^*\} \tag{8.9}$$

$$R_{av-L} = 1 + \sum_{i=1}^{\infty} \sum_{K_*=0}^{\infty} \left\{ \left[1 - \sum_{s=0}^{K_*-1} \frac{\mu^s}{s!} e^{-\mu} \right]^i - \left[1 - \sum_{s=0}^{K_*} \frac{\mu^s}{s!} e^{-\mu} \right]^i \right\} \times p\{D^{(i)} | K_*\} \tag{8.10}$$

where $p\{D^{(i)} | K^*\}$ and $p\{D^{(i)} | K_*\}$ are evaluated using (8.6). It is important to highlight that (8.9) is the absolute upper bound for the average number of transmissions. However, this is not the case with the lower limit described by (8.10) due to our pessimistic assumption of $P_B^{(i)}$. But (8.10) is useful because it allows us to investigate the effects of the time-varying multiuser interference on the system performance. The absolute lower bound on R_{av} can be evaluated in a similar way,

$$R_{av-AL} = 1 + \sum_{i=1}^{\infty} \sum_{K_*=0}^{\infty} \left\{ \left[1 - \sum_{s=0}^{K_*-1} \frac{\mu^s}{s!} e^{-\mu} \right]^i - \left[1 - \sum_{s=0}^{K_*} \frac{\mu^s}{s!} e^{-\mu} \right]^i \right\} \times \left[p\{D^{(1)} | K_*\} \right]^{i-1} \times \prod_{j=1}^{i} p\{D^{(j)} | K_*\} \tag{8.11}$$

It is also noted that the expressions in (8.9), (8.10), and (8.11) are related in the following manner,

$$R_{av-AL} \le R_{av-L} \le R_{av-AU} \tag{8.12}$$

Since $1/R_{av}$ is the average portion of a packet which is received successfully in each transmission, and μ is the average number of packets generated during each time slot, the system throughput is given by,

$$\beta = \mu/R_{av} \tag{8.13}$$

It can be easily shown that (8.13) reduces to (8.2), the familiar expression for throughput of a conventional slotted DS/CDMA ALOHA when packet combining is not considered. The channel utilization efficiency is dictated by the normalized throughput η,

$$\eta = \frac{\mu}{R_{av}} \times \psi \times \frac{1}{PG} \tag{8.14}$$

which is defined as the number of information bits correctly received per second per unit bandwidth [bits/s/Hz] (i.e., data throughput per unit bandwidth). The scalar ψ in (8.14) corresponds to the percentage of the message information bits in a data frame. Hence, $\psi = (k_d - k_h)/N_d$ and $\psi = k_d/(N_d + N_h)$ for the conventional DS/CDMA ALOHA and the packet combining systems, respectively.

8.2.2.2 Unslotted DS/CDMA ALOHA

In an unslotted (without frame synchronization) system, the packets are transmitted on the channel as soon as they are generated. Consequently, each transmitted packet experiences a random multiuser interference pattern corresponding to the evolution of channel traffic (asynchronous packet arrivals and departures) during the transmission interval. This imposes more severe computational difficulty when compared to the slotted case.

The probability distributions for the maximum and minimum number of interfering users within a packet reception interval in an unslotted system have been developed in [96] by considering the following three situations: (a) the maximum interference level over the interval $[0, T]$ is z; (b) the interference level is constant and equal to z over the entire interval; and (c) the minimum interference level over the interval is z. These distributions are given in terms of the Poisson density function $f_{\mu}(.)$ and the Poisson cumula-

tive distribution function $F_{\mu}(z) = \sum_{w=0}^{z} f_{\mu}(w)$,

$$g_{\mu\_max}(z) = f_{\mu}(z)\{\mu(z+1-\mu)f_{\mu}(z) + [(z+1-\mu)^2+\mu]F_{\mu}(z)\}/(z+1) \quad (8.15)$$

$$g_{\mu\_min}(z) = f_{\mu}(z)\{(\mu+1-z)f_{\mu}(z) + \mu^{-1}[(\mu-z)^2+\mu][1-F_{\mu}(z)]\} \quad (8.16)$$

By exploiting the knowledge of these probability density functions, and following the steps as we have outlined for the slotted case in Section 8.2.2.1, it can be easily shown that the average number of transmissions for the unslotted DS/CDMA ALOHA with packet combining is bounded by (8.17) and (8.18),

$$R_{av} \le 1 + \sum_{i=1}^{\infty}\sum_{K^*=0}^{\infty}\left\{\left[\sum_{s=0}^{K^*} g_{\mu\_max}(s)\right]^i - \left[\sum_{s=0}^{K^*-1} g_{\mu\_max}(s)\right]^i\right\} \times p\{D^{(i)}|K^*\} \quad (8.17)$$

$$R_{av} \ge 1 + \sum_{i=1}^{\infty}\sum_{K_*=0}^{\infty}\left\{\left[1-\sum_{s=0}^{K_*-1} g_{\mu\_min}(s)\right]^i - \left[1-\sum_{s=0}^{K_*} g_{\mu\_min}(s)\right]^i\right\} \times \left[p\{D^{(1)}|K_*\}\right]^{i-1} \times \prod_{j=1}^{i} p\{D^{(j)}|K_*\} \quad (8.18)$$

Once again, the corresponding absolute lower and absolute upper bounds on the normalized throughput can be attained using the definition in (8.14).

8.2.3 ACK Sensitivity

ARQ transactions in a Selective-Repeat retransmission request system with a noisy feedback channel is illustrated in Fig. 8.3. When an ACK or NAK is missed, the previous transmission is repeated. A missed NAK has no effect on the throughput performance because the response will be interpreted as a NAK anyway. The missed ACK, however, causes an extra transmission. Its effect is to increase the R_{av} by a factor $P_F/(1-P_F)$ for an ACK failure probability of P_F. It is important to highlight that if the receiver

receives a packet that already has been accepted, an ACK is sent to the transmitter, and the packet will be discarded.

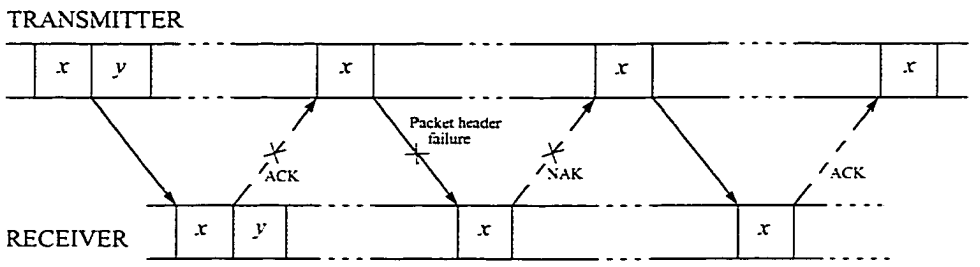

Fig. 8.3 ARQ transactions in a Selective-Repeat retransmission request system with a noisy feedback channel.

8.2.4 Packet Header Sensitivity

When a header is missed, the transmission is wasted. If P_H denotes the packet header failure probability, then P_H is the fraction of messages wasted. Consequently, if R_{av} transmissions must be received to deliver a message successfully, then $R_{av}/(1-P_H)$ transmissions must be sent. It is evident that its effect is to decrease the system throughput by the same factor. As an example, the resulting R_{av-AU}, taking into account both packet header and ACK sensitivities, for the slotted DS/CDMA ALOHA with packet combining is,

$$R_{av-AU} = \frac{1}{(1-P_H)} \sum_{i=1}^{\infty} \sum_{K^*=0}^{\infty} \left(\left[\sum_{s=0}^{K^*} \frac{\mu^s}{s!} e^{-\mu} \right]^i - \left[\sum_{s=0}^{K^*-1} \frac{\mu^s}{s!} e^{-\mu} \right]^i \right) \times p\{D^{(i)} | K^*\} + \frac{1}{(1-P_H)(1-P_F)} \tag{8.19}$$

where the header failure probability is computed as,

$$P_H = \sum_{K^*=0}^{\infty} \frac{\mu^{K^*}}{K^*!} e^{-\mu} \sum_{x=t_h+1}^{N_h} \binom{N_h}{x} \left[P_b^{(1)}\left(K^*+1\right) \right]^x \left[1 - P_b^{(1)}\left(K^*+1\right) \right]^{N_h - x} \tag{8.20}$$

8.3 Performance of Combined Multipath and Packet Diversity (2-D Receiver)

Rake reception is an excellent strategy to exploit the autocorrelations properties of the PN spreading signature waveforms by resolving and combining the multipath components to obtain spread spectrum diversity. In practice, the diversity improvement attained by combining many demodulator fingers actually declines beyond some optimal value, as each tap has already improved statistics, and because of surmounting combination losses of many fingers. Hence, in this section an analytical closed form expression to evaluate the average bit error rate of the coherent binary phase shift keying (BPSK) signal, after combining the finite $M \leq L$ tap decisions (i.e., M-fingers) from each of the B packets (time-diversity branches), is outlined. The analysis can be easily extended to other fading conditions as well, following the moment generating function (MGF) approach presented in Chapter 3.

Following the analysis for maximal-ratio combining in [12], the probability of bit error conditioned on a fixed set of path gain is,

$$P_b(\gamma_b) = \frac{1}{2}\text{erfc}\left[\sqrt{\gamma_b}\right] = \frac{1}{\pi}\int_0^{\pi/2} \exp\left[-\gamma_b \csc^2(\theta)\right] d\theta \tag{8.21}$$

where γ_b denotes the instantaneous received signal-to-noise ratio (SNR), defined as,

$$\gamma_b = \sum_{i=1}^{B} \sum_{l=1}^{M} \gamma_{il} \tag{8.22}$$

and the notation γ_{il} corresponds to the instantaneous received SNR for the ith packet and lth multipath component. In the preceding section, the bounds on throughput and packet error probability are derived by considering that multiple copies of the same packet are affected in a similar manner (i.e., same number of interfering users). This allows us to assume γ_{il} are statistically identical with respect to index i, yielding $\bar{\gamma}_{1l} = \bar{\gamma}_{2l} = \ldots = \bar{\gamma}_{Bl} = \bar{\gamma}_l$. If we assume the branch fading as well as branch noises to be statistically independent, then the characteristics function for γ_b is simply the product

of their individual characteristics functions, i.e.,

$$\psi_{\gamma_b}(jv) = \prod_{l=1}^{M} \frac{1}{(1-jv\bar{\gamma}_l)^B} = \sum_{l=1}^{M} \sum_{i=1}^{B} \frac{A_{li}}{(1-s\bar{\gamma}_l)^i} \tag{8.23}$$

where

$$A_{li} = \frac{1}{(B-i)!\ (-\bar{\gamma}_l)^{B-i}} \frac{d^{B-i}}{ds^{B-i}} \left\{ \prod_{\substack{k=1, \\ k \neq l}}^{M} \frac{1}{(1-s\bar{\gamma}_k)^B} \right\} \Bigg|_{s=1/\bar{\gamma}_l} \tag{8.24}$$

and $\bar{\gamma}_l$ is the average SNR for path l of the target receiver is given by [99],

$$\bar{\gamma}_l \cong \frac{E\left[\beta_l^2\right]}{\frac{2}{3N} \sum_{j=1,\, j\neq l}^{L} E\left[\beta_j^2\right] + \frac{2K}{3N} \sum_{j=1}^{L} E\left[\beta_j^2\right] + \frac{N_o}{E_b}} \tag{8.25}$$

where β_j corresponds to the channel gain of the jth path. With the assumption of an exponentially decaying power delay profile, (8.25) reduces to,

$$\bar{\gamma}_l = \left[\frac{2(K+1)}{3N} \sum_{j=1, j\neq l}^{L} e^{-(j-l)\delta} + \frac{2K}{3N} + \left\{ \frac{N_o}{E_b E\left[\beta_1^2\right]} \right\} e^{(l-1)\delta} \right]^{-1} \tag{8.26}$$

because $E\left[\beta_j^2\right] = E\left[\beta_1^2\right] e^{-(j-1)\delta}$. Parameter δ in (8.26) represents the decay rate of the multipath intensity profile (MIP).

The inverse Fourier transform of the characteristic function in (8.23) yields the probability density function of γ_b in the form,

$$f_{\gamma_b}(x) = \sum_{l=1}^{M} \sum_{i=1}^{B} A_{li} \frac{x^{i-1}}{(i-1)!\,(\bar{\gamma}_l)^i} \exp\left(\frac{-x}{\bar{\gamma}_l}\right) \tag{8.27}$$

Therefore, the average probability of bit error for BPSK with combined spread spectrum and packet diversity, conditioned on $K+1$ active users, is given by,

$$P_b^{(B)}(K+1) = \sum_{l=1}^{M}\sum_{i=1}^{B} A_{li}\int_0^{\infty}\frac{1}{2}\operatorname{erfc}(\sqrt{x})\frac{x^{i-1}}{(i-1)!\,(\bar{\gamma}_l)^i}\exp\left(\frac{-x}{\bar{\gamma}_l}\right)dx \tag{8.28}$$

The definite integral in (8.28) has a known closed-form solution (e.g., [100]),

$$\begin{aligned}
&\int_0^{\infty}\frac{1}{2}\operatorname{erfc}(\sqrt{x})\frac{x^{i-1}}{(i-1)!\,(\bar{\gamma}_l)^i}\exp\left(\frac{-x}{\bar{\gamma}_l}\right)dx \\
&\quad = (2i-1)!\;{}_2F_1\left(i, i+\frac{1}{2}, i+1, \frac{-1}{\bar{\gamma}_l}\right)\Big/\left[2^{2i}(\bar{\gamma}_l)^i(i-1)!\,i!\right] \\
&\quad = \left[\frac{1}{2}(1-\Delta_l)\right]^i\sum_{w=0}^{i-1}\binom{i-1+w}{w}\left[\frac{1}{2}(1+\Delta_l)\right]^w
\end{aligned} \tag{8.29}$$

where $\Delta_l = \sqrt{\bar{\gamma}_l/(1+\bar{\gamma}_l)}$. Hence, the closed-form bit-error rate expression is obtained by substituting (8.24) and (8.29) into (8.28).

Alternatively, the performance of the two-dimension diversity receiver (i.e., combined packet and spread-spectrum diversity) in a Rayleigh fading channel may be evaluated using Eq. (8.30):

$$P_b^{(B)}(K+1) = \frac{1}{\pi}\int_0^{\pi/2}\phi_\gamma\left[\sec^2(\theta)\right]d\theta = \frac{1}{\pi}\int_0^{\pi/2}\prod_{i=1}^{B}\prod_{l=1}^{M}\frac{d\theta}{\left[1+\bar{\gamma}_{il}\sec^2(\theta)\right]} \tag{8.30}$$

For different fading environments, one just need to substitute an appropriate expression for the MGF $\phi_\gamma(.)$ in Eq. (8.30). As well, Eq. (8.28) can be further simplified for the uniform multipath intensity profile ($\delta = 0$) case, i.e.,

$$P_b^{(B)}(K+1) = \left[\frac{1}{2}(1-\Delta)\right]^{MB}\sum_{w=0}^{MB-1}\binom{MB-1+w}{w}\left[\frac{1}{2}(1+\Delta)\right]^w \tag{8.31}$$

By choosing different values of M, the trade-off between performance and receiver com-

plexity can be investigated. For instance, the performance of a single correlation receiver can be readily evaluated by setting $M = 1$. On the other hand, by selecting $M = L$, the performance of the optimum coherent receiver is realized.

8.4 Numerical Results

We now present some representative numerical results which give an indication of the performance improvement provided by packet combining. Each packet in the conventional DS/CDMA ALOHA consists of $N_d = 127$ bits, and FEC is assumed to correct up to $t_d = 4$ bits, i.e., a $(127, 99, 4)$ BCH code. For simplicity, we assume that the same cyclic code will be used for both error correction and error detection. Whereas, the packet combining systems will have an additional $N_h = 31$ bits tagged preceding the message block, as illustrated in Fig. 8.2. The packet header is assumed to be protected by $(31, 11, 5)$ BCH code, unless stated otherwise. Gold codes of period 63 are employed as a spreading sequence. Therefore, $N = 63$ because each bit is encoded with 63 chips. For the Rayleigh multipath fading model, we assume that the maximum number of resolvable paths L to be 5, the MIP decay rate parameter $\delta = 1$, and the average received SNR of the first arriving path, in the absence of multiuser and self-interference, is fixed at $E[\beta_1^2] E_b/N_0 = 15$ dB.

Fig. 8.4 compares the frame error probabilities for two different block sizes and error correction capabilities. It is evident from this figure that the packet header failure rate is significantly lower than that of the message frame. This suggests that the likelihood of a message block being received correctly when its corresponding header block was missed is negligible. The difference in the error performance is due to two factors: (a) the header frame length is smaller than the message block size, and therefore it is more robust to random channel errors; (b) error protection for the header section is greater (i.e., lower code rate), thereby further reducing the frame error rate.

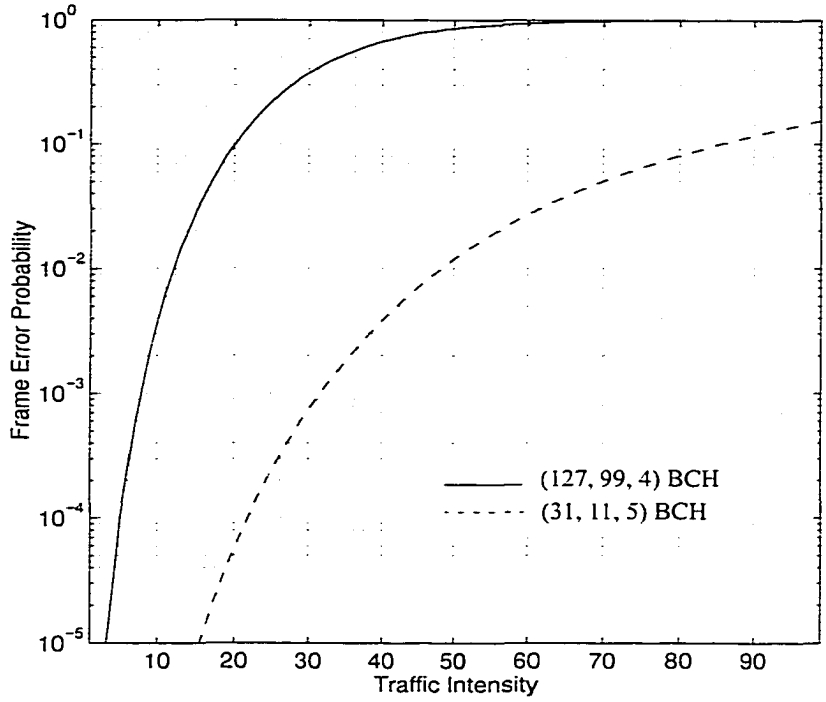

Fig. 8.4 Comparison between the message (solid curve) and packet header (dashed curve) failure rates as a function of offered traffic.

The tightness of the bounds on throughput and packet error probability are depicted in Fig. 8.5. As expected, the throughput characteristics for the conventional DS/CDMA ALOHA (denoted as Type-I HARQ) exhibits behavior that is typical of random access systems, with throughput initially increasing with the channel traffic and then decreasing as the load[4] increases beyond the channel "capacity". In order to make a fair comparison between the conventional and the proposed packet combining system (i.e., isolate the effect of the different message block size), N_d is maintained to be identical for both systems. The header information bits (k_h = 11 bits) in the conventional DS/CDMA ALOHA will have the same protection level as the message information bits of length $(k_d - k_h)$. This is because a packet retransmission will be initiated unless both the

4. In this thesis, we have used the terminologies "offered traffic", "traffic intensity" and "channel traffic" synonymously.

header and message fields were received correctly. Therefore, in this case it is only wasteful to allocate extra redundancy bits for protecting the packet header. Comparison between the upper bound and the absolute upper bound for throughput curves of the packet combining system (obtained by substituting (8.10) and (8.11) into (8.14), respectively) indicate that the bound on packet error rate is very tight over a wide range of offered traffic. Hence, P_i is a very good approximation for $P_B^{(i)}$ in the analysis of throughput and/or delay performance. However this is not the case for the average number of transmissions, when the effect of multiuser interference is taken into account. While this bound (given by expressions (8.9) and (8.10)) is reasonably tight at low and moderate values of μ, it becomes weak as the traffic intensity increases. This observation is attributed to the fact that the difference between K^* and K_* becomes significant at higher ranges of offered load.

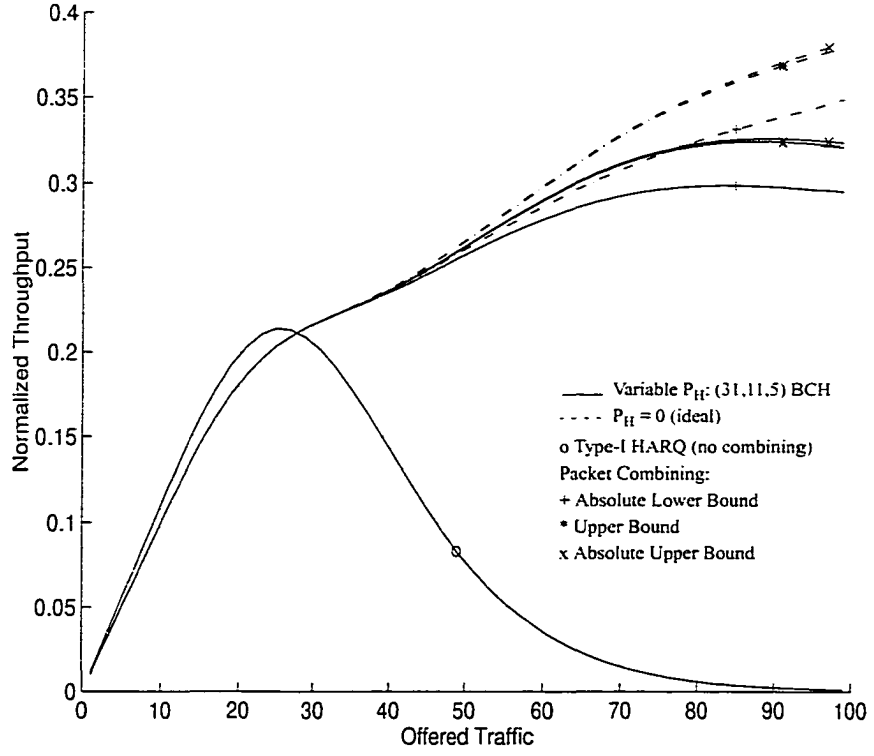

Fig. 8.5 Bounds on throughput performance of a slotted DS/CDMA ALOHA with Poisson traffic: (a) $P_H = 0$, and (b) variable P_H - (31,11,5) BCH code.

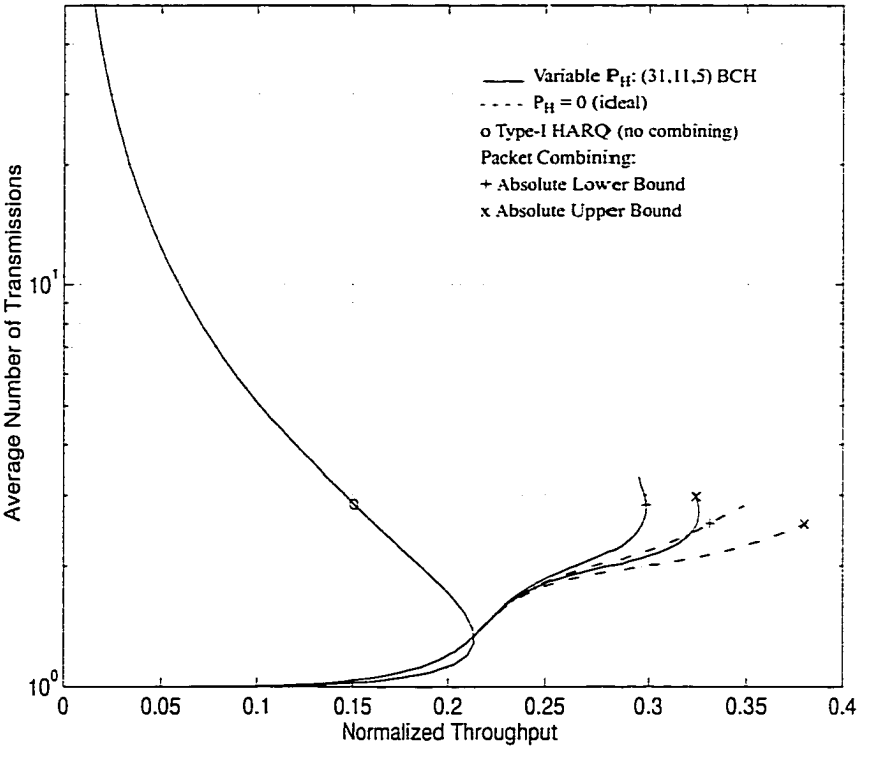

Fig. 8.6 Delay-throughput characteristics of a slotted random access packet CDMA with and without retransmission diversity combining in an error-free feedback channel.

In Fig. 8.6, delay-throughput performance of slotted DS/CDMA networks (with and without packet combining) are plotted for different packet header failure rates. It is clear that the type-I hybrid ARQ system is still inherently unstable. But this serious problem can be mitigated by introducing some form of diversity reception. Notice that when the traffic intensity is low, the proposed packet combining scheme has the net effect of reducing the normalized throughput, compared to the performance curve of the conventional DS/CDMA ALOHA. This is because additional parity bits (fixed overhead) are sent in each transmission for protecting the packet header. However, as the traffic intensity increases, the former performs better because of its ability to exploit packet diversity which reduces the retransmission frequency. Packet combining also dramatically reduces

the average number of transmissions necessary before a packet is decoded successfully, thereby improving the delay performance of the type-I hybrid ARQ system.

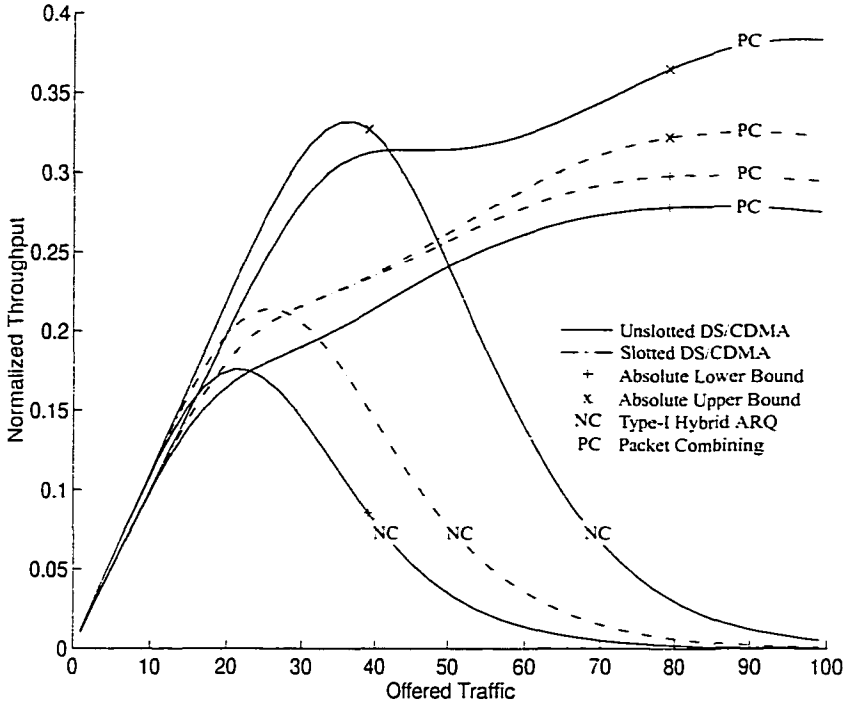

Fig. 8.7 Bounds on normalized throughput for the slotted and unslotted random access spread-spectrum radio networks with Poisson traffic arrival, and $P_F = 0$.

Fig. 8.7 examines the impact of packet combining on channel utilization efficiency of an unslotted random access DS/CDMA. This scenario is important because of the pure ALOHA-like implementation complexity and robustness advantages associated with completely uncoordinated channel access. While there is a 2:1 capacity differential (i.e., 0.368 versus 0.184) between slotted and unslotted fixed packet length narrowband ALOHA networks, unslotted operation results in a much smaller penalty (perhaps only 10-30%) for packet CDMA. It is also apparent from this figure that the throughput for the slotted random-access packet-switched DS/CDMA system falls in between the absolute upper and lower bounds for the unslotted DS/CDMA system. This is true for both

the packet combining and no combining cases. Because of the nature of the functional dependence of the error probability on the number of simultaneous transmissions, it is expected that the absolute lower bound is closer to the actual throughput than the absolute upper bound. Therefore, we conjecture that the throughput for an unslotted system falls between the absolute upper bound for the slotted system and the absolute lower bound for the unslotted system. Similar observations and conclusions were drawn for a conventional frequency-hopped spread-spectrum multiple access network in [96].

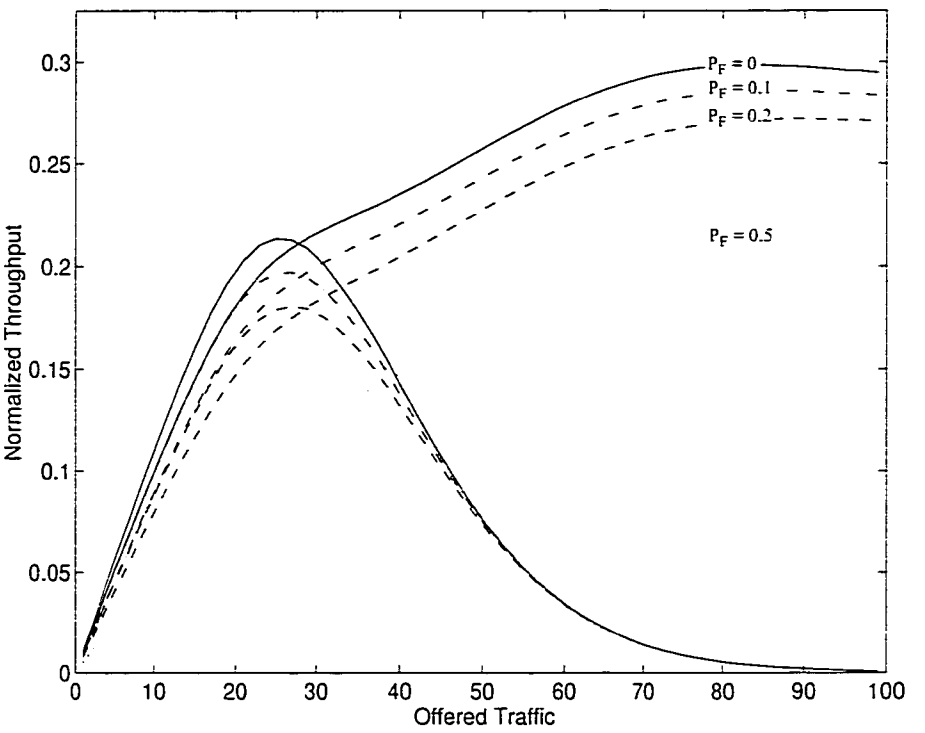

Fig. 8.8 Throughput performance of a slotted DS/CDMA ALOHA with and without packet combining in the presence of a noisy feedback channel. The packet header is assumed to be protected with a (31,11,5) BCH code.

From Fig. 8.8, it is obvious that feedback channel errors (i.e., missed ACK) only causes graceful degradation to the network performance. Hence, we can conclude that in practice the reduction in the throughput performance due to P_F will be negligible since

the ACK messages are normally protected by a low-rate code and their packet size is usually short. On the other hand, the system throughput may decline rather rapidly as the load increases, depending on the protection level of the packet header (see Fig. 8.5 and Fig. 8.6). This observation is attributed to the fact that packet diversity may not be realized if the header block is corrupted. This reduction, however, can be restored by adopting an adaptive multi-copy packet header transmission strategy or other approaches that will reduce the header failure probability. Analysis of such schemes are beyond the scope of this thesis.

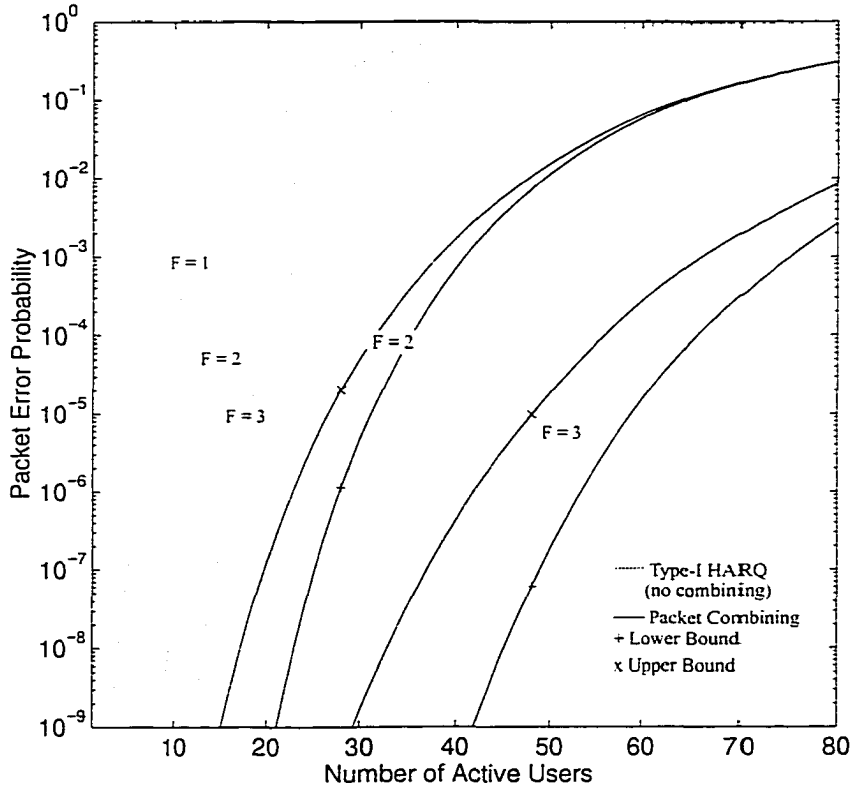

Fig. 8.9 Comparison of packet error probability between a type-I hybrid ARQ scheme and the proposed packet combining technique in a Rayleigh multipath fading environment.

It is also worth noting that the network stability issue can be alleviated by limiting the maximum number of packet retransmissions (in situations where a large number of retransmissions occur), but at the expense of packet reliability. Let notation $F-1$ denote the maximum allowable packet retransmissions in a truncated ARQ protocol. Packet error probability can be used as a reliability metric in an hybrid ARQ protocol with finite (small) number of transmissions because its reliability is mainly determined by the decoding failure, rather than the undetectable error probability. While the delay performance for the proposed packet combining scheme is identical with that of the conventional DS/CDMA ALOHA when $F = 2$ (only single retransmission is allowed), the system reliability is significantly better for the former than the latter, as shown in Fig. 8.9. As well, the packet error rate for the multicopy transmission system is identical with the absolute upper bound of the packet combining system (with its corresponding F). From Fig. 8.9, we can conclude that packet combining can significantly improve the reliability of the truncated ARQ protocol, or alternatively support a larger number of simultaneous users for a given reliability index. As an example, the conventional type-I HARQ with two retransmissions ($F = 3$) can only facilitate up to 17 simultaneous users (on average) at $P_B = 10^{-5}$. On the other hand, the packet combining system can accommodate up to 46 users with the same number of retransmissions. This is particularly interesting in that a considerable improvement is attained with only a modest increase in the buffer requirements and processing complexity of the conventional system.

8.5 Conclusions

A steady-state performance analysis has been presented for both slotted and unslotted random access packet-switched DS/CDMA networks in conjunction with packet combining. This technique is highly advantageous for systems which can tolerate a certain delay and operate over highly time-varying channels. To facilitate the analysis, we have derived simple and computationally efficient formulas for evaluating the average number of transmissions and throughput of this new system with Poisson traffic. Numerical

results reveal that the proposed adaptive retransmission diversity combining system yields a higher maximum throughput in comparison with the conventional DS/CDMA ALOHA, and helps to sustain a high level of throughput over a wide range of offered traffic (at the expense of only a slight increase in implementation complexity). Packet combining also dramatically reduces the average number of transmissions necessary before a packet is received correctly, thereby improving the delay performance of the type-I hybrid ARQ system. Missed ACK and controlled header failure rate only cause graceful degradation of the network performance. Besides ensuring a more stable network, the reliability of a truncated ARQ protocol can be substantially enhanced by employing packet diversity.

Appendix 8A

Expressions (8A.5) and (8A.7) derived in this appendix enable us to evaluate both the upper and lower bounds on (8.8) efficiently. For mathematical simplification but without any loss in generality, let us assume that m_1 will take the maximum value for the number of interfering users among the combined packets, i.e., $m_1 = max(m_1, m_2, ..., m_i)$. Hence, the unconditional average number of transmissions R_{av} is upper-bounded by,

$$R_{av} \le 1 + \sum_{i=1}^{\infty} \left\{ \sum_{m_1=0}^{\infty} \sum_{m_2=0}^{\infty} \cdots \sum_{m_i=0}^{\infty} f_\mu(m_1) f_\mu(m_2) \ldots f_\mu(m_i) \times p\{D^{(i)} \mid m_1\} \right\} \quad (8A.1)$$

where $p\{D^{(i)} \mid m_1\} = p\{D^{(i)}(m_1, m_1, ..., m_1)\}$. Subsequently, (8A.1) can be restated as,

$$R_{av} \le 1 + \sum_{i=1}^{\infty} \left[\sum_{m_1=0}^{\infty} f_\mu(m_1) \left\{ \sum_{m_2=0}^{\infty} f_\mu(m_2) \cdots \sum_{m_i=0}^{\infty} f_\mu(m_i) \right\} \times p\{D^{(i)} \mid m_1\} \right] \quad (8A.2)$$

The right-hand side of (8A.2) can be re-written in the form of a binomial series, i.e.,

$$\text{RHS} = 1 + \sum_{i=1}^{\infty}\left[{}^{i}C_1 \sum_{m_1=0}^{\infty} f_{\mu}^{1}(m_1)\left\{\sum_{t=0}^{m_1-1}\frac{\mu^t}{t!}e^{-\mu}\right\}^{i-1} + {}^{i}C_2 \sum_{m_1=0}^{\infty} f_{\mu}^{2}(m_1)\left\{\sum_{t=0}^{m_1-1}\frac{\mu^t}{t!}e^{-\mu}\right\}^{i-2} + \ldots + {}^{i}C_j \sum_{m_1=0}^{\infty} f_{\mu}^{j}(m_1)\left\{\sum_{t=0}^{m_1-1}\frac{\mu^t}{t!}e^{-\mu}\right\}^{i-j} + \ldots + \sum_{m_1=0}^{\infty} f_{\mu}^{i}(m_1)\right] \times p\{D^{(i)} \mid m_1\} \quad (8A.3)$$

where the binomial coefficient is defined as ${}^{a}C_b = \frac{a!}{(a-b)!b!}$.

Therefore, Eq. (8A.3) can be simplified as,

$$\text{RHS} = 1 + \sum_{i=1}^{\infty}\sum_{m_1=0}^{\infty}\left[\sum_{k=1}^{i} {}^{i}C_k f_{\mu}^{k}(m_1)\left\{\sum_{t=0}^{m_1-1}\frac{\mu^t}{t!}e^{-\mu}\right\}^{i-k}\right] \times p\{D^{(i)} \mid m_1\} \quad (8A.4)$$

which reduces to,

$$\text{RHS} = 1 + \sum_{i=1}^{\infty}\sum_{m_1=0}^{\infty}\left\{\left[\sum_{t=0}^{m_1}\frac{\mu^t}{t!}e^{-\mu}\right]^{i} - \left[\sum_{t=0}^{m_1-1}\frac{\mu^t}{t!}e^{-\mu}\right]^{i}\right\} \times p\{D^{(i)} \mid m_1\} \quad (8A.5)$$

The lower bound on R_{av} can be obtained in a similar way. Let us now define $m_1 = min(m_1, m_2, \ldots\ldots, m_i)$. Hence,

$$R_{av} \geq 1 + \sum_{i=1}^{\infty}\left[{}^{i}C_1 \sum_{m_1=0}^{\infty} f_{\mu}^{1}(m_1)\left\{\sum_{t=m_1+1}^{\infty}\frac{\mu^t}{t!}e^{-\mu}\right\}^{i-1} + {}^{i}C_2 \sum_{m_1=0}^{\infty} f_{\mu}^{2}(m_1)\left\{\sum_{t=m_1+1}^{\infty}\frac{\mu^t}{t!}e^{-\mu}\right\}^{i-2} + \ldots + {}^{i}C_j \sum_{m_1=0}^{\infty} f_{\mu}^{j}(m_1)\left\{\sum_{t=m_1+1}^{\infty}\frac{\mu^t}{t!}e^{-\mu}\right\}^{i-j} + \ldots + \sum_{m_1=0}^{\infty} f_{\mu}^{i}(m_1)\right] \times p\{D^{(i)} \mid m_1\} \quad (8A.6)$$

which can be re-stated in a compact form,

$$R_{av} \geq 1 + \sum_{i=1}^{\infty}\sum_{m_1=0}^{\infty}\left\{\left[\sum_{t=m_1}^{\infty}\frac{\mu^t}{t!}e^{-\mu}\right]^{i} - \left[\sum_{t=m_1+1}^{\infty}\frac{\mu^t}{t!}e^{-\mu}\right]^{i}\right\} \times p\{D^{(i)} \mid m_1\} \quad (8A.7)$$

Notice that (8A.7) is equivalent to the expression described by (8.10).

Chapter 9

Analysis and Optimization of Adaptive Multicopy Transmission ARQ Protocols for Time-Varying Channels

Automatic repeat-request (ARQ) schemes have received considerable attention for data transmission because of its simplicity, and are highly reliable compared to the forward-error correction (FEC) schemes [102]. Among the various known ARQ protocols, Go-Back-N (hereafter, simply referred as GBN) is very popular for terrestrial communications because it provides a good trade-off in terms of implementation complexity and performance. However, for systems that impose large propagation delays (such as satellite communication links), Selective-Repeat (SR) is a better candidate. Another class of ARQ protocols has evolved by exploiting the benefits of both ARQ and FEC schemes [104]. Consequently hybrid approaches offer superior performance at the expense of increased implementation complexity.

A major drawback of repeat-request strategies is that their throughput is not constant (unlike the case with FEC) and it falls rapidly with increasing channel error rate [101]. In order to address this issue, many adaptive ARQ protocols have been suggested in literature [104]-[111]. For instance in [109]-[111], the authors suggested varying the forward error correction rate to compensate for the fluctuations in the channel conditions. In [108] and [105]-[107], different block (packet) sizes and multi-copy transmission

schemes were used as adaptation mechanisms, respectively. The underlying premise is that if accurate channel state information (CSI) is exploited to dynamically change the protocol operation modes, then obviously higher throughput can be realized over a wide-range of error probability, versus a fixed (nonadaptive) algorithm. Fortunately, the frequency of the acknowledgment messages provides a natural source of channel state information. Hence, no additional circuitry is needed for channel state estimation (CSE). It should be pointed out that most of these studies, with the exception of [105], do not take into account the effects of unreliable feedback channel in their adaptation algorithm. This is an important consideration since the CSI is extracted from the received acknowledgment messages. Besides quantifying the degree of performance degradation, one should also answer the question as to how the selection of the CSE design parameters is affected by this form of errors (reflects the robustness of the algorithm). Other known channel estimation techniques include signal power measurements and pilot tone transmissions [117], which involves estimation and signal processing complexity.

In this chapter, we consider the CSE method outlined in [105], where channel conditions are estimated by counting the contiguous positive acknowledgments (ACKs) and/or contiguous negative acknowledgments (NACKs). As we will describe shortly, this technique is simple, yet can yield an accurate estimate of the channel condition. The reliability of this algorithm improves at high signalling rates or in a slowly-varying environment. Notice that in [105], the author modelled the adaptive ARQ system by a *simple Markov chain* with two states. However, this representation becomes void if the design variables are selected to be larger than unity because now the present state probabilities will be dependent on a specified number of previous state values, and therefore $Pr\{X_n | X_0, X_1, ..., X_{n-1}\} \neq Pr\{X_n | X_{n-1}\}$. Hence, an accurate analytical model to analyze the performance of this adaptive ARQ system is developed in this paper by representing the adaptive system by an *r-order Markov chain* (*multiple Markov process*) [120]

instead. As well, Yao [105] used trial methods to obtain the system design variables, and consequently does not provide sufficient guidelines to choose appropriate values for these parameters. In contrast, here we adopt the Broyden-Fletcher-Goldfarb-Shanno (BFGS) algorithm [115], a well-known nonlinear optimization technique to obtain the suboptimal values for these parameters in a systematic and efficient manner. Moreover, in [105] no attempt was made to verify as to how the selection of these design parameters is affected by feedback channel errors. These questions are answered here. Furthermore, our work extends the results presented in [105]: (a) by studying a more general case of mixed-mode ARQ strategy with transitions between any two arbitrary t-copy GBN schemes, (b) by outlining an efficient and systematic approach to acquire the suboptimal design parameters, (c) by providing a quantitative measure of the appropriateness of the selected design variables (reliability criterion), (d) by investigating the asymptotic properties of the estimated throughput expression, and (e) by presenting simple expressions to estimate the suboptimal design parameters, both in noisy and noiseless feedback channels. Additionally, we have also evaluated the performance of Weldon's Selective - Repeat ARQ strategy with transitions between two operation modes.

This chapter has the following organization: The operation of an adaptive Go-Back-N ARQ strategy and CSI acquisition techniques are described in Section 9.1. Section 9.2 details the throughput analysis for t-copy GBN and Weldon's SR ARQ strategies. Subsequently, exact analytical expressions for computing the throughput cross-over probability between any two multicopy transmission modes are derived. In Section 9.3, application of a Quasi-Newton optimization method to find the suboptimal design parameters is outlined. Selected numerical results are presented in Section 9.4. Finally in Section 9.5, the main points are summarized and conclusions restated.

9.1 System Description

For convenience, a brief description for each of the parameters affecting the throughput performance is summarized in Table 9.1.

Table 9.1 Description of the notations used in the throughput analysis.

Notations	Explanation
t_1, t_2	Number of identical message blocks sent in each transmission in case of a Go-Back-N scheme or number of copies of a block retransmitted to handle a NACKed codeword for the Selective-Repeat ARQ strategy. The subscripts 1 and 2 denote the low- and high-channel error rate states, respectively.
α, β	Design variables that correspond to the count of contiguous NACKs and ACKs, respectively. If the transmitter receives α contiguous NACKs while in state L (or β contiguous ACKs while in state H), it will switch its operation mode from t_1-copy transmission to t_2-copy transmission scheme (or vice-versa).
P_{L_i}, P_{H_i}	Steady-state probabilities for each of the low- and high-channel error rate states, respectively.
P_L, P_H	Sum of steady-state probabilities of all the individual states in their respective low- and high channel error rate groups, and therefore correspond to the fraction of time that the adaptive system operates in a t_1-copy and t_2-copy transmission modes, respectively.
P_e	Channel block error probability (i.e, message frame error rate).
P_f	Feedback channel error rate (i.e, probability than an acknowledgment message is corrupted).
P_{co}	Channel block error probability at which the throughput of one ARQ protocol cross-over that of another in a noise-free feedback channel (hereafter, simply referred as throughput cross-over probability).
$P_{co\text{-}noisy}$	Throughput cross-over probability in the presence of a noisy feedback channel.
T	Throughput efficiency of the adaptive system.
N	Block storage of the link (has the same meaning as in the basic Go-Back-N scheme, as well as the size of the finite buffer in the Selective-Repeat protocol to store the error-free frames).
$E(\alpha, \beta)$	Quality criterion that indicates the appropriateness of the selected design variables in terms of matching the performance curve of the proposed CSE scheme with the desired performance envelope.
W_k	User defined weight sequence that provides additional flexibility in matching different data samples with varying accuracy.

9.1.1 ARQ System Operation

The forward channel is considered to have a finite number of states associated with distinct channel conditions. As an example, Fig. 9.1 depicts an adaptive Go-Back-N ARQ strategy with transition between two operation modes. State L and H correspond to low and high channel error rate conditions, respectively.

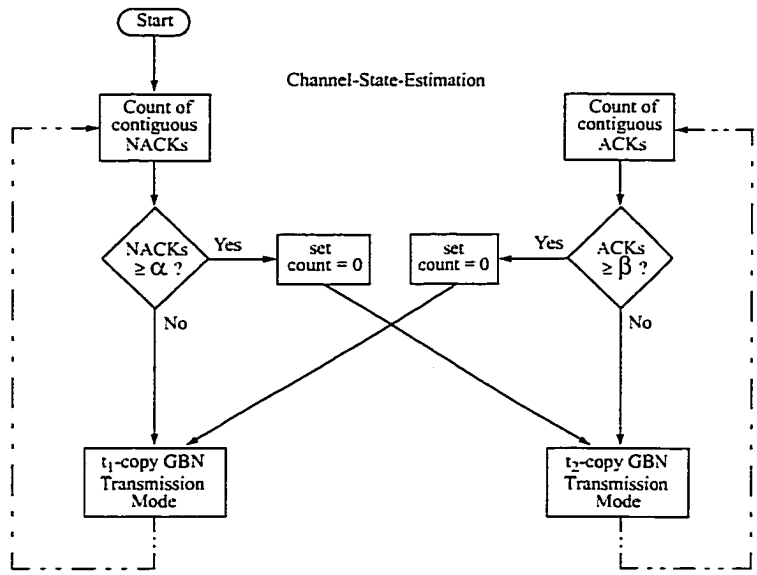

(a) System description of an adaptive Go-Back-N ARQ strategy.

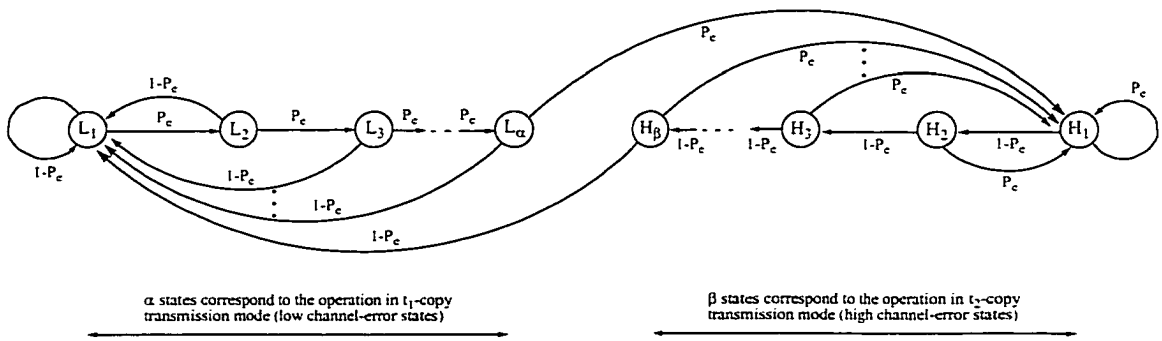

(b) (α+β)-state Markov chain representation.

Fig. 9.1 An example of the proposed ARQ scheme illustrating the transition between two operation modes.

The transmitter operates in a t_1-copy GBN transmission mode while in state L. When the channel condition degrades, it switches to t_2-copy GBN transmission mode. The operation of t-copy GBN is the same as pure Go-Back-N except that t copies of a data block are sent in each transmission. Notice that $t_2 > t_1$ because we have to provide greater amount of redundancy to improve the overall system throughput and delay char-

acteristics at high channel error rates. The decision regarding the transitions between different operation modes is made based on the received acknowledgment messages. In our example, the transmitter assumes that the channel condition transits from state L to H upon receiving α contiguous NACKs or erasure symbols. On the other hand, if the transmitter receives β contiguous ACKs, then the transmitter would consider that the channel is traversing from state H to state L. Similar to [105] and [118], we assume that the feedback channel error can only make ACK and NACK messages indistinguishable and the transmitter will handle this erred ACK/NACK message (erasure symbol) as a NACK. This form of error process is referred as "product-approximation" in [116]. Such an assumption is reasonable since the undetectable error probability can be made very small by proper selection of error detecting codes [104].

Since the transition from one state to another depends on the number of contiguous NACKs or number of contiguous ACKs that have been received, i.e., $Pr\{X_{n+1} | X_0, X_1, \ldots, X_n\} = Pr\{X_{n+1} | X_{n-\alpha+1}, \ldots, X_n\}$, we can represent the proposed adaptive system precisely by an r-order Markov process. It is straightforward to transform a multiple Markov process into a simple one by expanding the number of states defined for the system and correspondingly increasing the size of the transition matrix. Then the adaptive ARQ system can be characterized by an $(\alpha + \beta)$ -state Markov chain whose state space is partitioned into two groups of α low-channel error rate states and β high-channel error states, as illustrated in Fig. 9.1(b). The $(\alpha + \beta) \times (\alpha + \beta)$ state transition matrix can be easily constructed (tabulated) from Fig. 9.1(b). After some mathematical manipulations, we obtain the following steady-state probabilities:

$$P_{L_i} = \frac{(1-\lambda)^{\beta}\lambda^{i-1}}{(1-\lambda)^{\beta-1}\left[1-\lambda^{\alpha}\right]+\lambda^{\alpha-1}\left[1-(1-\lambda)^{\beta}\right]}, i \in \{1, 2, \ldots, \alpha\}, \qquad (9.1)$$

$$P_{H_i} = \frac{\lambda^{\alpha}(1-\lambda)^{i-1}}{(1-\lambda)^{\beta-1}\left[1-\lambda^{\alpha}\right]+\lambda^{\alpha-1}\left[1-(1-\lambda)^{\beta}\right]}, i \in \{1, 2, \ldots, \beta\}, \qquad (9.2)$$

where $\lambda = P_e (1-P_f) + P_f$, P_f and P_e denote the feedback channel error probability and message block error probability, respectively.

Since the adaptive system operates in a t_1-copy GBN transmission mode while in any of the L_i states, it is useful to define a new parameter $P_L = \sum_{i=1}^{\alpha} P_{L_i}$ which dictates the steady-state probability of the channel at low channel error rate group,

$$P_L = \sum_{i=1}^{\alpha} P_{L_i} = \frac{(1-\lambda)^{\beta-1}\left[1-\lambda^{\alpha}\right]}{(1-\lambda)^{\beta-1}\left[1-\lambda^{\alpha}\right] + \lambda^{\alpha-1}\left[1-(1-\lambda)^{\beta}\right]}. \tag{9.3}$$

Similarly, the steady-state probability of the channel at high channel error rate group is given by,

$$P_H = \sum_{i=1}^{\beta} P_{H_i} = \frac{\lambda^{\alpha-1}\left[1-(1-\lambda)^{\beta}\right]}{(1-\lambda)^{\beta-1}\left[1-\lambda^{\alpha}\right] + \lambda^{\alpha-1}\left[1-(1-P_e)^{\beta}\right]}. \tag{9.4}$$

The throughput of this new adaptive scheme is therefore an average of the throughput values of the two operation modes, i.e.,

$$T = P_L T_L + P_H T_H = P_L T_L + (1-P_L) T_H, \tag{9.5}$$

and throughput performance for each of the operation modes are derived in Section 9.2.

9.1.2 Channel State Estimation

Perhaps the most difficult problem in implementing an adaptive scheme is finding a simple real-time adaptive algorithm. In other words, the channel error characteristics should be identified within a few block transmissions while preserving simplicity. Typically, the channel is monitored by counting the number of retransmissions during an observation interval (*OBI*) and comparing that number with a set of thresholds to determine the channel condition [109]. If *OBI* is large, then the delay in reacting to a change in the channel could be significant. On the other hand, very small values of *OBI* will not provide a reli-

able CSI decision. It should be pointed out that more reliable CSI can be achieved by exploiting a more complex decision statistics, such as the exact number of erroneous bits in the received packet. Such techniques allow the predicted bit-error rate (BER) to converge to the "true" BER much faster. However, considerable overhead requirements and the added complexity are not likely to be justified in practical applications.

In [108], a method for estimating the BER was outlined. By accumulating the values of total number of n-bits blocks in error (TNBE) and total number of n-bits blocks (TNB) over a long period, the expression (9.6) does provide a real-time adaptation,

$$P_b \approx TNBE/(TNB \times n) . \tag{9.6}$$

However, as pointed out in [112], such a long term bit error rate is meaningless as a description of practical communication channels, because real channels often have errors occurring in bursts. To provide a more reasonable estimate of the instantaneous block error probability, weighted sum of errors should be considered. This ensures that the influence of the most recent errors is the largest. Two other CSE methods were presented in [109] and [105]. In the former scheme, the authors predict the channel conditions by scoring the outcome of the decoding process. It has been shown that the statistical sequential inspection scheme will require, on average, fewer samples (and therefore shorter observation interval) to detect this change than with a fixed sample size approach. In our analysis we adopt the CSE proposed in [105]. Specifically, in Appendix 9A we have shown that the selection of the design parameters is not very sensitive to the feedback channel errors. Unfortunately this is not the case for throughput performance.

The CSE scheme considered in this chapter addresses a few shortcomings found in some other approaches. First, by counting the contiguous ACKs or NACKs, we place a greater emphasis on the influence of most recent errors. Consequently, our measurements tend to estimate the desired instantaneous block error probability parameter more realistically, and therefore can make a reliable decision much faster than the traditional channel monitoring technique. Next, this CSE method allows us to choose a wide-range of suboptimal design parameters which can be properly selected depending on the rate at which

the channel statistics vary and the mode switching reliability criterion. Finally, the computation of the suboptimal design variables involves very simple operations and, if necessary, can be performed in real-time for both noiseless and noisy feedback channels.

9.2 Throughput Analysis

In this section, throughput performance for multi-copy transmission of Go-Back-N and Selective-Repeat ARQ protocols are presented. Subsequently, we seek to find exact analytical expressions for computing the break point of the channel error probability where the performance of one ARQ scheme is better than the other, so that the overall system throughput can be optimized. The knowledge of this throughput cross-over probability is essential in the design of mixed-mode ARQ strategies because the operation mode switching will occur at the vicinity of this intersection point.

9.2.1 Multi-copy Transmission of Go-Back-N ARQ Protocol

The operation of the t-copy GBN scheme is the same as the basic GBN ARQ strategy, except that t identical copies of a data block are sent in each transmission. The transmitter considers block i as being correctly received if at least one of the t copies has been positively acknowledged by the receiver. However, a retransmission of block i is required when all the copies of block i have been negatively acknowledged.

Let s denote the number of data frames which can possibly be sent during the round trip propagation delay of the channel, i.e.,

$$s = \left\lceil \frac{RT_{prop}}{n} \right\rceil = N-1, \tag{9.7}$$

where R is the transmission rate in bits/s, T_{prop} denotes the round trip propagation delay in seconds, n corresponds to total number of bits per frame, and N has the same meaning as in the basic Go-Back-N scheme (block storage of the link). Notation $\lceil x \rceil$ indicates the smallest integer larger than or equals to x. Notice that $t < s + 1$ because it will

be pure waste of time sending more copies than the channel round-trip propagation delay.

In the t-copy GBN ARQ system, a retransmission is requested only if all the t original transmissions of a particular codeword were detected in error, which always involves resending $(s+t)$ data frames. Consequently, the average number of transmissions for a codeword to be successfully received and acknowledged is [104][106],

$$\begin{aligned} R_{t-GBN} &= t(1-\zeta) + (s+2t)(1-\zeta)\zeta + (2s+3t)(1-\zeta)\zeta^2 + \cdots \\ &= \sum_{q=0}^{\infty} (1-\zeta)[qs + (q+1)t]\zeta^q \end{aligned} \tag{9.8}$$

where $\zeta = [1-(P_c+P_u)(1-P_f)]^t$, P_c denotes the probability that a received packet contains no error, P_u is the probability that a received codeword contains an undetectable error pattern, and P_f corresponds to the feedback channel error probability. In arriving to (9.8), we have assumed that the packet error process is independent and identically distributed. The effects of packet error correlations on the system performance have been examined in a greater detail by Zorzi and Rao [121]. Using identities $\sum_{i=0}^{\infty} y^i = 1/(1-y)$ and $\sum_{i=1}^{\infty} iy^i = y/(1-y)^2$ allows us to simplify (9.8) as,

$$R_{t\text{-}GBN} = \frac{t+s\zeta}{1-\zeta} = \frac{t+s[1-(P_c+P_u)(1-P_f)]^t}{1-[1-(P_c+P_u)(1-P_f)]^t}. \tag{9.9}$$

Since the undetectable error probability P_u can be made very small by proper selection of error detecting codes [104], virtually an error-free transmission can be attained. For example, the (2047, 2014) triple-error correcting primitive BCH code satisfies the following tight bound [103],

$$P_u \le 2^{-(n-k)}\{1 + (1-2\varepsilon)^n - 2(1-\varepsilon)^n\}, \tag{9.10}$$

where ε and k correspond to the channel bit-error rate and the number of information

bits in a packet size of length n, respectively. Consequently, the error event of a system employing such a code can be made very small by using only a moderate number of parity bits. Since $P_c + P_u + P_e = 1$, we can substitute $P_c + P_u = 1 - P_e$ in (9.9), where P_e is the probability that the received block contains a detectable error pattern (hereafter, we shall refer P_e as frame error rate). Then the throughput efficiency of the t-copy GBN scheme is given by,

$$T_{t-copy\ GBN} = \frac{k}{n} \times \frac{1 - [1 - (1-P_e)(1-P_f)]^t}{t + (N-1)[1 - (1-P_e)(1-P_f)]^t} = \frac{\eta[1-\lambda^t]}{t + (N-1)\lambda^t}, \quad (9.11)$$

where $\eta = k/n$ is the code rate of error detecting code. Notice that (9.11) reduces to the throughput of pure GBN strategy when $t = 1$, and throughput of pure SR ARQ scheme when both $t = 1$ and $N = 1$. Similarly, (9.11) reduces to the familiar expression in [113] when $P_f = 0$.

We now derive the exact throughput cross-over probability between any two arbitrary t-copy transmission of Go-Back-N ARQ strategies. After some algebraic manipulations, the throughput difference between the t_1-copy and t_2-copy GBN transmission protocols is given by,

$$\begin{aligned} \Delta_T &= T_{t_2-copy\ GBN} - T_{t_1-copy\ GBN} \\ &= \frac{k}{n} \times \frac{(t_1 - t_2) + (N + t_2 - 1)\lambda^{t_1} - (N + t_1 - 1)\lambda^{t_2}}{\left[t_1 + (N-1)\lambda^{t_1}\right]\left[t_2 + (N-1)\lambda^{t_2}\right]} \end{aligned} \quad (9.12)$$

It is evident that the denominator of (9.12) is always greater than zero. Thus, with the assumption of noisy feedback channel and $t_2 > t_1$, the t_2-copy transmission strategy outperforms the t_1-copy transmission scheme when the numerator term of (9.12) is positive, namely,

$$(1-\lambda)\times\Big(\Big[1+\lambda+\lambda^2+\ldots+\lambda^{t_1-1}\Big](t_1-t_2) + \Big[\lambda^{t_1}+\lambda^{t_1+1}+\ldots+\lambda^{t_2-1}\Big](N+t_1-1)\Big)>0 \tag{9.13}$$

For an error-free feedback link, (9.13) can be simplified as,

$$(1-P_e)\times\Big(\Big[1+P_e+P_e^2+\ldots+P_e^{t_1-1}\Big](t_1-t_2) + \Big[P_e^{t_1}+P_e^{t_1+1}+\ldots+P_e^{t_2-1}\Big](N+t_1-1)\Big)>0 \tag{9.14}$$

For the specific case of $t_1 = 1$, (9.13) reduces to,

$$(1-\lambda)\left[\lambda^{t_2-1}+\lambda^{t_2-2}+\lambda^{t_2-3}+\ldots+\lambda-\frac{t_2-1}{N}\right]>0 \tag{9.15}$$

It is important to mention here that the t-copy transmission protocol performs better than the pure Go-Back-N ARQ strategy only if (9.15) is satisfied. In other words, if $P_e > P_{co-noisy}$ or $P_f > P_{co}$, and $P_e < 1$, then multi-copy transmission approach yields higher throughput than the pure Go-Back-N protocol. The throughput cross-over probability is obtained by solving for P_e when inequalities in (9.13), (9.14) and (9.15) are replaced with equalities. Selected numerical examples are illustrated in Table 9.2 (a) and Table 9.2 (b). The knowledge of this exact probability (which can be computed numerically) is essential in the design of our adaptive protocol because the switching will occur at the vicinity of this transition point.

As well, comparison between (9.13) and (9.14) reveals an interesting relationship between the cross-over probability for the noiseless and noisy feedback channels,

$$P_{co-noisy} = \frac{P_{co}-P_f}{(1-P_f)} \tag{9.16}$$

Table 9.2 (a) Examples of throughput cross-over probability between any two arbitrary t-copy GBN transmission schemes with the assumption of error-free feedback channel and N=10.

	Throughput Cross-over Probability, P_{co}				
t	2	3	4	5	6
1	0.10000	0.17082	0.23304	0.28711	0.33426
2	-	0.35037	0.42640	0.48519	0.53231
3	0.35037	-	0.53301	0.58763	0.62996
4	0.42640	0.53301	-	0.65246	0.69038

Table 9.2 (b) Throughput cross-over probability between different t-copy GBN transmission and the pure Go-Back-N schemes in the presence of feedback channel errors. N is assumed to be 5.

	Throughput Cross-over Probability, $P_{co\text{-}noisy}$					
t	$P_f = 0$	$P_f = 0.001$	$P_f = 0.05$	$P_f = 0.10$	$P_f = 0.20$	T_{co}/η
2	0.20000	0.19920	0.15789	0.11111	0	0.44444
3	0.30623	0.30553	0.26971	0.22914	0.13278	0.31182
4	0.38937	0.38875	0.35723	0.32152	0.23671	0.23877
5	0.45532	0.45477	0.42665	0.39480	0.31914	0.19306

Table 9.2 (c) Examples of throughput cross-over probability between any two arbitrary t-copy SR transmission schemes with the assumption of error-free feedback channel and N=25.

	Throughput Cross-over Probability, P_{co}				
t	2	3	4	5	6
1	0.04000	0.07446	0.10726	0.13797	0.16668
2	-	0.21629	0.27735	0.32679	0.36809
3	0.21629	-	0.38426	0.43787	0.48075
4	0.27735	0.38426	-	0.51070	0.55259

9.2.2 Weldon's Selective-Repeat ARQ Protocol

Consider a two level Weldon's SR ARQ system (hereafter, referred as t-copy SR) for which the receiver has a finite buffer N to store the error-free frames, when a received word is detected in error. As in Section 9.2.1, the quantity N corresponds to the block storage of the link. We refer to [107] for a detailed description of the operation of this ARQ scheme. Following the analysis presented in [107], the throughput efficiency of this protocol can be easily obtained as,

$$T_{t-copy\ SR} = \frac{\eta\left[1-\lambda^{t}\right]}{1+\lambda t+\lambda^{t}\left[(N-1)\lambda-1\right]}, \tag{9.17}$$

where parameters λ and η are as defined in (9.4) and (9.11), respectively. It is evident that (9.17) reduces to the expression given in [107] when the feedback channel is assumed to be error-free. The difference in throughput performance of the t_2-copy and t_1-copy SR protocols is,

$$\Delta_T = \eta \times \frac{\lambda\left[(t_1-t_2)+(N+t_2-1)\lambda^{t_1}-(N+t_1-1)\lambda^{t_2}\right]}{\left[1+(N-1)\lambda^{t_2+1}+\lambda t_2-\lambda^{t_2}\right]\left[1+(N-1)\lambda^{t_1+1}+\lambda t_1-\lambda^{t_1}\right]}. \tag{9.18}$$

Notice that the denominator of (9.18) is always greater than 0 since $0 \le \lambda \le 1$, $t \ge 1$ and $t-\lambda^{t-1} \ge 0$. Whereas, the numerator of (9.18) can be rewritten as,

$$\begin{aligned}(1-\lambda) \times \Big(&\left[1+\lambda+\lambda^2+\ldots+\lambda^{t_1-1}\right](t_1-t_2) \\ &+\left[\lambda^{t_1}+\lambda^{t_1+1}+\ldots+\lambda^{t_2-1}\right](N+t_1-1) \Big) > 0, \end{aligned} \tag{9.19}$$

which is similar to (9.13). Then, the throughput cross-over probability is computed by letting (9.19) equal to 0, and then solving the polynomial for P_e. Selected examples are illustrated in Table 9.2 (c).

9.3 Quasi-Newton Optimization

In this section, we outline the use of the BFGS algorithm [115], a well-known non-linear optimization technique, to compute the suboptimal values of the CSE design variables in a systematic and efficient manner. This methodology is particularly attractive in cases where a large number of variables need to be optimized simultaneously (multi-dimensional optimization). Additionally, in this chapter we have introduced a user defined weight sequence that provides greater flexibility in matching different data points with varying accuracy.

9.3.1 Problem Formulation

Consider the adaptive ARQ strategy depicted in Fig. 9.1, and let $T(P_e)$ and $\hat{T}(P_e)$ denote the throughput performance of the desired (ideal) and adaptive ARQ protocol respectively. Our task is to find the optimal design parameters such that $\hat{T}(P_e)$ best approximates $T(P_e)$ in the sense that the total estimation error is minimized,

$$\begin{aligned} \underset{[\alpha,\beta]\in\mathcal{Z}}{\text{minimize}} \quad E(\alpha,\beta) &= \int_0^1 W\left[T(P_e)-\hat{T}(P_e)\right]^2 dP_e \\ &\cong \Delta \sum_{k=1}^{K} W_k\left[T(P_{ek})-\hat{T}(P_{ek})\right]^2 \\ \text{subject to:} \quad & \alpha_{min} < \alpha < \alpha_{max} \\ & \beta_{min} < \beta < \beta_{max} \end{aligned} \tag{9.20}$$

where K denotes the sample size, P_{ek} corresponds to the block error probability of the kth sample, W_k is the user defined weight sequence that provides additional flexibility in matching different points with varying accuracy, and the optimization variables can assume any value from the set $\mathcal{Z}$, which consists of positive integers. In other words, the mean square error (MSE) function is our objective function, and its local minimum point contains the information of the optimal design parameters, $\mathbf{x}^* = [\alpha^* \ \beta^*]^T$. Discrete determination of $E(\alpha,\beta)$ is valid if the step size Δ between the consecutive data points

is selected to be relatively small. In this paper, we decide to choose the samples to be equally-spaced in the region $0 \le P_e \le 1$, with a step-size of $\Delta = 0.0010$. It is apparent that the objective function depicted in (9.20) serves as a reliability indicator of our CSE algorithm. For the sake of illustration, consider an error-free feedback channel scenario. Then, the envelope of the desired throughput performance curve is described by,

$$T(P_{ek}) = \begin{cases} T_{Lk} = \dfrac{1-P_{ek}^{t_1}}{t_1 + (N-1)P_{ek}^{t_1}} & \text{if } 0 \le P_{ek} \le P_{co} \\ T_{Hk} = \dfrac{1-P_{ek}^{t_2}}{t_2 + (N-1)P_{ek}^{t_2}} & \text{if } P_{co} < P_{ek} \le 1 \end{cases}, \tag{9.21}$$

and the throughput expression for the proposed adaptive scheme is,

$$\hat{T}(P_{ek}) = P_{Lk}\,T_{Lk} + P_{Hk}\,T_{Hk}, \tag{9.22}$$

with the steady-state probabilities given by (9.3)-(9.4). P_{co} is the throughput cross-over probability between t_1-copy and t_2-copy transmission schemes when $P_f = 0$ (noise-free return channel), and the system throughput for low- and high error rate state are denoted as T_{Lk} and T_{Hk}, respectively.

As we will describe shortly, the optimal solution to our problem (i.e., when the performance curve of the proposed CSE scheme coincides with the desired performance envelope over the entire $0 \le P_e \le 1$ range) exists in the infinite α-β space [see Appendix 9A]. In this case, the steady-state probabilities (P_L and P_H) will be equal at $P_{ek} = P_{co}$. Hence, it can be readily shown that the optimal design parameters are related by,

$$\begin{aligned} \frac{\beta^* - 1}{\alpha^* - 1} &= \frac{\ln(P_{co})}{\ln(1-P_{co})} - \frac{\ln\left[1 + P_{co}^{\alpha-1}(1-2P_{co})\right]}{(\alpha-1)\ln(1-P_{co})} \\ &= \left\{ \frac{\ln(1-P_{co})}{\ln(P_{co})} - \frac{\ln\left[1 + (1-P_{co})^{\beta-1}(2P_{co}-1)\right]}{(\beta-1)\ln(1-P_{co})} \right\}^{-1} \\ &\approx \frac{\ln(P_{co})}{\ln(1-P_{co})} \end{aligned} \tag{9.23}$$

Since the optimal solution (i.e., local minimum point) does not lie in a reasonable value range, one can resort to the suboptimal solutions with some sacrifice in performance. If we select α and β values to be very large, then this scheme will lose its ability to adapt to moderately fast channel variations. On the other hand, extremely small values of α and β will result in premature (unnecessary) switching, and poor fit to the desired performance curve. Therefore we have introduced additional boundary constraints to the design parameters, which will be specified by the channel behavior and/or the intended application. In our minimization problem, these boundary constraints can be eliminated via transformation $y = \dfrac{e^{z} - e^{-z}}{e^{z} + e^{-z}} \equiv \tanh(z)$. The hyperbolic tangent is a monotonically increasing function with respect to z that maps the entire 1-D space $-\infty < z < \infty$ to $-1 < \tanh(z) < 1$. Subsequently, it is easy to show that the linear relationship described in (9.24) gives a map from $(-\infty, \infty)$ to (x_{min}, x_{max}) ,

$$x = \left(\frac{x_{max} - x_{min}}{2}\right)\tanh(z) + \left(\frac{x_{max} + x_{min}}{2}\right). \tag{9.24}$$

Finally the objective function for an unconstrained optimization is obtained by substituting $[\alpha \;\; \beta]^{T} = \begin{bmatrix} 0.5(\alpha_{max} - \alpha_{min})\tanh(z_{\alpha}) + 0.5(\alpha_{max} + \alpha_{min}) \\ 0.5(\beta_{max} - \beta_{min})\tanh(z_{\beta}) + 0.5(\beta_{max} + \beta_{min}) \end{bmatrix}$ into (9.20), and minimizing the MSE function with respect to $\mathbf{z} = [z_{\alpha} \; z_{\beta}]^{T}$, i.e.,

$$\underset{[z_{\alpha}, z_{\beta}] \in \mathcal{R}}{\text{minimize}} \quad E(z_{\alpha}, z_{\beta}) \cong \Delta \sum_{k=1}^{K} W_k \left[T(P_{ek}) - \hat{T}(P_{ek})\right]^2, \tag{9.25}$$

where $\mathcal{R}$ consists of the set of real numbers. The corresponding gradient function (first-order partial derivatives) can be obtained without much difficulty.

9.3.2 Optimization Algorithm

In quasi-Newton algorithms only the gradient vector needs to be computed, and it is unnecessary to manipulate or invert the Hessian matrix H. Additionally, if the initial matrix S_0 is positive definite, then the updating formula for S_{k+1} will yield a sequence of positive definite matrices even for a non-quadratic function. This guarantees that the next search direction to be a descent direction. The BFGS recursion formula is contrived to be an approximation of H^{-1}, and is given by,

$$S_{k+1} = S_k + \left\{1 + \frac{\gamma_k^T S_k \gamma_k}{\gamma_k^T \delta_k}\right\} \frac{\delta_k \delta_k^T}{\gamma_k^T \delta_k} - \frac{\delta_k \gamma_k^T S_k + S_k \gamma_k \delta_k^T}{\gamma_k^T \delta_k} \tag{9.26}$$

where $\gamma_k = g_{k+1} - g_k$, $\delta_k = -\alpha_k S_k g_k$, α_k is a scaling factor obtained using line search, and g_k corresponds to the gradient vector.

The algorithm of the BFGS method to obtain the suboptimal design parameters is summarized as follows:

Step 1: Initialization:

(a) Input initial values for x_0 and convergence criterion ε.

(b) Set $k \leftarrow 0$ and $S_0 \leftarrow I_n$ (I_n corresponds to an $n \times n$ identity matrix, where n is the length of matrix x_0).

(c) Compute $f(x_0)$ and g_0.

Step 2: (a) Set feasible direction $d_k \leftarrow -S_k g_k$.

(b) Find α_k, the value of scaling factor c that minimizes $f(x_k + cd_k)$ using a line search routine.

(c) Set $\delta_k \leftarrow \alpha_k d_k$ and $x_{k+1} \leftarrow x_k + \delta_k$.

Step 3: Check if convergence has been achieved by using an appropriate criterion:

IF $\|\delta_k\| < \varepsilon$, then do:

Declare $\hat{x}^* = x_{k+1}$ and $f(\hat{x}^*) = f(x_{k+1})$ as suboptimal solutions.

End.

ELSE goto Step 4.

Step 4: Update new search direction:

(a) Compute g_{k+1}.

(b) Set $\gamma_k \leftarrow g_{k+1} - g_k$.

(c) Compute BFGS updating formula S_{k+1} using Eq. (9.26).

(d) Set $k \leftarrow k+1$ and goto Step 2.

9.4 Computational Results and Remarks

In this section, we present a few examples to illustrate the system design and performance evaluation of the proposed adaptive repeat-request strategy. Table 9.2 (a) and Table 9.2 (c) depict the throughput cross-over probability between any two arbitrary t-copy GBN and t-copy SR transmission modes respectively, with the assumption of noiseless feedback channel. These values were obtained by computing the roots of the polynomial described in (9.14). As we have shown in the preceding sections, the knowledge of this exact cross-over probability is essential because it determines the selection of the system design variables. Whereas, Table 9.2 (b) displays the throughput cross-over probability between different t-copy GBN and the pure Go-Back-N schemes in the presence of feedback channel errors. Similar to the above, these cross-over probabilities were computed numerically by solving (9.13) for P_e. Alternatively, if the knowledge of P_{co} is available, $P_{co-noisy}$ can be easily obtained via relationship given in (9.16). It was also observed that the cross-over throughput value remain constant regardless of the ACK/NACK error rates, if $P_f \leq P_{co}$.

We now describe the trends observed from the solutions obtained via the Quasi-Newton optimization approach. Table 3 depicts the suboptimal design parameters and their corresponding total estimation error for various adaptive GBN ARQ systems, by modelling the forward link as a partitioned Markov chain with (α + β) states. It is apparent from this table that α always assumes the value of α_{max} (i.e., suboptimal solution exists on the boundary of the specified region), and the objective function approaches its absolute minimum point as the upper limit for α increases. This trend challenges the conclusion drawn in [105]. Additionally, we observe that for each α there exists an optimum value for β that minimizes the error function.

Table 9.3 Suboptimal design parameters and their corresponding error function (MSE) for different values of t, N and α_{max}. The forward-channel is modelled by a partitioned Markov chain with two channel state groups, associated with the pure GBN (i.e., $t_1 = 1$) and t-copy GBN transmission (i.e., $t_2 = t$) modes; and W_k is assigned to be unity for all data points.

t	N	$\alpha_{max} = 1$		$\alpha_{max} = 3$		$\alpha_{max} = 5$		$\alpha_{max} = 10$	
		$\hat{x}^* = [\alpha\ \beta]^T$	$E(\hat{x}^*)$	$\hat{x}^* = [\alpha\ \beta]^T$	$E(\hat{x}^*)$	$\hat{x}^* = [\alpha\ \beta]^T$	$E(\hat{x}^*)$	$\hat{x}^* = [\alpha\ \beta]^T$	$E(\hat{x}^*)$
2	5	$[1\ 3]^T$	3.17×10^{-4}	$[3\ 15]^T$	1.33×10^{-5}	$[5\ 30]^T$	1.90×10^{-6}	$[10\ 66]^T$	1.67×10^{-7}
	10	$[1\ 7]^T$	2.33×10^{-4}	$[3\ 45]^T$	4.81×10^{-6}	$[5\ 89]^T$	6.31×10^{-7}	$[10\ 198]^T$	5.54×10^{-8}
3	5	$[1\ 1]^T$	6.18×10^{-4}	$[3\ 7]^T$	3.93×10^{-5}	$[5\ 14]^T$	6.31×10^{-6}	$[10\ 30]^T$	5.67×10^{-7}
	10	$[1\ 4]^T$	4.51×10^{-4}	$[3\ 20]^T$	1.45×10^{-5}	$[5\ 39]^T$	2.00×10^{-6}	$[10\ 86]^T$	1.76×10^{-7}
4	5	$[1\ 1]^T$	5.89×10^{-4}	$[3\ 5]^T$	5.94×10^{-5}	$[5\ 9]^T$	1.12×10^{-5}	$[10\ 18]^T$	1.00×10^{-6}
	10	$[1\ 2]^T$	5.40×10^{-4}	$[3\ 12]^T$	2.24×10^{-5}	$[5\ 23]^T$	3.29×10^{-6}	$[10\ 50]^T$	2.95×10^{-7}

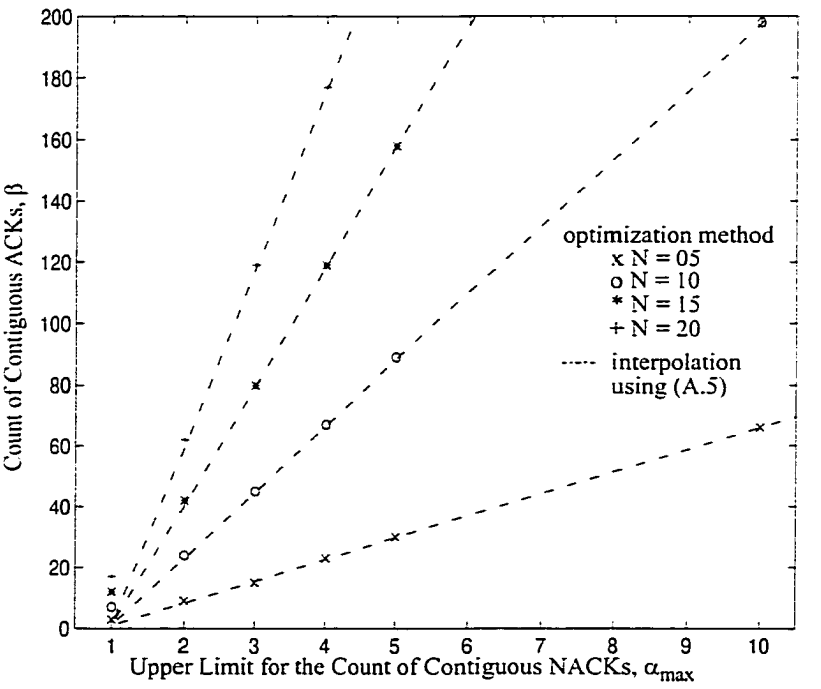

Fig. 9.2 Relationship between the suboptimal design variables of an adaptive multi-mode GBN ARQ protocol (i.e., $t_1 = 1$ and $t_2 = 2$), as a function of α_{max} and the buffer size N.

It is also worthwhile to investigate as to how these suboptimal design parameters will be related to each other, so that we can interpolate the results in broader ranges. The asymptotic property of the estimated throughput expression is examined in Appendix 9A. However, this property only provides the relationship between the design variables at the absolute minimum point (which lies in the infinite space). Consequently, the application of optimization technique becomes increasingly beneficial in studying the behavior of this interaction under realistic system considerations (i.e., finite α-β space). Interestingly, our optimization results reveal that the relationship between $\hat{\alpha}^*$ and $\hat{\beta}^*$ can be well approximated by (9A.3) or (9A.4) when α is quite small, and by a linear function (9A.5) as α increases. Fig. 9.2 describes this interaction graphically for an adaptive GBN ARQ protocol with $t_1 = 1$, $t_2 = 2$, and varying buffer sizes N. Notice that the gradient for each of these lines (in the linear portion) takes the value $\ln(P_{co}) / \ln(1 - P_{co})$, which suggests that the relationship attained from the asymptotic analysis seem to hold true in other regions as well. Another trend to note here is that the ratio β/α becomes larger as the buffer size increases (corresponding to systems with large roundtrip delay), but declines for higher values of t (refer to Table 9.3).

Fig. 9.3 illustrates the throughput performance of a multi-mode GBN ARQ protocol for three different sets of suboptimal design parameters. It is apparent from this figure that the adaptive system provides higher throughput than other comparable nonadaptive ARQ schemes, under a wide-range of error rate conditions. Moreover, it is shown that our optimized $\{\alpha, \beta\}$ pairs yield a very close fit to the envelope of the desired performance curve even by limiting the optimization variables values to a moderate range. Since increasing α beyond 2 or 3 in this example will result only in a slight improvement of the quality criterion, these values (with their corresponding β) appear to be a good compromise in terms of the accuracy in matching to the desired performance curve, avoiding unnecessary switching between various protocols ('ping-pong effect') and at the same time sustaining the ability to adapt to fast variations experienced on wireless channels. It is also interesting to highlight at this point that the selection of $[\alpha = 1, \beta = 10]$ (coarse estimation[1] of the channel condition based on conventional channel monitoring method

with $OBI = 10$) is not optimal in terms of mode switching reliability (i.e., $E(1, 10) = 2.79 \times 10^{-4}$ versus $E(1, 7) = 2.33 \times 10^{-4}$), as well as the rate at which it can react to the fluctuations in the channel statistics. Next, by looking at the performance curves of $[\alpha = 1, \beta = 7]$ and $[\alpha = 2, \beta = 24]$, we conclude that a substantial gain in curve fitting can be realized by selecting a slightly larger value for α and its corresponding β value. This is intuitively satisfying since the reliability of the switching will be improved by considering the effects of the most recent errors, i.e., reducing the number of false alarms.

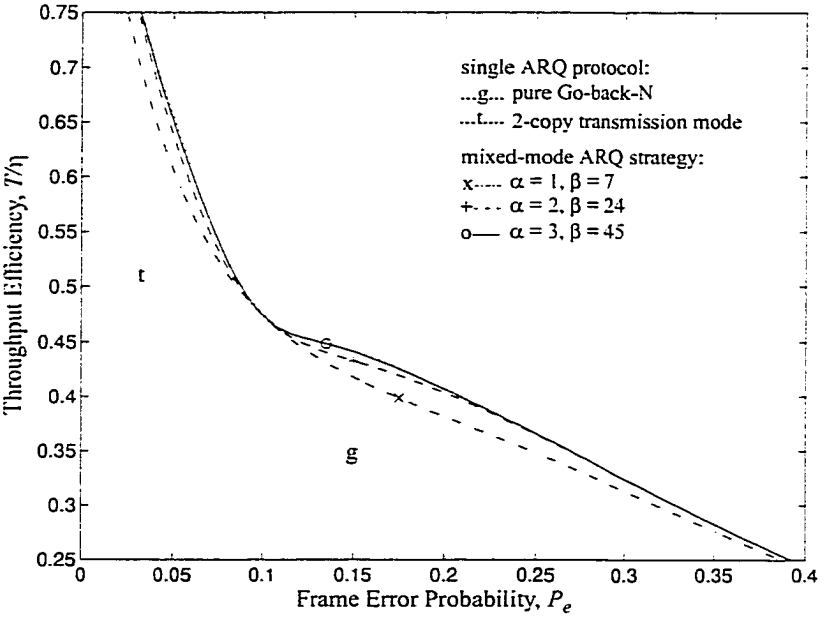

Fig. 9.3 Performance comparison of the proposed adaptive GBN ARQ system with different sets of suboptimal design parameters for N=10, t_1=1, and t_2=2.

---

1. This is actually an optimistic approximation because the protocol switches its operation mode to the 2-copy transmission immediately after receiving a NACK, rather than continue monitoring the incoming acknowledgment messages for the remaining duration of the observation interval and then switch to the 2-copy GBN strategy. Consequently, the anticipated throughput reduction in the conventional channel monitoring approach is associated with the idle time (delay) incurred before reacting to the changing channel conditions.

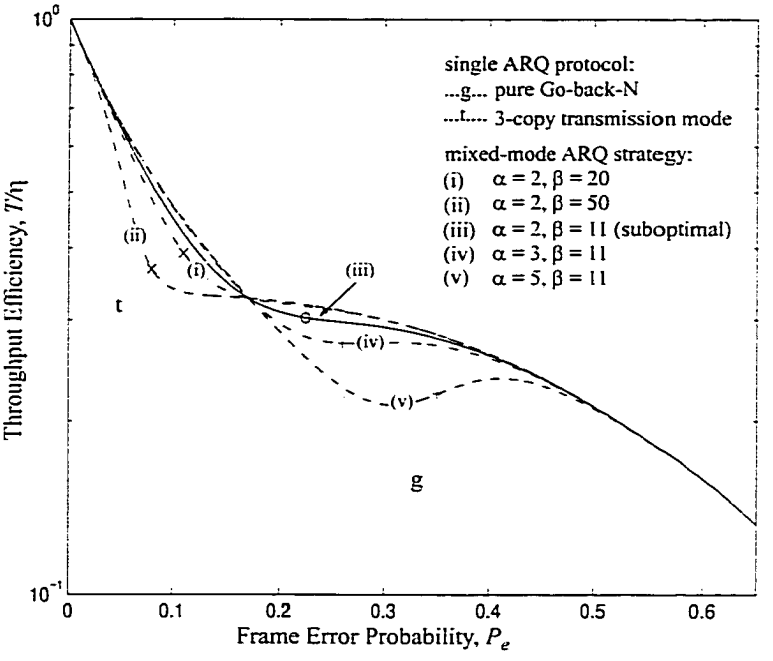

Fig. 9.4 Sensitivity of the selection of the design variables (α and β) on the throughput performance of a mixed-mode GBN ARQ protocol. N, t_1 and t_2 are assumed to be 10, 1 and 3, respectively.

Comparisons of the throughput performance for various settings (sensitivity analysis) of the design variables are illustrated graphically in Fig. 9.4. It is evident that a larger value of α (while keeping β identical) relates to a higher probability of being in State L. As a consequence, this selection yields much lower throughput within the error range slightly greater than the throughput cross-over probability (although an improved performance is attained at the lower error rates). Similarly, a larger value of β translates into a higher probability while being in state H, and therefore its performance curve tends to be closer to the 2-copy transmission scheme for a wider range of the channel error rates. These trends also validate the observations (a) and (b) in Appendix 9A.

Table 9.4 depicts the suboptimal CSE design parameters for the adaptive GBN ARQ system illustrated in Fig. 9.1, with different user defined weight sequences. Notation $W_{x:y}$ denotes the weight coefficients assigned to each of the data points in the follow-

ing two regions: $0 \le P_e \le P_{co}$ (Region A) and $P_{co} < P_e \le 1$ (Region B). For instance, $W_{10:1}$ will amplify the mean square error function by a factor of 10 in region A compared to the same amount of mismatch in region B. This translates into matching different data points with varying accuracy. Whereas, $W_{1:1}$ dictates that identical weights will be assigned to all data points in the region $0 \le P_e \le 1$. With the declining weight assignments from region A to region B, the ratio β/α of the suboptimal design variables are also lowered compared to the identical weights scenario, as anticipated. On the other hand, a higher weight assignment for region B relates to a higher probability of being in state H, and therefore requires a larger value for β when α is fixed.

Table 9.4 Suboptimal CSE design parameters for the adaptive GBN ARQ system depicted in Fig. 9.1, with different user defined weight sequences W_k. System parameters: $N = 10$, $t_1 = 1$ and $t_2 = 2$.

Weight Coefficients $W_{x:y}$	$W_{1:1}$	$W_{5:1}$	$W_{10:1}$	$W_{100:1}$	$W_{1:5}$	$W_{1:10}$	$W_{1:100}$
α	2	2	2	2	2	2	2
β	24	20	18	12	29	31	38
β/α	12.00	10.00	9.00	6.00	14.50	15.50	19.00
α	4	4	4	4	4	4	4
β	67	62	59	52	72	74	82
β/α	16.75	15.50	14.75	13.00	18.00	18.50	20.5

Table 9.5 Sensitivity of the CSE design variables to the feedback channel error in a mixed-mode Go-Back-N ARQ strategy with $N = 5$, $t_1 = 1$ and $t_2 = 2$.

Feedback channel error rate	$\alpha_{max} = 1$	$\alpha_{max} = 2$	$\alpha_{max} = 3$	$\alpha_{max} = 5$	$\alpha_{max} = 10$
$P_f = 0.00$	$[1\ 3]^T$	$[2\ 9]^T$	$[3\ 15]^T$	$[5\ 30]^T$	$[10\ 66]^T$
$P_f = 0.05$	$[1\ 3]^T$	$[2\ 9]^T$	$[3\ 15]^T$	$[5\ 30]^T$	$[10\ 66]^T$
$P_f = 0.10$	$[1\ 4]^T$	$[2\ 9]^T$	$[3\ 16]^T$	$[5\ 30]^T$	$[10\ 66]^T$
$P_f = 0.15$	$[1\ 6]^T$	$[2\ 11]^T$	$[3\ 17]^T$	$[5\ 30]^T$	$[10\ 66]^T$

Whereas in Table 9.5, the sensitivity of the design parameters to the feedback channel errors is investigated. It is evident that the suboptimal solutions remain unchanged if P_f is kept small, regardless the value of α. As well, the selection of the design variables appears to be independent of the feedback channel errors when α is chosen to be quite large. This observation is validated by the our asymptotic analysis in Appendix 9A. On the other hand, if α is quite small but P_f approaches very closely to P_{co}, then there is a noticeable increase in the ratio $\hat{\beta}^*/\hat{\alpha}^*$. This can be easily explained by noting that the system should only operate in a 2-copy transmission mode when $P_f \geq P_{co}$, and therefore it is desirable to have the ratio $\beta/\alpha \to \infty$. Although the suboptimal β may vary considerably in this regime, but we found that the quality criterion (MSE function) appears not to be very sensitive to this change.

In Fig. 9.5 and Fig. 9.6, throughput performance of the adaptive GBN and SR systems are plotted as a function of the frame error probability, and for different ACK/ NACK error rates. Although the throughput cross-over probability has changed due to feedback channel errors, the discrepancy between the adaptive ARQ curve with the desired performance envelope appears to be not influenced by this type of errors. These figures also indicate that the throughput performance is not severely affected unless the acknowledgment error rates are excessively large ($P_f > 0.01$). In general, the magnitude of the feedback channel error is usually much lower than the forward channel because the packet sizes are much shorter and these acknowledgment messages can be heavily protected by a low-rate FEC code. However for large P_f scenarios, the degradation in the system performance can be restored by introducing additional redundancy (i.e., by implementing a similar adaptive strategy used in the forward-link on the feedback channel). Analysis of such schemes is beyond the scope of this paper and shall be considered as part of our future study.

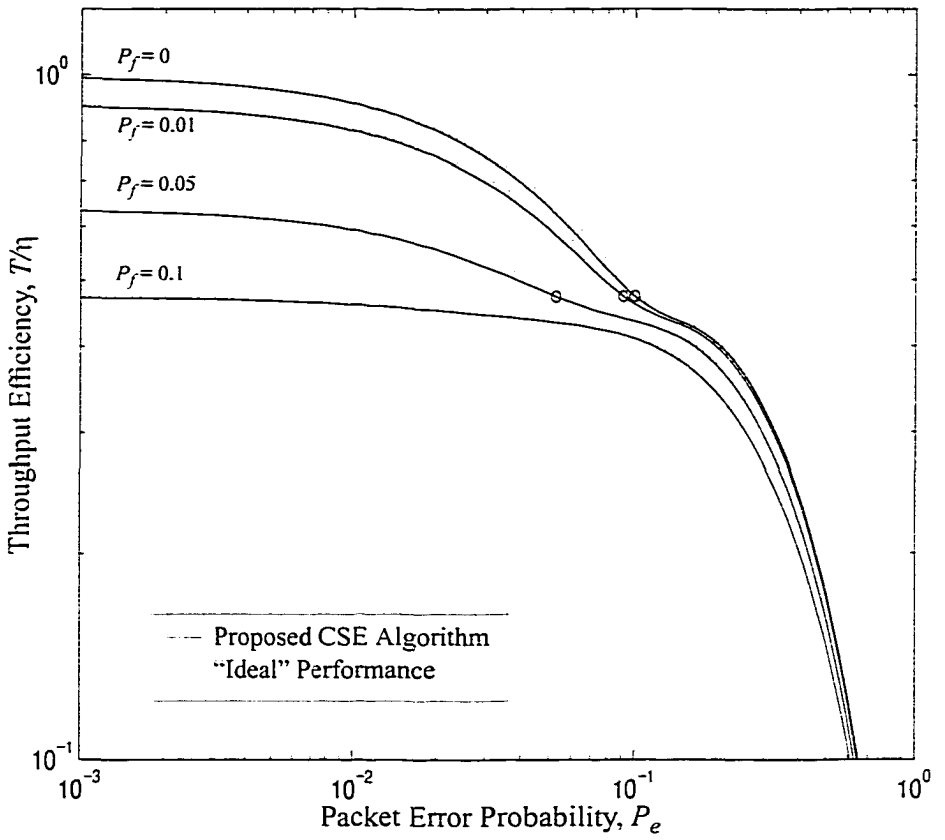

Fig. 9.5 Effects of feedback channel errors on the throughput performance of a mixed-mode GBN ARQ strategy with $t_1 = 1$, $t_2 = 2$, and $N = 10$. To obtain these curves, the design variables are selected to be $\alpha = 2$ and $\beta = 24$.

Table 9.6 Comparison between the interpolated β and the suboptimal $\hat{\beta}^*$ for an adaptive SR ARQ system with $N = 25$, $t_1 = 1$, $t_2 = 2$ and $P_f = 0$.

α	$c = \dfrac{\ln\lceil P_{co}\rceil}{\ln\lceil 1 - P_{co}\rceil}$	Interpolated integer value of $\beta = c(\alpha - 1) + 1$	β estimated using (9A.4)	Suboptimal $\hat{\beta}^*$ via optimization method
2	78.8515	80	81	98
3		159	159	169
5		316	316	322

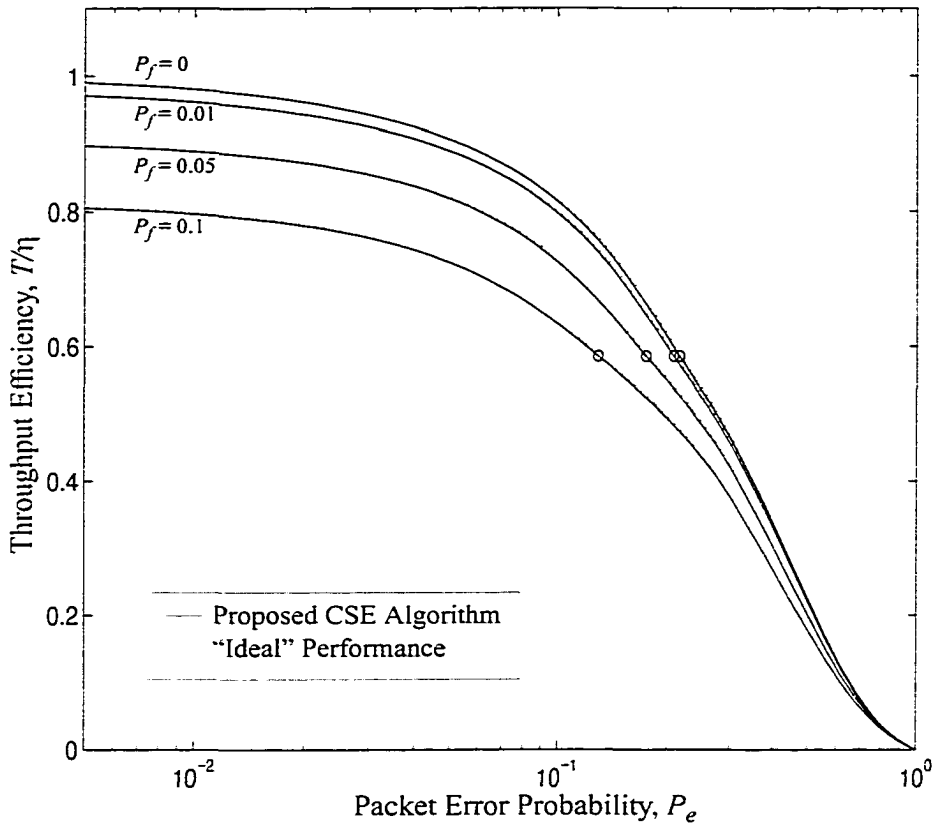

Fig. 9.6 Performance of an adaptive multi-copy SR ARQ system (i.e., $t_1 = 2$, $t_2 = 3$, and $N = 25$) in the presence of unreliable feedback channel. α and β for the CSE algorithm are assumed to be 3 and 15, respectively.

As might be anticipated, the deviation of the suboptimal solutions from the interpolated asymptotic properties becomes larger with decreasing α [see Table 9.6]. This observation becomes more pronounced in situations where the ratio described in (9A.5) is very large, (i.e., when the throughput cross-over probability is very small). For instance, the suboptimal solution and its corresponding interpolated CSE parameters for an adaptive SR ARQ system with $t_1 = 1$, $t_2 = 2$, and $N = 25$ are $\hat{x}^* = [2\ 98]^T$ and $\hat{x}_{interpolated} = [2\ 80]^T$, respectively. However, the objective function (MSE) appears not to be very sensitive to the variations in the quantity β, i.e., $E(2, 98) = 9.81 \times 10^{-8}$ and $E(2, 80) = 2.10 \times 10^{-7}$.

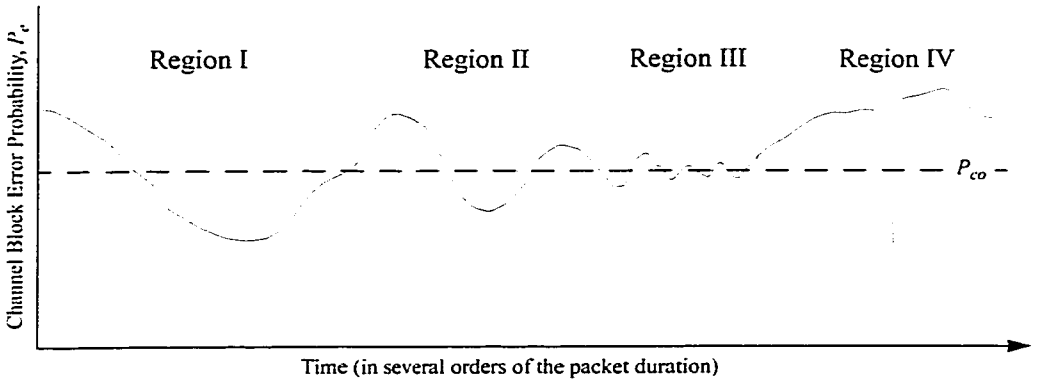

Fig. 9.7 Trade-offs and/or considerations for the selection of the CSE design variables in a moderate or slowly varying channels (i.e., variable-error-rate channels).

Fig. 9.7 summarizes some of the considerations for selecting the design parameters in a variable-error-rate channel. The proposed CSE algorithm aims to adapt to the slow variations of the long-term signal fading statistics rather than the rapid fluctuations of the short-term signal strength due to multipath fading. While in region I (i.e., local mean evolves very slowly), one would choose a moderate value for the design variables to achieve an improved mode switching reliability. However when the rate at which P_e crosses P_{co} increases (i.e., in region II), it would be desirable to select the suboptimal $[\alpha, \beta]$ pair as small as possible so that it can quickly react to the change in the channel conditions. On the other hand, a slightly larger value for α and its corresponding β may be appropriate if the channel condition is changing very rapidly (as shown in region III). This eliminates the need for too frequent switching between the two protocols, but at the expense of some sacrifice in performance. Moreover, it may become prohibitive to accurately track the channel condition in this situation (due to inability to acquire a reliable CSI), which in turn can results in a poorer performance (if the adaptive ARQ system is not 'synchronized' with the changing channel condition). Whereas in region IV, a moderate value for the design variables is again preferred to reduce the 'false-alarms'. Taking into account all these factors, and realizing that a close fit to the desired performance envelope can be attained even with a reasonably small α, we suggest that α be selected

in the range of 2 to 4 for practical systems, with its corresponding suboptimal β.

Finally, Fig. 9.8 illustrates the performance comparison of a mixed-mode GBN ARQ protocol and the single ARQ protocols for a Rayleigh faded channel at two different Doppler rates. Using a fade threshold model, the expression for the block error rate is given by [122],

$$P_e = 1 - \exp\left[-\frac{0.693}{\rho^2} - \frac{2\psi f_D}{\rho}\exp\left(-\frac{0.693}{\rho^2}\right)\right] \tag{9.27}$$

where ρ denotes the median received signal amplitude to threshold ratio, ψ is the message length in seconds, and f_D corresponds to the Doppler frequency for a vehicle speed V and carrier frequency f_c. When ψf_D goes to infinity the message becomes very long compared to fading process, and consequently P_e approaches unity. As well, the block error probability remains constant for vehicle speeds inversely related to the message duration [122]. This is intuitively satisfying since the probability of error depends on the message duration relative to the fading process. For moderate and fast fading channels or longer packet lengths, it is reasonable to assume that the probability of a transmission failure for one block is independent of that for other blocks [124]. Typically, $f_D = 80$ Hz for fast fading and $f_D = 40$ Hz for moderate fading. These fading rates correspond to 48 km/h speed and 24 km/h speed at a carrier frequency of 1800 MHz, respectively. While the effect of bit correlations within a packet is taken into account in (9.27), the expression do not consider time-correlation between adjacent packets. Moreover, independent block error probability is implicitly assumed in the derivations of (9.5) and (9.11), for analytical tractability. As a result, the results presented in this chapter are applicable for the moderate and fast fading channels where the statistical independence assumption between neighbouring packets is not violated. For a very slow fading channel (e.g., $f_D = 1.34$ Hz), one should resort to the rigorous treatment on this subject by Justin Chuang [123] and Li Fung Chang [124] where they carefully examined the throughput performance of several basic ARQ protocols in a time-correlated Rayleigh fading channel and used instantaneous block error probability for the computation of

throughput performance with the aid of computer simulations and estimation techniques.

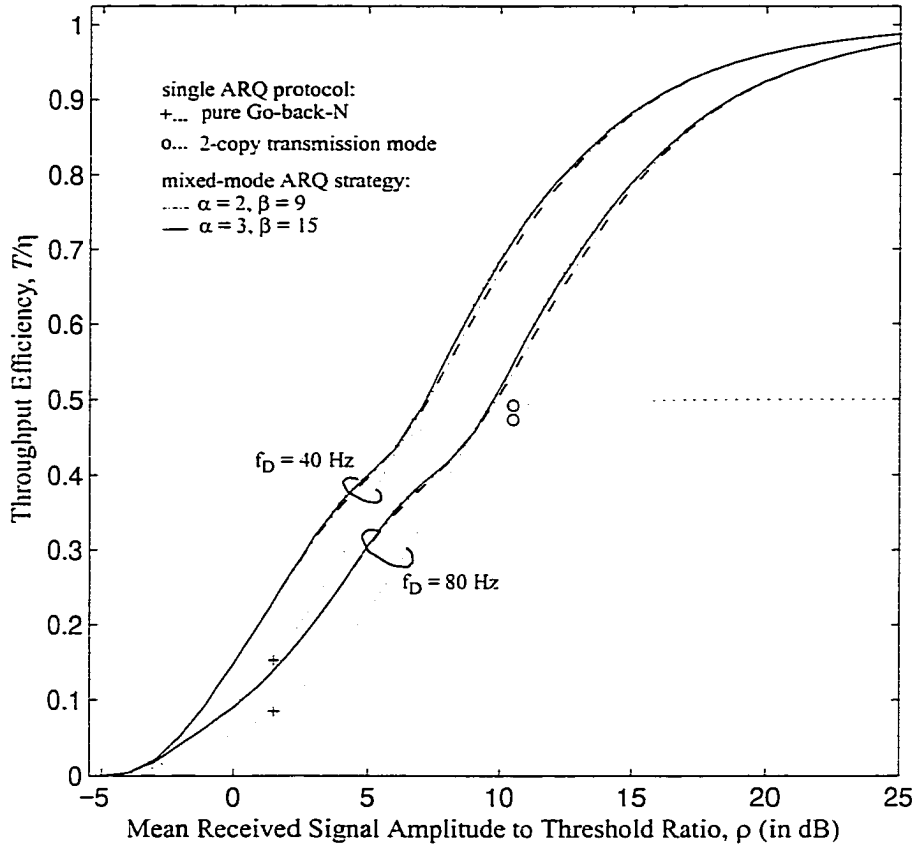

Fig. 9.8 Performance comparison of the proposed multi-mode GBN ARQ system (with suboptimal design parameters) and the single ARQ protocols for a Rayleigh faded channel at two different Doppler rates. N, t_1, t_2 and ψ are assumed to be 5, 1, 2, and 0.01, respectively.

From Fig. 9.8, we observe that the throughput increases monotonically as ρ increases. Since fast fading (i.e., f_D = 80 Hz) introduces errors which are more randomly distributed in time than caused by a smaller Doppler rate, it causes more retransmissions of groups of N frames for GBN ARQ protocol than the latter. In other words, the discrepancy between the throughput performance for a channel at f_D = 40 Hz and f_D = 80 Hz is attributed to the fact that the probability of a packet failure rate in a channel with burst errors is much lower than a channel with purely random errors. We also

note that the performance curve of the mixed-mode GBN ARQ scheme with $[\alpha= 2, \beta= 9]$ deviates slightly farther away from the desired performance envelope at a higher Doppler rate. This may be attributed to the "false-alarm" phenomena that we have described in region IV of Fig. 9.7. Hence, we can conclude that the design parameters are relatively insensitive to the short-term fading rate (for the independent block error probability case), as long as their values are not too small.

9.5 Conclusions

A simple channel state estimation scheme suitable for wireless packet data communications has been studied. The channel state information is extracted from the frequency of the received contiguous ACKs and NACKs acknowledgment messages at the transmitter. The effectiveness of this algorithm has been highlighted by analyzing the performance of adaptive multicopy transmission GBN and SR protocols. In particular, a systematic and efficient approach for computing the suboptimal CSE design variables has been outlined. The optimization results reveal that this CSE algorithm can provide a reliable CSI (accurate estimate of the channel conditions) within only a few block transmissions, while preserving simplicity. Additionally, it has been shown that the proposed CSE algorithm is robust against feedback channel errors since the selection of the design variables are not very sensitive to this type of errors.

Asymptotic properties of the estimated throughput expression have been investigated. The asymptotic analysis can be considered complementary to the analysis performed in a finite region of the α-β space using the optimization approach. Subsequently, a simple formula to estimate the suboptimal design parameters is suggested. This approximation becomes quite accurate especially when the throughput cross-over probability is quite large or as the value of α increases. Finally, this CSE method also allows us to choose a wide-range of suboptimal design parameters depending on the evolution of the channel statistics, i.e., based on the rate at which the channel block error probability crosses P_{co} and the mode switching reliability criterion.

Appendix 9A

In this appendix, we analyze the asymptotic properties of the estimated throughput expression. This is motivated by the trends observed from our optimization results which suggests that the optimal solution for the design variables lies in the infinite region. Therefore, here we attempt to show analytically that the observation is valid, and subsequently investigate the relationship between the design parameters at the optimum point. For mathematical simplifications, we model the forward-link by a partitioned Markov chain with two channel state groups, and assume a noiseless feedback channel. Then, P_L in (9.5) can be re-written in the form,

$$P_L = \left\{1 + \left(\frac{P_e^{\alpha-1}}{1-P_e^{\alpha}}\right)\left(\frac{1-(1-P_e)^{\beta}}{(1-P_e)^{\beta-1}}\right)\right\}^{-1} . \tag{9A.1}$$

We note the following observations:

(a) If $\alpha \to \infty$ with finite β, then $\underset{\substack{\alpha \to \infty \\ \text{finite } \beta}}{\text{Limit}} \hat{T}(P_e) = T_L$ since $P_L \to 1$ (because $\underset{x \to 0}{\text{limit}} \frac{x}{1-x} = 0$) and $P_H = (1-P_L) \to 0$.

(b) If $\beta \to \infty$ with finite α, then $\underset{\substack{\beta \to \infty \\ \text{finite } \alpha}}{\text{Limit}} \hat{T}(P_e) = T_H$ since $P_L \to 0$ and $P_H \to 1$.

(c) If both $\alpha, \beta \to \infty$, (9A.1) can be well approximated as,

$$\begin{aligned} P_L &\approx \left\{1 + \frac{P_e^{\alpha-1}}{(1-P_e)^{\beta-1}}\right\}^{-1} \\ &= \left[1 + \exp\left((\alpha-1)\ln(1-P_e)\left(\frac{\ln(P_e)}{\ln(1-P_e)} - \frac{\beta-1}{\alpha-1}\right)\right)\right]^{-1} \end{aligned} \tag{9A.2}$$

(i) If $\frac{\ln(P_e)}{\ln(1-P_e)} - \frac{\beta-1}{\alpha-1} = 0$, then $\underset{\alpha, \beta \to \infty}{\text{Limit}} \hat{T}(P_e) = 0.5(T_L + T_H)$.

(ii) If $\frac{\ln(P_e)}{\ln(1-P_e)} - \frac{\beta-1}{\alpha-1} < 0$,

then $\underset{\alpha, \beta \to \infty}{\text{Limit}} \hat{T}(P_e) = T_H$ since $P_L \to 0$ and $P_H \to 1$.

(iii) If $\frac{\ln(P_e)}{\ln(1-P_e)} - \frac{\beta - 1}{\alpha - 1} > 0$,

then $\underset{\alpha, \beta \to \infty}{\text{Limit}} \hat{T}(P_e) = T_L$ since $P_L \to 1$ and $P_H \to 0$.

Therefore by forcing the observations in (c) at the throughput cross-over probability, i.e., $P_e = P_{co}$, we achieve the best fit to the desired (ideal) performance curve over a wide range of channel error probability. Notice that for $P_e > P_{co}$ (observation (ii)), the throughput performance of the adaptive protocol converges towards T_H. On the other hand, when $P_e < P_{co}$ (observation (iii)), $\hat{T}(P_e)$ approaches T_L very closely. Finally, when $P_e = P_{co}$, we have $\hat{T}(P_e) = T_L = T_H$. Hence, we have shown that the best fit happens (which corresponds to the local minimum point of our objective function) when both the parameter values approaches infinity. However, it should be stressed that the asymptotic analysis has no practical significance (because it assumes the channel to be quasi-stationary) except for providing useful insights regarding the interaction of the design variables, as well as a rule of thumb allowing a handy calculation of the α for a given β (suboptimal solutions), or vice-versa. The relationship between the design parameters at the optimum point can be easily attained by letting $P_L = P_H$ at the throughput cross-over probability, and then solve the equation for α or β,

$$\alpha = 1 + \left\{ \frac{(\beta - 1)\ln(1 - P_{co}) - \ln\left[1 + (1 - P_{co})^{\beta - 1}(2P_{co} - 1)\right]}{\ln(P_{co})} \right\} \qquad (9A.3)$$

$$\beta = 1 + \left\{ \frac{(\alpha - 1)\ln(P_{co}) - \ln\left[1 + P_{co}^{\alpha - 1}(1 - 2P_{co})\right]}{\ln(1 - P_{co})} \right\} \qquad (9A.4)$$

Since $\alpha^* \gg 1$ and $\beta^* \gg 1$, a good approximation for (9A.3) and (9A.4) is given by,

$$\frac{\beta_\infty - 1}{\alpha_\infty - 1} \approx \frac{\ln (P_{co})}{\ln (1 - P_{co})}. \tag{9A.5}$$

In the presence of feedback channel errors,

$$P_L = \left\{ 1 + \left(\frac{\lambda^{\alpha - 1}}{1 - \lambda^{\alpha}} \right) \left(\frac{1 - (1 - \lambda)^{\beta}}{(1 - \lambda)^{\beta - 1}} \right) \right\}^{-1}. \tag{9A.6}$$

Applying the steps outlined for an error-free feedback channel, but now forcing the corresponding three observations from (9A.6) at the new throughput cross-over probability, i.e., $P_e = P_{co-noisy}$, we have

$$\frac{\beta_\infty - 1}{\alpha_\infty - 1} \approx \frac{\ln (\lambda_{co})}{\ln (1 - \lambda_{co})},$$

where $\lambda_{co} = P_{co-noisy}(1 - P_f) + P_f$.

It is apparent from (9.16) that $\lambda_{co} = P_{co}$, and therefore we have shown that the optimum $[\alpha^* \ \beta^*]^T$ value is independent of the quality of the feedback channel. In other words, the selection of the design variables for the proposed CSE algorithm is not strongly influenced or affected by the feedback channel errors.

Chapter 10

Evaluation of Self-Reconfigurable ARQ Systems with Adaptive Packet Length in a Slowly Varying Mobile Radio Environment

Automatic repeat request (ARQ) error control schemes are practically appealing for providing reliable packet data transmissions over two-way wireless communication links, owing to their simplicity and high system reliability. On the other hand, a major drawback of the repeat-request strategies is that their throughput is not constant (unlike the case with forward-error correction schemes) and it falls rapidly with increasing channel error rate [101]. In order to address this issue, many adaptive[1] ARQ protocols have been suggested in literature [109]-[127]. For instance in [109], [110] and [111], the authors suggested to vary the forward error correction rate to compensate for the fluctuations in the channel conditions. In [108] and [125], adaptive block (packet) size strategy was adopted. Whereas, in [105]-[107] and [127], different multi-copy transmission schemes were used as adaptation mechanisms. The underlying premise is that if accurate channel state information is exploited to dynamically change the protocol coding rate, packet length or the operation modes, then obviously higher throughput can be realized over a wide-range of error probabilities, versus a fixed (nonadaptive) algorithm.

---

1. It is worth noting that error detection with retransmission itself is an adaptive system because the redundant information is only transmitted when errors occur. The protocol throughput efficiency can be further enhanced by optimizing its parameters such as the packet length and/or the code rate.

Adaptive ARQ schemes rely on a certain algorithm to estimate the channel conditions and then adjust the protocol parameters accordingly. Ideally, the knowledge of instantaneous packet error probability is required. But this involves accurate estimation of the signal strength (via signal power measurement or with pilot tone transmission) as well as the mobile terminal velocity (need a speed sensor at the receiver), which give rise to signal processing complexity. Alternatively, a reliable channel state information (CSI) can be attained by exploiting a complex decision statistics such as the exact number of erroneous bits in a received packet, and periodically transmitting the information to the transmitter. Certainly the efficiency of the exchange improves with the frequency of the feedback packets, but at the expense of a larger consumption of return-channel capacity. While such techniques allow the predicted packet error rate (PER) to converge to the "true" PER quite rapidly, the considerable overhead requirement and added complexity are not likely to be justified in practical applications. Fortunately, the frequency of the retransmission requests provide a natural source of CSI. Hence no additional circuitry is required for estimating the channel state (except for the knowledge of either the received signal strength or the mobile terminal velocity if both of these parameters are changing with time). Since an indirect method is employed to predict the variation in the channel condition, the effectiveness of the adaptive system is mainly dictated by the rate at which the estimated PER converges to the instantaneous PER.

Typically, the channel is monitored by counting the number of retransmissions during an observation interval (OBI) and comparing that number with a set of thresholds to determine the channel condition [109]. If OBI is large, then the delay in reacting to a change in the channel could be significant. On the other hand, very small values of OBI will not provide a reliable CSI decision. In [108], a method for estimating the bit-error rate (BER) was outlined. By accumulating the values of total number of n-bits blocks in error (TNBE) and total number of n-bits blocks (TNB) over a long period, the expression (10.1) does provide a real-time adaptation,

$$P_b \approx TNBE / (TNB \times n) \; . \tag{10.1}$$

However, as pointed out in [112], such a long term bit error rate is meaningless as a description of practical communication channels, because real channels often have errors occurring in bursts. To provide a more reasonable estimate of the instantaneous block error probability, weighted sum of errors should be considered. This ensures that the influence of the most recent errors is the largest. More recently, Rice and Wicker suggested to predict the channel conditions by scoring the outcome of the decoding process [109]. It has been shown that the statistical sequential inspection scheme will require, on average, fewer samples (and therefore shorter observation interval) to detect this change than with a fixed sample size approach.

Whereas in [125], Hara and others performed a simulation study for the stop-and-wait (SAW-ARQ) protocol with adaptive packet length by employing the traditional channel monitoring algorithm. They constructed a permanent look-up table based on the parameters for very fast fading situation, and therefore its usage is restrictive (limited). By contrast, in this chapter we have developed an analytical framework to analyze the performance of this algorithm and present closed-form expressions to update the PER table in real-time (rather than a permanent look-up table). This robust adaptation strategy is desirable in many practical applications where both the mobile terminal speed (or the Doppler frequency) and the received mean signal strength are slowly varying. In addition, we propose three other simple algorithms to implement an adaptive ARQ protocol with variable packet lengths. Numerical results reveal that these algorithms perform remarkably well in spite of their simplicity. In particular, the algorithm based on counting the contiguous positive and/or negative acknowledgment messages provides a reliable CSI within only a few block transmissions, and requires the shortest observation interval among these four schemes. Explicit expressions to construct the PER look-up table are derived, and rule of thumb for handy calculations of the suboptimal design parameters in certain algorithms is found. As an illustrative example, the throughput performance of selective-repeat (SR-ARQ) protocol with adaptive packet length is furnished.

10.1 Throughput Analysis

In this section, throughput performance for adaptive packet length of SR-ARQ and SAW-ARQ protocols are presented. First, we determine the optimal packet length which maximizes the throughput efficiency in a Rayleigh fading channel. Subsequently, we seek to find exact analytical expressions for computing the break points of the channel block error probability where the performance with a specified packet length is better than the other, so that the overall system throughput can be optimized. The knowledge of these throughput cross-over probabilities (entries in the PER table) are essential in the design of the adaptive ARQ strategies because the packet length adaptation will occur at the vicinity of these intersection points.

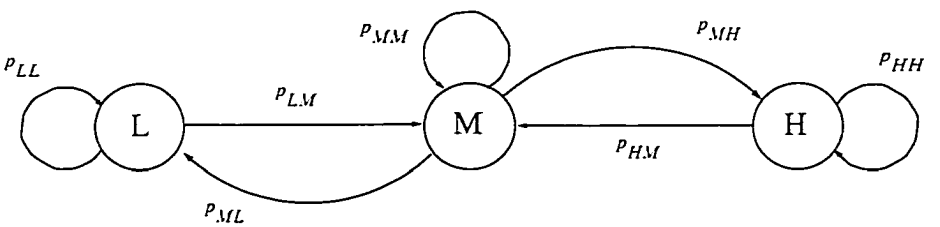

Fig. 10.1 Markov chain representation for an adaptive ARQ protocol with three different packet lengths.

The forward channel is considered to have a finite number of states associated with distinct channel conditions. As an example, Fig. 10.1 depicts an adaptive ARQ strategy with transition between three different packet lengths. State L, M and H correspond to low, moderate and high channel error rate conditions, respectively. The packet length is assumed to be n_1 bits while in state L. When the channel condition degrades, the number of information bits in a packet is reduced to $n_2 - h$ bits, where h denotes the number of overhead bits in each packet. The decision regarding the transitions between different packet lengths is made based on the received acknowledgment messages as well as from the measurement of either the received mean signal strength or the speed of the mobile terminal. On the other hand, when the transmitter considers that the channel is traversing

from state H to state M, the packet length is adapted from n_3 to n_2 bits. Notice that $n_3 < n_2 < n_1$ because short packets are less likely to encounter fades than long packets. But they are more burdened by overheads. The two contradicting requirements suggest that the optimal packet length vary at different channel error rates.

Now the throughput of this adaptive scheme with three controllable packet lengths is simply an average of the throughput performance with their individual packet lengths, i.e.,

$$\hat{T}_A = P_L T_L + P_M T_M + P_H T_H, \tag{10.2}$$

where T_i and P_i denote the throughput efficiency and steady-state probability of the channel while in state i ($i \in \{L, M, H\}$), respectively. The steady-state probabilities are dependent on a specific algorithm employed for sensing the channel condition, and will be derived in Section 10.2.

10.1.1 Stop-and-Wait ARQ Protocol

SAW-ARQ is the simplest form of repeat request error control strategy but inherently inefficient due to the idle time spent waiting for an acknowledgment of each transmitted codeword. Consequently, this scheme is only suitable for terrestrial communications with short propagation delays, and low data rate applications.

10.1.1.1 Optimal Packet Length

Using a fade threshold model [128][122] where both the average gap length and average burst length obey exponential density laws, the probability of packet success (i.e., received signal level is above the threshold level) in a Rayleigh fading channel can be readily obtained as

$$P_C = \exp\left[-\rho - f_D\sqrt{2\pi\rho}\,T_b\right], \tag{10.3}$$

where ρ corresponds to the ratio between the threshold power level and the mean received power level, and $T_b = n/R$ is the packet duration at signalling rate R. It is noted that the threshold power level is fixed by the type of modulation and transmission

techniques employed, and the quality of service desired. Parameter $f_D = v/\lambda_c$ is the Doppler frequency with v and λ_c denote the mobile speed and the carrier wavelength, respectively. The approximate packet success probability predicted by the threshold model is quite accurate and has been verified by experimental results [122].

The throughput efficiency of SAW-ARQ scheme is then given by,

$$T = \frac{n-h}{n+\Delta}\exp\left[-\rho - \frac{nf_D\sqrt{2\pi\rho}}{R}\right], \tag{10.4}$$

where Δ is the number of bits that could have been transmitted during the period equivalent to the roundtrip propagation delay, had the transmitter not been idle, waiting for an acknowledgment.

Differentiating (10.4) with respect to n, and then solving it for maximum throughput (i.e., setting the derivative to 0), we obtain a closed-form expression for the optimal packet length,

$$n_{opt} = \frac{1}{2}\left[h - \Delta + \sqrt{(h+\Delta)^2 + \frac{4(h+\Delta)}{\Omega}}\right], \tag{10.5}$$

where $\Omega = f_D\sqrt{2\pi\rho}/R$. Therefore, the maximum attainable throughput with adaptive packet length can be expressed as,

$$T_{opt} = \frac{\Omega}{4}(h+\Delta)\left[\sqrt{1+\frac{4}{\Omega(h+\Delta)}} - 1\right]^2 \times \exp\left(-\rho - \frac{\Omega}{2}\left[h - \Delta + \sqrt{(h+\Delta)^2 + \frac{4(h+\Delta)}{\Omega}}\right]\right). \tag{10.6}$$

10.1.1.2 Determination of Packet Error Rate Table

We now derive the exact throughput cross-over probability, P_{co}, between any two arbitrary packet length of SAW-ARQ scheme. After some algebraic manipulations, the throughput difference between the two fixed packet length protocols is [129],

$$\Psi = \frac{\exp(-\rho - \Omega n_{i+1})}{(n_i + \Delta)(n_{i+1} + \Delta)} \times [(n_{i+1} - h)(n_i + \Delta) - (n_i - h)(n_{i+1} + \Delta)\exp(\Omega n_{i+1} - \Omega n_i)] \quad (10.7)$$

where the notation n_i denotes the number of bits in a packet while the adaptive system is in state i. It is evident that the denominator of (10.7) is always greater than zero. Thus with the assumption of $n_i > n_{i+1}$, the throughput efficiency of SAW-ARQ with packet size n_{i+1} bits is higher than that of n_i bits per block if the numerator of (10.7) is positive, namely,

$$\Omega = \frac{f_D\sqrt{2\pi\rho}}{R} \geq \frac{1}{(n_i - n_{i+1})} \ln\left[\frac{(n_i - h)(n_{i+1} + \Delta)}{(n_i + \Delta)(n_{i+1} - h)}\right]. \quad (10.8)$$

Consequently, for a fixed ρ, the packet length is adapted from n_i to n_{i+1} if the estimated block error probability is greater than (10.9), and vice-versa if the estimated block error probability is less than (10.10) [129]:

$$P_{co(i,i+1)}^{(U)} = 1 - \exp\left[-\rho - \frac{n_i}{(n_i - n_{i+1})} \ln\left(\frac{(n_i - h)(n_{i+1} + \Delta)}{(n_i + \Delta)(n_{i+1} - h)}\right)\right], \quad (10.9)$$

$$P_{co(i,i+1)}^{(L)} = 1 - \exp\left[-\rho - \frac{n_{i+1}}{(n_i - n_{i+1})} \ln\left(\frac{(n_i - h)(n_{i+1} + \Delta)}{(n_i + \Delta)(n_{i+1} - h)}\right)\right]. \quad (10.10)$$

Similarly for a fixed f_D, the corresponding throughput cross-over probability entries of the PER table are [129]:

$$P_{co(i,i+1)}^{(U)} = 1 - \exp\left[-\rho_{co(i,i+1)} - \frac{n_i}{(n_i - n_{i+1})} \ln\left(\frac{(n_i - h)(n_{i+1} + \Delta)}{(n_i + \Delta)(n_{i+1} - h)}\right)\right], \quad (10.11)$$

$$P_{co(i,i+1)}^{(L)} = 1 - \exp\left[-\rho_{co(i,i+1)} - \frac{n_{i+1}}{(n_i - n_{i+1})} \ln\left(\frac{(n_i - h)(n_{i+1} + \Delta)}{(n_i + \Delta)(n_{i+1} - h)}\right)\right], \quad (10.12)$$

where

$$\rho_{co(i,i+1)} = \left(\frac{R}{\sqrt{2\pi} f_D (n_i - n_{i+1})} \ln\left[\frac{(n_i - h)(n_{i+1} + \Delta)}{(n_i + \Delta)(n_{i+1} - h)}\right]\right)^2. \quad (10.13)$$

10.1.2 Selective-Repeat ARQ Protocol

Selective-repeat retransmission scheme yields the highest throughput efficiency among the class of basic ARQ protocols. This is because the transmitter retransmits only those blocks which were detected in error, but requires resequencing buffers at the receiver. Therefore, SR-ARQ strategy is preferred for applications with large propagation delays (e.g., satellite communication links) and/or high signalling rates (i.e., high-speed modems).

10.1.2.1 Optimal Packet Length

Throughput formula for the ideal SR-ARQ scheme (i.e., no overflows) can be easily derived from that of SAW-ARQ by ignoring the terms associated with propagation delay. Substituting $\Delta = 0$ in (10.4), (10.5) and (10.6), we obtain the expressions for the throughput efficiency, optimal packet length and the maximum achievable throughput with optimal packet length for the SR-ARQ scheme:

$$T = \frac{n-h}{n}\exp\left[-\rho - n\Omega\right], \tag{10.14}$$

$$n_{opt} = \frac{1}{2}\left[h + \sqrt{h^2 + \frac{4h}{\Omega}}\right], \tag{10.15}$$

$$T_{opt} = \frac{\Omega h}{4}\left[\sqrt{1 + \frac{4}{\Omega h}} - 1\right]^2 \exp\left(-\rho - \frac{\Omega}{2}\left[h + \sqrt{h^2 + \frac{4h}{\Omega}}\right]\right). \tag{10.16}$$

It should be pointed out that our analysis for the SR-ARQ protocol with adaptive packet length is strictly valid if the channel is evolving very slowly (so that (10.14) will be a good approximate for the steady-state throughput in a given state). But this requirement can be relaxed without any loss of generality for both SAW-ARQ and Go-Back-N ARQ strategies.

Fig. 10.2 depicts the throughput performance curves for various fixed packet lengths and an adaptive SR-ARQ scheme with optimal packet length at a fixed ρ. It is evident that by dynamically adapting the number of information bits in a packet in an

appropriate manner to the changing channel conditions, a higher throughput efficiency can be realized over a wide-range of Doppler fading rates.

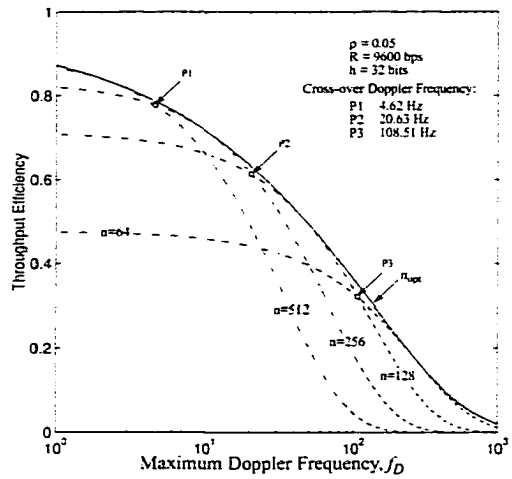

Fig. 10.2 Performance comparison between the adaptive and fixed packet length SR-ARQ systems in a Rayleigh fading channel at ρ=0.05.

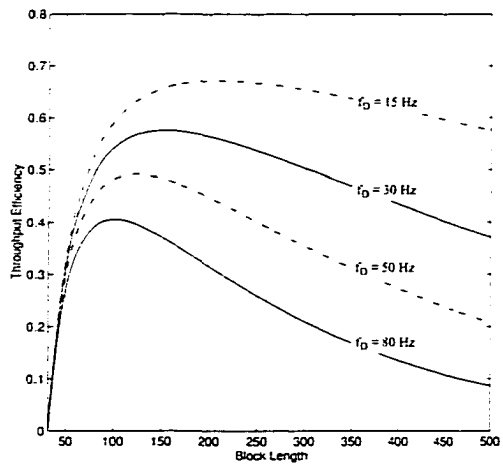

Fig. 10.3 Throughput curves of SR-ARQ protocol plotted as a function of the block size (obtained using (10.14) with ρ = 0.05, h = 32 bits and R = 9600 bps).

Also notice that we can still achieve a very good performance (closely approaching the ideal performance curve) even by adjusting the packet length within a set of geometrically related integers as the channel condition fluctuates. This is because the throughput versus block size curve at various Doppler rates do not show a sharp peak, but rather a wide interval spread around the maximum (optimal packet length), as shown in Fig. 10.3.

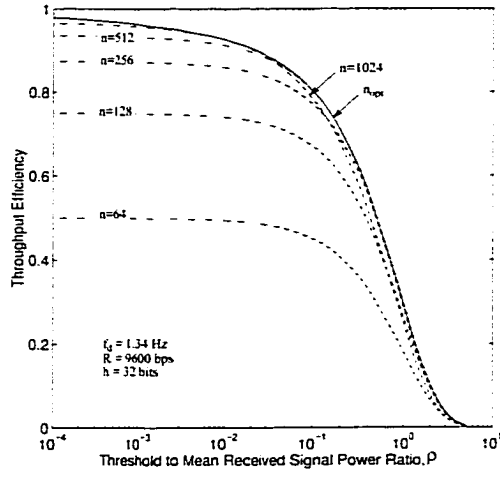

(a) Slow fading channel, $f_D = 1.34$ Hz

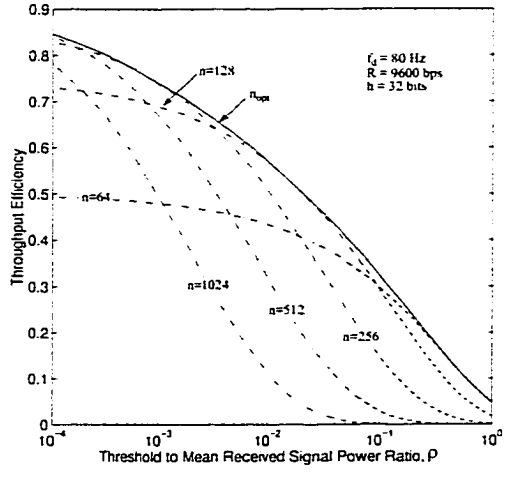

(b) Fast fading channel, $f_D = 80$ Hz

Fig. 10.4 Throughput performance of fixed and variable packet length SR-ARQ systems in a Rayleigh fading channel at a fixed f_D.

Whereas in Fig. 10.4, the throughput performance for different packet lengths are plotted as a function of ρ for a fixed f_D. Typically, f_D = 80 Hz for fast fading and f_D = 1.34 Hz for slow fading [125]. These fading rates correspond to 30 mi/h speed and 0.5 mi/h speed at a carrier frequency of 1800 MHz, respectively. Comparison between Fig. 10.4(a) and Fig. 10.4(b) reveal that the adaptive packet length strategy is less effective when Doppler fading rate is very small (i.e., very slow fading) even if the dynamic range of ρ is quite large. However for moderate and fast moving terminals (i.e., fast fading scenario), block size adaptation is an effective technique for improving the system throughput over the variable-error-rate channel.

10.1.2.2 Determination of Packet Error Rate Table

Similar to our treatment for the SAW-ARQ scheme, we first determine the intersection point between two throughput curves for SR-ARQ which corresponds to the block sizes n_i and n_{i+1}. Then it can be shown that at the cross-over point, the following condition is satisfied,

$$\Omega_{co} = \frac{1}{(n_i - n_{i+1})} \ln\left[\frac{n_{i+1}(n_i - h)}{(n_i + \Delta)(n_{i+1} - h)}\right]. \tag{10.17}$$

It follows that the entries for the PER table of the adaptive SR-ARQ are computed by substituting $\Delta = 0$ in (10.9) and (10.10) if ρ is known, or using formulas (10.11) to (10.13) (with $\Delta = 0$) when knowledge about f_D is available.

Suppose the initial packet length is chosen to be n_i bits. Then this packet length will be remain unchanged if the instantaneous PER (or the estimated PER) is greater than $P^{(L)}_{co(i-1,i)}$ but less than $P^{(U)}_{co(i,i+1)}$. A shorter packet size of n_{i+1} bits will be selected if the block error probability is greater than $P^{(U)}_{co(i,i+1)}$, and a longer packet length if the instantaneous PER is less than $P^{(L)}_{co(i-1,i)}$. As an example, Table 10.1 illustrates the entries of a PER table for the following two different cases: (i) measurement or the knowledge of the average signal power is available; and (ii) mobile terminal velocity

(can be obtained using speed sensor) or the Doppler fading rate is known.

Table 10.1(a) PER table for a given $\rho = 0.05$. $R = 9.6$ kbps and $h = 32$ bits.

Controllable Packet Size Range $n_i = 2^{1-i} \times 512, i = 1, 2, 3, \ldots$	Throughput cross-over probability	
$n_1 = 512$	-	0.1714
$n_2 = 256$	0.1122	0.3011
$n_3 = 128$	0.1847	0.5772
$n_4 = 064$	0.3658	-

Table 10.1(b) PER table for a very slow fading situation ($f_D = 1.34$ Hz). $h = 32$ bits and $R = 9.6$ kbps.

Controllable Packet Size Range $n_i = 2^{1-i} \times 512, i = 1, 2, 3, \ldots$	Throughput cross-over probability	
$n_1 = 512$	-	0.5187
$n_2 = 256$	0.4843	1.0000
$n_3 = 128$	1.0000	1.0000
$n_4 = 064$	1.0000	-

Table 10.1(c) PER table for a fast fading condition ($f_D = 80$ Hz). $R = 9600$ bps and $h = 32$ bits.

Controllable Packet Size Range $n_i = 2^{1-i} \times 512, i = 1, 2, 3, \ldots$	Throughput cross-over probability	
$n_1 = 512$	-	0.1290
$n_2 = 256$	0.0668	0.2677
$n_3 = 128$	0.1457	0.5946
$n_4 = 064$	0.3919	-

In order to attain the maximum throughput, the entries in the PER table should be continuously updated because they are dependent on both f_D and ρ. Expressions (10.9)-(10.13) provide closed-form formulas for updating these entries in real-time (instead of a permanent look-up table). It is apparent that these formulas only require the measure-

ment of a single parameter (either the mean received signal power or the speed of the mobile terminal) to estimate the instantaneous block error probability via an indirect method. Moreover in a reverse-link communication (from the mobile terminal to the base-station), the knowledge of the Doppler frequency is usually acquired at no additional cost because the moving vehicles are usually equipped with speedometer. Then the block size can be adapted to the fluctuations in ρ, without having to measure the received signal strength, by using (10.11), (10.12) and a simple indirect channel state estimation scheme.

10.2 Channel State Estimator

Perhaps the most difficult problem in implementing an adaptive scheme is finding a simple real-time adaptive algorithm. In other words, the channel error characteristics should be identified within a few block transmissions while preserving simplicity. Although a reliable CSI can be acquired by continuously measuring the received signal power and the speed of the mobile terminal, this is not preferable in terms of implementation. Therefore in practice, the frequency of retransmission request during an observation interval is used to sense the changes in the channel condition. Since an indirect method is employed to detect the fluctuations in the channel condition, the effectiveness of the adaptive system is mainly dictated by the rate at which the estimated PER converges to the instantaneous PER. In light of these considerations, we will study the performance of four simple channel state estimation (CSE) algorithms, which may be used to implement an adaptive ARQ system.

10.2.1 Maximum Likelihood PER with Fixed Observation Interval (Algorithm A)

Traditionally the CSI is acquired by counting the number of retransmissions during an observation interval (OBI) and comparing that number with a set of thresholds to determine the channel condition [109]. This algorithm is based on maximum likelihood estimate for the packet error probability [129] with an identical OBI for all the channel

states (see Appendix 10A). The packet length control strategy is summarized as follows:

(i) During an observation interval, the packet length n_i is kept unchanged.

(ii) The block error probability is calculated as,

$$P_B(n_i) = \frac{\text{No. of NACKs}}{\text{OBI}} = \frac{\text{No. of NACKs}}{\text{No. of ACKs + No. of NACKs}} \tag{10.18}$$

(iii) The packet length in the subsequent OBI is determined according to,

n_{i-1} is chosen if $P_B(n_i) < P_{co(i-1,i)}^{(L)}$,

n_i is selected if $P_{co(i-1,i)}^{(L)} \le P_B(n_i) \le P_{co(i,i+1)}^{(U)}$,

n_{i+1} is chosen when $P_B(n_i) > P_{co(i,i+1)}^{(U)}$

Hara et. al. [125] have investigated the performance of this algorithm via simulation and furnish a permanent PER table for a very fast fading condition. By contrast, in this paper we have developed a theoretical framework to analyze the performance of this algorithm and present closed-form expressions to update the PER table in real-time (instead of a permanent look-up table for achieving an improved throughput efficiency).

Let us consider an adaptive ARQ strategy with a set of three controllable packet sizes, namely $\{n_2 = 256, n_3 = 128, n_4 = 64\}$, and a fixed observation interval of 10 acknowledgment messages. R, h and f_D are assumed to be 9600 bps, 32 bits and 50 Hz, respectively. The adaptive ARQ strategy can be represented by a simple Markov chain with three states as illustrated in Fig. 10.1. Then we obtain the following steady-state probabilities,

$$P_L = \frac{p_{43}\,p_{32}}{p_{23}\,p_{34} + p_{23}\,p_{43} + p_{43}\,p_{32}}, \tag{10.19}$$

$$P_M = \frac{p_{23}\,p_{43}}{p_{23}\,p_{34} + p_{23}\,p_{43} + p_{43}\,p_{32}}, \tag{10.20}$$

$$P_H = \frac{p_{23}\,p_{34}}{p_{23}\,p_{34} + p_{23}\,p_{43} + p_{43}\,p_{32}}, \tag{10.21}$$

where $\{p_{23}, p_{34}\}$ and $\{p_{32}, p_{43}\}$ are obtained using (10.22) and (10.23), respectively:

$$p_{ab} = \sum_{w=\lceil OBI \times P_{co(a,b)}^{(L)} \rceil}^{OBI} {}^{OBI}C_w [1 - P_B(n_a)]^{OBI-w} [P_B(n_a)]^w, \qquad (10.22)$$

$$p_{ba} = \sum_{w=0}^{\lfloor OBI \times P_{co(a,b)}^{(L)} \rfloor} {}^{OBI}C_w [1 - P_B(n_b)]^{OBI-w} [P_B(n_b)]^w, \qquad (10.23)$$

for $a \in \{2, 3\}$ and $b = a + 1$.

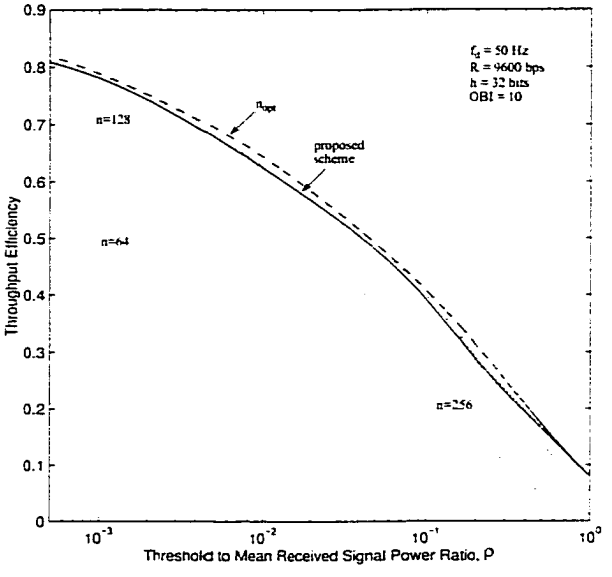

Fig. 10.5 Performance of an adaptive SR-ARQ protocol with three controllable packet lengths based algorithm A (maximum likelihood PER with fixed observation interval).

Fig. 10.5 compares the performance of the proposed adaptive scheme with that of the fixed block length SR-ARQ systems as well as the maximum attainable throughput (with optimal block length) curve. It is apparent that the performance of the adaptive system with three controllable packet sizes closely resembles the envelope of the corresponding three fixed packet length performance curves. The performance of this adaptive system

can be improved slightly by optimizing the observation interval. In selecting the value for OBI, the following factors must be taken into consideration:

(a) If the OBI is very large, then the delay incurred before reacting to a change in the channel could be significant;

(b) On the other hand, very small values for the OBI will not provide a reliable CSI decision.

The generalization of this algorithm for an adaptive system with more than three states is straight-forward.

10.2.2 Maximum Likelihood PER with Variable Observation Interval (Algorithm B)

This CSE algorithm is similar to that of algorithm A except that now the observation interval can be chosen to be different at each distinct state. This relaxation provides a greater flexibility in selecting the design parameters (i.e., observation interval) associated with each state, and therefore this CSE algorithm has the potential to yield a superior performance than algorithm A. Alternatively, this algorithm could be designed to react much faster to the changing channel condition (i.e., shorter OBI) without significantly affecting the performance. In order to evaluate the performance of this algorithm, equation (10.22) and (10.23) should be modified as shown below:

$$p_{ab} = \sum_{w=\left\lceil OBI_a \times P_{co(a,b)}^{(L)} \right\rceil}^{OBI_a} {}^{OBI_a}C_w \left[1 - P_B(n_a)\right]^{OBI_a - w} \left[P_B(n_a)\right]^w, \qquad (10.24)$$

$$p_{ba} = \sum_{w=0}^{\left\lfloor OBI_b \times P_{co(a,b)}^{(L)} \right\rfloor} {}^{OBI_b}C_w \left[1 - P_B(n_b)\right]^{OBI_b - w} \left[P_B(n_b)\right]^w, \qquad (10.25)$$

for $a \in \{2, 3\}$ and $b = a + 1$.

10.2.3 Variable Observation Interval with Weighted Success or Error Events (Algorithm C)

Let us consider an adaptive ARQ system with two controllable packet lengths, and define the observation intervals associated with the low- and high-channel error rate states to be α and β, respectively. The channel estimator would consider that the channel condition is transiting from state L to state H if all the received acknowledgments messages during that observation interval (i.e., α) are NACKs. Hence the transition probability is $p_{LH} = [P_B(n_L)]^{\alpha}$. On the other hand, if the transmitter receives β contiguous ACKs during the observation window of length β, then the block length will be adapted from n_H to n_L bits. The transition probability from state H to state L is therefore $p_{HL} = [1-P_B(n_H)]^{\beta}$. Then the steady-state probabilities are given by,

$$P_L = \frac{p_{HL}}{p_{LH}+p_{HL}} = \frac{[1-P_B(n_H)]^{\beta}}{[P_B(n_L)]^{\alpha}+[1-P_B(n_H)]^{\beta}}, \tag{10.26}$$

$$P_H = \frac{p_{LH}}{p_{LH}+p_{HL}} = \frac{[P_B(n_L)]^{\alpha}}{[P_B(n_L)]^{\alpha}+[1-P_B(n_H)]^{\beta}}, \tag{10.27}$$

and the expressions for the desired and estimated throughput performance of this adaptive SR-ARQ with two controllable packet lengths are given by (10.28) and (10.29), respectively:

$$T_A(\rho) = \begin{cases} T_L = \dfrac{n_L-h}{n_L}\exp\left[-\rho-\dfrac{n_L f_D\sqrt{2\pi\rho}}{R}\right] & \text{if } \rho_{min} \le \rho \le \rho_{co(L,H)} \\ T_H = \dfrac{n_H-h}{n_H}\exp\left[-\rho-\dfrac{n_H f_D\sqrt{2\pi\rho}}{R}\right] & \text{if } \rho_{co(L,H)} < \rho \le \rho_{max} \end{cases}, \tag{10.28}$$

$$\hat{T}_A(\rho) = P_L T_L + P_H T_H, \tag{10.29}$$

where $(\rho_{max}-\rho_{min})$ dictates the dynamic range of the parameter ρ.

Exploiting the asymptotic property of the steady-state probabilities when $\{\alpha, \beta\} \rightarrow \infty$, it can be easily shown that the optimal solution to our problem (i.e., when the performance curve of the proposed CSE scheme coincides with the desired performance envelope) lies in the infinite α-β space (i.e., assumes a quasi-stationary channel). In this case, the steady-state probabilities (P_L and P_H) will be equal at the cross-over point. It follows that the optimal design parameters are related by,

$$\frac{\beta^*}{\alpha^*} = \frac{\ln\left[P_{co(L,H)}^{(U)}\right]}{\ln\left[1 - P_{co(L,H)}^{(L)}\right]}. \tag{10.30}$$

Since the optimal solution does not lie in a reasonable value range, one can resort to the suboptimal solutions with some sacrifice in performance. If we select α and β values to be very large, then this scheme will lose its ability to adapt to moderately fast channel variations. On the other hand, extremely small values of α and β will result in premature (unnecessary) switching, and poor fit to the desired performance curve. Therefore we have introduced additional boundary constraints to the design parameters, which will be specified by the channel behavior and/or the intended application.

The problem of finding the suboptimal design parameters (i.e., α and β) may be accomplished via an optimization approach [126] such that $\hat{T}_A(\rho)$ best approximates $T_A(\rho)$ in the sense that the total estimation error is minimized,

$$\begin{aligned} &\text{minimize} \quad E(\alpha, \beta) \cong \Delta \sum_{k=1}^{K} W_k\left[T_A(\rho_k) - \hat{T}_A(\rho_k)\right]^2 \\ &[\alpha, \beta] \in Z \\ &\text{subject to:} \quad \alpha_{min} < \alpha < \alpha_{max} \\ &\qquad\qquad\quad \beta_{min} < \beta < \beta_{max} \end{aligned} \tag{10.31}$$

where K corresponds to the sample size, ρ_k denotes the threshold to signal power ratio of the kth sample, W_k is the user defined weight sequence that provides additional flexibility in matching different points with varying accuracy. The optimization variables,

α and β, can assume any value from the set Z, which consists of positive integers. In our minimization problem, these boundary constraints can be eliminated via transformation $y = \dfrac{e^{z} - e^{-z}}{e^{z} + e^{-z}} \equiv \tanh(z)$.

Table 10.2 Comparison between the interpolated β (from asymptotic analysis) and the suboptimal $\hat{\beta}^*$ (via Quasi Newton optimization method) for an adaptive SR ARQ system based on algorithm C. It is assumed that $h = 32$ bits, $R = 9600$ bps, $f_D = 50$ Hz, $n_L = 256$ bits and $n_H = 128$ bits.

α	$c = \dfrac{\ln\left[P_{co(L,H)}^{(U)}\right]}{\ln\left[1 - P_{co(L,H)}^{(L)}\right]}$	Interpolation Technique		Quasi-Newton optimization method	
		Integer value of $\beta = c\alpha$	$E(\alpha, \beta)$	Suboptimal $\hat{\beta}^*$	$E(\alpha, \beta)$
1	8.0147	8	4.4507×10^{-6}	13	1.4919×10^{-6}
2		16	5.7136×10^{-7}	19	3.8271×10^{-7}
3		24	1.7035×10^{-7}	26	1.3973×10^{-7}
10		80	4.6296×10^{-9}	81	4.5040×10^{-9}

From Table 10.2 it is evident that the discrepancy between the suboptimal design parameters obtained via the optimization approach and the interpolation of Eq. (10.30) diminishes as α and β gets larger, as anticipated. Therefore, Eq. (10.30) provides a rule of thumb allowing a handy calculation of β for a given $\alpha > 1$, or vice versa.

From Fig. 10.6 we observe that this CSE algorithm yields a very close match to the desired performance envelope even with relatively small α and β (i.e., a shorter OBI is required to acquire a reliable CSI compared to the algorithm A). Consequently, this scheme outperforms the traditional channel monitoring system in terms of the ability to react to rapid fluctuations in the channel condition. This is because we have placed a greater emphasis on the influence of most recent errors, and therefore our measurements tend to estimate the instantaneous block error probability parameter more realistically.

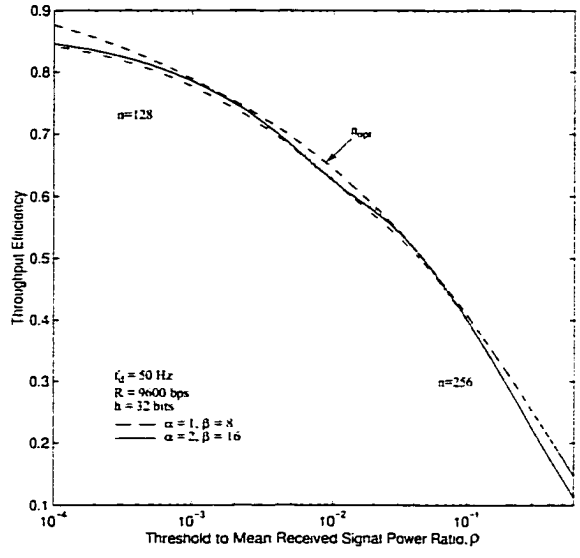

Fig. 10.6 Performance of an adaptive SR-ARQ protocol with two controllable packet lengths based algorithm C (variable OBI with weighted success or error events).

However, this algorithm may not be very effective for an adaptive ARQ system with more than two controllable packet lengths because it lacks the flexibility in choosing suitable values for the observation intervals in the intermediate channel error states. As a consequence, the practical application of this algorithm is restricted to a Markov chain with two channel error states.

10.2.4 Sliding Observation Window(s) with Weighted Success or Error Events (Algorithm D)

In this algorithm, the CSI is gathered by monitoring the count of contiguous ACKs and/or NACKs. Therefore the observation interval could be different even in a particular channel-error state (consequently, overcomes the major limitation of algorithm C for systems with more than two controllable packet sizes). Although this algorithm was first proposed by Yao [105], the author failed to accurately model this adaptive ARQ system. The

simple Markov chain representation in [105] becomes void if the design variables are selected to be larger than unity because now the present state probabilities will be dependent on a specified number of previous state values, and therefore $Pr\{X_n | X_0, X_1, \ldots, X_{n-1}\} \neq Pr\{X_n | X_{n-1}\}$.

Since the transition from one state to another depends on the number of contiguous NACKs or ACKs that have been received, i.e.,

$$Pr\{X_{n+1} | X_0, X_1, \ldots, X_n\} = Pr\{X_{n+1} | X_{n-\alpha+1}, \ldots, X_n\} ,$$

we can represent the proposed adaptive system precisely by an r-order Markov (multiple Markov process) process. It is straightforward to transform a multiple Markov process into a simple one by expanding the number of states defined for the system and correspondingly increasing the size of the transition matrix.

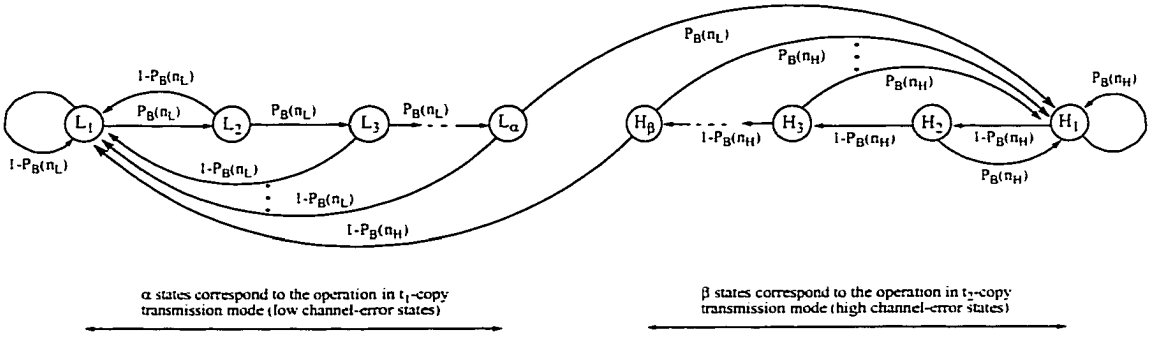

Fig. 10.7 (α+β)-state Markov chain representation for an adaptive ARQ strategy with two controllable packet lengths.

As an example consider an adaptive SR-ARQ system with two controllable packet lengths. The CSE assumes that the channel condition transiting from state L to H upon receiving α contiguous NACKs. On the other hand, if the transmitter receives β contiguous ACKs, then the CSE would consider that the channel is traversing from state H to state L. Then the adaptive ARQ system can be characterized by an $(\alpha + \beta)$ -state Markov chain whose state space is partitioned into two groups of α low-channel error rate states

and β high-channel error states, as illustrated in Fig. 10.7. The $(\alpha+\beta) \times (\alpha+\beta)$ state transition matrix can be easily constructed (tabulated) from this figure.

After some mathematical manipulations, we obtain the following steady-state probabilities [129]:

$$P_{L_x} = \frac{[1-P_B(n_H)]^{\beta}[P_B(n_L)]^{x-1}}{\dfrac{[1-P_B(n_H)]^{\beta}\left[1-[P_B(n_L)]^{\alpha}\right]}{1-P_B(n_L)} + \dfrac{[P_B(n_L)]^{\alpha}\left[1-[1-P_B(n_H)]^{\beta}\right]}{P_B(n_H)}}, \quad (10.32)$$

$$P_{H_y} = \frac{[P_B(n_L)]^{\alpha}[1-P_B(n_H)]^{y-1}}{\dfrac{[1-P_B(n_H)]^{\beta}\left[1-[P_B(n_L)]^{\alpha}\right]}{1-P_B(n_L)} + \dfrac{[P_B(n_L)]^{\alpha}\left[1-[1-P_B(n_H)]^{\beta}\right]}{P_B(n_H)}}, \quad (10.33)$$

where $x \in \{1, 2, \ldots, \alpha\}$ and $y \in \{1, 2, \ldots, \beta\}$, respectively.

Since the adaptive system operates with a packet length while in any of the L_x states, it is useful to define a new parameter $P_L = \sum_{x=1}^{\alpha} P_{L_x}$ which dictates the steady-state probability of the channel at low channel error rate group,

$$\begin{aligned} P_L &= \sum_{x=1}^{\alpha} P_{L_x} \\ &= \frac{[1-P_B(n_H)]^{\beta}\left[1-[P_B(n_L)]^{\alpha}\right]/[1-P_B(n_L)]}{\dfrac{[1-P_B(n_H)]^{\beta}\left[1-[P_B(n_L)]^{\alpha}\right]}{1-P_B(n_L)} + \dfrac{[P_B(n_L)]^{\alpha}\left[1-[1-P_B(n_H)]^{\beta}\right]}{P_B(n_H)}} \end{aligned} \quad (10.34)$$

Similarly, the steady-state probability of the channel at high channel error rate group is given by,

$$P_H = \frac{[P_B(n_L)]^{\alpha}\left[1-[1-P_B(n_H)]^{\beta}\right]/P_B(n_H)}{\dfrac{[1-P_B(n_H)]^{\beta}\left[1-[P_B(n_L)]^{\alpha}\right]}{1-P_B(n_L)} + \dfrac{[P_B(n_L)]^{\alpha}\left[1-[1-P_B(n_H)]^{\beta}\right]}{P_B(n_H)}} \quad (10.35)$$

Following our treatment for algorithm C, the relationship between the optimal design parameters can be found by exploiting the asymptotic properties of the estimated throughput expression:

$$\beta^* = \frac{1}{\ln\left[1-P_{co(L,H)}^{(L)}\right]} \ln\left\{\frac{\left[1-P_{co(L,H)}^{(U)}\right]\left[P_{co(L,H)}^{(U)}\right]^{\alpha^*}}{P_{co(L,H)}^{(L)} + \left[1-P_{co(L,H)}^{(L)}-P_{co(L,H)}^{(U)}\right]\left[P_{co(L,H)}^{(U)}\right]^{\alpha^*}}\right\} \quad (10.36)$$

$$\alpha^* = \frac{\ln\left\{\frac{\left[P_{co(L,H)}^{(L)}\right]\left[1-P_{co(L,H)}^{(L)}\right]^{\beta^*}}{1-P_{co(L,H)}^{(U)} + \left[P_{co(L,H)}^{(L)}+P_{co(L,H)}^{(U)}-1\right]\left[1-P_{co(L,H)}^{(L)}\right]^{\beta^*}}\right\}}{\ln\left[P_{co(L,H)}^{(U)}\right]} \quad (10.37)$$

Table 10.3 Comparison between the interpolated β (from the asymptotic analysis) and the suboptimal $\hat{\beta}^*$ (via Quasi Newton optimization method [9]) for an adaptive SR ARQ system based on algorithm D. It is assumed that $h = 32$ bits, $R = 9600$ bps, $f_D = 50$ Hz, $n_L = 256$ bits and $n_H = 128$ bits.

α	Interpolation Technique		Quasi-Newton optimization method	
	Integer value of β using (10.36)	$E(\alpha, \beta)$	Suboptimal $\hat{\beta}^*$	$E(\alpha, \beta)$
1	3	3.7665×10^{-5}	7	5.4330×10^{-6}
2	8	4.0663×10^{-6}	12	1.4878×10^{-6}
3	15	7.1246×10^{-7}	18	4.6308×10^{-7}
4	23	2.0381×10^{-7}	25	1.7424×10^{-7}
10	71	6.8577×10^{-9}	71	6.8577×10^{-9}

As might be anticipated, the deviation of the suboptimal design parameters from the interpolated asymptotic properties of the throughput expression becomes larger with decreasing α (see Table 10.3). Nevertheless, the interpolated value can be used as a good initial point for the optimization routine. However, when the ratio $\ln\left[P_{co(L,H)}^{(U)}\right] / \ln\left[1-P_{co(L,H)}^{(L)}\right]$ gets much closer to unity (or alternatively, the upper and lower limits of the channel cross-over probability is approximately 0.5) the value pre-

dicted using (10.36) is quite accurate even for very small α. In fact, both the interpolated and the suboptimal β yield almost identical results for $n_L = 128$ bits and $n_H = 64$ bits (i.e., $P_{co(L,H)}^{(L)} = 0.4732$ and $P_{co(L,H)}^{(U)} = 0.6488$).

Now consider an adaptive ARQ scheme with three controllable packet lengths. The system operation is illustrated in Fig. 10.8, and its corresponding Markov-chain representation is shown in Fig. 10.9. Notice that in the medium channel error-rate state, the proposed channel estimation scheme permits distinct OBI for the count of contiguous ACKs and the count of contiguous NACKs, respectively, instead of a fixed OBI associated with each of the channel-error states.

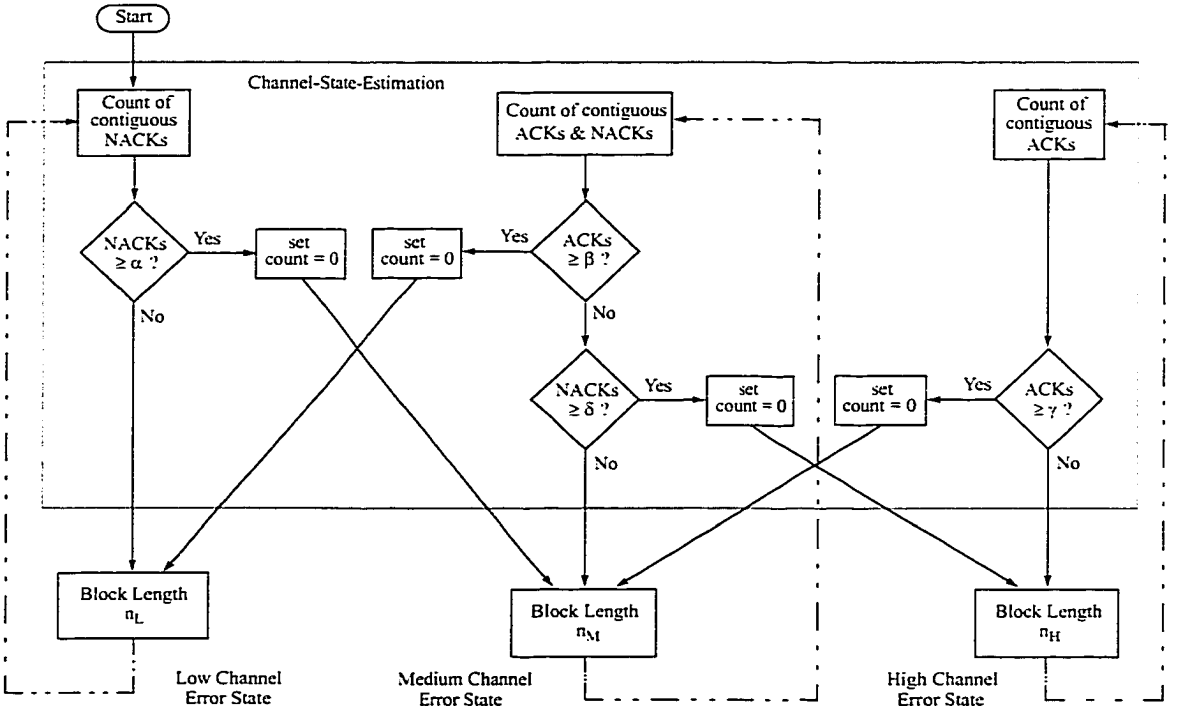

Fig. 10.8 System description of the proposed adaptive ARQ strategy (algorithm D) illustrating the transition between three block lengths.

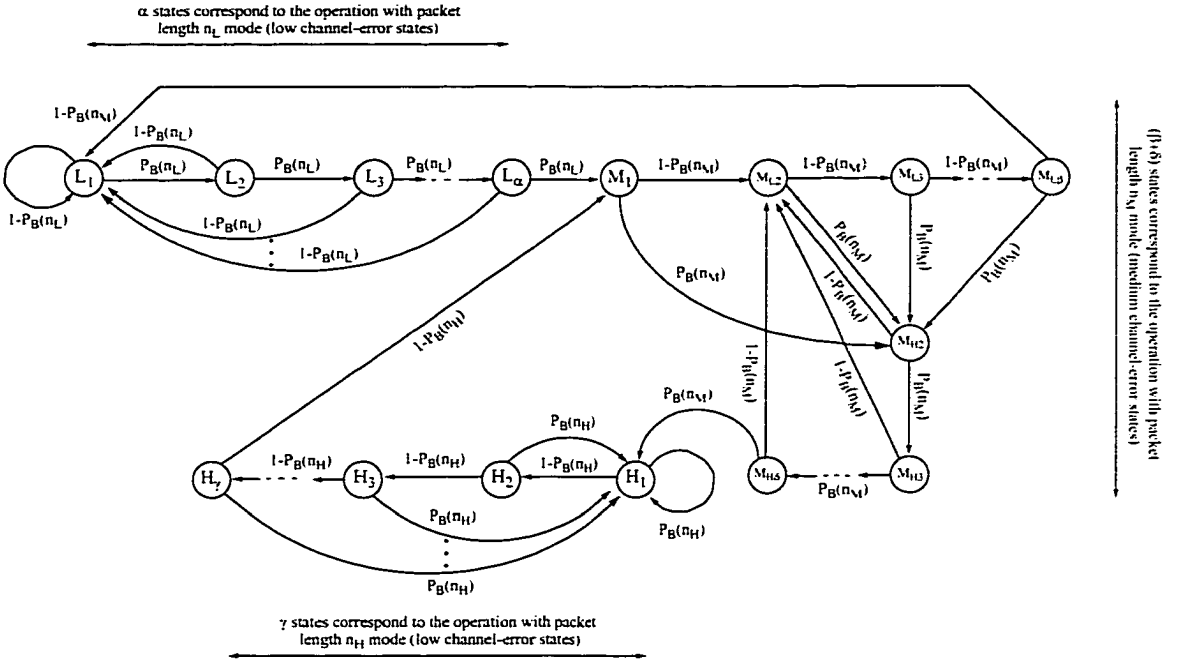

Fig. 10.9 $(\alpha+\beta+\gamma+\delta)$-state Markov chain representation for an adaptive ARQ strategy with three controllable packet lengths (based on algorithm D).

After some tedious calculations, we arrive to the following steady-state probabilities:

$$P_{L_i} = \frac{1}{\Lambda}(1-P_{eM})^{\beta-1}(1-P_{eH})^{\gamma}\left[1-P_{eM}^{\delta}\right]P_{eL}^{i-1},\quad i=1,2,\ldots,\alpha \tag{10.38}$$

$$P_{H_i} = \frac{1}{\Lambda}P_{eL}^{\alpha}P_{eM}^{\delta-1}\left[1-(1-P_{eM})^{\beta}\right](1-P_{eH})^{i-1},\quad i=1,2,\ldots,\gamma \tag{10.39}$$

$$P_{M_1} = \frac{1}{\Lambda}(1-P_{eH})^{\gamma}P_{eL}^{\alpha}\left[(1-P_{eM})^{\beta-1}\left[1-P_{eM}^{\delta}\right]+P_{eM}^{\delta-1}\left[1-(1-P_{eM})^{\beta}\right]\right] \tag{10.40}$$

$$P_{M_{Li}} = \frac{1}{\Lambda}P_{eL}^{\alpha}(1-P_{eH})^{\gamma}\left[1-P_{eM}^{\delta}\right](1-P_{eM})^{i-2},\quad i=2,3,\ldots,\beta \tag{10.41}$$

$$P_{M_{Hi}} = \frac{1}{\Lambda}P_{eL}^{\alpha}(1-P_{eH})^{\gamma}\left[1-(1-P_{eM})^{\beta}\right]P_{eM}^{i-2},\quad i=2,3,\ldots,\delta \tag{10.42}$$

where $P_{eL} = P_B(n_L)$, $P_{eM} = P_B(n_M)$, $P_{eH} = P_B(n_H)$, and

$$\Lambda = (1-P_{eM})^{\beta-1}(1-P_{eH})^{\gamma}\left[1-P_{eM}^{\delta}\right]\left[1-P_{eL}^{\alpha}\right]/(1-P_{eL}) + P_{eL}^{\alpha}P_{eM}^{\delta-1}\left[1-(1-P_{eM})^{\beta}\right]\left[1-(1-P_{eH})^{\gamma}\right]/P_{eH} + (1-P_{eH})^{\gamma}P_{eL}^{\alpha}\left[1-P_{eM}^{\delta}\right]\left[1-(1-P_{eM})^{\beta}\right]/\left[P_{eM}(1-P_{eM})\right] \quad (10.43)$$

Finally, the steady-state probability of the low, medium and high channel error-rate groups are given by (10.44), (10.45) and (10.46), respectively:

$$P_L = \sum_{i=1}^{\alpha} P_{L_i} = \frac{(1-P_{eM})^{\beta-1}(1-P_{eH})^{\gamma}\left[1-P_{eM}^{\delta}\right]\left[1-P_{eL}^{\alpha}\right]}{\Lambda(1-P_{eL})} \quad (10.44)$$

$$P_M = P_{M_1} + \sum_{i=2}^{\beta} P_{M_{Li}} + \sum_{i=2}^{\delta} P_{M_{Hi}} = \frac{(1-P_{eH})^{\gamma}P_{eL}^{\alpha}\left[1-P_{eM}^{\delta}\right]\left[1-(1-P_{eM})^{\beta}\right]}{\Lambda P_{eM}(1-P_{eM})} \quad (10.45)$$

$$P_H = \sum_{i=1}^{\gamma} P_{H_i} = \frac{P_{eL}^{\alpha}P_{eM}^{\delta-1}\left[1-(1-P_{eM})^{\beta}\right]\left[1-(1-P_{eH})^{\gamma}\right]}{\Lambda P_{eH}} \quad (10.46)$$

Our results reveal that this simple scheme can yield a reliable estimate of the channel condition within only a few block transmissions. For instance, if $[n_L, n_M, n_H] = [256, 128, 64]$ bits respectively (see Fig. 10.8), then we have $[\alpha, \beta, \delta, \gamma] = [1, 7, 4, 3]$, $[2, 12, 5, 4]$, $[2, 12, 10, 7]$, etc. as possible suboptimal solutions, obtained via optimization method. As well, since the CSE based on algorithm D requires the shortest period to accurately detect a change in the channel condition among the four schemes presented in this chapter, it is an excellent choice for implementing an adaptive ARQ strategy over wireless links. This algorithm also permits a flexible selection of the design variables for an adaptive system with an arbitrary number of controllable packet lengths. The generalization of this self-reconfigurable ARQ protocol with more than three controllable packet lengths is straight-forward from the analysis (methodology) presented in this chapter.

10.3 Conclusions

Four simple CSE algorithms to implement an adaptive ARQ scheme over slowly varying mobile radio channels have been studied. The channel state information is extracted from the frequency of the received contiguous ACKs and NACKs acknowledgment messages at the transmitter. The effectiveness of these algorithms has been highlighted by analyzing the performance of an adaptive packet length SR-ARQ protocol. Simple formulas to estimate the suboptimal design parameters are suggested. Numerical results reveal that the algorithms perform remarkably well, in spite of their simplicity. Specifically, the CSE algorithm based on counting the contiguous positive and/or negative acknowledgment messages provides a reliable CSI within only a few block transmissions, and requires the shortest observation interval among these four schemes. This algorithm also permits a flexible selection of the design variables for an adaptive system with an arbitrary number of controllable packet lengths.

Appendix 10A

In this appendix we will show that the channel estimation scheme based on algorithm A or B is essentially based on maximum likelihood estimation for the packet error probability. Suppose in an observation interval of $(x+y)$ packets, x packet have been received successfully and y packets are received in error. Then the likelihood function can be written as,

$$Z = \frac{(x+y)!}{x!y!}(1-P_B)^x (P_B)^y, \tag{10A.1}$$

and logarithm of the likelihood function as,

$$\log_{10} Z = x\log_{10}(1-P_B) + y\log_{10} P_B + \text{constant} \tag{10A.2}$$

The most convenient way to obtain the maximum likelihood estimator is to examine all the local maxima of log-likelihood function, i.e.,

$$\frac{d\log_{10}Z}{dP_B} = \frac{-x}{1-P_B} + \frac{y}{P_B} = 0 \Leftrightarrow \frac{y}{x+y} = P_B \tag{10A.3}$$

$$\frac{d^2\log_{10}Z}{dP_B^2} = \frac{-x}{(1-P_B)^2} - \frac{y}{P_B^2} < 0, \quad \text{since } x \geq 0, y \geq 0, x+y > 0 \text{ and } 0 \leq P_B \leq 1 \tag{10A.4}$$

Hence it is evident from (10A.3) and (10A.4) that in an observed proportion of the samples, $y/(x+y)$ is the maximum likelihood estimate of P_B, the packet error probability.

Chapter 11

Conclusions

In this chapter, a brief summary of results described in the previous chapters is given, and suggestions for further research are made.

11.1 Summary of the Dissertation

The dissertation focuses on accurate and efficient analysis of wireless digital communication systems in multiuser and multipath fading environments. Diversity techniques are employed to mitigate the detrimental effects of channel fading while adaptive ARQ strategies may be used to improve the overall system throughput in a slowly time-varying channel.

In Chapter 2, we derive several new unified expressions for computing the probability of outage in cellular mobile radio systems by exploiting either the Laplace inversion formula or Gil-Pelaez inversion theorem (Fourier inversion method). These methods handle non-integer Nakagami fading indexes, unequal Rice factors, dissimilar shadowing spreads, unequal transmit powers, correlated interferers as well as all the common fading distributions (Rayleigh, Rice, Nakagami-m, Nakagami-q, lognormal-Rice, Suzuki and lognormal-Nakagami-m). Both the interference-limited and the minimum signal power constraint (due to receiver noise floor) situations are considered. The exact outage probability is expressed in terms of a single finite-range integral. The integral may be approximated very precisely by a Gauss-Chebychev quadrature (GCQ) formula requiring the knowledge of the moment generating function (MGF) at only a small number of points. An estimate of the remainder term is also derived. The proposed techniques lend themselves to a powerful tool for outage analysis since they do not impose any restrictions while being easy to program. Moreover, our analytical framework, based on statistical

decision theory, can be used to assess the compatibility and applicability of previously published approaches that treat noise as cochannel interference or consider a minimum detectable receiver signal threshold, in the presence of receiver noise. Some previous studies have suggested approximating Rician desired signal statistics by a Nakagami-m model to circumvent the difficulty in evaluating the outage in Rician fading. We asses the suitability of this approximation by providing a comparison study of the outage performance in these two fading conditions. Surprisingly, some basic results for Nakagami-m channel have been overlooked, which has led to misleadingly optimistic results with the Nakagami-m approximation model.

Chapter 3 briefly surveys some of the diversity techniques commonly used in cellular radio and satellite communication systems to mitigate the detrimental effects of signal fading. Subsequently, two unified approaches for evaluating the average symbol error probability (SER) of a wide class of coherent, differentially coherent and noncoherent communication systems in different fading environments are presented. All common diversity combining techniques (maximal-ratio combining (MRC), equal-gain combining (EGC), selection combining (SDC), and switched combining (SWC)) are studied. In the first approach, our novel derivation relies upon the properties of the MGF of the signal-to-noise ratio (SNR) in the fading channel without diversity reception, the use of an alternative exponential form of the one-dimension and two-dimension complementary error functions, and the application of GCQ formulas. In the second approach, we require the knowledge of six Fourier Transforms, characteristic function (CHF) of SNR, and the application of GCQ formulas. While the MGF method (i.e., the first approach) fails to analyze the EGC diversity case, it usually leads to a more concise solution for other diversity combining methods such as MRC, SDC and SWC compared to the CHF method. Our method is computationally stable and the closed-form expressions (in the form of a rapidly converging series) derived in this chapter can approximate the true average SER within any degree of accuracy.

Exact integral expressions for calculating the average SER of multilevel quadrature amplitude modulation (MQAM) in conjunction with L-fold antenna diversity on arbitrary Nakagami fading channel are derived in Chapter 4. Both MRC (in independent and correlated fading) and EGC (in independent fading) predetection diversity combining techniques have been considered. Exact closed-form SER expressions for three restricted Nakagami fading cases (MRC reception) are also derived. An exact analysis of EGC for MQAM has not been reported previously despite its practical interest. Remarkably, the

exact SER integrals can also be replaced by a finite-series using a GCQ formula. A useful procedure for computing the confluent hypergeometric series is also presented in the appendix. Our unified expressions handle arbitrary fading parameters as well as dissimilar mean signal strengths across the diversity branches. The generality and computational efficiency of these new formulas render themselves as a powerful tool for SER analysis in different fading conditions.

In Chapter 5, the MGF of SNR at the output of a dual-branch SWC combiner is derived. The first-order derivative of the MGF with respect to the switching threshold is also derived. These expressions are obtained for the general case of correlated fading and nonidentical diversity branches, and hold for any common fading distributions. The optimum switching threshold (in a minimum error rate sense) is obtained by solving a nonlinear equation which is formed by using the first-order derivative of the MGF. This nonlinear equation can be simplified for several special cases. For independent and identically distributed diversity branches, the optimal switching threshold in closed-form is derived for three generic forms of the conditional error probability. For correlated Rayleigh or Nakagami-m fading with identical branches, the optimal switching threshold in closed-form is derived for the non-coherent binary modulation formats. We show that previous published results as special cases of our unified expression.

In Chapter 6, we derive a new closed-form formula for the MGF of the output SNR of a dual-diversity selection combiner in bivariate Nakagami-m fading with positive integer fading severity index using a circular contour integral representation for the generalized Marcum-Q function, $Q_m(a, b)$. This result involves only elementary functions and holds for any value of the ratio a/b in $Q_m(a, b)$. As an aside, we have shown that previous integral representations for $Q_m(a, b)$ can be obtained from a contour integral and also derive a new, single finite-range integral representation for $Q_m(a, b)$. A new infinite series expression for the MGF with arbitrary m is also derived. These MGFs can be readily used to unify the evaluation of average error performance of the dual-branch SC for coherent, differentially coherent and noncoherent communications systems.

In Chapter 7, we examined a new reduced-complexity rake receiver structure which is particularly attractive for high-speed wireless communications in indoor wireless channel. Subsequently, a general expression is derived to quantify the average bit

error rate performance of a maximum amplitude selection diversity (MA/SD) rake receiver over Nakagami multipath fading channels. This includes all possible conditions of signal strengths and arbitrary fading parameters. This low-complexity receiver architecture is practically appealing because of its simplicity as well as its ability to operate effectively even at high signalling rates. While the MRC combiner with perfect channel fading estimation outperforms the proposed MA/SD scheme, the latter yields superior performance when inaccurate channel estimation is considered (i.e., with Gaussian error in the combiner weighting factors). Simple yet accurate expressions for rapid evaluation of MRC and SDC diversity performance in a Nakagami fading channel with arbitrary parameters are also presented. A bound on the magnitude of the remainder term is also derived using a complex-variable method. This new bound is highly desirable since it does not require the evaluation of higher order derivatives, which can be difficult, time consuming and tedious. More importantly, it allows us to choose an appropriate value for n (upper limit for the truncated series) that satisfies a prescribed error tolerance. Numerical examples reveal that the number of samples of MGF required to achieve a specified accuracy declines rapidly with a higher average received SNR per channel, but increases when the channel has a strong line-of-sight path. It is shown that the series expression is virtually exact for sufficiently large n (say, 15) and SNR over 0 dB. The expression breaks down when the SNR approaches $-\infty$ dB.

In Chapter 8, an adaptive retransmission diversity combining scheme is investigated for both slotted and unslotted random access packet-switched code division multiple access (DS/CDMA ALOHA) systems over a frequency selective Rayleigh fading channel. Multiple received noisy packets are combined on a bit by bit basis to form a single, more reliable packet. A novel mechanism to ensure a reliable packet combining operation is outlined. It is shown that packet combining is an effective mechanism for enhancing the network throughput and delay performance of the conventional DS/CDMA ALOHA, while sustaining a reasonable receiver complexity. This scheme is highly advantageous for systems which can tolerate a certain delay and operate over highly time-varying channels. Sensitivity of the system performance to the packet header failure rate and in the presence of feedback channel errors have been investigated.

Chapter 9 outlines an efficient method to concurrently optimize a multiplicity of design variables for continuous selective-repeat (SR) and go-back-N (GBN) ARQ strategies, both in noiseless and noisy feedback channels. For these ARQ protocols, we adapt either the number of identical message blocks sent in each transmission (in case of GBN

scheme) or the number of copies of a block retransmitted to handle a NACKed codeword (for the SR protocol) dynamically to the estimated channel condition. The channel state information is obtained by counting the contiguous acknowledgment (ACK or NACK) messages. Exploiting the asymptotic properties of the steady-state probability expressions, we show analytically that the optimum solution indeed lies in the infinite space. Subsequently, a simple expression to estimate the suboptimal design parameters is suggested. Our approach of minimizing the mean square error function yields to a quantitative study of the appropriateness of the selected parameters. Exact analytical expressions that allows us to compute the throughput cross-over probability between any two arbitrary multicopy transmission modes are derived. The results provide fundamental insights into how these key parameters interact and determine the system performance.

The throughput of conventional ARQ protocols, such as the stop-and-wait, go-back-N and selective-repeat, can also be improved by dynamically adapting the protocol packet length to changes in channel conditions. Such action requires a method for sensing the channel state and detecting a change in it. Fortunately, the frequency of retransmission requests in ARQ error control schemes provides a natural source of channel state information (CSI). Chapter 10 examines four simple algorithms to implement such an adaptive system in a slowly varying mobile radio channel. Our numerical results reveal that in spite of their simplicity, the algorithms performs remarkably well. In particular, the algorithm based on counting the contiguous positive and/or negative acknowledgment messages provides a reliable CSI within only a few block transmissions, and requires the shortest observation interval among these four schemes. This algorithm also permits a flexible selection of the design variables for an adaptive system with an arbitrary number of controllable packet lengths.

11.2 Suggestions for Further Work

The following are interesting topics which may be pursued for future work. Some of this work is already in progress.

- Extension of the EGC receiver analysis in Rician and Nakagami-Hoyt fading channels and also perform the comparison between the CHF, Fourier series and Hermitian approximation methods in terms of their computational complexity.
- Accurate analysis of digital communications systems in band-limited channels

(to study the performance degradation due to intersymbol interference) and in the presence of cochannel interference.

- A useful method for studying the error floor phenomena in Turbo codes in different fading environments. In fact, one no longer needs to invoke the Chernoff-Union bound since we can now analyze the exact union bound very efficiently.
- Analysis of BDPSK with post-detection EGC.
- Analysis of a simple packet combining strategy using majority logic on the hard decisions at the bit level.
- Simple techniques for evaluating the Gaussian probability integral $Q(x)$ and the generalized Marcum-Q function $Q_M(a, b)$ with arbitrary M.
- Analysis of average diversity combiner in multipath fading environment.
- Since there is a strong analogy between the conditional error-rate performance for diversity reception of an i.i.d. L-path received signal and the pair-wise error probability of two-sequences (length L) of i.i.d. faded symbols, one may characterize the performance of error correction coded communication systems (e.g., convolutional, trellis) over fading channels using the approach outlined in this dissertation. In particular, the analyses for MRC and EGC are directly applicable for the evaluation of pair-wise error probability with the known and unknown channel state information, respectively.

"It is dangerous to put limits on wireless"

- Guglielmo Marconi (1932)

Bibliography

[1] G. L. Stuber, *Principles of Mobile Communications*, Kluwer Academic Publishers, 1996.

[2] W. C. Jakes, *Microwave Mobile Communications*, IEEE Press, New Jersey, 1974.

[3] J. -P. Linnartz, *Narrowband Land-mobile Radio Networks*, MA:Artech, 1993.

[4] A. A. Abu-Dayya and N. C. Beaulieu, "Outage Probabilities of Cellular Mobile Radio Systems with Multiple Nakagami Interferers," *IEEE Trans. Vehic. Technology*, Vol. 40, pp. 757-767, Nov. 1991.

[5] Y. D. Yao and A. U. H. Sheikh, "Investigation into Cochannel Interference in Microcellular Mobile Radio Systems," *IEEE Trans. Vehic. Technology*, Vol. 41, pp. 114-123, Feb. 1992.

[6] R. F. Diesta and J. -P. Linnartz, "Using Laplace Transforms to Compute Performance of Mobile Radio Links," *Proc. PIMRC'94*, pp. 301-305, 1994.

[7] Q. T. Zhang, "Outage Probability in Cellular Mobile Radio Due to Nakagami Signal and Interferers with Arbitrary Parameters," *IEEE Trans. Vehic. Technology*, Vol. 45, pp. 364-372, May 1996.

[8] C. Tellambura and V. K. Bhargava, "Outage Probability Analysis for Cellular Mobile Radio Systems Subject to Nakagami Fading and Shadowing," *IEICE Trans. Commun.*, pp. 1416-1423, Oct. 1995.

[9] T. T. Tjhung, C. C. Chai and X. Dong, "Outage Probability for Lognormal-Shadowed Rician Channels," *IEEE Trans. Vehic. Technology*, Vol. 46, pp. 400-407, May 1997.

[10] C. Tellambura, A. J. Mueller and V. K. Bhargava, "Analysis of M-ary Phase-Shift-Keying with Diversity Reception for Land-Mobile Satellite Channels," *IEEE Trans. on Vehic. Technology*, Vol. 46, pp. 910-922, November 1997.

[11] L. -C. Wang and C. -T. Lea, "Co-channel Interference Analysis for Shadowing Rician Channels," *IEEE Commun. Letters*, Vol. 2, pp. 67-69, March 1998.

[12] J. G. Proakis, *Digital Communications*, New York: McGraw-Hill, 3rd. Ed., 1995.

[13] R. S. Hoyt, "Probability Functions for the Modulus and Angle of the Normal Complex Variate," *Bell System Tech. Journal*, Vol. 26, pp. 318-359, 1947.

[14] M. Abramowitz and I. A. Stegun, *Handbook of Mathematical Functions*, National Bureau of Standards, Applied Mathematics Series 55, 1964.

[15] C. Tellambura and A. Annamalai, "A Unified Numerical Approach for Computing the Outage Probability for Mobile Radio Systems," submitted to the IEEE Communications Letters, 1998.

[16] E. Biglieri, G. Caire, G. Taricco and J. Ventura-Traveset, "Simple Method for Evaluating Error Probabilities," *IEE Electronics Letters*, Vol. 32, pp. 191-192, Feb. 1996.

[17] J. Gil-Pelaez, "Note on the Inversion Theorem," *Biometrika*, Vol. 38, pp. 481-482, 1951.

[18] A. Annamalai, C. Tellambura and V. K. Bhargava, "A General Approach for Evaluating the Outage Probability in Microcellular Mobile Radio Systems," submitted to the IEEE ICC'99.

[19] S. Stein, "Fading Channel Issues in System Engineering," *IEEE J. Selected Areas Commun.*, Vol. 5, pp. 68-69, February 1987.

[20] A. Paulraj, "Diversity Techniques," pp. 213-223, *The Communications Handbook*, J. D. Gibson Ed., IEEE Press, New Jersey, 1996.

[21] M. Schwatz, W. R. Bennett and S. Stein, *Communication Systems and Techniques*, McGraw-Hill, New York, 1966.

[22] C. Tellambura, A. J. Mueller and V. K. Bhargava, "BER and Outage Probability for the Land Mobile Satellite Channel with Maximal Ratio Combining," *IEE Electronics Letters*, April 1995.

[23] T. S. Rappaport, *Wireless Communications: Principles and Practice*, Prentice Hall, New Jersey, 1996.

[24] A. J. Mueller, *Issues in Diversity and Adaptive Error Control Coding for Wireless Communications*, M. A. Sc Thesis, Dept. of Electrical and Computer Engineering, University of Victoria, September 1995.

[25] M. Nakagami, "The m-distribution - A General Formula of Intensity Distribution of Rapid Fading," in *Statistical Methods of Radio Wave Propagation*, W. G. Hoffman Ed., Oxford, England: Pergamon, 1960, pp. 3-36.

[26] E. Lutz, D. Cygan, M. Dippold, F. Dolainsky and W. Papke, "The Land Mobile Satellite Communication Channel - Recordings, Statistics and Channel Model," *IEEE Trans. Vehicular Technology*, Vol. 40, pp. 375-386, May 1991.

[27] A. Annamalai, C. Tellambura and V. K. Bhargava, "Efficient Computation of MRC Diversity Performance in a Nakagami Fading Environment with Arbitrary Parameters" *IEE Electronics Letters*, June 1998, pp. 1189-1190.

[28] M. K. Simon and D. Divsalar, "Some New Twists to Problems Involving the Gaussian Probability Integral," *IEEE Trans. on Communications*, Vol. 46, February 1998.

[29] A. Annamalai, C. Tellambura and V. K. Bhargava, "Error Performance of L-branch MRC and EGC Diversity Reception of MQAM in Generalized Fading Channels," submitted to the *IEEE Trans. on Communications*, 1998.

[30] C. Tellambura, "Evaluation of the Exact Union Bound for Trellis Coded Modulations over Fading Channels," *IEEE Trans. Communications, Vol. 44*, pp. 1693-1699, December 1996.

[31] A. Annamalai, C. Tellambura and V. K. Bhargava, "Unified Analysis of MPSK and MDPSK with Diversity Reception in Different Fading Environments," IEE Electronics Letters, Vol. 34, No. 16, 6th August 1998, 1564-1565.

[32] S. Chennakeshu and J. B. Anderson, "Error rates for Rayleigh fading multichannel reception of MPSK signals," *IEEE Trans. on Communications*, Vol. 43, pp. 338-346, February/March/April 1995.

[33] R. F. Pawula, S. O. Rice and J. H. Roberts, "Distribution of the phase angle between two vectors perturbed by Gaussian noise," *IEEE Trans. on Communications*, Vol. 30, pp. 1828-1841, August 1982.

[34] A. Abu-Dayya and N. C. Beaulieu, "Analysis of Switched Diversity System on Generalized-Fading Channels," IEEE Trans. Communications, Vol. 42, pp. 2959-2966, Nov. 1994.

[35] A. Abu-Dayya and N. C. Beaulieu, "Switched Diversity on Microcellular Rician Channels," IEEE Trans. Vehicular Technology, Vol. 43, pp. 970-976, Nov. 1994.

[36] M. K. Simon and M. -S. Alouini, Tutorial Notes TU 08: A Unified Approach to the Error Probability Analysis of Digital Communication over Generalized Fading Channels, IEEE Global Telecommunications Conference, Sydney, 8-12 Nov. 1998.

[37] C. Tellambura and V. K. Bhargava, "Unified Error Analysis of DQPSK in Fading Channels," IEE Electronics Letters, Vol. 30, No. 25, pp. 2110-2111, Dec. 1994.

[38] R. F. Pawula, "A New Formula for MDPSK Symbol Error Probability" IEEE Communications Letters, Vol. 2, pp. 271-272, Oct. 1998.

[39] X. Dong, N. C. Beaulieu and P. H. Wittke, "Two Dimensional Signal Constellations for Fading Channels," IEEE GLOBECOM, Communication Theory Mini Conference, pp. 22-27, 8-12 Nov. 1998.

[40] M. Simon and M. Alouini, "A Unified Approach to Performance Analysis of Digital Communication over Generalized Fading Channels," Proc. IEEE, Vol. 86, September 1998, pp. 1860-1877.

[41] M. Alouini and A. Goldsmith, "A Unified Approach for Calculating Error Rates of Linearly Modulated Signals over Generalized Fading Channels," Proc. ICC'98, Atlanta, pp. 459-464, June 1998.

[42] S. Sampei, *Applications of Digital Wireless Technologies to Global Wireless Communications*, Prentice Hall, New Jersey, 1997.

[43] T. Sunaga and S. Sampei, "Performance of Multi-Level QAM with Post-Detection Maximal-Ratio Combining Space Diversity for Digital Land Mobile Radio Communications," *IEEE Trans. Vehic. Tech.*, 294-301, August 1993.

[44] C. J. Kim, Y. S. Kim, G. Y. Jung and H. J. Lee, "BER Analysis of QAM with MRC Space Diversity in Rayleigh Fading Channel," *Proc. PIMRC'95*, Toronto, pp. 482-485, September 1995.

[45] J. Lu, T. T. Tjhung and C. C. Chai, "Error Probability Performance of L-branch Diversity Reception of MQAM in Rayleigh Fading," *IEEE Trans. Commun.*, Vol. 46, pp. 179-181, February 1998.

[46] A. Annamalai, C. Tellambura and V. K. Bhargava, "Error Performance of M-ary QAM with MRC Diversity Reception in a Nakagami Fading Channel," *IEEE International Symposium on Wireless Communications Digest*, pp. 44, May 1998.

[47] F. J. Altman and W. Sichak, "A Simplified Diversity Communication System for Beyond the Horizon Links," *IRE Trans. Commun. Systems, Vol. 4*, pp. 50-55, March 1956.

[48] N. C. Beaulieu, "An Infinite Series for the Computation of the Complementary Probability Distribution Function of a Sum of Independent Random Variables and Its Application to the Sum of Rayleigh random Variables," *IEEE Trans. Commun., Vol. 38*, pp. 1463-1474, September 1990.

[49] N. C. Beaulieu and A. Abu-Dayya, "Analysis of Equal Gain Diversity on Nakagami Fading Channels," *IEEE Trans. Commun.*, Vol. 39, pp. 225-234, February 1991.

[50] A. Abu-Dayya and N. C. Beaulieu, "Microdiversity on Rician Fading Channels," *IEEE Trans. Communications*, Vol. 42, June 1994, pp. 2258-2267.

[51] W. T. Webb and L. Hanzo, *Modern Quadrature Amplitude Modulation: Principles and Applications for Fixed and Wireless Channels*, IEEE Press, New York, 1994.

[52] I. S. Gradshteyn and I. M. Ryzhik, *Table of Integrals, Series and Products*, Academic Press, 5th edition, 1995.

[53] E. Biglieri, G. Caire, G. Taricco and J. Ventura-Traveset, "Simple Method for Evaluating Error Probabilities," *IEE Electronics Letters*, Vol. 32, February 1996, pp. 191-192.

[54] V. Aalo, "Performance of Maximal-Ratio Diversity Systems in a Correlated Nakagami-Fading Environment," IEEE Trans. Communications, Vol. 43, August 1995, pp. 2360-2369.

[55] P. Z. Peebles, *Probability, Random Variables and Random Signal Principles*, McGraw-Hill, 1993.

[56] G. B. Rybicki, "Dawson's Integral and Sampling Theorem," *Computers in Physics*, Vol. 3, pp. 85-87, March 1989.

[57] A. Erdelyi, *Higher Transcendental Functions*, Vol. 1, McGraw-Hill, 1953.

[58] A. Annamalai, C. Tellambura and V. K. Bhargava, "Analysis of Maximal-Ratio and Equal-Gain Diversity Systems for MQAM on Generalized Fading Channels," submitted to the *IEEE ICC'99*.

[59] H. Suzuki, "A Statistical Model for Urban Radio Propagation," *IEEE Trans. Communications*, Vol. 25, July 1977, pp. 673-679.

[60] A. J. Rustako Jr., Y. S. Yeh and R. R. Murray, "Performance of Feedback and Switch Space Diversity 900 MHz FM Mobile Radio Systems with Rayleigh Fading," IEEE Trans. Communications, Vol. 21, pp. 1257-1268, Nov. 1993.

[61] W. E. Shortall, "A Switched Diversity Receiving System for Mobile Radio," IEEE Trans. Communications, Vol. 21, pp. 1269-1275, Nov. 1973.

[62] F. Adachi, T. Hattori, K. Hirade and T. Kamata, "A Periodic Switching Diversity Technique for a Digital FM Land Mobile Radio," IEEE Trans. Vehicular Technology, Vol. 27, pp. 211-219, Nov. 1978.

[63] M. A. Blanco and K. J. Zdunek, "Performance and Optimization of Switched Diversity Systems for Detection of Signals with Rayleigh Fading," IEEE Trans. Communications, Vol. 27, pp. 1887-1895, Dec. 1979.

[64] M. Blanco, "Diversity Receiver Performance in Nakagami Fading," Proc. 1983 IEEE Southeastern Conference, Orlando, pp. 529-532.

[65] C. Tellambura, A. Annamalai and V. K. Bhargava, "Unified Analysis of Switched Diversity Systems in Independent and Correlated Fading Channels," submitted to the *IEEE Trans. Communications*.

[66] A. Annamalai, C. Tellambura and V. K. Bhargava, "A Unified Approach to Performance Evaluation of Switched Diversity in Independent and Correlated Fading Channels," submitted to *IEEE WCNC'99*.

[67] S. Okui, "Probability of Co-Channel Interference for Selection Diversity Reception in the Nakagami-m Fading Channel," *IEE Proceedings-I*, Vol. 139, No. 1, February 1992, pp. 91-94.

[68] F. Adachi, K. Ohno and M. Ikura, "Postdetection Selection Diversity Reception with Correlated Unequal Average Power Rayleigh Fading Signals for P/4-shift QDPSK Mobile Radio," *IEEE Trans. Vehic. Tech.*, May 1992, pp. 199-210.

[69] G. Fedele, L. Izzo and M. Tanda, "Dual Diversity Reception of M-ary DPSK Signals over Nakagami Fading Channels," *Proc. PIMRC*, Toronto, Sept. 1995, pp. 1195-1201.

[70] G. Fedele, "N-Branch Diversity Reception of M-ary DPSK Signals in Slow and Nonselective Nakagami Fading," *European Trans. Telecommunications*, Vol. 7, March/April 1996, pp. 119-123.

[71] M. Simon and M. -S. Alouini, "A Unified Performance Analysis of Digital Communication with Dual Selective Combining Diversity over Correlated Rayleigh and Nakagami-m Fading Channels," *IEEE Trans. Communications*, Vol. 47, No. 1, January 1999, pp. 33-43.

[72] M. K. Simon, "A New Twist on the Marcum Q-Function and Its Applications," *IEEE Communications Letters*, Vol. 2, February 1998, pp. 39-41.

[73] C. W. Helstrom, *Elements of Signal Detection and Estimation*, Prentice-Hall, New Jersey, 1995.

[74] C. C. Tan and N. C. Beaulieu, "Infinite Series Representation of the Bivariate Rayleigh and Nakagami-m Distributions," *IEEE Trans. Communications*, Vol. 45, No. 10, October 1997, pp. 1159-1161.

[75] M. Simon and M. -S. Alouini, "A Simple Single Integral Representation of the Bivariate Rayleigh Distribution" *IEEE Communications Letters*, Vol. 2, May 1998, pp. 128-130.

[76] J. W. Craig, "A New, Simple and Exact Results for Calculating the Probability of Error for Two Dimensional Signal Constellations," *IEEE Milcom'91* Conference Record, pp. 25.5.1-25.5.5.

[77] A. Salmasi and K. S. Gilhousen, "On the System Design Aspects of CDMA Applied to Digital Cellular and Personal Communications Networks," *Proc. IEEE VTC'91*, pp. 57-62, May 1991.

[78] M. Kavehrad and P. J. McLane, "Performance of Low-Complexity Channel Coding and Diversity for Indoor Wireless Communications," *AT&T Tech. Journal, Vol. 64*, pp. 1927-1965, Oct. 1985.

[79] T. Eng and L. B. Milstein, "Coherent DS-CDMA Performance in Nakagami Multipath Fading," *IEEE Trans. Commun., Vol. 43*, pp. 1134-1143, Feb./March/ April 1995.

[80] T. Eng, N. Kong and L. B. Milstein, "Comparison of Diversity Combining Techniques for Rayleigh Fading Channels," *IEEE Trans. Commun., Vol. 44*, pp. 1117-1129, September 1996.

[81] R. Wong, A. Annamalai and V. K. Bhargava, "Evaluation of Predetection Diversity Techniques for Rake Receivers," *Proc. IEEE PACRIM'97*, pp. 227-230, Victoria, August 20-22, 1997.

[82] G. Chyi, J. G. Proakis and C. M. Keller, "On the Symbol Error Probability of Maximum Selection Diversity Reception Schemes over a Rayleigh Fading Channel," *IEEE Trans. Commun., Vol. 37*, pp. 79-83, January 1989.

[83] E. A. Neasmith and N. C. Beaulieu, "A New Look at Selection Diversity," *Proc. WIRELESS'96*, pp. 191-206, 8-10 July, 1996.

[84] A. Annamalai, "Micro-Diversity Reception of Spread-Spectrum Signals on Nakagami Fading Channels," to appear in the *IEEE Trans. on Commun.*, 1998.

[85] W. Magnus, F. Oberhettinger and R. P. Soni, *Formulas and Theorems for Special Functions of Mathematical Physics*, Vol. 52, Springer-Verlag, New York, 1966.

[86] M. Abramowitz and I. A. Stegun, *Handbook of Mathematical Functions,* National Bureau of Standards, Applied Mathematics Series 55, 1964.

[87] G. Efthymoglou, V. Aalo and H. Helmken, "Performance Analysis of Coherent DS-CDMA Systems in a Nakagami Fading Channel with Arbitrary Parameters," *IEEE Trans. Vehic. Tech.*, Vol. 46, No. 2, May 1997, pp. 289-297.

[88] M. J. Gans, "The Effect of Gaussian Error in Maximal Ratio Combiners," *IEEE Trans. Commun. Tech.*, Vol. 19, August 1971, pp. 492-500.

[89] R. A. Silverman, *Complex Analysis with Applications*, Dover Publications, 1974.

[90] M. B. Pursley, "The Role of Spread-Spectrum in Packet Radio Network," *Proc. IEEE, Vol. 75*, pp. 116-134, Jan. 1987.

[91] D. Raychaudhuri, "Performance Analysis of Random Access Packet-Switched Code Division Multiple Access Systems," *IEEE Trans. Commun., Vol. 29*, pp. 895-901, June 1981.

[92] R. D. J. van Nee, R. N. van Wolfswinkel and R. Prasad, "Slotted ALOHA and Code Division Multiple Access Techniques for Land-Mobile Satellite Personal Communications," *IEEE JSAC, Vol. 13*, pp. 382-388, Feb. 1995.

[93] D. Chase, "Code combining - A Maximum-Likelihood Decoding Approach for Combining an Arbitrary Number of Noisy Packets," *IEEE Trans. Commun., Vol. 33*, pp 385-393, May 1985.

[94] S. Souissi and S. B. Wicker, "A Diversity Combining DS/CDMA System with Convolutional Encoding and Viterbi Decoding," *IEEE Trans. Vehic. Tech., Vol. 44*, pp. 304-312, May 1995.

[95] A. M. Y. Bigloo, T. A. Gulliver and V. K. Bhargava, "A Slotted Frequency-Hopped Multiple-Access Network with Packet Combining," *IEEE J. Selected Areas Commun., Vol. 14*, pp. 1859-1865, Dec. 1996.

[96] M. B. Pursley, "Frequency-Hop Transmission for Satellite Packet Switching and Terrestrial Packet Radio Networks," *IEEE Trans. Information Theory, Vol. 32*, pp. 652-667, Sept. 1986.

[97] R. K. Morrow and J. S. Lehnert, "Bit-to-Bit Error Dependence in Slotted DS/ SSMA Packet Systems with Random Signature Sequences," *IEEE Trans. Commun.*, pp. 1052-1061, Oct. 1989.

[98] D. L. Lu and J. F. Chang, "Analysis of ARQ Protocols via Signal Flow Graph," *IEEE Trans. Commun., Vol. 37,* pp. 245-251, March 1989.

[99] A. Annamalai, *Issues in DS-CDMA Integrated Wireless Access Networks*, M. A. Sc. Thesis, University of Victoria, British Columbia, Canada, 1997.

[100] R. L. Peterson, R. E. Ziemer and D. E. Borth, *Introduction to Spread Spectrum Communications*, Prentice Hall, New Jersey, 1995.

[101] S. B. Wicker, *Error Control Systems for Digital Communication and Storage*, Prentice-Hall, New Jersey, 1995.

[102] V. K. Bhargava, D. Haccoun, R. Matyas and P. Nuspl, *Digital Communications by Satellite*, Wiley, New York, 1981.

[103] T. Kasami, T. Klove and S. Lin, "Error Detection with Linear Block Codes," *IEEE Trans. Inform. Theory, Vol. 29,* pp. 131-136, January 1983.

[104] S. Lin, D. J. Costello and M. J. Miller, "Automatic-Repeat-Request Error-Control Schemes," *IEEE Communication Mag., Vol. 22,* pp. 5-17, December 1984.

[105] Y.-D. Yao, "An Effective Go-Back-N ARQ Scheme for Variable-Error-Rate Channels," *IEEE Trans. Commun., Vol. 43,* pp. 20-23, January 1995.

[106] H. Bruneel and M. Moeneclaey, "On Throughput Performance of Some Continuous ARQ Strategies with Repeated Transmissions," *IEEE Trans. Commun., Vol. 34,* pp. 244-249, March 1986.

[107] E. J. Weldon, "An Improved Selective-Repeat ARQ Strategy," *IEEE Trans. Commun., Vol. 30,* pp. 480-486, March 1982.

[108] A. C. Martins and J. C. Alves, "ARQ Protocols with Adaptive Block Size Perform Better over a Wide Range of Bit Error Rates," *IEEE Trans. Commun., Vol. 38,* pp. 737-739, June 1990.

[109] M. Rice and S. B. Wicker, "A Sequential Scheme for Adaptive Error Control over Slowly Varying Channels," *IEEE Trans. Commun., Vol. 42,* pp. 1533-1543, February/March/April 1994.

[110] S. Kallel and C. Leung, "Analysis of Memory and Incremental Redundancy ARQ Schemes over a Nonstationary Channel," *IEEE Trans. Commun., Vol. 40,* pp. 1474-1480, September 1992.

[111] B. Vucetic, "An Adaptive Coding Scheme for Time-Varying Channels," *IEEE Trans. Commun., Vol. 39,* pp. 653-663, March 1991.

[112] V. I. Johannes, "Improving on Bit Error Rate," *IEEE Communication Mag., Vol. 22,* pp. 18-20, December 1984.

[113] N. D. Birrell, "Pre-emptive Retransmission for Communications over Noisy Channels," *IEE Proc. Part F, Vol. 128,* pp. 393-400, 1981.

[114] W. -S. Lu, *Lecture Notes - ELEC 603 Engineering Design by Optimization II*, University of Victoria, 1996.

[115] R. Fletcher, *Practical Methods of Optimization*, Volume 1 - Unconstrained Optimization, Wiley, New York, 1980.

[116] R. Cam and C. Leung, "Throughput Analysis of Some ARQ Protocols in the Presence of Feedback Errors," *IEEE Trans. Commun., Vol. 45,* pp. 35-44, January 1997.

[117] H. Li and J. Cavers, "An Adaptive Filtering Technique for Pilot-Aided Transmission Systems," *IEEE Trans. Vehic. Technology, Vol. 40,* pp. 532-545, August 1991.

[118] D. L. Lu and J. F. Chang, "Analysis of ARQ Protocols via Signal Flow Graph," *IEEE Trans. Commun., Vol. 37,* pp. 245-251, March 1989.

[119] A. Annamalai, L. Freiberg and V. K. Bhargava, "Analysis and Optimization of an Adaptive Go-Back-N ARQ Protocol for Time-Varying Channels," *Proc. International Symposium on Personal, Indoor and Mobile Radio Communications*, pp. 447-451, September 1997.

[120] J. L. Doob, *Stochastic Processes*, Wiley, New York, 1953.

[121] M. Zorzi and R. R. Rao, "On the Statistics of Block Errors in Bursty Channels," *IEEE Trans. Commun., Vol. 45*, pp. 660-667, June 1997.

[122] R. A. Comroe and D. J. Costello, "ARQ Schemes for Data Transmission in Mobile Radio Systems," *IEEE J. Select. Areas Commun., Vol. 2,* pp. 472-481, July 1984.

[123] J. C. I. Chuang, "Comparison of Two ARQ Protocols in a Rayleigh Fading Channel," *IEEE Trans. Vehic. Technology, Vol. 39,* pp. 367-373, November 1990.

[124] Li Fung Chang, "Throughput Estimation of ARQ Protocols for a Rayleigh Fading Channel Using Fade- and Interfade-Duration Statistics," *IEEE Trans. Vehic. Technology, Vol. 40*, pp. 223-229, February 1991.

[125] S. Hara, A. Ogino, M. Araki, M. Okada and N. Morinaga, "Throughput Performance of SAW-ARQ Protocol with Adaptive Packet Length in Mobile Packet Data Transmission," *IEEE Trans. Vehicular Technology, Vol. 45,* pp. 561-569, August 1996.

[126] A. Annamalai, V. K. Bhargava and W. S. Lu, "On Adaptive Go-Back-N ARQ Protocol for Variable-Error Rate Channels," *IEEE Trans. Communications*, Vol. 46, pp. 1405-1408, Nov. 1998.

[127] A. Annamalai and V. K. Bhargava, "Analysis and Optimization of Adaptive Multicopy Transmission ARQ Protocols for Time-Varying Channels," *IEEE Trans. Communications, Vol. 46*, pp. 1356-1368, October 1998.

[128] S. A. Mahmoud, J. S. DaSilva and H. M. Hafez, "Optimal Packet Length for Fading Land Mobile Data Channels," *Proc. ICC'80,* pp. 61.3, June 1980.

[129] A. Annamalai and V. K. Bhargava, "Efficient ARQ Error Control Strategies with Adaptive Packet Length for Mobile Radio Networks," *Proc. 1998 IEEE ICUPC*, Florence, 5-9 October, 1998.